Traitement et valorisation des retours en tête : De la mesure à la modélisation

Perrine Devos

N°d'ordre NNT : 2023ISAL0056

THESE de DOCTORAT DE L'INSA LYON, membre de l'Université de Lyon

Ecole Doctorale N° 206
(Ecole doctorale de chimie de Lyon)

Spécialité / discipline de doctorat : Génie des Procédés

Soutenue publiquement le 12/09/2023, par :
Perrine Devos

Traitement et valorisation des retours en tête : de la mesure à la modélisation

---

Devant le jury composé de :

BUFFIERE, Pierre	Professeur des Universités	INSA-Lyon	Président
SPERANDIO, Mathieu	Professeur des Universités	INSA-Toulouse	Rapporteur
FLORES ALSINA, Xavier	Senior Researcher	Technical University of Denmark - DTU	Rapporteur
VANEECKHAUTE, Céline	Associate Professor	Université Laval	Examinatrice
GRAU, Paloma	Full Professor	Tecnun	Examinatrice
GILLOT, Sylvie	Directrice de recherche	INRAE	Directrice de thèse
ARNAULT, Camille	Ingénieure	Agence de l'eau Rhône Méditerranée Corse	Invitée
FILALI, Ahlem	Chargée de recherche	INRAE	Invitée

N°d'ordre NNT : 2023ISAL0056

THESE de DOCTORAT DE L'INSA LYON, membre de l'Université de Lyon

Ecole Doctorale N° 206
(Ecole doctorale de chimie de Lyon)

Spécialité / discipline de doctorat : Génie des Procédés

Soutenue publiquement le 12/09/2023, par :
Perrine Devos

Traitement et valorisation des retours en tête : de la mesure à la modélisation

---

Devant le jury composé de :

BUFFIERE, Pierre	Professeur des Universités	INSA-Lyon	Président
SPERANDIO, Mathieu	Professeur des Universités	INSA-Toulouse	Rapporteur
FLORES ALSINA, Xavier	Senior Researcher	Technical University of Denmark - DTU	Rapporteur
VANEECKHAUTE, Céline	Associate Professor	Université Laval	Examinatrice
GRAU, Paloma	Full Professor	Tecnun	Examinatrice
GILLOT, Sylvie	Directrice de recherche	INRAE	Directrice de thèse
ARNAULT, Camille	Ingénieure	Agence de l'eau Rhône Méditerranée Corse	Invitée
FILALI, Ahlem	Chargée de recherche	INRAE	Invitée

INSTITUT NATIONAL DES SCIENCES APPLIQUÉES LYON

Département de la Formation par la Recherche et des Études Doctorales (**FEDORA**)

Bâtiment INSA direction, 1er étage
37, av. J. Capelle
69621 Villeurbanne Cédex
fedora@insa-lyon.fr

Référence : TH0960_Perrine DEVOS
L'INSA Lyon a mis en place une procédure de contrôle systématique via un outil de détection de similitudes (logiciel Compilatio). Après le dépôt du manuscrit de thèse, celui-ci est analysé par l'outil. Pour tout taux de similarité supérieur à 10%, le manuscrit est vérifié par l'équipe de FEDORA. Il s'agit notamment d'exclure les auto-citations, à condition qu'elles soient correctement référencées avec citation expresse dans le manuscrit.

Par ce document, il est attesté que ce manuscrit, dans la forme communiquée par la personne doctorante à l'INSA Lyon, satisfait aux exigences de l'Etablissement concernant le taux maximal de similitude admissible.

SIGLE	ECOLE DOCTORALE	NOM ET COORDONNEES DU RESPONSABLE
CHIMIE	**CHIMIE DE LYON** **https://www.edchimie-lyon.fr** Sec. : Renée EL MELHEM Bât. Blaise PASCAL, 3e étage secretariat@edchimie-lyon.fr	**M. Stéphane DANIELE** C2P2-CPE LYON-UMR 5265 Bâtiment F308, BP 2077 43 Boulevard du 11 novembre 1918 69616 Villeurbanne **directeur@edchimie-lyon.fr**
E.E.A.	**ÉLECTRONIQUE, ÉLECTROTECHNIQUE, AUTOMATIQUE** **https://edeea.universite-lyon.fr** Sec. : Stéphanie CAUVIN Bâtiment Direction INSA Lyon Tél : 04.72.43.71.70 secretariat.edeea@insa-lyon.fr	**M. Philippe DELACHARTRE** INSA LYON Laboratoire CREATIS Bâtiment Blaise Pascal, 7 avenue Jean Capelle 69621 Villeurbanne CEDEX Tél : 04.72.43.88.63 **philippe.delachartre@insa-lyon.fr**
E2M2	**ÉVOLUTION, ÉCOSYSTÈME, MICROBIOLOGIE, MODÉLISATION** **http://e2m2.universite-lyon.fr** Sec. : Bénédicte LANZA Bât. Atrium, UCB Lyon 1 Tél : 04.72.44.83.62 secretariat.e2m2@univ-lyon1.fr	**Mme Sandrine CHARLES** Université Claude Bernard Lyon 1 UFR Biosciences Bâtiment Mendel 43, boulevard du 11 Novembre 1918 69622 Villeurbanne CEDEX **sandrine.charles@univ-lyon1.fr**
EDISS	**INTERDISCIPLINAIRE SCIENCES-SANTÉ** **http://ediss.universite-lyon.fr** Sec. : Bénédicte LANZA Bât. Atrium, UCB Lyon 1 Tél : 04.72.44.83.62 secretariat.ediss@univ-lyon1.fr	**Mme Sylvie RICARD-BLUM** Institut de Chimie et Biochimie Moléculaires et Supramoléculaires (ICBMS) - UMR 5246 CNRS - Université Lyon 1 Bâtiment Raulin - 2ème étage Nord 43 Boulevard du 11 novembre 1918 69622 Villeurbanne Cedex Tél : +33(0)4 72 44 82 32 **sylvie.ricard-blum@univ-lyon1.fr**
INFOMATHS	**INFORMATIQUE ET MATHÉMATIQUES** **http://edinfomaths.universite-lyon.fr** Sec. : Renée EL MELHEM Bât. Blaise PASCAL, 3e étage Tél : 04.72.43.80.46 infomaths@univ-lyon1.fr	**M. Hamamache KHEDDOUCI** Université Claude Bernard Lyon 1 Bât. Nautibus 43, Boulevard du 11 novembre 1918 69 622 Villeurbanne Cedex France Tél : 04.72.44.83.69 **hamamache.kheddouci@univ-lyon1.fr**
Matériaux	**MATÉRIAUX DE LYON** **http://ed34.universite-lyon.fr** Sec. : Yann DE ORDENANA Tél : 04.72.18.62.44 yann.de-ordenana@ec-lyon.fr	**M. Stéphane BENAYOUN** Ecole Centrale de Lyon Laboratoire LTDS 36 avenue Guy de Collongue 69134 Ecully CEDEX Tél : 04.72.18.64.37 **stephane.benayoun@ec-lyon.fr**
MEGA	**MÉCANIQUE, ÉNERGÉTIQUE, GÉNIE CIVIL, ACOUSTIQUE** **http://edmega.universite-lyon.fr** Sec. : Stéphanie CAUVIN Tél : 04.72.43.71.70 Bâtiment Direction INSA Lyon mega@insa-lyon.fr	**M. Jocelyn BONJOUR** INSA Lyon Laboratoire CETHIL Bâtiment Sadi-Carnot 9, rue de la Physique 69621 Villeurbanne CEDEX **jocelyn.bonjour@insa-lyon.fr**
ScSo	**ScSo*** **https://edsciencessociales.universite-lyon.fr** Sec. : Mélina FAVETON INSA : J.Y. TOUSSAINT Tél : 04.78.69.77.79 melina.faveton@univ-lyon2.fr	**M. Bruno MILLY** Université Lumière Lyon 2 86 Rue Pasteur 69365 Lyon CEDEX 07 **bruno.milly@univ-lyon2.fr**

*ScSo : Histoire, Géographie, Aménagement, Urbanisme, Archéologie, Science politique, Sociologie, Anthropologie

DEVOS Perrine

Sidestream treatment and recovery in wastewater treatment plants: from measurement to modelling

PhD supervisors:

Sylvie Gillot, INRAE, UR REVERSAAL, Lyon, France
Ahlem Filali, UR PROSE, Antony, France
Paloma Grau, CEIT & Tecnun, Donostia, Spain

RESUME

Dans un contexte d'évolution de la STEP (Station d'épuration) vers la StaRRE (Station de Récupération des Ressources de l'Eau), le procédé de digestion anaérobie des boues d'épuration connait des développements croissants. Ce procédé peut être installé de manière conventionnelle en traitant les boues produites sur un site mais également de manière centralisée en traitant les boues des stations d'épuration voisines. Enfin, ce procédé peut également être précédé d'une étape de prétraitement comme l'hydrolyse thermique afin d'améliorer les performances de digestion anaérobie et de déshydratation. L'installation d'un digesteur résulte en la production d'un centrat, également appelé retours en tête ou flux secondaires, suite à la déshydratation des boues digérées. Ce flux peut contenir des quantités importantes d'azote et/ou de phosphore qui peuvent être accrues dans le cas de digesteurs centralisés ou lors de la présence d'un prétraitement. Il convient donc de valoriser ou de traiter ces flux pour d'une part ne pas détériorer les performances des installations de traitement des eaux résiduaires, et d'autre part maximiser les ressources qu'elles contiennent. L'objectif de la thèse était d'accroitre les connaissances sur les caractéristiques des flux secondaires et sur les possibilités de traitement de l'azote et de valorisation du phosphore contenus dans ces flux. Les résultats permettront d'apporter des éléments pour choisir un procédé de traitement de l'azote et du phosphore.

La revue de la littérature a dans un premier temps permis de quantifier l'azote et le phosphore des flux secondaires pour différents types de digestion anaérobie (conventionnelle et avec hydrolyse thermique). Pour une digestion anaérobie mésophile conventionnelle, la concentration médiane d'azote ammoniacale est de 810 mg $N\text{-}NH_4$/L et de 1890 mg $N\text{-}NH_4$/L pour une digestion anaérobie avec hydrolyse thermique. Pour le phosphore, la quantité dans les flux secondaires peut varier de 1 à 400 mg $P\text{-}PO_4$/L et dépend du type de traitement du phosphore appliqué sur la file principale de traitement des eaux. Cependant, aucune différence entre la digestion conventionnelle et la digestion avec hydrolyse thermique n'a été observée pour la concentration en phosphate. Cette revue de littérature permet également de compiler les données sur les matières en suspension (MES), la demande chimique en oxygène (DCO) et sur les ions (Al^{3+}, Ca^{2+}, Cl^-, $Fe^{2+/3+}$, Mg^{2+}, K^+, Na^+, SO_4^{2-}). Une forte variabilité est constatée entre les stations d'épuration notamment pour les ions, avec une concentration qui s'étend de 10 à 320 mg/L pour les ions calcium et de 1 à 95 mg/L pour les ions magnésium. La variabilité pour ces deux ions peut être expliquée par la dureté de l'eau, différente d'une région à une autre, et à la précipitation de ces ions dans le digesteur. La revue s'intéresse également aux différents procédés existants pour le traitement et la valorisation de l'azote et du phosphore et souligne les caractéristiques des retours en tête qui pourraient impacter les performances de ces procédés. Parmi les procédés les plus développés, la récupération du phosphore sous forme de struvite peut voir ses performances diminuées dues à la présence élevée de matières en suspension et de calcium. Le procédé de nitritation partielle / anammox peut quant à lui être impacté par une multitude de composés et en particulier par les matières organiques et les matières en suspension.

Dans un second temps, les paramètres d'un modèle de digestion anaérobie couplé à la précipitation du phosphore ont été ajustés. L'innovation apportée par ce travail de thèse porte sur la prise en compte la dureté de l'eau lors de l'étape de calage des constantes de précipitation. Les deux digesteurs étudiés présentent des concentrations en calcium, magnésium, phosphate et alcalinité différentes et sont opérés avec des boues de stations d'épuration à pleine échelle. La procédure de calage proposée inclut le calage de la fraction de DCO inerte et des constantes cinétiques de

précipitation par la méthode de Monte Carlo par chaînes de Markov. Une correction du modèle a été effectuée pour inclure la fraction de potassium, calcium et magnésium organique dans les boues afin de mieux représenter leurs concentrations dans les boues digérées. Les résultats des simulations ont montré que les constantes cinétiques des minéraux $MgCO_3$, $CaCO_3$ et phosphate de calcium amorphe (ACP en anglais) impactent la concentration finale de phosphate, calcium, magnésium et d'alcalinité. L'identification d'un jeu de paramètre unique pouvant être appliqué aux deux digesteurs n'a pas été possible et un calage spécifique pour chaque digesteur a dû être réalisé. Les résultats de simulation donnent des valeurs de phosphate dans les boues digérées cohérentes quand les valeurs par défaut des constantes cinétiques de précipitation sont appliquées. En revanche, un ajustement des cinétiques de précipitation est nécessaire pour obtenir des concentrations en calcium et magnésium dans les boues digérées proches de celles mesurées, particulièrement dans le cas du digesteur présentant des concentrations élevées en calcium (207 mg/L) et magnésium (67 mg/L).

Enfin, une étude de scénarios a été réalisée afin d'évaluer les quantités de phosphore et d'azote pour un digesteur centralisé mélangeant différents types de boues. Les boues diffèrent par le type de traitement de phosphore appliqué sur la file eau et par le niveau de concentration de calcium, magnésium et carbone inorganique (dureté de l'eau). Cette étude propose également une évaluation simplifiée des coûts opérationnels et du bilan carbone d'un procédé de récupération du phosphore sous forme de struvite et du traitement biologique de l'azote par nitrification/dénitrification et nitritation partielle/anammox dans la configuration un et deux étages. Le modèle calé précédemment pour différents niveaux de dureté de l'eau a été employé dans l'analyse de scenarios. Les résultats montrent que la quantité de phosphate dans les boues est impactée par le type de traitement du phosphore et par le niveau de dureté de l'eau. En effet, le digesteur avec des boues provenant de déphosphatation biologique présente les concentrations en phosphate les plus élevées dans les boues digérées. En revanche, pour ce même digesteur, la quantité de phosphate est divisée par un facteur 2.4 lorsque la dureté de l'eau passe d'un niveau bas (concentration dans les boues de Ca^{2+} = 50 mg/L et Mg^{2+} = 20 mg/L) à haut (Ca^{2+} = 410 mg/L et Mg^{2+} = 166 mg/L). On note également que pour une dureté de l'eau basse ou moyenne, la récupération de phosphate dans les retours de digestion anaérobie de boues sans traitement spécifique du phosphore peut être considérée comme viable ([P-PO_4] > 50 mg/L). Ces résultats s'expliquent par des taux de précipitation important dans le digesteur pour de fortes duretés de l'eau. Concernant le traitement biologique de l'azote, une attention particulière doit être portée aux émissions de protoxyde d'azote qui dominent le bilan carbone des procédés de traitement des flux secondaires et en particulier dans le cas du procédé de nitritation partielle/anammox en deux étages.

ABSTRACT

As the wastewater treatment plant (WWTP) evolves towards the Water Resources Recovery Facility (WRRF), the anaerobic digestion of sewage sludge is undergoing increasing development. This process can be operated conventionally, treating the sludge produced on one site, or centrally, treating sludge from surrounding facilities. The anaerobic digestion process can also be preceded by a pre-treatment step such as thermal hydrolysis to improve anaerobic digestion and dewatering performance. The installation of a digester results in the production of a centrate, also called sidestreams or reject water, generated by the dewatering of digested sludge. This stream can contain significant quantities of nitrogen and/or phosphorus, which can be increased in the case of a centralised digester or when a pre-treatment is used. The aim of the thesis was to increase knowledge on the characteristics of sidestreams and on the potential routes for nitrogen and/or phosphorus treatment in these streams. The results will provide a basis for selecting a nitrogen and phosphorus treatment process.

A throughout literature review was first made to quantify the nitrogen and phosphorus amounts in sidestreams for different types of anaerobic digestion (conventional and with thermal hydrolysis). For conventional mesophilic anaerobic digestion, the median concentration of ammonia is 810 mg NH4-N/L and 1890 mg NH4-N/L for anaerobic digestion with thermal hydrolysis. For phosphorus, the concentration in sidestreams can vary from 1 to 400 mg PO_4-P/L and depends on the type of phosphorus treatment applied in the water mainline. However, no difference in phosphate concentration was observed between conventional digestion and digestion with thermal hydrolysis. This literature review also compiles data on suspended solids (SS), chemical oxygen demand (COD) and ions (Al^{3+}, Ca^{2+}, Cl^-, $Fe^{2+/3+}$, Mg^{2+}, K^+, Na^+, SO_4^{2-}). There is a significant variability between the different facilities, particularly for ions, with concentrations ranging from 10 to 320 mg/L for Ca^{2+} and from 1 to 95 mg/L for Mg^{2+}. The variability for these two ions can be explained by water hardness, which varies from one region to another, and by the precipitation of these ions in the digester. The review also looks at the various existing processes that exist to treat or recover nitrogen and phosphorus, and highlights the characteristics of sidestreams that could have an impact on the performance of these processes. Among the most developed processes, the recovery of phosphorus in the form of struvite may see its performance diminished due to the high presence of suspended solids and calcium. The partial nitritation / anammox process can be impacted by a multitude of compounds and in particular by organic and suspended matter.

Next, the parameters of an anaerobic digestion model coupled with phosphorus precipitation were adjusted. The innovative aspect of this doctoral work is the specific focus on the water hardness for the calibration of the precipitation constants. The two anaerobic digesters studied have different concentrations of calcium, magnesium, phosphate and alkalinity and are operated with full scale sewage sludge. The proposed calibration procedure includes calibration of the inert COD fraction and the precipitation kinetic constants using the Bayesian Monte Carlo method. A model correction was performed to include the fraction of organic potassium, calcium and magnesium in the sludge, in order to better represent their concentrations in the digested sludge. Simulation results showed that the kinetic constants of the minerals $MgCO_3$, $CaCO_3$ and Amorphous calcium phosphate (ACP) impact the final concentration of phosphate, calcium, magnesium and alkalinity. Identifying a single set of parameters that could be applied to both digesters was not possible, thus a specific calibration had to be carried out for each digester. The simulation results give consistent phosphate values in the digested sludge with default values of the precipitation kinetic constants. On the other hand, the precipitation kinetics had to be calibrated to obtain calcium and magnesium concentrations in the

digested sludge closed to the measured ones, particularly in the case of the digester with high calcium (207 mg/L) and magnesium (67 mg/L) concentrations.

Finally, a scenario analysis was carried out to assess the phosphorus and nitrogen contents for a centralised digester mixing different types of sludge. The sludges differ by the type of phosphorus treatment applied in the water line and by the level of concentration of calcium, magnesium and inorganic carbon (water hardness). This study also provides a simplified assessment of the operational costs and carbon footprint of a process for phosphorus recovery in the form of struvite and for biological treatment of nitrogen by nitrification/denitrification and partial nitritation/anammox in one- and two-stage configurations. The model previously calibrated in the thesis for different levels of water hardness was used in the scenario analysis. The results show that the amount of phosphate in the sludge is impacted by the type of phosphorus treatment and the level of water hardness. Indeed, the digester with sludge from biological phosphorus removal has the highest phosphate concentrations in the digested sludge. On the other hand, for the same digester, the quantity of phosphate is divided by a factor of 2.4 when the water hardness goes from low (concentration in the sludge of Ca^{2+} = 50 mg/L and Mg^{2+} = 20 mg/L) to high (Ca^{2+} = 410 mg/L and Mg^{2+} = 166 mg/L). For low or medium water hardness, phosphate recovery in anaerobic sludge digestion sidestreams without specific phosphorus treatment can be considered technically and economically viable ([P-PO4] > 50 mg/L). These results can be explained by high precipitation rates in the digester at high water hardness levels. As far as biological treatment of nitrogen is concerned, particular attention needs be paid to nitrous oxide emissions, which dominate the carbon balance of sidestream processes, particularly in the case of the two-stage partial nitrification/anammox process.

LIST OF PUBLICATIONS AND COMMUNICATIONS

Publications

- Devos, P., Filali, A., Grau, P., Gillot, S., 2023. Sidestream characteristics in water resource recovery facilities: A critical review. Water Res. 232, 119620. https://doi.org/10.1016/j.watres.2023.119620
- Devos, P., Elduayen-Echave, B., Filali, A., Gillot, S., Grau, P., 2023. Systematic calibration of a sewage sludge anaerobic digestion model with multiple mineral precipitation using full-scale data. Submitted to *Journal of Water Process Engineering.*

International Conferences

- Devos P., Filali A., Grau P., Gillot S. (2021) Characterisation of sidestreams for nutrient recovery implementation. Virtual 4th IWA Resource Recovery Conference (IWARR2021), 5-8 September 2021. (Poster presentation)
- Devos P., Filali A., Grau P., Gillot S. (2022) Ionic Strength Characterisation of Sidestreams in WRRFs: towards Nutrient Recovery Implementation. Virtual IWA water and resource recovery conference (IWA WWRR2022), 10 – 13 April 2022 (Oral presentation)
- Devos P., Filali A., Grau P., Gillot S. (2023) Validation of an AD model including multiple mineral precipitation to optimise P recovery in a centralised sludge anaerobic digester. 8th IWA Water Resource Recovery Modelling Seminar (WRRmod2022+), Stellenbosh, South Africa, 18-22 January 2023 (Poster presentation)

National conference

- Devos P., Bouniol, E., Kninech, B., Guthi, R., Tondera, K., Béline, F., Chazarenc, F., Boram, K., Buffière, P. Gillot, S. (2023) Biodégradabilité des eaux résiduaires urbaines, des boues d'épuration et des retours en tête. 102nd ASTEE Congress, Nice, France, 6-8 June 2023.
- Devos P., Filali A., Grau P., Gillot S. (2022) Sidestream characterisation in municipal WWTPs. Study of ion concentration for phosphorus and nitrogen recovery. 101st ASTEE Congress, Dunkerque, France, 14-16 June 2022. (Oral presentation)

Webinar and workshops

- Devos P., Filali A., Grau P., Gillot S. (2020) Sidestream characterisation in municipal WWTPs for phosphorus and nitrogen recovery. Scientific day CODEGEPRA Lyon, France, 19 November 2020. (Oral presentation).
- Devos P., Filali A., Grau P., Gillot S. (2021) Sidestream characterisation in municipal WWTPs for the implementation of phosphorus and nitrogen recovery processes. Academic morning Axelera, Lyon, France, 21 January 2021. (Oral presentation).
- Devos P., Filali A., Grau P., Gillot S. (2021) Will the wastewater treatment plant of the future be able to recover water resources? Webinar H2O Lyon et Réseaux Rivieres TV - Feet in the

water: from the lab to the field, sharing our knowledge, Lyon, France, 22 March 2021. (Oral presentation).

- Devos P., Filali A., Grau P., Gillot S. (2021) Sidestream characterisation. Workshop: Plant-wide modelling challenges with data and bottlenecks at full-scale WRRFs. Virtual 7th IWA Water Resource and Recovery Modelling Seminar (WRRmod2021), 21-25 August 2021. (Oral presentation)

- Devos P., Filali A., Grau P., Gillot S. (2021) Phosphorus and nitrogen recovery in anaerobic digestion sidestreams from municipal wastewater treatment plants (WWTPs). H_2O Lyon day, France, 25 November 2021. (Poster presentation).

- Devos P., Filali A., Grau P., Gillot S. (2023) Practicability of models in full-scale applications for resource recovery. Young water professional workshop. 8th IWA Water Resource Recovery Modelling Seminar (WRRmod2022+), Stellenbosch, South Africa, 18-22 January 2023 (Oral presentation)

- Devos P., Filali A., Grau P., Gillot S. (2023) Fate of ions in full-scale sludge line: from measurements to modelling. Workshop: Integrated modelling for Climate Resilient Water Resource Recovery Facilities of the Future. 8th IWA Water Resource Recovery Modelling Seminar (WRRmod2022+), Stellenbosch, South Africa, 18-22 January 2023 (Oral presentation)

TABLE OF CONTENT

LIST OF FIGURES

LIST OF TABLES

CHAPTER 1 – GENERAL INTRODUCTION

1.1 From a wastewater treatment plant to a water resource recovery facility

Before the 1970's, the main purpose of conventional wastewater treatment plants (WWTPs) was the removal of suspended solids, the elimination of pathogens and the treatment of organic compounds. From 1970, the removal of nitrogen and phosphorus started to be addressed due to environmental concerns (Metcalf & Eddy Inc. et al., 2003). In France, these discharge standards from the European directive 91/271/EEC continue to be applied and more stringent standards are expected in the near future (Laperche, 2022).

Following the Rio United Nations conference on environment and development in 1992, the concept of sustainable urban water management emerged (Larsen and Gujer, 1997). This was an opportunity to restate the functions of urban water including the integration of agriculture and nutrient cycles. Indeed, wastewater treatment plants are connected to nutrient cycles because part of nitrogen and phosphorus applied as fertiliser in agriculture ends up in wastewater. Historically, urban water management aimed to return nutrient to the countryside soil but this practice was lost with the introduction of cheap fertilizers (Cordell et al., 2009). The recent concerns of sustainable development and the development of circular economy concepts led to paradigm shift consisting in converting wastewater from an unwanted substance to a valuable resource (Bakan et al., 2022). As a result, WWTPs are now considered to be Wastewater Resource Recovery Facilities (WRRFs) from which valuable products can be covered. The wastewater sector started to include the recovery of: water, nutrients (phosphorus, nitrogen and potassium), bioenergy (methane, biodiesel, bio-hydrogen), heat, cellulosic fibres, metals and a wide range of platform biochemicals (enzymes, extracellular polymers, volatile fatty acids, etc.) (Pradel et al., 2016; Varennes et al., 2023; Yadav et al., 2022). In particular, the industry has focused a lot of efforts on the recovery of nitrogen and phosphorus due to regulations and the obligation to reduce their concentrations before discharge in the environment (Latimer et al., 2016).

The recovery of nitrogen and phosphorus could contribute to the reduction of greenhouse gas (GHG) induced by the fertiliser production (Qadir et al., 2020). Conventionally, ammonia fertiliser is produced by the Haber–Bosch process, an energy intensive process contributing to approximatively 1.5% of carbon dioxide emissions (Capdevila-Cortada, 2019). Part of nitrogen produced ends up in sewage from which it is removed from sewage biologically and returned to the air mainly in the form of dinitrogen gas (Khiewwijit et al., 2015). This treatment step also generates GHG emissions associated with energy (mainly for aeration) and chemical consumption as well as direct emissions of nitrous oxide (N_2O), a by-product of biological nitrogen removal processes, having a global warming potential 273 times that of CO_2 for a 100-year timescale (Pörtner et al., 2022).

Phosphorous used in mineral phosphorus fertilisers come from phosphate rock and is classified as a critical raw material by the European Commission (Egle et al., 2016) as it is expected to be depleted within next 45–100 years (Sengupta et al., 2015). In such context, recycling nutrients from wastewater is regaining importance as it could fill 13.4% of the global demand for these nutrients in agriculture according to Qadir et al. (2020).

To achieve this paradigm shift from a WWTP to a WRRF, one of the options is to consider the facility in a partition-release-recover configuration. This configuration relies on a first step of chemical

oxygen demand (COD) and nutrient accumulation in the solids, a second step of nutrient release with the anaerobic digestion process, and a final step of digested sludge treatment (D. J. Batstone et al., 2015). This PhD work mainly focusses on the last step related to nitrogen and phosphorus management (recovery or treatment) in the liquid phase obtained after the dewatering of the digested sludge.

1.2 Anaerobic digestion of sewage sludge and the emergence of sidestream management questions

Anaerobic Digestion was developed for the first time in a wastewater treatment plant in England in 1895 to recover biogas to fuel street lamps in Exeter (Nanda and Sarangi, 2022). This process has been implemented more widely with the development of activated sludge systems due to the large volumes of sewage sludge generated and that needed to be reduced and stabilised (Moletta, 2008). In the context of resource recovery, AD has been evaluated as one of the most efficient technologies for bio-energy production (Vaneeckhaute et al., 2014). In addition, to boost AD and dewatering performance, several sludge pre-treatments have been developed (Carrère et al., 2010). Among them, the thermal hydrolysis process (THP) is the most applied technology and existing full-scale references have so far reported an enhancement of biogas production and organic matter removal after THP pre-treatment (Kor-Bicakci and Eskicioglu, 2019).

However, AD also concentrates the remaining nutrients in the digested sludge, more especially in the liquid phase of the sludge. Once dewatered, this liquid phase, also called sidestream, centrate, reject water or supernatant, is sent back to the main wastewater treatment line. This internal sidestream contains up to 25% of the total nitrogen load and up to 30% of the total phosphorus load to the facilities (Couturier et al., 2001; Grulois et al., 1993; Ueno and Fujii, 2001). Sludge pre-treatments increase the quantity of nitrogen in sidestream and can generate streams with high concentration of refractory compounds in the case of thermal hydrolysis process (Barber, 2016; Bougrier et al., 2008; Dwyer et al., 2008b). However, the total nitrogen and phosphorus loads can vary from one WWTP to another due to the different wastewater composition, to the treatment applied for nutrient and phosphorus removal in the mainstream treatment line and to the operating conditions of the digester (concentration of the sludge, temperature, etc.).

High nutrient content in sidestreams can lead to increased energy consumption in the mainstream treatment line and degradation of effluent quality (Cullen et al., 2013; Janus and van der Roest, 1997; Preisner et al., 2020), especially when the facility operates close to full capacity. In such conditions, sidestream processes are good opportunities for upgrading nitrogen or phosphorus treatment capacity without needing to expand existing works (van Loosdrecht and Salem, 2006). Indeed it was suggested that managing sidestreams in mainstream treatment line is not always the most cost effective solutions because streams will be diluted and larger biological reactors and higher aeration demand may be required (Eskicioglu et al., 2018; Janus and van der Roest, 1997; Wett and Alex, 2003). Recovery processes in sidestreams could be highly efficient due to the high nutrient concentration (Latimer et al., 2016). Different sidestream processes have been developed and to choose the most appropriate one, an understanding of the different processes and tools as modelling to evaluate their impacts on the WRRF are paramount. Modelling is one of them.

1.3 Sidestream processes for nitrogen and phosphorus removal

Sidestream processes generally address only one particular component (either nitrogen or phosphorus), thus the removal or recovery of both nutrients involve the implementation of a combination of processes. They lie on biological and physico-chemical mechanisms and have different levels of technology readiness while implying different operational costs. Figure 1.1 is based on the level of technological readiness levels (TRLs), from TRL 4 (technology validation in laboratory environment) for the bioelectrochemical system to the maximum level of TRL 9 (successful operations of the technology in real environment) for nitrification/denitrification. The classification according to operational costs has been done based on figures found in scientific literature (see appendix of Chapter 1). Each process listed in Figure 1.1 is briefly described in the following paragraphs.

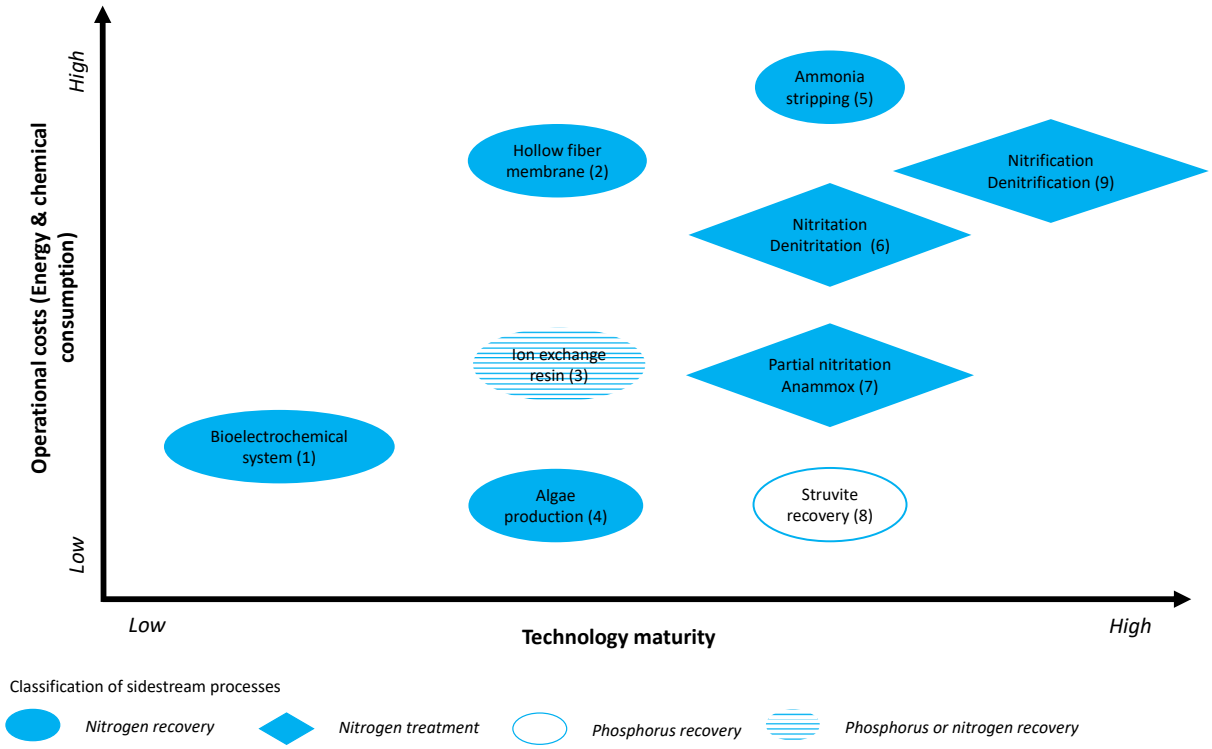

Figure 1.1 – Classification of the different sidestream processes described in the literature according to their purpose (treatment or recovery), maturity and operational costs. Main references for the classification of the technologies: (1) Barua et al., 2019 ; (2) Eskicioglu et al., 2018 ; (3) Sengupta et al., 2015 ; (4) Eskicioglu et al., 2018 ; (5) Ye et al., 2018 ; (6) Bowden et al., 2015 ; (7) Lackner et al., 2014 ; (8) Le Corre et al., 2009 ; (9) Bowden et al., 2015

1.3.1 Biological sidestream processes for N treatment

In the literature, nitrification/denitrification, nitritation/denitritation, partial nitritation/anammox, aerobic digestion and algae production are the biological processes employed to remove nitrogen in sidestreams (Eskicioglu et al., 2018; Ye et al., 2018). They all have applications at pilot-scale or full-scale but the most applied one is the partial nitritation/anammox system (Lackner et al., 2014) because less oxygen and no biodegradable COD are required compared to nitritation/denitritation or nitrification/denitrification.

Sidestream biological nitrogen removal by nitrification/denitrification has been mostly applied in sequencing batch reactors operated independently of the mainstream treatment line. However,

some applications were also developped to achieve bioaugmentation of the main line (Husband et al., 2010; Krhutkova et al., 2006). This is the case of the BABE (Bio Augmentation Batch Enhanced) technology in which part of the return activated sludge is fed into sidestream reactor in order to treat nitrogen in sidestream but also to produce a biomass with a high nitryfing activity (Berends et al., 2000; Salem et al., 2004) which can then seed the main treatment line. This can be achieved thanks to the high nitrogen load with concentration of $N\text{-}NH_4$ in the range of 800 to 1300 mg/L (Metcalf & Eddy Inc. et al., 2003) and elevated temperature in sidestreams. One of the system limit is the temperature shock between sidestreams and mainstream line (Bowden et al., 2015).

Shortcut nitrogen removal can be achieved by selectively inhibiting nitrite-oxidizing bacteria while retaining the activites of ammonia-oxidizing bacteria and denitrifiers. This process, know as nitritation/denitritation process, reduces carbon requirement for denitrification by 40% and aeration energy demand for nitrification by 25% (Turk and Mavinic, 1986). The most well known commercialised technology is the SHARON process (Hellinga et al., 1998; Perret et al., 2018).

The discovery of anaerobic ammonium oxidising (anammox) bacteria in the late 90s, let to the developpement of an energy and carbon efficient technology for nitrogen removal: partial nitritation and anammox (PN/A). It comprises two consecutive processes: ammonia-oxidising bacteria aerobically oxidise part of the ammonium load into nitrite (PN, Partial Nitritation), then anammox bacteria convert ammonia and nitrite formed to nitrogen gas and a small fraction of nitrate. Those two processes can be achieved in a single reactor (1-stage configuration) or in two separate reactors (2-stage configuration). Compared to conventional nitrogen removal through nitrification/denitrification, PN/A saves 60% of the aeration costs without a need for exogenous carbon dosing (Lackner et al. 2014). However, the process can be responsible of high N_2O emissions (Schaubroeck et al., 2015).

For algae production, the application at full scale is relatively scarce. This process allows the recovery of algae that can be used for biofuel production for example (Eskicioglu et al., 2018). However, this process is suitable in warm countries and the harvesting of the algale produced is still a complicated step of the process (Al Momani and Örmeci, 2020; Marazzi et al., 2019).

1.3.2 Physico-chemical processes for N recovery

Physico chemical processes have been developed with a focus on recovery rather than treatment. They are less implemented at full scale compared to biological processes and are mainly developed at pilot scale. Different solutions have been found in the literature: ammonia stripping and absorption, membrane filtration, ion exchange resin, electrodialysis and bio electrochemical systems (Eskicioglu et al., 2018; Ye et al., 2018). Ammonia stripping is based on the liquid gas equilibrium where ammonia from the liquid phase is transferred to the gas phase before being sent to an air scrubber for ammonia absorption into an acid. The recovered solution can be used as fertiliser but only one full scale application have been found in the literature (Sagberg et al., 2006).

For membrane filtration, hollow fiber membrane contactor or reverse osmosis can be used. Only hollow fiber membrane contractor has been applied at full scale (Eskicioglu et al., 2018). Ammonia passes through the membrane and an acid is used as a draw solution to recover nitrogen. For ion exchange resin, electrodialysis and bio electrochemical system, only pilot-scale applications have been found (Sengupta et al., 2015). Electrodialysis process uses an electric current to migrate ions to the cathode or anode and trap them on ion exchange membranes and obtained a concentrated ammonia solutions (Ward et al., 2018). In bioelectrochemical systems, the oxidation of organics produces

electrons used as energy for the migration of NH_4^+ ions from the anode to the cathode in order to maintain charge neutrality (de Fouchécour et al., 2022). In the cathode chamber, NH_4 is transformed into NH_3 thanks to the high pH value to be recovered (Nancharaiah et al., 2016).

These processes have been developed more recently and their development is slow due to their energy requirements: around 26-28 kWh/kgN treated for ammonia stripping and 3 to 6 kWh/kgN treated for biolectrechemical system; while, PN/anammox and nitrification/denitrification has an energy consumption respectively of 4.2 kWh/kgN and 12 kWh/kgN treated (Barua et al., 2019; Ye et al., 2018). Considering that bioelectrochemical systems are not mature enough for full-scale applications, biological processes are more economical from an energy consumption perspective.

1.3.3 Physico-chemical processes for P recovery

For P recovery and treatment, the most applied process is based on precipitation mechanisms to recover P in the form of struvite ($MgNH_4PO_4 \cdot 6H_2O$) (Le Corre et al., 2009). This process was implemented first to help reduce struvite clogging issues in pumps and pipes (Kleemann et al., 2015) and is increasingly being seen as a recovery solution. In the literature, one full scale installation of calcium phosphate recovery (Eggers et al., 1991) rather than struvite have been found as well as an application of electrodialisys for P recovery at lab or pilot scale (Ward et al., 2018).

1.3.4 Research needs for a better implementation of sidestream processes

Nutrient removal in sidestreams could constitute a key element in the evolution of wastewater treatment plant towards a water resource recovery facility. Indeed, these streams are highly concentrated in nitrogen and phosphorus and a variety of processes are emerging at different scales to provide recovery solutions. However, the knowledge on sidestream characteristics are scattered and limited in the literature and they mostly address mainly one component: nitrogen or phosphorus without giving information of other characteristics. An effort must be made to gain a deeper understanding of these streams as the performance of processes could depend on other components or species as the ions (as for example: Ca^{2+}, K^+, Mg^{2+}, Cl^-, Na^+, SO_4^{2-}), total suspended solids or residual chemical oxygen demand. In view of recovery, most of these processes lie on physico-chemical equilibrium and could be impacted by the different ions in solution (Ye et al., 2018). The quality of sidestreams could indeed have consequences on process performance and on the quality of the recovered products (Lizarralde et al., 2019) but little research has been done to date. For example, the presence of calcium can impact the quality of struvite by also generating other minerals as calcium phosphates (Le Corre et al., 2005) but these different minerals are generally not included when assessing the potential for phosphorus recovery.

1.4 Evaluating sidestream process performance

The assessment of sidestream process performance depends both on the performance of the process as such and on the impact that this process has on the entire WRRF. In scientific literature, most scenario analyses use effluent quality and operational costs including chemical and energy consumption to assess the suitability of a process (De Ketele et al., 2018; Fernández-Arévalo et al., 2017a; Hodgson and Sharvelle, 2019). Additionally, many studies evaluate the potential for P recovery (Flores-Alsina et al., 2021; Lizarralde et al., 2019; Solon et al., 2017) and try to maximise it by optimising P release (Bouzas et al., 2019; Martí et al., 2017). While most of these studies are able to predict the quantity of struvite produced, its quality is seldom studied (Vaneeckhaute et al., 2018b).

More recently, carbon footprint was considered to take into account the climate footprint of the facilities and the urgent need to reduce anthropogenic greenhouse gas emissions sources. For the evolution towards a WRRF, an effort has to be made to include the carbon footprint as a performance indicator in addition of operational aspects, effluent quality and resource recovery potential (Solon et al., 2019a).

1.5 Ability of anaerobic digestion models to predict sidestream characteristics and evaluate sidestream management scenarios

To evaluate scenarios with sidestream processes, many authors used mechanistic models, in particular anaerobic digestion models coupled with activated sludge models to simulate the whole WWRF. These models representing the whole plant are also called Plant Wide Models (PWM) and different libraries of models have been developed in the last years: the PWM approach detailed in Grau et al. (2007) and Lizarralde et al. (2015), the benchmark simulation model (Gernaey et al., 2014), the biological nutrient removal model (Barat et al., 2013), the PWM South Africa (Ikumi, 2020), and the generic nutrient recovery model (Vaneeckhaute et al., 2018b).

However, ADM1 showed some limitations to correctly estimate pH and phosphate concentrations due to simplifying assumptions, such as considering solutions with ideal behaviour, or neglecting solid-liquid transformations (Batstone et al., 2012). In the first ADM1 version, the precipitation of phosphorus into the anaerobic digester where not considered which leads to an overestimation of phosphate in the digested sludge and resulting sidestreams. Therefore, in recent publications, this model was updated with a more comprehensive physico-chemical framework (Batstone and Flores-Alsina, 2022) including activity corrections for non-ideal behaviour and precipitation with phosphate of the following metals: calcium, magnesium, iron, aluminium. More extensive models have also been developed to describe interactions between sulphur, iron and phosphorus (Hauduc et al., 2019; Kazadi Mbamba et al., 2019; Solon et al., 2017), as well as more advanced precipitation models with particle size distribution of the minerals formed (Elduayen-Echave et al., 2019). In addition, to be able to calculate the carbon footprint of the different plants, models have been upgraded to describe N_2O emissions (Flores-Alsina et al., 2011; Mannina et al., 2019; Massara et al., 2018).

With these new extensions, recent studies have been able to validate the quantity of P in sidestreams and then assess different scenarios for P recovery. However, there is no information on the quality on the recovered product which is essential for marketing. In the work of Vaneeckhaute et

al. 2018, a sensitivity analysis was carried out to analyse the impact of the characteristics of the substrate fed to the digester on the performance of phosphorus and nitrogen recovery. The impact of calcium on the quality of the recovered struvite was demonstrated but the model was not validated using data from full-scale facilities. Models including the extensions with S/P/Fe and N_2O emissions have not yet been applied to full-scale data and are generally used to compare different scenarios (Flores-Alsina et al., 2014; Solon et al., 2017).

In conclusion, the evaluation of the potential of nutrient recovery in sidestreams using anaerobic digestion model coupled with the physico-chemical framework can be an interesting tool. However, this model has been developed recently and few full-scale applications have been published. Moreover, in these applications, the procedure for the calibration of the precipitation model parameters is not always specified. Therefore, there is no generic calibration procedure when applying this model to another application and the range of values in which the precipitation model parameters can vary is not clear. In order to apply this model widely more full-scale applications are necessary, considering not only phosphorus but also other ions such as calcium and magnesium and studying the impact of the precipitation parameters on the model results.

1.6 Research questions and thesis outline

The objective of this doctoral research was to provide a framework for selecting a sidestream process depending on the types of sewage sludge and the resulting characteristics of sidestreams. In order to support the choice of a sidestream process for nitrogen and phosphorus treatment or recovery, an effort has been made to include not only operational performance indicators but also to focus on carbon footprint and on the quality of the product recovered in sidestreams. To establish this framework, the thesis is divided into 3 main chapters and focuses first on sidestream characteristics, then studies in detail the AD model coupled with precipitation mechanisms and ends with the use of this model to conduct a scenario analysis for a sludge line treating different types of sewage sludge. The content of each chapter is detailed below.

Chapter 2 provides an analysis of the data collected in the literature on the characteristics of sidestreams (Figure 1.2). Concentration ranges for the different characteristics have been extracted and are analysed for a conventional mesophilic anaerobic digester with and without thermal hydrolysis pre-treatment. The impacts of sidestream characteristics and concentrations found in the literature on the performance of several treatment or recovery processes are discussed.

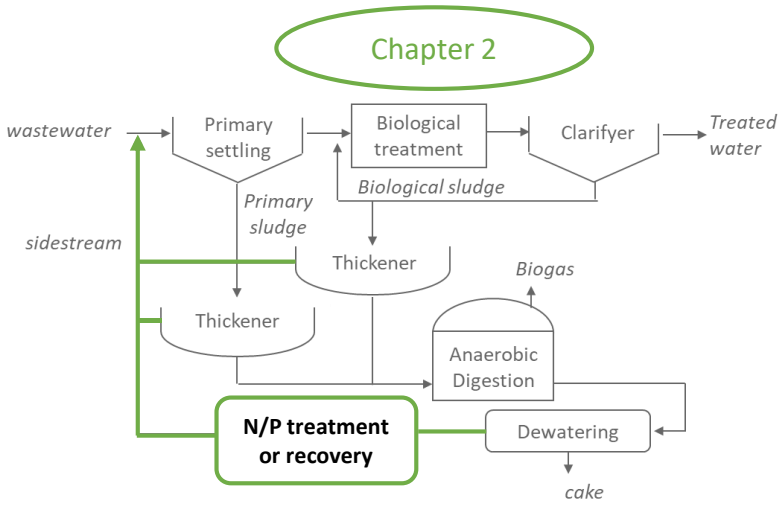

- What are the characteristics of sidestream?
- Which processes can be installed for sidestream treatment or recovery ?
- Is the performance of these processes affected by certain characteristics of sidestreams ?

Figure 1.2 - Outline of chapter 2

Chapter 3 investigates the calibration and validation of the anaerobic digestion model coupled with the physico-chemical framework with a focus on the precipitation models (Figure 1.3). The objective is not only to validate the quantity of phosphorus but also of magnesium and calcium in the digested sludge to obtain reliable estimation of the quantity and the quality of struvite that can be recovered in sidestreams. A systematic calibration procedure is applied to two different anaerobic digesters treating full-scale sludge with different concentrations of Ca, P, Mg and inorganic carbon. The parameters of the precipitation model to be calibrated are discussed. This chapter is based on the results of measurement campaigns from two other projects to which the PhD thesis was involved. The first project “DESINTEGBOUES”, led by INRAE, focuses on the analysis of the operation of a mesophilic anaerobic digester located at the Reventin Vaugris WWRF (France). The second project “MAGNYFOS”, led by CEIT, is about the assessment of phosphorus recovery potential in Tudela WRRF (Spain) in which the implementation of a thermophilic anaerobic digester is planned.

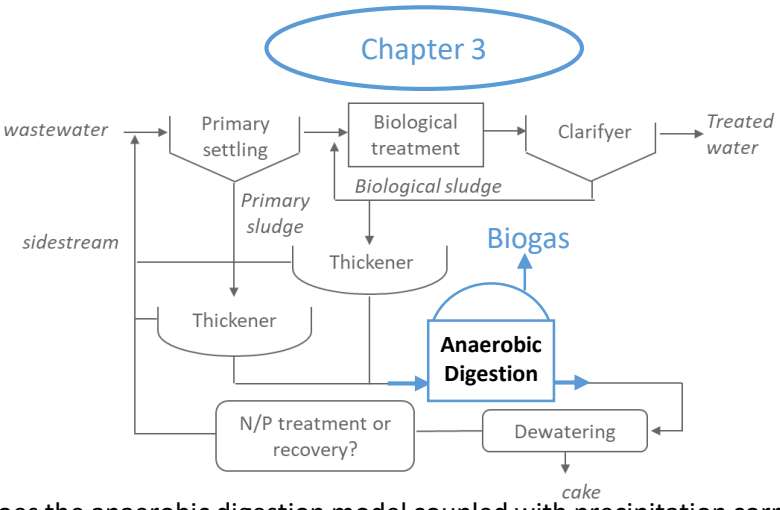

- Does the anaerobic digestion model coupled with precipitation correctly predict sludge and sidestream characteristics ?
- How can this model be calibrated to correctly predict the different concentration of ions in sidestreams?

Figure 1.3 - Outline of chapter 3

In *Chapter 4*, calibrated models of Chapter 3 are used to carry out a scenario analysis evaluating the impact of different sludge characteristics on different sidestreams management (Figure 1.4). Simulations of anaerobic digestion process are performed with sludge of different origins in terms of phosphorus treatment in the mainline, and containing different levels of Ca, Mg and inorganic carbon. Simulation results allowed calculating the quantity of nitrogen or phosphorus to be removed, the operational costs and the carbon footprint of a struvite recovery process and a nitrogen treatment unit by nitrification-denitrification or by partial nitritation / anammox. . The recovery of phosphorus as struvite has been selected because the process has been developed at full scale but still arise question about the interest for this process when the WRRF is operating without enhanced biological phosphorus removal or when the concentration of calcium is high. The biological nitrogen treatment with partial nitritation / anammox or by the conventional nitrification – denitrification process were also selected because they are both applied at full-scale but the issue with N_2O emissions are known to be detrimental in the carbon footprint of such processes. This chapter was carried out in the framework of the Pierre Bénite (France) WWRF project which focussed on the implementation of a mesophilic anaerobic digester treating internal sludge and sludge from the surrounding WRRFs. Ultimately, the findings of this chapter can serve as a basis for the choice of sidestream processes.

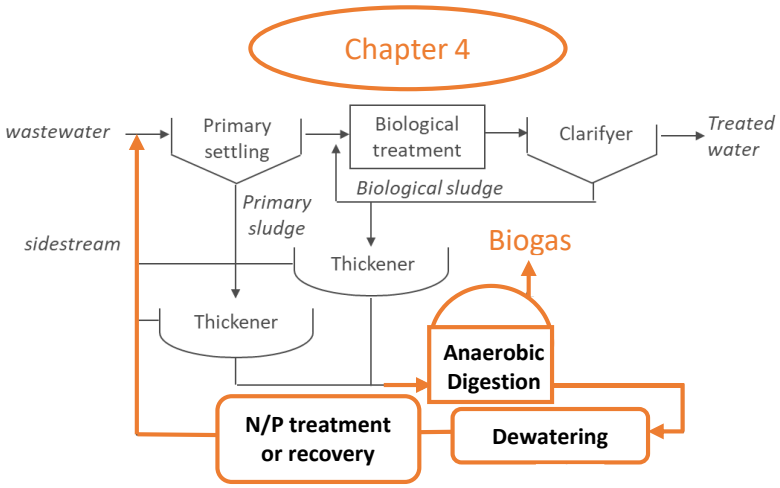

- How do different types of sludge and different water hardnesses influence the recovery potential in sidestreams ?
- What is the influence of these anaerobic digestion sidestreams on the performance of N treatment and P recovery process ?

Figure 1.4 - Outline of Chapter 4

Chapter 5 summarises each chapter and provide main conclusions of this doctoral work. The conclusion chapter first details the main findings of the literature review on sidestream processes and existing processes. For the AD model coupled with multiple mineral precipitation, recommendations for the calibration procedure and perspectives are provided. To help select a sidestream process, and especially, for phosphorus recovery and biological nitrogen treatment, the last chapter also discusses the important points to take into consideration. Areas for future research are highlighted, focusing on the possible evolution of plant-wide models to better predict sidestream characteristics.

CHAPTER 2 - SIDESTREAM CHARACTERISTICS IN WATER RESOURCE RECOVERY FACILITIES: A CRITICAL REVIEW

2.1 Abstract

This review compiles information on sidestream characteristics that result from anaerobic digestion dewatering (conventional and preceded by a thermal hydrolysis process), biological and primary sludge thickening. The objective is to define a range of concentrations for the different characteristics found in literature and to confront them with the optimal operating conditions of sidestream processes for nutrient treatment or recovery. Each characteristic of sidestream (TSS, VSS, COD, N, P, Al^{3+}, Ca^{2+}, Cl^{-}, $Fe^{2+/3+}$, Mg^{2+}, K^{+}, Na^{+}, SO_4^{2-}, heavy metals, micro-pollutants and pathogens) is discussed according to the water resource recovery facility configuration, wastewater characteristics and implications for the recovery of nitrogen and phosphorus based on current published knowledge on the processes implemented at full-scale. The thorough analysis of sidestream characteristics shows that anaerobic digestion sidestreams have the highest ammonium content compared to biological and primary sludge sidestreams. Phosphate content in anaerobic digestion sidestreams depends on the type of applied phosphorus treatment but is also highly dependent on precipitation reactions within the digester. Thermal Hydrolysis Process (THP) mainly impacts COD, N and alkalinity content in anaerobic digestion sidestreams. Surprisingly, the concentration of phosphate is not higher compared to conventional anaerobic digestion, thus offering more attractive recovery possibilities upstream of the digester rather than in sidestreams. All sidestream processes investigated in the present study (struvite, partial nitritation/anammox, ammonia stripping, membranes, bioelectrochemical system, electrodialysis, ion exchange system and algae production) suffer from residual TSS in sidestreams. Above a certain threshold, residual COD and ions can also deteriorate the performance of the process or the purity of the final nutrient-based product. This article also provides a list of characteristics to measure to help in the choice of a specific process.

2.2 Highlights

- The review provides concentration ranges for sidestream characteristics in WWRFs
- THP mainly affects COD and N content in anaerobic digestion sidestream
- The effect of THP on P is not significant due to precipitation inside AD
- A list of characteristics to measure before selecting sidestream processes is given

This chapter was published as:

Devos, P., Filali, A., Grau, P., Gillot, S., 2023. Sidestream characteristics in water resource recovery facilities: A critical review. Water Res. 232, 119620. https://doi.org/10.1016/j.watres.2023.119620

2.3 Introduction

Wastewater characteristics have been studied for decades because they are key to design and optimise the operation of wastewater treatment processes. The usual characteristics of urban wastewater (including total solids, organic matter, total nitrogen, total phosphorous and organic matter biodegradability) from different countries is well-documented, especially in view of process modelling (Rieger et al., 2012), and experimental methods to characterise the composition of wastewater have been established and benchmarked (Gillot and Choubert, 2010; van Loosdrecht et al., 2016). At the same time, there is a growing interest in the characterisation of both the solid and the liquid phase of sewage sludge. This interest is primarily motivated by the need to reduce sludge volumes and associated sludge management costs (Zhen et al., 2017) as well as to maximise their reuse as fertiliser (Kacprzak et al., 2017). One of the current concerns is the concentration of heavy metals and emerging contaminants when sludge disposal route is land application (Appels et al., 2010; Steele et al., 2022).

As part of sewage sludge management in water resource recovery facilities (WRRFs), sludge thickening and dewatering units result in the production of different types of sidestreams, also called “reject water”, “centrate”, “supernatant” or “filtrate”, recycled into the main wastewater treatment line. The major concern about these streams arise with the overall tightening of WRRFs effluent standards (Preisner et al., 2020) and the development of anaerobic digestion (AD) that generates a nutrient-rich supernatant (Gourdet et al., 2017). In the context of a wastewater identified as a resource rather than a waste stream, AD has proved to be an essential technology as it reduces sludge volume, stabilises sludge and more importantly recovers energy as methane (Appels et al., 2011). Sidestreams in WRRFs equipped with AD can contain up to 25% of the total nitrogen load and 10% of the total phosphorus load to the facilities (Couturier et al., 2001; Grulois et al., 1993). This phosphorus load can be even higher (up to 30%) when enhanced biological phosphorus removal (EBPR) is implemented in the water line (Ueno and Fujii, 2001). Also, to boost AD and dewatering performance, several sludge pre-treatments have been developed (Carrère et al., 2010). Among them, the thermal hydrolysis process (THP) is the most applied technology and existing full-scale references have so far reported an enhancement of AD performance after THP pre-treatment (Kor-Bicakci and Eskicioglu, 2019).The main drawback of THP is that it generates streams with high concentration of refractory compounds and an increase in sidestream ammonia concentration (Barber, 2016; Bougrier et al., 2008; Dwyer et al., 2008b).

High nutrient content in sidestreams can lead to increased energy consumption and degradation of effluent quality (Cullen et al., 2013; Janus and van der Roest, 1997), especially when the facility operates close to full-scale capacity. In such conditions, sidestream processes are good opportunities for upgrading treatment capacity without needing to expand existing works (van Loosdrecht and Salem, 2006). The main biological processes for the treatment of nitrogen in sidestreams includes: nitritation-denitritation, nitrification-denitrification, partial nitritation / anammox, bioaugmentation and algae production (Eskicioglu et al., 2018).

Sidestream processes also offer an excellent opportunity for nutrient recovery, essential for sustaining the food production industry. Currently, nitrogen-based fertilisers are mainly produced by the energy-intensive Haber–Bosch process, while rock phosphate is the main raw material in phosphorus-based fertilisers (Nancharaiah et al., 2016; Shaddel et al., 2019). The implementation of these production routes on the long-term is questioned because (1) phosphorus depletion is expected by 2100 (Van Vuuren et al., 2010) and (2) fertilizers production currently accounts for more than 1% of the world's emissions of greenhouse gases (GHG) (Kehrein et al., 2020). Municipal wastewater is

thus an interesting nutrient-source as its nitrogen and phosphorus content accounts respectively for 14% and 7% of the global fertilizer demand (Qadir et al., 2020). Several reviews present in detail the technologies available for nutrient recovery from wastewater. They are mainly based on physical, physicochemical, and bio-electrochemical mechanisms (Guilayn et al., 2020; Vaneeckhaute et al., 2017; Ye et al., 2018). Struvite precipitation, ammonia stripping, membrane filtration, electrodialysis, bio-electrochemical system, ammonia and phosphate sorption are the most investigated processes. Performances of such processes depend on sidestream characteristics. Their efficiency, the capacity for nutrient removal, the energy and chemical consumption and the quality of recovered products have to be specified. The nutrient-based products must also comply with the current N and P fertilizer characteristics and legislation. In addition, to complete COD, N and P fractionation, the detailed ionic strength of sidestreams is necessary to correctly design and model treatment or recovery processes as they are mainly based on physicochemical reactions. This information is especially required as input of the new advanced plant wide models that couple biokinetics with physicochemical framework (Flores-Alsina et al., 2015; Kazadi Mbamba et al., 2015a; Lizarralde et al., 2015; Solon et al., 2015; Vaneeckhaute et al., 2018b).

Despite the growing interest in the implementation of sidestream processes, a complete characterisation of this stream is relatively scarce and sparse in the literature. Published data include phosphorus (Martí et al., 2017), nitrogen (Kassouf et al., 2020), COD fractionation (Noutsopoulos et al., 2018) and ionic composition (Bhuiyan et al., 2009). However, no synthesis compares sidestream characteristics from different WRRFs, considering a large number of components (solids concentration, COD, biodegradability, N, P, ions, heavy metals and ionic composition) that constitute wastewater (Metcalf & Eddy Inc. et al., 2003).

This review article compiles and analyses literature data of sidestream characteristics from different locations in WRRFs. The aim is to bring knowledge on sidestream characteristics to assist in selection, design and modelling of sidestream processes. Data are questioned in order to choose the most optimal operating conditions of the main sidestream processes and to identify potential limits of application. Implications in terms of plant wide modelling are also mentioned, in order to improve sidestream description and nutrient recovery options. Finally, the need for data on characterisation of sidestreams are highlighted to support the development of processes that can improve environmental and economic impacts of WRRFs.

2.4 Literature Data Compilation

The set of data used in this study results from the compilation of information from 87 documents (peer-reviewed and grey literature). The characteristics found have been classified according to the source of sidestreams:

- biological sludge for sidestreams resulting from the thickening of biological sludge
- primary sludge for sidestreams resulting from the thickening of primary sludge
- anaerobic digestion for sidestreams resulting from the dewatering of digested sludge
- THP anaerobic digestion for sidestreams resulting from the dewatering of digested sludge preceded by a thermal hydrolysis process (THP).

The collection and description of the data can be found on the french repository “DataGouv” (https://doi.org/10.57745/FOHRHY). Only papers with clear information on sidestream sources were selected. Sidestreams from full-scale measurements only were included in the dataset.

All figures presented in this document have been generated with RStudio software version 4.1.2. Most of the data is presented in the form of a violin plot overlaid on a boxplot. Outliers have been detected with the Bonferroni test (Bretz et al., 2010) for each boxplot when the p-value is below 5%. They are indicated in the figures (in grey) but are not included in the calculation of the median nor in the count of the total number of values. The different sources of sidestreams were statistically compared using the Kruskal-Wallis test. The pairwise comparison using the Wilcoxon test was also used to compare the impact of different WRRF configurations. In addition, correlations between different parameters were identified using the Spearman test.

2.5 Sidestream Characteristics

In the following, sidestream characteristics are first described in terms of major pollutants (TSS, COD and nutrients): concentrations and mass loads are analysed. The ionic composition of sidestreams are then described, as well as pH, alkalinity and temperature. Collected data mainly refer to streams from the anaerobic digestion of sewage sludge. A few data on sidestreams from primary or biological sludge thickening are also presented, when available.

2.5.1 Major pollutants in sidestreams

2.5.1.1 Concentration of Total Suspended Solids (TSS) and Volatile Suspended Solids (VSS)

Figure 2.1 presents the TSS concentrations in sidestreams from anaerobic digestion preceded or not by a THP. TSS concentrations are highly variable from one study to another. This variability is partly due to the sampling methodology as most of the values have been obtained on grab samples. There is no significant difference between both types of sidestreams which means that TSS concentration in sidestreams is mainly driven by other factors than the presence of a THP, such as the dewatering unit performance. Interestingly, most of the data compiled on anaerobic digestion sidestreams came from centrifuges. The centrifuge has a solid capture rate between 95% and 99% depending on sludge conditioning (Metcalf & Eddy Inc. et al., 2003). Considering a TSS concentration in digested sludge of 25 g/L, the TSS concentration in sidestreams from an anaerobic digester would not exceed 1500 mg/L. Outliers in Figure 2.1 are much higher than this value, indicating that the centrifuge may sometimes underperform. Besides, variability of water content and particle size of sludge induced by sludge transport and storage can impact the demand for polymers, and therefore the performance of the dewatering unit (Andreoli et al., 2007; Henze and Comeau, 2008). Anaerobic digestion sidestream has a median VSS to TSS ratio of 70% (Figure 2.1 B). A value in the range of 55 – 75% is expected (Bowden et al., 2015) which corresponds to volatile solids (VS) range for digested sludge (Andreoli et al., 2007).

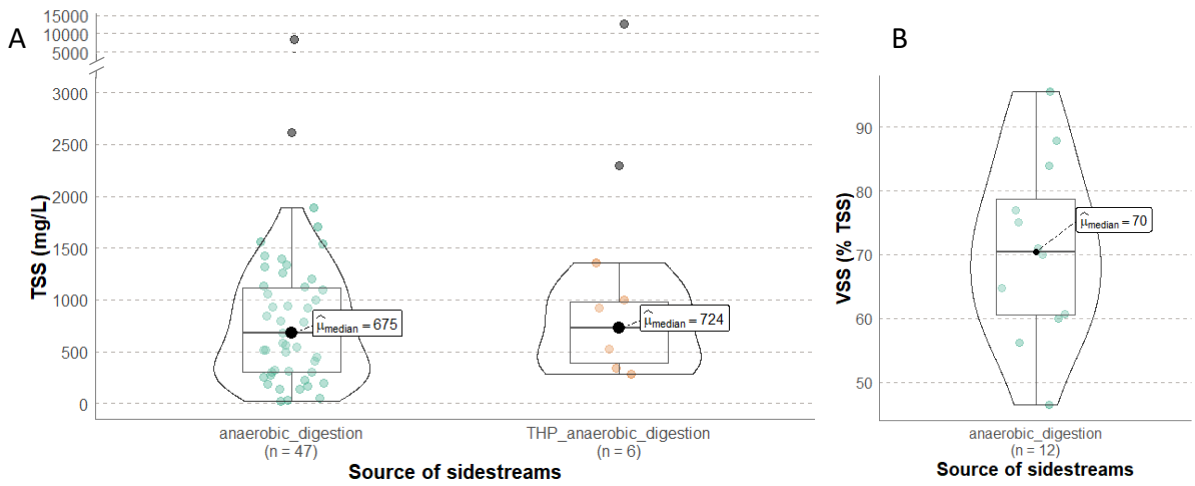

Figure 2.1 - Literature data compilation of TSS (A) and VSS (B) in sidestreams from anaerobic digestion and from anaerobic digestion preceded by a THP

2.5.1.2 Concentration of Chemical Oxygen Demand (COD)

The concentrations of total COD and soluble COD are significantly different between anaerobic digestion and THP anaerobic digestion sidestreams (Figure 2.2). As for TSS, there is a large variability of COD concentration which is explained by the significant correlation between total COD and TSS. The difference of total COD concentration between both types of sidestreams is mainly due to the higher soluble COD concentration in THP anaerobic digestion sidestreams, induced by a higher solubilisation rate (Barber, 2016; Devos et al., 2020). Part of this additional soluble COD has been reported to be refractory compounds produced through the Maillard and Amadori reaction that also impacts the effluent COD of the WRRF. The amount of refractory compounds produced is dependent on the temperature of THP, and becomes significant at a temperature higher than 160°C (Toutian et al., 2020). For six facilities in Berlin (without sidestream processes) and for different THP temperatures the increase in effluent soluble COD was estimated to be in the range of 2 – 15 mg/L (Toutian et al., 2020). Another study reported that THP implementation in five facilities led to a 3 – 8 mg/L increase of effluent COD concentration, depending on the quantity of primary sludge versus the quantity of biological sludge (Svennevik et al., 2020).

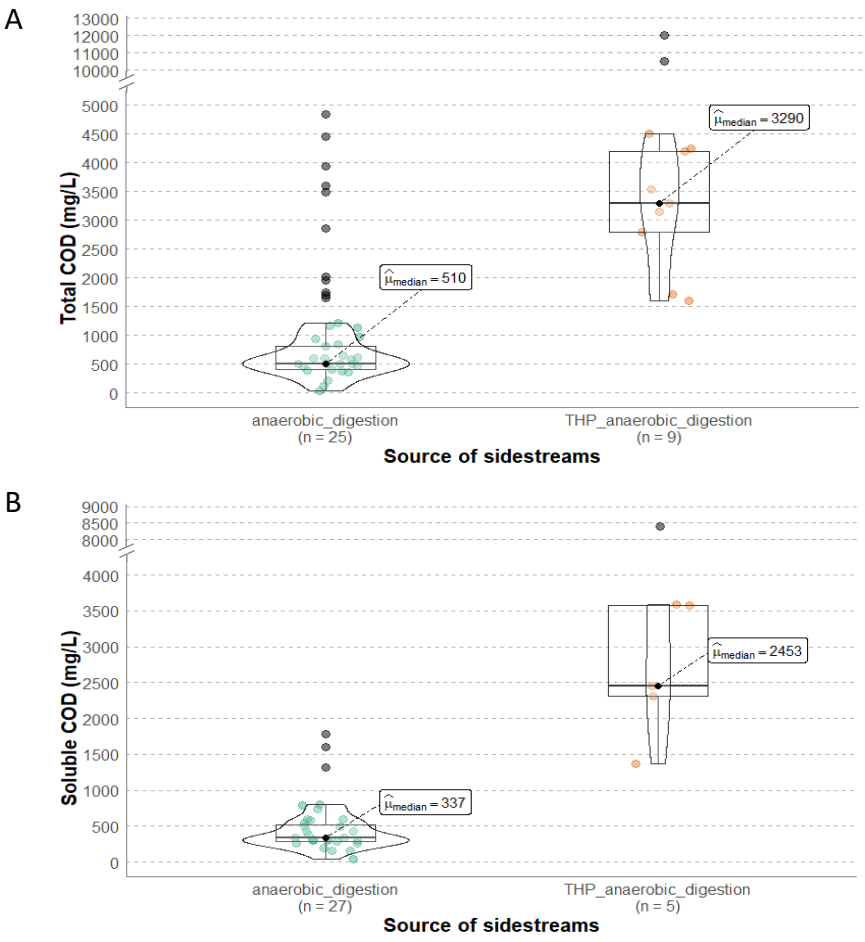

Figure 2.2 - Literature data compilation of Total COD (A) and Soluble COD (B) in sidestreams from anaerobic digestion and from anaerobic digestion preceded by a THP

The concentration of total COD in biological sludge sidestreams and in the treated water are usually close except in the case of thickening unit malfunction. The concentration of COD in primary

sludge sidestreams is similar to wastewater and is in the range of 250 – 800 mg/L (Constantine, 2006). However, higher values of 823 mg/L (Roldán et al., 2020) and up to 4244 mg/L have been encountered probably due to sludge loss following a rain event in the gravity thickener (Noutsopoulos et al., 2018).

2.5.1.3 Organic matter biodegradability in sidestreams

Table 2.1 shows COD biodegradable fractions in sidestreams based on literature review. For a given type of sidestreams, results show a large variability explained on the one hand by varying methods employed to characterise the biodegradability and on the other hand by differences in operating conditions of AD and THP (T°C, sludge concentration, retention time). The fractionation of COD into different classes of biodegradability (slowly biodegradable, rapidly biodegradable, inert soluble and particulate) is essential for design, operation purposes and modelling (Gillot and Choubert, 2010). However, more data are required to compare the sludge biodegradability after anaerobic digestion and THP anaerobic digestion sidestreams. Primary sludge thickening sidestreams has a biodegradable fraction similar to wastewater generally between 54 – 88 % (Gillot and Choubert, 2010) of total COD. The biodegradable fraction of biological sludge thickening sidestreams is similar to the one of treated wastewater which is generally 70 to 80% lower than the untreated wastewater.

Table 2.1 - COD fractionation in sidestreams based on literature data

Method	***Type of sidestream***	***Biodegradable fraction (%total COD)***	***Reference***
Ultimate BOD test	Conventional AD	55%	(Akhiar et al., 2017)
Respirometry	Conventional AD	14%	(Im and Gil, 2019)
N/A	Conventional AD	15%	(Liu et al., 2014)
Respirometry	Conventional AD	57%	(Noutsopoulos et al., 2018)
Continuous aeration of centrate	THP + AD	27%	(Gupta et al., 2015)
Respirometry	THP + AD	40%	(Noutsopoulos et al., 2018)
Respirometry	Primary sludge	82%	(Noutsopoulos et al., 2018)
Respirometry	Biological sludge	15%	(Noutsopoulos et al., 2018)

2.5.1.4 Concentration of nitrogen species

For conventional mesophilic anaerobic digesters, the resulting ammonium (N-NH_4) concentration in sidestreams typically ranges from 400 mg/L to 1 300 mg/L (Metcalf & Eddy Inc. et al., 2003) which is in line with present data (Figure 2.3).

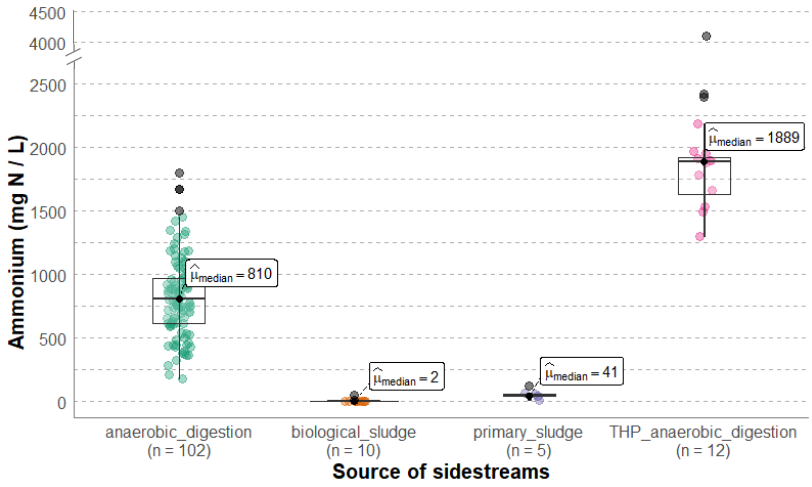

Figure 2.3 - Literature data compilation of ammonium ion concentrations in sidestreams from different sources of sidestreams

Variability of N-NH_4 can be linked to the quantity of wash water used in the dewatering unit (Metcalf & Eddy Inc. et al., 2003) and to AD operating conditions (sludge concentration, VS removal). N-NH_4 is significantly higher in anaerobic digestion with THP compared to AD without THP, which is explained by the fact that THP favours (1) an increase in the sludge concentration in the digester due to reduced viscosity (Urrea et al., 2015), (2) a higher solubilisation rate (Dwyer et al., 2008a; Wilson and Novak, 2009) and (3) an increase in biodegradation of organic matter and therefore of proteins content (Bougrier et al., 2008). Likewise, increased release of ammonium in the digester is expected. It was reported that total ammonium release per mass of volatile solids removed is equivalent for conventional mesophilic AD and THP whatever the sludge type (Wilson et al., 2011). Soluble nitrogen in AD dewatering sidestreams is mainly in the form of ammonium and soluble organic nitrogen accounts for a maximum of 10% of soluble TKN. Of this soluble organic nitrogen fraction, approximately 50% is considered non-biodegradable. The soluble organic nitrogen is believed to be produced through cell metabolism and decay of the anaerobic bacteria and waste activated sludge. Therefore, typical digester sidestream will add approximately 0.2 mg/L of refractory dissolved organic nitrogen to the WRRF effluent (Metcalf & Eddy Inc. et al., 2003). A recent survey on soluble organic nitrogen content in treated wastewater reported an average final concentration of 0.93 mg/L with a range of 0 – 2.5 mg/L (Galvagno et al., 2016). Therefore, the non-biodegradable fraction brought by AD dewatering sidestreams will account for approximatively 25% of final organic nitrogen. This quantity can be higher with THP pre-treatment (Ahuja, 2015).

As expected, N-NH_4 concentration in biological sludge and primary sludge sidestreams is significantly lower compared to anaerobic digestion sidestreams. However, the formation of anaerobic zones in thickening units such as gravity thickener or dissolved air flotation can lead to sludge hydrolysis thus favouring ions release, which can explain outliers of 50 mg/L for biological sludge

sidestreams and 123 mg/L for primary sludge sidestreams (not clearly visible in Figure 2.3 due to the scaling).

2.5.1.5 Concentration of phosphate

Phosphate (P-PO_4) concentration for different sources of sidestreams is shown in Figure 2.4. The concentration of phosphate in biological sludge and primary sludge sidestreams is significantly lower compared to anaerobic digestion sidestreams. Outliers in Figure 2.4 with very high concentrations of phosphate (up to 180 mg/L) for biological sludge sidestreams was attributed by Barat et al. (2009) to the formation of anaerobic zones in the thickener. This phenomenon is unlikely to happen in fast thickening processes such as centrifuge, rotary drum or belt press (Wild et al., 1997). In addition, as THP increases phosphorus solubilisation, a higher phosphate content in AD dewatering sidestreams was expected compared to conventional digestion (Khunjar et al., 2019). Surprisingly this was not supported by literature data. Whilst the intracellular phosphorus can be released during THP, this phosphorus can be directly immobilized by metallic ions such as Mg^{2+}, $Fe^{2+/3+}$, Ca^{2+} and Al^{3+} (Han et al., 2020). Consequently, the phosphorus content in the THP return liquor does not differ from the one of conventional AD. This result was found without considering the different types of applied phosphorus treatment because more data is needed to complete this comparative analysis.

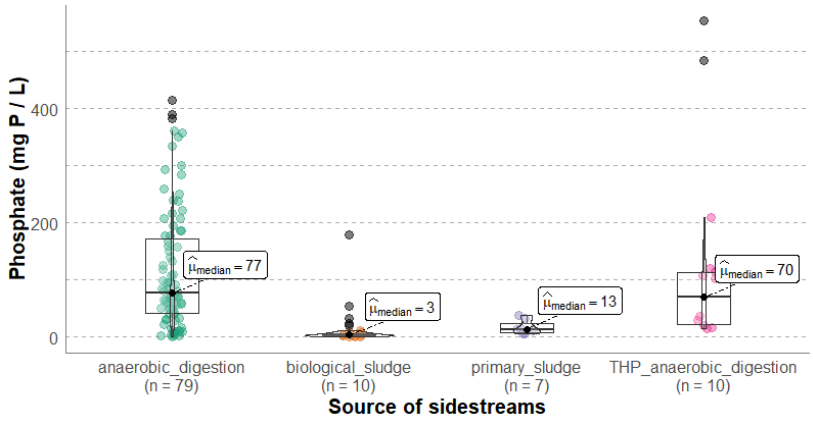

Figure 2.4 - Literature data compilation of phosphate concentrations in sidestreams from different sources of sidestreams

To investigate the high phosphate concentration variability in anaerobic digestion sidestreams, Figure 2.5 shows phosphate concentration according to the phosphorus treatment type installed in the water line: enhanced biological phosphorus removal (EBPR), chemical phosphorus removal, a combination of both biological and chemical phosphorus removal and no specific phosphorus treatment. Only WRRFs operated with EBPR lead to higher phosphate in anaerobic digestion sidestreams compared to chemical phosphorus removal and no specific phosphorus treatment. The high phosphate concentration range for biological phosphorus removal and the combination of biological with chemical phosphorus removal can be attributed to different level of precipitation inside the anaerobic digester and different iron dosage.

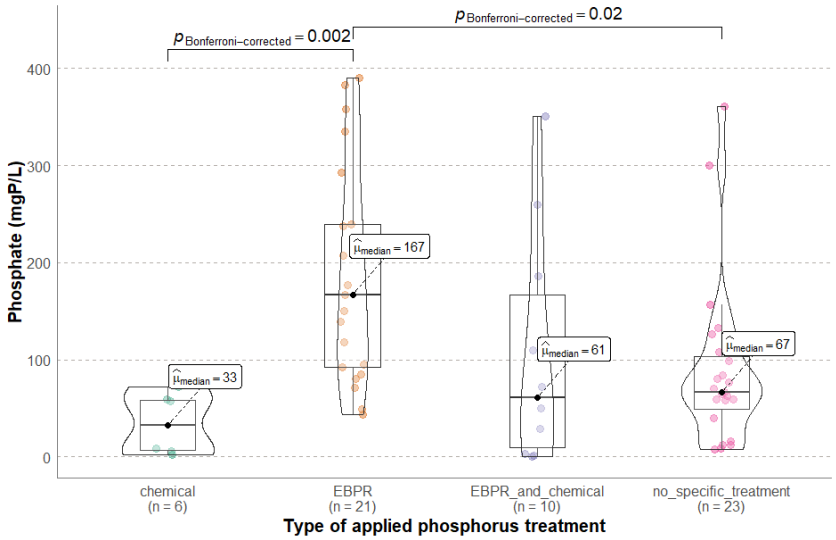

Figure 2.5 - Literature data compilation of phosphate concentrations in anaerobic digestion sidestreams for different type of phosphorus treatment

2.5.1.6 Contribution to the inlet mass flows

The flow of the different sources of sidestreams accounts for less than 5% of the total flow at the WRRF inlet (Figure 2.6). Mass flow of total COD and TSS also represent less than 5% of the total mass flow at WRRF inlet for biological sludge and anaerobic digestion sidestreams. Primary sludge can excess this 5% threshold, especially after a rain event. As expected, the highest sidestream contribution for total phosphorus and total nitrogen comes from anaerobic digestion sidestreams. Regarding the nitrogen mass flow, sidestreams from anaerobic digestion contribute on average to 17% of the nitrogen mass flow at the WRRF inlet, which is much higher than the contribution of biological sludge sidestreams (1%) and primary sludge sidestreams (3 – 8%). The variability of the nitrogen mass flow is due to the the wide range of N-NH_4 concentration found in anaerobic digestion sidestreams and the different load of nitrogen at the WRRF inlet. Phosphorus mass flow depends on the type of phosphorus treatment implemented in the water line similarly to the concentration of phosphate in anaerobic digestion sidestreams. For WRRFs with EBPR, anaerobic digestion sidestreams can contribute up to 34% of the total phosphorus mass flow. Mass flow of total phosphorus from primary sludge sidestreams and biological sludge sidestreams can exceed 5% especially when the thickening unit favours the formation of anaerobic zones (gravity thickener, dissolved air flotation).

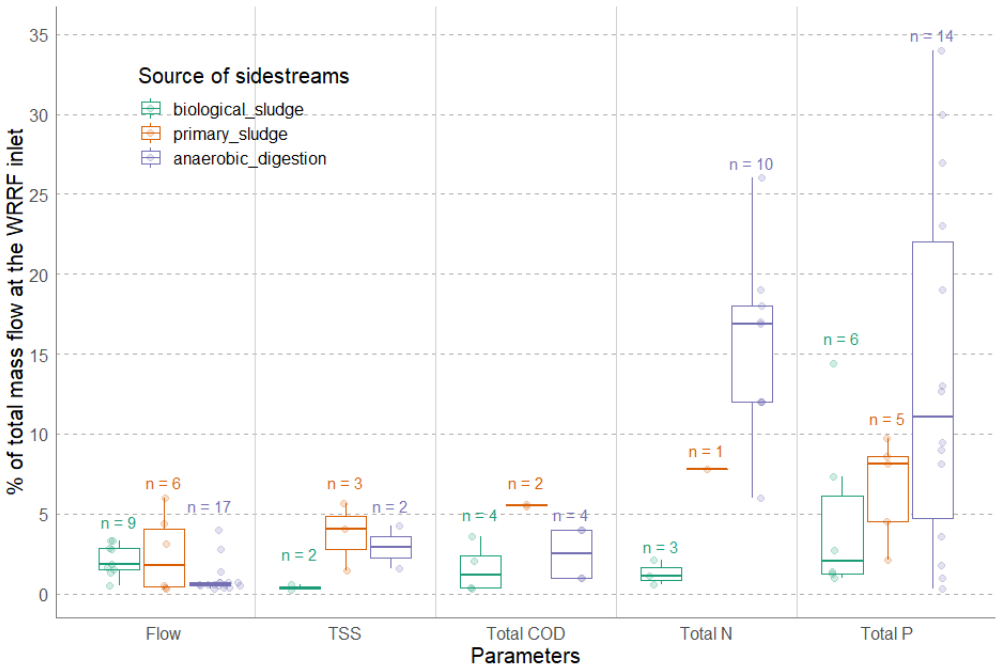

Figure 2.6 - Literature data compilation showing the contribution of the different sidestreams to the WRRF inlet mass flows

2.5.2 Ionic composition of sidestreams

Figure 2.7 shows the concentration of different ions in sidestreams from anaerobic digestion. The concentration of aluminium (Al^{3+}) and iron ions ($Fe^{2+/3+}$) is very low because these metals precipitate easily with phosphorus or sulphur (Wilfert et al., 2015). Only a high salt dosage can lead to residual iron or aluminium in the soluble phase. The addition of salts lead to a large variability of chloride (Cl^-) concentration from one study to another. This variability can be explained by different dose of salts or chemicals applied within the WRRF but also during disinfection of potable water or in sewers (Howe et al., 2012). Calcium (Ca^{2+}), magnesium (Mg^{2+}), potassium (K^+), sodium (Na^+) and sulphate (SO_4^2) concentrations depend on tap water characteristics that result from the distribution network, water source and treatment, geographical location and geology (Hori et al., 2021). The higher the concentration at the WRRF inlet, the higher the concentration in sidestreams. A study on tap water characteristics also indicated a positive correlation between Na^+ and Cl^- and between Ca^{2+}, Mg^{2+} and alkalinity (Banks et al., 2015). Positive correlations between Ca^{2+} and Mg^{2+} and Na^+ and Cl^- have also been found in anaerobic digestion sidestreams with the dataset used in the present study (p value < 5%).

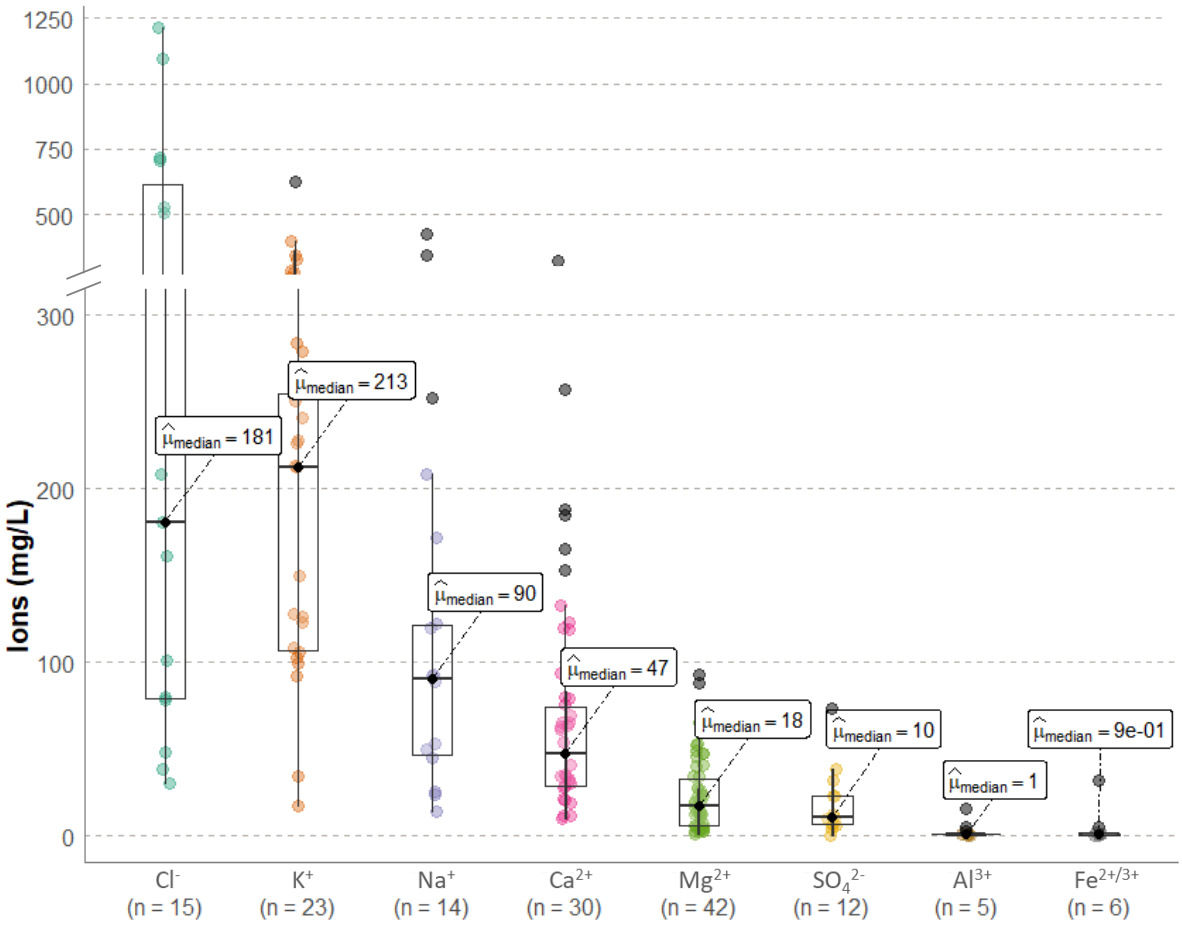

Figure 2.7 - Literature data compilation of the different ions in anaerobic digestion sidestreams

Table 2.2 shows typical ion concentrations for domestic wastewater. The concentration range are systematically more extensive in sidestreams with values that can be very different compared to wastewater. Sulphate concentration is lower in sidestreams compared to wastewater because sulphur is usually removed from wastewater to prevent H_2S formation in the digester and it can also be stripped as H_2S gas. For the other ions, the concentration in sidestreams may results from (1) the addition of industrial wastewater to be treated in the urban WRRF, (2) their accumulation in sludge and subsequent reaction of precipitation / dissolution in the digester and in the thickening or dewatering unit and (3) the addition of chemicals such as lime. For example, calcium concentration in wastewater can increase up to 500 – 1500 mg/L with industrial wastewater (Arabi and Nakhla, 2008). Besides, calcium, potassium and magnesium are present in wastewaters as organic or inorganic forms. These ions can accumulate in sludge and Ca^{2+} and K^{+} removal of 23% and 38% in wastewater has been observed in a WRRF in Iran (Hosseinipour Dizgah et al., 2018). Therefore, during anaerobic digestion, there is a release of ions which can then lead to precipitation as phosphates and carbonates of calcium and/or magnesium (Martí et al., 2008). Consequently, even if wastewater characteristics have an impact on the quantity of ions in sidestreams, the concentration of ions throughout the plant can vary. As an example, a WRRF performing nutrient removal reported Ca^{2+}, Mg^{2+} and K^{+} concentrations of respectively 63, 12 and 284 mg/L in sidestreams; whereas, the concentration in wastewater was respectively of 131, 26 and 27 mg/L (Martí et al., 2017). In the latter example, Ca^{2+} and Mg^{2+} have a

lower concentration in sidestreams compared to WRRF inlet but the opposite occurs for K^+ because K^+ do not precipitate in high extent in digester (Barat et al., 2009).

Table 2.2 - Typical ion concentrations in wastewater

Ions (mg/L)	*Concentration range in wastewater (mg/L)*	*Reference*
calcium	20 – 120 but with industrial wastewater 500 – 1500 mg/L	(Arabi and Nakhla, 2008)
magnesium	5 – 74 mg/L	(Barat et al., 2009; Wilfert et al., 2016)
potassium	11 – 32 mg/L	(Metcalf & Eddy Inc. et al., 2003)
sodium	50 – 250 mg/L	(Arienzo et al., 2009)
sulphate	24 – 72 mg/L	(Metcalf & Eddy Inc. et al., 2003)

2.5.3 Alkalinity, pH and Temperature

Figure 2.8 presents alkalinity in sidestreams from anaerobic digestion and THP anaerobic digestion. A significant difference between both types of sidestreams is observed. The high alkalinity concentration in THP anaerobic digestion is due to the retention of carbon dioxide in the digester bulk liquid to balance the positively charged ammonium ion at the typical pH range of the digesters (Metcalf & Eddy Inc. et al., 2003). The correlation between alkalinity and ammonia has been confirmed with the set of data (p value < 5%). In addition, the mass N-NH_4:alkalinity is similar between anaerobic digestion (0.24 ± 0.12) and THP anaerobic digestion (0.27 ± 0.2). The alkalinity in primary sludge and biological sidestreams (699 mg/L and 409 mg/L, respectively) are lower than anaerobic digestion sidestreams because of the lower ammonia concentration.

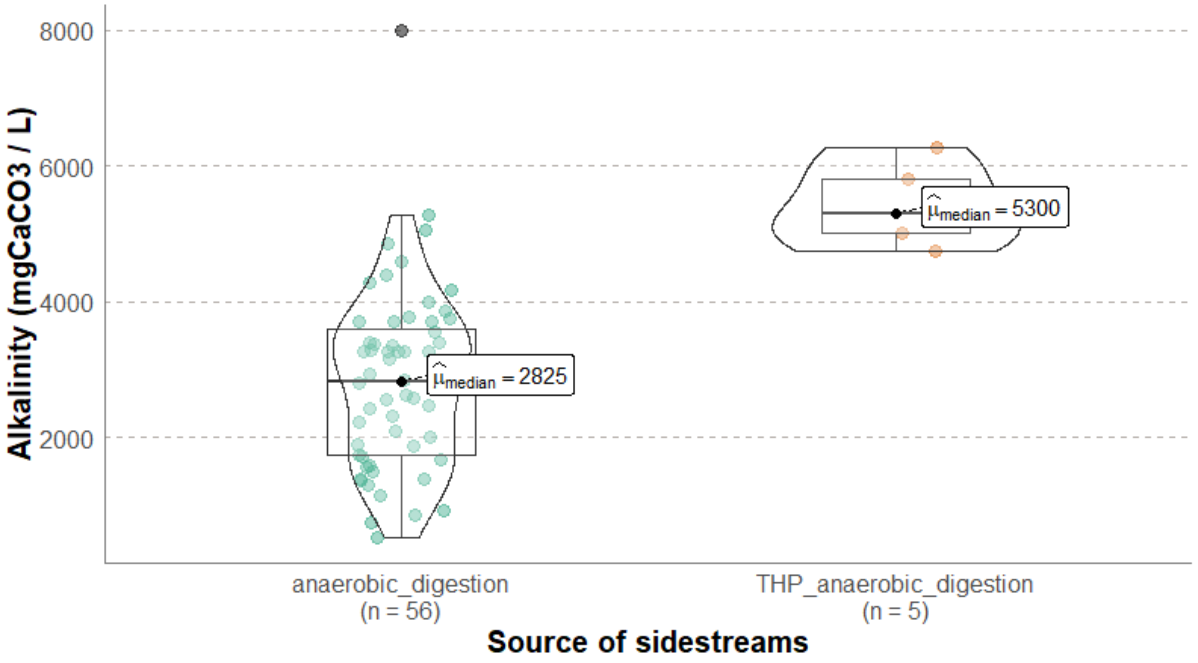

Figure 2.8 - Literature data compilation of alkalinity in sidestreams from anaerobic digestion and THP anaerobic digestion

The pH values from anaerobic digester sidestreams (not shown) ranged from 6.6 to 8.6 (median value of 7.8). This pH is in the high range of typical pH of digesters (6.5 – 7.5) (Paul and Liu, 2012). The low pH values can be due to CO_2 stripping in dewatering units (van Rensburg et al., 2003). pH in primary sludge and biological sludge sidestreams ranged from 6.3 to 7.6.

The temperature in anaerobic digestion sidestreams is comprised between 18°C and 27°C. This reflects the cooling between the outlet of the anaerobic digester (35 - 38°C) and the dewatering unit.

2.5.4 Heavy metals, micro-pollutants and pathogens

Sidestreams valorisation through a nitrogen or a phosphorus based-product is possible only if the latter complies with the regulations with reference to trace elements, including heavy metals, micropollutants and pathogens (Rey-Martínez et al., 2022). Indeed, heavy metals can be incorporated into the crystal, in case of struvite recovery, reducing the purity of the product (Muys et al., 2020; Uysal et al., 2010). In Table 2.3, heavy metal concentrations in sidestreams are compared with their concentrations in wastewater. The concentrations in sidestreams can be higher than in wastewater due to the accumulation of metals in sludge. In terms of fluxes, a study reported that AD dewatering sidestreams load contributed to 10%, 10%, 15%, 10%, 5%, 10%, 10% of the load entering the WRRF for Cd, Cr, Cu, Hg, Ni, Pb and Zn, respectively (Yoshida et al., 2015).

Table 2.3 - Heavy metals concentration in anaerobic digestion sidestreams compared to concentrations in wastewater

	Ranges in sidestreams	*References*	*maximum values in wastewater from 64 WRRFs* *(Vriens et al., 2017)*	*average values in wastewater from 6 WRRFs* *(Choubert et al., 2011)*
Cadmium (Cd)	0 – 0.017	(Ebbers et al., 2015; Karwowska et al., 2016)	0.000365	0.00020
Copper (Cu)	0.025 – 0.1477	(Bohutskyi et al., 2015; Ebbers et al., 2015; Karwowska et al., 2016; Ledda et al., 2015; Romero Villegas et al., 2017; Shao et al., 2019; Zhao et al., 2018)	0.052	0.054
Nickel (Ni)	0.01 – 0.2	(Ebbers et al., 2015; Karwowska et al., 2016; Shao et al., 2019; Zhao et al., 2018)	0.067	0.0103
Lead (Pb)	0.02 – 0.11	(Ebbers et al., 2015; Karwowska et al., 2016; Zhao et al., 2018)	0.0019	0.0065
Zinc (Zn)	0.014 – 0.28	(Bohutskyi et al., 2015; Ebbers et al., 2015; Karwowska et al., 2016; Ledda et al., 2015; Romero Villegas et al., 2017; Shao et al., 2019; Uysal et al., 2010; Zhao et al., 2018)	0.059	0.137
Mercury (Hg)	0.426	(Uysal et al., 2010)	-	0.00040
Chromium (Cr)	0.01 – 0.0834	(Shao et al., 2019; Uysal et al., 2010; Zhao et al., 2018)	0.0036	0.00109

For organic micropollutants, information of their concentration in sidestreams have been found in the work of Yoshida et al. (2015) and Uysal et al. (Uysal et al., 2010) for the following species: bis(2- ethylhexyl)phthalate (DEHP), polychlorinated biphenyl (PCBs) and polycyclic aromatic hydrocarbons (PAHs)). The AD dewatering sidestreams load contribute to 15%, 5%, 30% of the load entering the WRRF for DEHP, PCBs and PAHs, respectively.

2.6 How do sidestream characteristics impact the choice of a treatment/valorisation process?

2.6.1 Struvite precipitation

Struvite ($MgNH_4PO_4 \cdot 6H_2O$) is a white crystalline substance precipitating in a theoretical molar ratio of 1:1:1 (NH_4:PO_4:Mg) (Le Corre et al., 2009). Struvite precipitation is usually used to recover phosphorus in AD dewatering sidestreams when P-PO_4 concentration is above 50 mg/L (Wu and Vaneeckhaute, 2022). This process was implemented first to help reduce struvite clogging issues in pumps and pipes (Kleemann et al., 2015). The different technologies available on the market generally use a fluidised bed column reactor due to different solid and hydraulic retention time as well as to facilitate the recovery of struvite (Ghosh et al., 2019).

Even if the performance of P recovery through struvite in sidestreams is over 90% (Jaffer et al., 2002; Münch and Barr, 2001; Parsons et al., 2001; Yoshino et al., 2003), the overall plant-wide efficiency is lower than 50% (Muys et al., 2020). The recovered struvite can be applied directly to the field as a slow-release fertiliser if permitted and proven to be a favourable option for agricultural use (Melia et al., 2017). The pH at which struvite may precipitate is one of the main factors influencing the crystallisation process (Le Corre et al., 2009). The pH in a struvite precipitation reactor is usually between 7.5 (Liu and Qu, 2017) and 9.5 (Daneshgar et al., 2019) with optimal conditions around 8.5 (Münch and Barr, 2001). As the pH in AD dewatering sidestreams is from 6.6 to 8.9, adding sodium hydroxide to adjust the pH above 8 can be required. Because Mg:P ratio from 1 to 2 enhances the degree of supersaturation (Desmidt et al., 2013), Mg is generally added to the precipitation reactor as magnesium chloride or magnesium oxide (Münch and Barr, 2001; Xavier et al., 2014). Consumption of high quantities of magnesium can limit the economic interest of struvite recovery technologies (Astals et al., 2021). Likewise, low-cost magnesium source have been envisaged such as magnesium from nano filtration of seawater (Shaddel et al., 2020). However, this option also brings others ions so a good knowledge of sidestreams is paramount before adding new sources of impurities (Lahav et al., 2013).

Other parameters can affect the performance of struvite reactors. TSS above a concentration of 1000 mg/L (Barnes et al., 2007) has been reported to interfere with crystal growth by reducing the aggregation of crystals, hence their final size (Muys et al., 2020). TSS, even at a low concentration under 20 mg/L, can also adsorb to the surface of struvite crystals and decrease struvite purity (Desmidt et al., 2015; Ping et al., 2016). Not only TSS but VSS content can be responsible of a low phosphate removal efficiency because organic material can react with ions both on the media and on the surface of crystal nucleus (Ping et al., 2016; Tong and Chen, 2007). Other ions play a significant role in the purity of the final product. Indeed, amorphous calcium phosphate, brucite, magnesium phosphate, calcite, newberyite, K-struvite can precipitate in sidestreams (Musvoto et al., 2000b).

The impact of Ca^{2+} in the purity of struvite depends on both Ca^{2+}:P-PO_4 and Ca^{2+}:Mg^{2+} molar ratio as well as the initial P-PO_4 concentration. For a Ca^{2+}: Mg^{2+} molar ratio over 0.5, struvite is heavily impacted by calcium and co-precipitated with amorphous calcium phosphate and calcium carbonate (Korchef et al., 2011; Tao et al., 2016), even sometimes for a Ca^{2+}:Mg^{2+} molar ratio between 0.2 and 0.5 (Yan and Shih, 2016) and from ratio over 1 no struvite can be formed (Le Corre et al., 2005). If initial concentration of phosphate is higher than 60 mg/L, there is no influence of calcium on struvite precipitation for a Ca^{2+}:Mg^{2+} molar ratio lower than 0.2. However, at concentration of phosphate lower than 40 mg/L, struvite was affected by the presence of calcium for every ratio of Ca^{2+}:Mg^{2+}. Consequently, calcium phosphate precipitation will be more interesting than struvite precipitation for wastewaters with low phosphate concentrations (Desmidt et al., 2013).

In addition, even if the heavy metals concentrations in sidestreams are very low, they can accumulate in the minerals precipitated. A concentration of mercury in sidestreams of 0.426 mg/L can result in a concentration of 4.23 mg/kg dry matter in struvite (Uysal et al., 2010) exceeding the limit of 1 mg/kg dry matter (European Commission, 2019). As far as pathogens are concerned, struvite crystallisation selectively seem to exclude them, leaving them in the anaerobic digestion sidestreams (Muys et al., 2020).

2.6.2 Partial nitritation – anaerobic ammonium oxidation (PN-anammox)

The PN-anammox process is the most innovative worldwide applied technology for nitrogen removal in WRRFs in recent years. The technologies used at full-scale are single-stage or separate-stage systems that can be divided into 3 goups: moving bed biofilm reactor, granular sludge processes or sequencing bed reactor (Lackner et al., 2014). In comparison to conventional nitrification - denitrification and to nitritation - denitritation, this process does not require supplemental carbon addition, consumes less oxygen (1.9 kg O_2/kg N instead of 4.6 kg O_2/kg N for nitrification-denitrification) and has lower sludge production (Van Hulle et al., 2010). The process transforms a mix of NH_4^+ and NO_2^- into N_2 and a small quantity of NO_3^- according to the following equation (Ahn, 2006):

$$NH_4^+ + 1.32\ NO_2^- + 0.66\ HCO_3^- + 0.13\ H^+ \rightarrow 0.066\ CH_2O_{0.5}N_{0.15} + 1.02\ N_2 + 2.03\ H_2O + 0.26\ NO_3^-$$

Under anoxic conditions, anaerobic ammonium oxidising bacteria (anammox) can oxidize ammonium to molecular nitrogen, using nitrite as the final electron acceptor and CO_2 as carbon donor. The doubling time of anammox bacteria is about 10-12 days at 35°C (Talan et al., 2021); therefore reactors providing high biomass retention time such as biofilm reactors are often used. This process has been applied worldwide particularly in sidestreams from anaerobic digestion because these warm effluents with high nitrogen and low carbon content comply with optimal growth conditions of anammox bacteria (Kartal et al., 2010). However, process instability has been noted in connection with high or varying TSS concentration. Increased TSS load affects sludge withdrawal and consequently active biomass content in the reactor (Lackner et al., 2014).

Inhibitions by soluble, colloids and particulate COD has also been reported in literature (Arora et al., 2021; Jin et al., 2012, 2016; Lackner et al., 2014; Talan et al., 2021). A low COD:N-NH_4 ratio, generally lower than 2 (Lackner et al., 2014), is recommended for the operation of the PN-anammox process. Indeed, for a COD:N-NH_4 ratio higher than 2, inhibition has been reported in a laboratory-scale reactor with particulate COD concentration as low as 300 mg/L (Chamchoi et al., 2008) which is expected in sidestreams from anaerobic digestion. Particulate COD and colloidal COD were identified as the main inhibitory parameters that decreased aerobic ammonium oxidising bacteria (AOB) rate. Under high levels of colloidal matter, oxygen transfer efficiency decreased, resulting in limited dissolved oxygen availability and consequently a poor nitrification performance. This was resolved by improving the dewatering process through an optimised polymer dosing to capture the colloidal fraction. No decrease of anammox activity was observed during operation of the reactor as long as the soluble COD concentration remained below 2500 mg/L (Zhang et al., 2016). This value corresponds to a COD:N-NH_4 ratio of 2.4 and creates inhibition of anoxic ammonium oxidizing bacteria due to competition with denitrifiying bacteria. Such competitions between heterotrophic bacteria that outcompete both AOB and anammox bacteria has been described by different authors, especially with THP and high COD content (Baeten et al., 2019; Molinuevo et al., 2009). To avoid such phenomena, a dilution was suggested to maintain a constant soluble COD concentration in the process and to decrease toxicity effects from refractory compounds especially for anaerobic digestion sidestreams preceded by THP that can reach elevated COD concentrations (Driessen et al., 2020). The potential

drawback of a higher dilution is the temperature drop (Zhang et al., 2016) below anammox optimal temperature growth rate of 30 – 40 °C (Shao et al., 2019).

A pH of 7–8 was reported to be suitable for anammox activity (Talan et al., 2021) and in range for avoiding inhibition by free ammonia and free nitrous acid. The inhibition at high pH is caused by the increase of free ammonia; however, a low pH value enhances free nitrous acid inhibition. A free ammonia concentration of 20 mg/L (Fernández et al., 2012) or even lower during process startup (Jung et al., 2007) can cause instability of the process (Figdore et al., 2011). This concentration is expected at a temperature of 27 °C, pH = 7.8 and a concentration of $N\text{-}NH_4$ of 810 mg/L. Dilution and pH control is one solution to stabilise the operation of deammonification processes (Lackner et al., 2014; Ochs et al., 2021). A gradual start up for biomass acclimation is nevertheless possible up to 150 mg $N\text{-}NH_3$/L (Aktan et al., 2012).

Inhibition of anammox activity by phosphate was reported for a wide range of concentration: 57.6 mg/L (Jin et al., 2012); 235 mg/L (Yang et al., 2019), 310 mg/L (Arora et al., 2021), 475 mg/L (Eskicioglu et al., 2018). However, the underlying mechanisms are still under debate and are likely to vary depending on many parameters such as: phosphate concentration, aggregate state (flocculated or densified biomass), pH conditions; degree of acclimation of the biomass and duration of the inhibition test (short vs long-term), among others. According to Zhang et al. (2017), the formation of dihydrogen phosphate ion, under weakly basic conditions and high phosphate concentration, may be responsible for the inhibition of the enzymes of the anammox reaction. This effect seems less pronounced in granules due to their multi-layer structure and higher extracellular polymeric substances levels that act as a protective layer for anammox bacteria. Biologically induced precipitation of calcium phosphate was confirmed in P/NA granular sludge and could be an additional explanation for the higher tolerance to phosphate stress of granules compared to anammox flocs (Johansson et al., 2017).

Although essential nutrients (Ca, K, Fe, Mg, Mn, Co, Cu, Mo, Ni, Zn) are usually sufficiently available in digested sewage sludge reject liquors (Burgess et al., 1999), fulvic and humic-like organic substances generated by the THP process are known for binding metal-ions, possibly reducing the bioavailability of essential trace elements (Zhang et al., 2018). Table 2.4 shows that Fe, Cu, Al and Zn content in sidestreams do not always meet the minimum requirements for biomass growth. To ensure optimal biological activity and growth of the biomass micronutrients, essential trace metals are sometimes dosed to the anammox reactor, especially for anaerobic digestion sidestreams with THP (Driessen et al., 2020). Besides, it has been reported that the specific anammox growth rate could be significantly enhanced by adding ferrous oxide (Zhang et al., 2022). High concentrations of heavy metals can inhibit anammox activity as it is reported in Table 2.4 but such elevated concentrations are not likely to be encountered in municipal WRRF sidestreams.

Table 2.4 - Comparison of trace elements requirements to inhibiting concentrations and concentrations found in anaerobic digestion sidestreams

Trace elements	*Requirements* *(Burgess et al., 1999)*	*Inhibiting concentrations* *(Zhang et al., 2022)*	*Concentrations in sidestreams from Table 2.2 and Table 2.3*
Ca	0.4 – 1.4	-	10 – 321
K	0.8 – 3	-	17 – 626
Fe	0.1 – 0.4	-	0.04 – 32
Mg	0.5 – 5.0	-	1 – 94
Mn	0.01 – 0.05	-	-
Cu	0.01 – 0.05	4.2	0.01 – 0.1477
Al	0.01 – 0.05	-	0.1 – 16
Zn	0.1 – 1	6.76	0.014 – 0.28
Mo	0.1 – 0.7	-	-
Co	0.1 – 5	-	-
Cd	-	7	0 – 0.017
Cr	-	8.96	0.010 – 0.198
Hg	-	2.3	0.42
Ni	-	3.6	0.005 – 0.2
Pb	-	4.3	0.03 – 0.11

Reduction of sulphate to H_2S often occurs in anaerobic digestion processes (Forouzanmehr et al., 2022) and in anammox-based system (Arora et al., 2021) inducing the presence of sulphide in sidestreams. In addition, one should also mention that sulphate can be biologically reduced to sulphide (Bi et al., 2020). The concentration of sulphide is mitigated by the formation of insoluble metal sulfide complexes in the anaerobic digester (Forouzanmehr et al., 2021). The intermediate sulphide produced biologically was reported in a review to inhibit anammox activity starting from a concentration of 32 mg/L (Jin et al., 2013).

2.6.3 Ammonia stripping

Stripping of ammonia lies on the liquid-gas equilibrium where ammonia from the liquid phase is transferred to a gas phase in a packed tower. The ammonia gas is then sent to an air scrubber for ammonia absorption to an acid, generally sulphuric acid, in order to recover a solution of ammonium sulphate ($(NH_4)_2SO_4$) (Boehler et al., 2015). This process has been applied at full-scale but it is generally not favourable from the energy and chemicals consumption point of view except for a niche market (Fernández-Arévalo et al., 2017b; Shaddel et al., 2019). The main bottlenecks of this process are scaling and fouling of the packing material, and the consequent high energy and chemical requirements. To avoid that, removal of Ca, Mg, carbonates and TSS is required (Gopalakrishnan et al., 2000). For a concentration of TSS higher than 1000 mg/L, a separation solid-liquid is required before entering the process (Vaneeckhaute et al., 2018a). The minimum alkalinity is 4000 mg/L as $CaCO_3$ to satisfy the pH requirements by stripping out CO_2 without the use of chemicals as NaOH (Vaneeckhaute et al., 2018c). The quantity of Cl^- above 20 kmol/m^3 (which corresponds to 564 mg/L) negatively impacts the NH_3 removal efficiency because it decreases the pH, while increasing the ionic strength of the solution (Vaneeckhaute et al., 2018c). As discussed in previous sections, these threshold levels can be reached in anaerobic digestion sidestreams and pre-treatment step is required when the conditions are not met for the correct operation of the process. Moreover, the minimum ammonia concentration for this process is 1000 mg/L to be economically viable (Wu and Vaneeckhaute, 2022). One study shows lower disadvantages by applying a thin film evaporator directly on digested sludge (Costamagna et al., 2020).

2.6.4 Emerging processes

Three emerging technologies are briefly presented in the following section, together with the main sidestream characteristics that may impact their performance according to literature data.

2.6.4.1 Membrane

Hollow-fiber membrane contactor is a promising technology for N recovery. In this system, ammonia passes through a microporous hydrophobic membrane and a sulfuric acid solution is used as draw solution to recover N as a valuable product (Robles et al., 2020). This technology has been applied at full-scale in only one WRRF (Seco et al., 2018; Richter et al., 2020) but the presence of suspended solids and colloidal materials can make the use of membrane-based technologies for separate treatment of AD sidestream difficult due to membrane fouling (Eskicioglu et al., 2018; Metcalf & Eddy Inc. et al., 2003; Wäeger-Baumann and Fuchs, 2012). Nevertheless, the optimisation of the materials used and recent works have shown an application of membranes for nitrogen recovery directly in digested sludge (Rivera et al., 2022). Regarding the final nitrogen-based product obtained, it can be contaminated by other ions present in the original substrate; therefore membranes should be consider with additional steps (TSS, COD and foreign ions removal) to obtain a pure ammonia product (Darestani et al., 2017; Beckinghausen et al., 2020). Application of forward osmosis membrane or membrane distillation have not been found for sidestream application because of excessive fouling (Vu et al., 2019).

2.6.4.2 Electrodialysis, bioeletrochemical system and ion exchange resin

Electrodialysis process uses an electric current to migrate ions to the cathode or anode and trap them on ion exchange membranes. A concentrated ammonia or phosphate solution is obtained (Ward et al., 2018). In bioelectrochemical systems, the oxidation of organics produces electrons used as energy for the migration of NH_4^+ ions from the anode to the cathode in order to maintain charge neutrality (de Fouchécour et al., 2022). In the cathode chamber, NH_4 is transformed into NH_3 thanks to the high pH value to be recovered (Nancharaiah et al., 2016). Ion exchange systems use resins which can exchange an ion adsorbed on the resin surface with a specific cation or anion in the centrate (Huang et al., 2020). Performance of these systems depend on electrode, membrane and resin fouling because high calcium, magnesium, TSS and carbonate can lead to significant deposit as calcium carbonate, struvite or accumulation of colloidal particles (Beckinghausen et al., 2020; Feng et al., 2017; Mondor et al., 2009). For the bioelectrochemical system, the low COD content in sidestreams limits its development at full scale and this technology is best suitable for wastewater rather than centrate (Al-Sahari et al., 2021). Phosphorus adsorption is also highly dependent of pH value because it affects the surface charges of the absorbent. The co-existing of different ions such as SO_4^{2-}, NO_3^- and Cl^- may inhibit P adsorption due to ions completion for the vacant adsorption sites (Song and Li, 2019; Ye et al., 2017).

2.6.4.3 Algae production

Microalgae-based wastewater treatment systems can be used for the removal of organic and inorganic carbon as well as for nutrients from wastewater (Al Momani and Örmeci, 2020). The main interest of this process lies in the production of a high growth rate algae biomass for biogas or biofuel production (Romero Villegas et al., 2017). The algae biomass has low carbon requirement which can be attractive for anaerobic digestion sidestreams treatment (Peralta et al., 2019). However, high content of TSS can negatively impact the growth of microalgae biomass because algal biomass can

then compete with other bacteria for N, P and alkalinity (Marazzi et al., 2019). Another limit of this process is the design of the algae culture system as harvesting the biomass produced is still a challenging step (Zhao et al., 2018).

2.7 Discussion

The selection of processes for nutrient treatment/recovery of anaerobic digestion sidestreams have been discussed based on current published information on their operation. Although of high importance, current literature review revealed that it is challenging to define operational limits of the processes with regards to sidestream characteristics based on full-scale data. Published data are indeed scarce, and most of the time only limited characteristics were evaluated or investigated. In addition, it is likely that reported threshold values for sidestream characteristics leading to a decrease of process performance or to an inhibition embed the effect of other operational parameters. It is therefore not excluded that process configuration, the way it is operated as well as the exposition time and the acclimation of the biomass to an inhibitor highly affects the range of reported values. This is especially critical when limited data are available.

Based on literature data, Figure 2.9 presents the most important parameters to be measured before choosing a specific process. Comparison of the ranges of concentrations found and the list of sidestream characteristics shows that the range of concentrations from literature is large in comparison to the inhibition mentioned in the previous sections. Consequently, installation of a pretreatment step for TSS or COD removal for example can be required to ensure stable process performance.

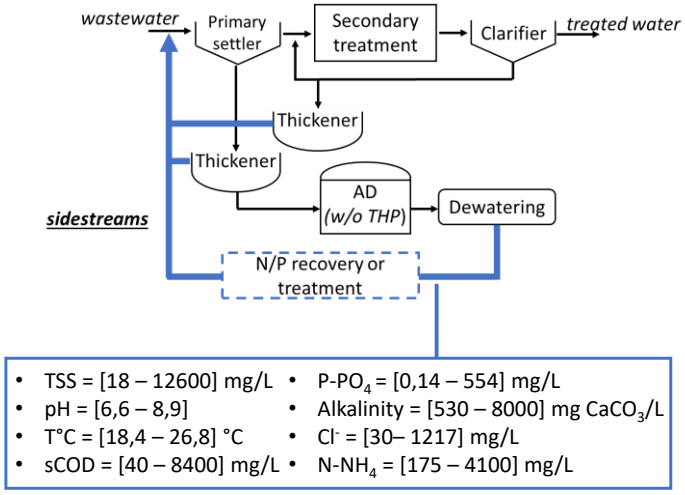

List of characteristics to be measured before implementation of the process

Process	Characteristics
Struvite precipitation	TSS, pH, $P\text{-}PO_4$, Ca^{2+}:Mg^{2+}
Partial Nitritation / Anammox	COD:$N\text{-}NH_4$, $P\text{-}PO_4$, pH, T°C
Ammonia stripping	Alkalinity, Cl^-, $N\text{-}NH_4$
Membrane	TSS, $N\text{-}NH_4$, $P\text{-}PO_4$, Ca^{2+}, Cl^-, Mg^{2+}, K^+, Na^+, SO_4^{2-}
Electrodialysis, BES & IEX resin	TSS, Alkalinity, $P\text{-}PO_4$, $N\text{-}NH_4$, Ca^{2+}, Mg^{2+}
Algae production	TSS, $N\text{-}NH_4$, $P\text{-}PO_4$

Figure 2.9 - Main characteristics of anaerobic digestion sidestreams and list of key characteristics for the implementation of sidestream processes

Nutrient recovery in sidestreams, and especially in anaerobic digestion sidestreams seem promising but a well-defined product with high purity is required if recovery as fertiliser is considered. For example, organic farmers have a need for a pure nitrogen fertilizer, rather than a combination that includes P or K (Beckinghausen et al., 2020). As seen in previous paragraphs other ions and organic matter can impact the purity of the final recovered product or the efficiency of the process to obtain these products. Therefore, more investigations have to be carried out on the feasibility of producing a product with higher purity considering the full ionic composition of AD dewatering sidestreams (Shaddel et al., 2019). THP can, in addition to improving the performance of anaerobic digestion, improve the possibilities of recovering nitrogen because the $N\text{-}NH_4$ content is higher in sidestreams

compared to a conventional digester sidestream. However, this does not apply for P which is released as phosphate upstream of the AD through the THP but then precipitates in the digester with Ca^{2+} and Mg^{2+}. The potential for P recovery upstream of AD needs to be more expanded as only a few examples exist to date (Bouzas et al., 2019). Nutrient recovery from primary sludge and biological sludge sidestreams has not been extensively explored. Indeed, the concentrations of phosphorus and nitrogen are lower than in the anaerobic digestion sidestreams. However, nutrient content in these sidestreams can be interesting for the recovery in some specific cases; especially when there is a thickening unit with high retention time as the release of ions is stimulated. In such specific context, sidestreams can be joined together and the process installed on this sidestream combination (Latimer et al., 2016). Overall, there is not always local demand for nitrogen or phosphorus fertiliser (Kehrein et al., 2020; Robles et al., 2020) and nutrient recovery technologies need a large quantity of energy and chemicals which induces higher environmental impacts (Pradel and Aissani, 2019).

Future research should focus on the definition of evaluation criteria that take into account the WRRF performance, effluent quality and operation costs, but also the environmental impacts, the efficiency of the recovery process and purity and the destination of the final product. To do so, there is an urgent need to develop shared databases with updated information on recovery processes including performance and operating conditions because there is a lack of information on recovery processes in real conditions (Puchongkawarin et al., 2015). Plant-wide modelling could also help in the choice and comparison of different routes to treat or valorise sidestreams. Even if some models already include precipitation as struvite (Lizarralde et al., 2019) or ammonia stripping (Vaneeckhaute et al., 2018b), they still need to be validated not only for the targeted nutrient but also considering the different compounds that can interact (Mg^{2+}, Ca^{2+}, $Fe^{2+/3+}$, SO_4^{2-}, K^+, Cl^-). Access to data from full-scale measurement campaigns is therefore essential in order to understand the full ionic distribution in different locations in the WRRF and to integrate new mechanisms into existing models.

2.8 Conclusions

Sidestream processes are increasingly being optimised to mitigate their effects on the water treatment line but also to recover nutrients in water resource recovery facilities. The implementation of such processes depends on sidestream characteristics. Ranges of concentrations of the main components observed in sidestreams at full scale have been discussed. To aid in the development, design and optimum operation of sidestream processes, this critical review identified the following key points:

1) Anaerobic digestion sidestreams contribute significantly to the nitrogen (17%) and phosphorus (11%) mass flows at the WRRF inlet. The quantity of phosphate in sidestreams depends on the type of applied phosphorus treatment with a median value of 33 mg/L for chemical phosphorus removal and of 167 mg/L for enhanced biological phosphorus removal.

2) The concentration of COD, N and alkalinity are higher in THP anaerobic digestion sidestreams than conventional anaerobic digestion. However, there is no difference in the phosphorus content because the phosphate release during THP is directly immobilised by others ions (Ca^{2+}, Mg^{2+}, $Fe^{2+/3+}$). Phosphorus recovery before anaerobic digestion should be considered in the presence of THP, and the quantity of Ca^{2+}, Mg^{2+} and $Fe^{2+/3+}$ should be quantified to assess the potential for P recovery.

3) The variability of ion concentrations (Al^{3+}, Ca^{2+}, Cl^{-}, $Fe^{2+/3+}$, Mg^{2+}, K^{+}, Na^{+}, SO_4^{2-}) depends on: (1) wastewater characteristics in particular the presence of industrial wastewater, (2) the use of chemicals such as iron chloride or lime and (3) dissolution and precipitation mechanisms in thickening or dewatering unit. The latter should be further investigated to better assess the impact of the full ionic composition on nutrient treatment or recovery.

4) All the characteristics previously mentioned can have an impact on sidestream processes. However, the definition of a concentration range or threshold value to ensure the successful operation of these processes is not a straightforward task. Indeed, the information about inhibitions is sparse in the literature and depends on a lot of different parameters (reactor configuration, scale, biomass acclimatisation, operating conditions). This review provides a list of characteristics to be measured in order to select the most suitable sidestream process for each specific application.

5) Future research should focus on further data acquisition, especially on the concentration of the different ions, to better assess the potential for nutrient recovery and to minimise the economic and environmental impact of WRRFs.

CHAPTER 3 - SYSTEMATIC CALIBRATION OF A SEWAGE SLUDGE ANAEROBIC DIGESTION MODEL WITH MULTIPLE MINERAL PRECIPITATION USING FULL SCALE DATA

3.1 Abstract

Including multiple mineral precipitation in anaerobic digestion (AD) models is important to accurately assess the quantity of phosphates (P-PO_4) in the liquid phase of digested sludge that can be recovered as a fertilizer in struvite precipitation reactors or by emerging processes such as ion exchange membranes. However, the performance of such processes is highly impacted by the presence of potassium (K^+) or calcium (Ca^{2+}) ions, which are most often neglected when validating precipitation models. The present study provides a calibration procedure of an AD model with multiple mineral precipitation using data from two ADs treating sludge with different biodegradability and concentration ranges of phosphorous (P), calcium (Ca), magnesium (Mg), potassium (K) and soluble inorganic carbon (SIC). This procedure includes the calibration of the inert COD fraction ($f_{XI,COD}$) and kinetic precipitation constants (K_r) using Bayesian Monte Carlo techniques. A model correction to include the fraction of organic Ca, Mg and K in sludge was found necessary to better represent Ca^{2+}, Mg^{2+} and K^+ in digested sludge. Monte Carlo simulation results reveal that some kinetic constants ($K_{r,MgCO3}$, $K_{r,CaCO3}$ and $K_{r,ACP}$) have an impact on final P-PO_4, Ca^{2+}, Mg^{2+} and alkalinity simulation results. However, a unique parameter set for both anaerobic digesters cannot be identified. Consequently, a site-specific calibration has to be performed. If the model gives acceptable results for P-PO_4 with precipitation parameters by default, $K_{r,MgCO3}$, $K_{r,CaCO3}$ and $K_{r,ACP}$ values need to be calibrated to obtain accurate Ca^{2+} and Mg^{2+} concentrations in the digested sludge, especially in case of high water hardness.

3.2 Highlights

- An AD model including precipitation kinetics was validated on two different anaerobic digesters by adjusting only $f_{XI,COD}$, $K_{r,CaCO3}$, $K_{r,MgCO3}$ and $K_{r,ACP}$.
- A model correction to include the organic Ca, Mg and K fraction in sludge was required.
- Precipitation models with parameters by default give a reasonable estimation of P-PO_4 content in digested sludge but fail to describe Mg^{2+} and Ca^{2+} content.
- $K_{r,CaCO3}$, $K_{r,MgCO3}$ and $K_{r,ACP}$ need to be calibrated for each anaerobic digester to estimate accurately the amount of Mg^{2+} and Ca^{2+} especially when having high water hardness.

This chapter was submitted as:
Devos, P., Elduayen-Echave, B., Filali, A., Gillot, S., Grau, P., 2023. Systematic calibration of a sewage sludge anaerobic digestion model with multiple mineral precipitation using full-scale data. Submitted to *Journal of Water Process Engineering.*

3.3 Introduction

In wastewater treatment, models describing the operation of anaerobic digesters have shown to be effective in estimating biogas production and digested sludge quantity either when studying the sludge line alone or when considering the interactions between water and sludge lines in plant wide models (PWM). Anaerobic digestion model 1 (ADM1) is the outcome of the IWA task group for mathematical modelling of anaerobic digestion processes on the development of a generic model for anaerobic digestion (Batstone et al., 2002). Since its first application, this model has been adapted and introduced into different model libraries such as: the PWM approach detailed in Grau et al. (2007) and Lizarralde et al. (2015), the benchmark simulation model (Gernaey et al., 2014), the biological nutrient removal model (Barat et al., 2013), the PWM South Africa (Ikumi, 2020), and the generic nutrient recovery model (Vaneeckhaute et al., 2018b). Original ADM1 includes biochemical reactions, acid-base equilibrium and liquid-gas transformations (Batstone et al., 2002). The model provided satisfactory results for the estimation of biogas production, solids removal and ammonium concentration in digested sludge (Astals et al., 2013; de Gracia et al., 2009; Razaviarani and Buchanan, 2015; Souza et al., 2013).

However, ADM1 showed limitations to calculate pH and estimate phosphate concentration correctly, due to simplifying assumptions, such as considering solutions with ideal behaviour, or neglecting solid-liquid transformations (Batstone et al., 2012). Therefore, in recent publications, the model was updated with a more comprehensive physico-chemical framework (Batstone and Flores-Alsina, 2022) including activity corrections for non-ideal behaviour and precipitation with phosphate of the following metals: calcium (Ca), magnesium (Mg), iron (Fe), aluminium (Al). More extensive models have also been developed to describe interactions between sulphur, iron and phosphorus (Hauduc et al., 2019; Kazadi Mbamba et al., 2019; Solon et al., 2017), as well as more advanced precipitation models with particle size distribution of the minerals formed (Elduayen-Echave et al., 2019).

Table 3.1 summarises the different publications on precipitation in AD models implemented in PWMs. In all references, precipitation kinetic constants have been fitted to batch experiments performed with synthetic water (Kazadi Mbamba et al., 2015a), anaerobic digestion sidestreams (van Rensburg et al., 2003) or digested sludge (Kazadi Mbamba et al., 2015b; Marti et al., 2008; Musvoto et al., 2000a). Once calibrated, models were applied to full-scale case studies with similar sludge characteristics (Flores-Alsina et al., 2021; Kazadi Mbamba et al., 2016; Martí et al., 2017; Roldán et al., 2020) or used to simulate a single mineral precipitation (Lizarralde et al., 2019). As seen in Table 3.1, some of the modelling results were evaluated based on the concentration of phosphate in the digested sludge (Kazadi Mbamba et al., 2016; Lizarralde et al., 2019, 2015). Other authors evaluated the model performance through its ability to predict COD, SS, P (total, soluble and PO_4-P), nitrogen (total, soluble, NH_4-N, NO_3-N) and total and soluble Ca, K and Mg concentrations in the effluent of the water line (Flores-Alsina et al., 2021; Martí et al., 2017; Roldán et al., 2020).

Table 3.1 - Summary of publications including an AD model with mineral precipitation in a plant wide model. Simulation results were obtained at steady state

Reference	Wastewater characteristics					Minerals considered	Calibrated parameters or reference of default parameters used	Model performance on $P\text{-}PO_4$ (percentage deviation between measured and modelled values)
	Mg^{2+} (mg/L)	Ca^{2+} (mg/L)	K^{+} (mg/L)	Inorganic carbon (mg/L)	TP:TSS			
Lizarralde et al., 2015	90	25	176	183	NA	Struvite	Musvoto et al., 2000a	12%
Kazadi Mbamba et al., 2016	53	47	35	75	0.024	Struvite / Amorphous calcium phosphate / Calcium carbonate	Kazadi Mbamba et al., 2015b	22%
Martí et al., 2017	27	132	27	NA	0.026	Amorphous calcium phosphate / Hydroxyapatite / Struvite / Newberyite / Vivianite / Strengite / Variscite / Calcium carbonate	Barat et al., 2013	NA
Lizarralde et al., 2019	10	5	176	95	NA	Struvite	Struvite kinetic constant ($K_{r,Stru}$)	2%
Roldán et al., 2020	66	133	38	NA	0.022	Amorphous calcium phosphate / Hydroxyapatite / Struvite/ Newberyite / Vivianite / Strengite / Variscite / Calcium carbonate	Barat et al., 2013	NA
Flores-Alsina et al., 2021	NA	NA	NA	NA	0.02	Struvite / Amorphous calcium phosphate / Calcium carbonate	Kazadi Mbamba et al., 2015b	NA

However, as the concentration of $P\text{-}PO_4$, Mg^{2+}, Ca^{2+} and K^{+} are rarely measured at full-scale anaerobic digestors, there are no calibrated and validated precipitation models using full-scale data. In addition, not all models take into account the organic Ca, Mg, and K contained in primary and biological sludge but only consider the P, Mg and K associated with the poly-phosphate accumulating organisms. The differences are important because this implies that the release of Ca, Mg and K during the anaerobic digestion process is not systematically accounted. Both aspects are worked through in this contribution by (i) including the organic Ca, Mg and K fractions in the model and (ii) calibrating a mathematical model that combines the ADM1 and precipitation kinetics in a systematic way. This will help the assessment of technologies favouring circular economy as nutrient recovery processes (struvite precipitation, bioelectrochemical systems or ion exchange processes); they indeed require a good knowledge of the concentration of ions in digested sludge because they can interfere or inhibit the main mechanisms (Devos et al., 2023; Lizarralde et al., 2021).

Therefore, in this work, the effect of two different sludge and anaerobic digester characteristics on the capability of the model to predict biogas production, TS, VS, $N\text{-}NH_4$, $P\text{-}PO_4$ as well as Ca^{2+} and Mg^{2+} has been evaluated. The anaerobic digesters modelled have different operating conditions: temperature, hydraulic retention times and, especially, water hardness (Ca, Mg and inorganic carbon concentrations). This work proposes a systematic calibration procedure to obtain reliable simulation results especially for the concentration of $P\text{-}PO_4$, Ca^{2+} and Mg^{2+} in the digested sludge.

3.4 Material and Methods

3.4.1 Anaerobic digesters

The studied anaerobic digesters are part of 2 WRRFs treating mainly domestic wastewater with a part of industrial wastewater from food industry. WRRF 1 is located in France and includes one mesophilic digester of 3200 m^3. The facility consists in a primary settler followed by a conventional activated sludge line for COD removal. The digester receives both thickened primary and biological sludges. WRRF 2 is located in Spain and part of the produced sludge is treated in one thermophilic pilot-scale digester (2.75 m^3). The plant includes primary settling and trickling filters for COD removal and nitrification. Both types of sludge are thickened with a centrifuge and a fraction is sent to the pilot scale digester.

3.4.2 Data collection and reconciliation

Historical data of the different WRRFs included continuous monitoring of the two digesters with daily sludge and biogas flowrates. In average, two weekly measurements on different variables were also available at the AD inlet and outlet (Table 3.2). The dataset collected corresponds to 1.5 years of data for WRRF 1 and 1 year for WRRF 2. In addition, a dedicated measurement campaign was carried out on each digester to obtain measured variables required for modelling, including COD and ion concentrations (Table 3.2). These periods are from day 62 to day 212 and from day 258 to day 288 for WRRF 1 and WRRF 2, respectively.

Table 3.2 - Description of the datasets collected for each anaerobic digester

	Historical data		Data of measurement campaigns (grab samples)	Size of the data set
	Variables measured each day	**Variables measured twice a week (grab samples)**		
WRRF 1	Sludge flowrate biogas production	AD inlet : TS, VS AD outlet: TS, VS, pH, alkalinity	AD inlet and outlet: COD (total and soluble), biodegradable COD, TS, TSS, VS, VSS, TKN, TP, N-NH_4, P-PO_4, Ca, Mg, K, Na, Ca^{2+}, Mg^{2+}, K^+, Na^+, Cl^-, Lipids, VFAs	1,5 year (487 days)
WRRF 2	Sludge flowrate	AD inlet: TS, VS, pH, alkalinity, N-NH4, COD soluble AD outlet: TS, VS, pH, alkalinity, N-NH4, COD soluble, biogas production	AD inlet and outlet: COD (total and soluble), COD biodegradable, TS, VS, TKN, TP, N-NH_4, P-PO_4, Ca^{2+}, Mg^{2+}, K^+, Na^+, Cl^-, Lipids, VFAs	1 year (365 days)

The measurement campaigns and plant data were analysed following the methodology proposed by Rieger et al. (2012). Graphical tools as box-plot charts were applied and specific ratios (VSS:TSS, Ca^{2+}:Ca, N-NH_4:soluble TKN, etc.) were calculated and compared to usual ranges (Metcalf & Eddy Inc. et al., 2003) to check data and detect potential outliers. Then, the validation and reconciliation of the collected data was performed through mass balances of total COD, mineral matter and total phosphorus for WRRFs 1 and 2 as well as for total nitrogen, calcium, magnesium, potassium and sodium only for WRRF 1 thanks to a more complete dataset (see Supplementary Information 2).

To construct a continuous vector for anaerobic digester inlet and outlet, non-measured data for TS, VS and pH were estimated using a first-order interpolation. Specific ratios obtained during the measurement campaigns were used on these continuous TS and VS vectors to construct the input model component vector.

3.4.3 Model Implementation

The digesters were simulated using the mathematical model detailed in Grau et al. (2007) and Lizarralde et al. (2015) and implemented in the WEST software by MIKE DHI®. The model is based on the components characterisation in their elemental mass and charge density. The list of the 61 model components (dissolved, particulate and gaseous compounds) that form the state variable vector and associated formula is given in the "Supplementary Information" file. In this model, the original X_C has been differentiated into X_{C1} for the particulate complex substrate and X_{C2} for the cell decay products (Huete et al., 2006).

The reactions included in this model are divided into three parts: biochemical, multiphase and chemical transformations. For anaerobic digestion, the selected biochemical transformations were: acidogenesis, acetogenesis, methanogenesis and phosphate accumulating organisms activity under anaerobic conditions. Additionally, extracellular transformations such as disintegration, enzymatic hydrolysis and endogenous respiration were considered. The model also considers multiphase transformations such as liquid-gas and liquid-solid reactions. All relevant acid-base and ion pairing reactions (chemical transformations) were incorporated based on the model components included in the biochemical, liquid-gas and liquid-solid models. Biochemical and multiphase transformations were described using ordinary differential equations, while chemical reactions were described using algebraic equations according to the Tableau method (Morel and Hering, 2013). For the model of the digester, three phases coexist: the aqueous, gas and solid phases. The interactions were defined between the aqueous and the gaseous phases and between the aqueous and the solid phases. This work is focused on the liquid-solid equilibrium, therefore, more details on these interactions is given in the next section.

3.4.4 Precipitation model

The precipitation and dissolution reactions considered in this work are the ones identified by Musvoto et al. (2000a,b) as the most common ones in WRRFs. These reactions include the following minerals: calcium carbonate ($CaCO_3$), magnesium carbonate ($MgCO_3$), amorphous calcium phosphate (ACP) ($Ca_3(PO_4)_2$), struvite ($MgNH_4PO_4.6H_2O$), K-struvite ($MgKPO_4.6H_2O$) and newberyite ($MgHPO_4.3H_2O$). The kinetic rate (ρ) proposed for precipitation in this work describes the mass transfer phenomena involved in the formation of solids: development of supersaturation and crystal growth. The kinetic rate (ρ) in mol L^{-1} day^{-1} is expressed as follow:

$$\rho = K_r * \left(IAP^{\frac{1}{v}} - K_{sp}{}^{\frac{1}{v}}\right)^n \quad (1)$$

Where:

K_r: kinetic rate for precipitation (day^{-1})

K_{sp}: solubility constant (mol L^{-1} base)

IAP: ionic activity product (mol L^{-1})

n: the order of the reaction (-)

v: total number of ions (-)

For a general precipitation-dissolution reaction:

$$aA \quad + bB \quad \leftrightarrow A_xC_y \tag{2}$$

If the ion activity product is higher than the solubility product, the solution is supersaturated and precipitation takes place; if not, dissolution occurs. The ionic activity product is as follows:

$$IAP = \{A\}^a * \{B\}^b \tag{3}$$

Where:

{A}: activity of species A (mol L^{-1})

a: number of ions A

The ionic strength is considered through the equation of Davies (Equation 5) to calculate the activity of each species as suggested in the work of Solon et al. (2015) and Capson-Tojo et al. (2020) when precipitation and anaerobic digestion are to be modelled because of the non-ideality of the solution.

$$\{A\} = \gamma_A * [A] \tag{4}$$

$$I = \frac{1}{2} \sum_i [i] * z_i^2 \tag{5}$$

$$\log(\gamma_i) = -A_{DH} * z_i^2 * \left[\frac{\sqrt{I}}{1+\sqrt{I}} - 0.3I\right] \tag{6}$$

Where:

I: Ionic strength (mol L^{-1})

A_{DH}: Debye-Hückel constant

[A|: concentration of species A (mol L^{-1})

γ_i: activity coefficient of species i (-)

z_i: charge of the species i (-)

3.4.5 Substrate characterisation and fractionation

Analyses performed on raw and digested samples collected during dedicated measurement campaigns are listed in Table 3.2. They were performed following standards methods (APHA, 2005). Sample supernatant was filtered through a 0.45 µm filter to analyse soluble compounds such as soluble COD (sCOD) and ions (Ca^{2+}, Cl^-, Mg^{2+}, K^+, Na^+, SO_4^{2-}, N-NH_4, P-PO_4). Biochemical potential (BMP) tests were conducted to determine biodegradable and inert COD fractions of the substrate according to the conventional procedure (Holliger et al., 2016). Total lipid content was determined through the percentage of hexane extractable materials (HEM) by the Soxhlet extraction method on dried sludge (Abdulhussein Alsaedi et al., 2022).

The COD of the substrate was fractionated into the following model components: S_I, S_{TVA}, S_{TBU}, S_{TPRO}, S_{TAC}, S_{AA}, S_{FA}, S_{SU}, X_{CH}, X_{PR}, X_{Li}, X_I. The other COD-based model components (S_P, S_{H2}, S_{CH4}, S_{O2}, X_{C1},

X_{C2}, X_N, X_{SU}, X_{AA}, X_{FA}, X_{C4}, X_{PRO}, X_{AC}, X_{H2}, X_{PAO}, X_{PHA}, X_P, G_{H2}, G_{CH4}, G_{O2}) were set to 0. Unlike other authors (Astals et al., 2013; Baquerizo et al., 2021; de Gracia et al., 2009) who used the composite model components X_C for COD fractionation, the particulate fraction of the substrate was defined herein as proteins, lipids, carbohydrates and inerts (X_{PR}, X_{Li}, X_{CH}, X_I). The removal of the Xc fraction has been recommended in several works as in the benchmark simulation model no. 2 (Nopens et al., 2009), in a review of ADM1 applications (Damien J. Batstone et al., 2015) and in a recent case study when dealing with sludge coming from WRRFs (Donoso-Bravo et al., 2020).

The particulate COD fraction (X_{PR}, X_{Li}, X_{CH}, X_I) was calculated following the method proposed by Girault et al. (2012). The inert fraction was obtained considering the theoretical methane production of 350 NmL(CH_4) $gCOD^{-1}$. Protein content was determined considering a ratio protein to organic nitrogen of 6.25.

$$\mathrm{f}_{XI,COD} = \frac{BMP\left(\frac{NmL\,CH_4}{gVS_{substrate}}\right)}{350\left(\frac{NmL\,CH_4}{gCOD}\right)} * VS * \frac{1}{particulate\ COD} \tag{7}$$

$$XI = \mathrm{f}_{XI,COD} * particulate\ COD \tag{8}$$

$$\mathrm{f}_{XPR,COD} = 6.25\,\frac{g_{protein}}{g_{organic\,N}} * (\mathrm{TKN} - \mathrm{TAN}) * 1.42\,\frac{g_{O_2}}{g_{protein}} * \frac{(1-f_{XI,COD})}{particulate\ COD} \tag{9}$$

$$XPR = \mathrm{f}_{XPR,COD} * particulate\ COD \tag{10}$$

$$\mathrm{f}_{XLI,COD} = 2.86\,\frac{g_{O_2}}{g_{lipid}} * HEM * \frac{(1-f_{XI,COD})}{particulate\ COD} \tag{11}$$

$$XLI = \mathrm{f}_{XLI,COD} * particulate\ COD \tag{12}$$

$$\mathrm{f}_{XCH,COD} = 1 - \mathrm{f}_{XPR,COD} - \mathrm{f}_{XLI,COD} - \mathrm{f}_{XI,COD} \tag{13}$$

$$XCH = \mathrm{f}_{XCH,COD} * particulate\ COD \tag{14}$$

Where particulate COD refers to the difference between total and soluble COD, TKN to total Kjeldahl nitrogen and TAN to total nitrogen as ammonia.

Regarding the soluble COD components (S_I, S_{TVA}, S_{TBU}, S_{TPRO}, S_{TAC}, S_{AA}, S_{FA}, S_{SU}), S_I was set to 0 as it represents less than 1% of total COD (Astals et al., 2013); S_{TVA}, S_{TBU}, S_{TPRO}, S_{TAC} were obtained with analytical measurements and S_{AA}, S_{FA}, S_{SU} were calculated as follows (Girault et al., 2012):

$$S_{AA} = S_{FA} = S_{SU} = \frac{1-(S_I - S_{TVA} - S_{TBU} - S_{TPRO} - S_{TAC})}{3} \tag{15}$$

Most of the ionic concentrations (S_{IP}, S_{IN}, S_{IC}, S_{Ca}, S_{Mg}, S_K, S_{Cl}, S_{Na}, S_{NO3}, S_{Fe}) were defined using the results of analytical measurements. S_{IC} is the sum of soluble CO_2, HCO_3^- and CO_3^{2-} and was deducted from the value of alkalinity. S_{Alk} was calculated according to the Tableau method (see Supplementary Information). The component X_{II} was defined as the difference between TSS and VSS.

For particulate inert phosphorus, as no specific analysis was carried on the speciation of phosphorus, the results of Saoudi et al. (2022) were applied to obtain an initial concentration of phosphorus bound to Ca (X_{ACP}) and to Fe (X_{FEPO4}).

Other input model components (S_{N2}, X_{FeCl3}, $X_{Fe(OH)3}$, X_{CaCO3} , X_{Stru}, X_{KStru}, X_{New}, G_{CO2}, G_{NH3}, G_{N2}, G_{O2}, G_{H2O}) have been set to 0 as they were assumed not present in feed sludge.

Once the reconciled dataset was obtained and the model input vector constructed, a control of the error induced by the fractionation from the characterisation of the substrate to the input model components was carried out. It consisted in performing a mass balance to check that the sum of the amount of COD, N, P, TSS attributed to the different model components corresponds to the total amount measured in the substrate. An error below 10% was considered acceptable as this corresponds to the experimental error.

3.4.6 Calibration procedure

Figure 3.1 summarises the different steps followed to calibrate the mathematical model. All simulations have been performed at steady state and for Steps 1 and 2, simulations have also been validated under dynamic conditions. Default values (Step 1) taken from ADM 1 were used for all kinetic parameters since they were originally determined for the digestion of municipal wastewater sludge (Batstone et al., 2002). For the precipitation model, the default values were taken from Ikumi and Harding (2020) as they were previously used for anaerobic digestion applications. The kinetic constants for precipitation have been calibrated only at steady state because the concentration of ions (P-PO_4, Mg^{2+}, Ca^{2+}, K^{+}) in the feed and digested sludge was stable according to measurement campaign data.

The calibration of the stoichiometric fraction $f_{XI,COD}$ of the substrate (Step 2) was done for each anaerobic digester by varying $f_{XI,COD}$ in the range of [0.3 - 0.6] determined from literature (Astals et al., 2013; de Gracia et al., 2009; Fisgativa et al., 2020b, 2018; Metcalf & Eddy Inc. et al., 2003). Then, to highlight the impact of adding organic Ca, Mg and K on simulation results for the concentration of Ca^{2+}, Mg^{2+} and K^{+}, the model was modified to consider these fractions in the sludge (Step 3). The objective of steps 4 and 5 was to calibrate the precipitation kinetic constants K_r to fit Ca^{2+}, Mg^{2+}, P-PO_4 and alkalinity. In step 4, an attempt was made to find a unique parameter set including $K_{r,CaCO3}$, $K_{r,MgCO3}$, $K_{r,ACP}$, $K_{r,Struvite}$, $K_{r,Kstruvite}$ and $K_{r,Newberyite}$ for both anaerobic digesters. Step 5 is also relative to the calibration of the precipitation kinetic constants but the calibration was done separately for each anaerobic digester.

For Steps 2, 4 and 5, the calibration procedure is based on Bayesian Monte Carlo techniques. For Step 1, the $f_{XI,COD}$ value was incremented by 0.01 in the range of 0.3 to 0.6 (31 simulations). For Steps 4 and 5, the Latin Hypercube Sampling (LHS) sampling method was used because there is more than one parameter to calibrate. In similar contributions, a minimum number of simulations of 150 for each analysed model parameter has been recommended (Benedetti et al., 2011). In this study, 6 parameters were selected ($K_{r,CaCO3}$, $K_{r,MgCO3}$, $K_{r,ACP}$, $K_{r,Struvite}$, $K_{r,Kstruvite}$ and $K_{r,Newberyite}$), so at least 900 steady-state simulations would be needed. To fine-tune the results, 2000 simulations for steps 4 and 5 were done. The comparison between the experimental and simulation results was done using the posterior probability density function from the Bayes theorem as it was applied in the work of Elduayen-Echave et al. (2021). The posterior probability density function $p(\theta|y)$ of the parameter set θ for the experimental data y was calculated as follows:

$$p(\theta|y) = \frac{M(\theta)^{-\frac{N_M}{2}}}{\sum M(\theta)^{-\frac{N_M}{2}}} \quad (16)$$

$$M(\theta) = \sum_{k=1}^{N_{obs}} \left| e_{N\,k}(\theta) \right|^2 \quad (17)$$

Where:

- θ the parameter set, here $f_{XI,COD}$ for step 2 and $K_{r,CaCO3}$, $K_{r,MgCO3}$, $K_{r,ACP}$, $K_{r,Struvite}$, $K_{r,Kstruvite}$, $K_{r,Newberyite}$ for steps 4 and 5
- N_{obs}: number of output variables to fit. To calibrate $f_{XI,COD,}$ the following output variables were considered: biogas production, TSS, VSS, N-NH_4 and alkalinity. To calibrate $K_{r,CaCO3}$, $K_{r,MgCO3}$, $K_{r,ACP}$, $K_{r,Struvite}$, $K_{r,Kstruvite}$ and $K_{r,Newberyite}$, the following output variables were considered: Ca^{2+}, Mg^{2+}, K^+ and alkalinity.
- $e_{N_k}(\theta)$: normalised difference between the measurement of each k variable and its corresponding simulation result.
- N_M: Adjustable parameter of the Bayes Theorem that is used to establish the relative weight for each parameter set.

Once in Step 5, Step 2 was double-checked because the amount of precipitated minerals can impact TS, pH and alkalinity.

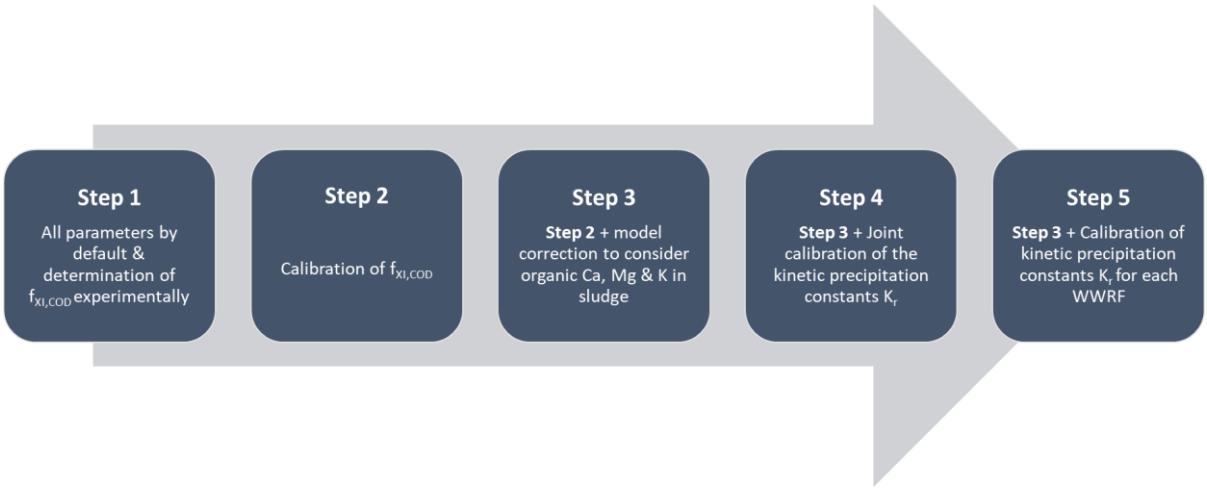

Figure 3.1 - Description of the different steps of the calibration procedure

3.5 Results and discussion

3.5.1 Differences between the two anaerobic digesters

Mixed and digested sludge characteristics of WRRFs 1 and 2 are reported in Tables 3.3 and 3.4. Table 3.4 presents the results obtained with data from the measurement campaigns, while Table 3.4 summarises historical data. Sludge from WRRF 2 has a solid concentration higher than WRRF 1 but a lower VS content, which results in a higher inert COD fraction ($f_{XI,COD}$). Mixed sludge from WRRF 1 has a higher content of P and P-PO_4 compared to WRRF 2. However, WRRF 2 is located in a region with hard water; consequently, very high content of Ca, Ca^{2+}, Mg, Mg^{2+} and inorganic carbon can be observed in its mixed and digested sludge. The anaerobic digester of WRRF 1 was operated with a hydraulic retention time (HRT) of 41 days which is twice as high as its design value (around 20 days) but volatile solids removal remained in the expected range of 45 – 65% (Metcalf & Eddy Inc. et al., 2003). Biogas production is in the conventional range according to biochemical methane potential values found in the literature (200 – 475 Nm^3 $kgVS^{-1}$) for both WRRFs (Guérin et al., 2017).

Table 3.3 - Characteristics of mixed and digested sludge determined during the dedicated measurement campaigns (mean value ± standard deviation (number of data)) for WRRFs 1 and 2

		WRRF 1		WRRF 2	
Parameter	**Unit**	**Mixed sludge**	**Digested sludge**	**Mixed sludge**	**Digested sludge**
COD	g COD g^{-1} VS	1.714 ± 0.03 (7)	1.524 ± 0.16 (9)	1.724 (1)	1.31 (1)
sCOD	g sCOD g^{-1} COD	0.041 ± 0.014 (9)	0.035 ± 0.012 (9)	0.17 (1)	0.40 (1)
$f_{XPR,COD}$	g COD protein g^{-1} pCOD	0.275 ± 0.036 (11)	NA	0.159 (1)	NA
$f_{XLI,COD}$	g COD lipids g^{-1} pCOD	0.063 (1)	NA	0.207 (1)	NA
$f_{XCH,COD}$	g COD carbohydrate g^{-1} pCOD	0.382 (1)	NA	0.209 (1)	NA
$f_{XI,COD}$	g COD inert g^{-1} pCOD	0.3 (1)	NA	0.43 (1)	NA
TKN	g TKN g^{-1} TSS	0.062 ± 0.006 (9)	0.12 ± 0.006 (11)	0.095 (1)	0.134 (1)
TP	g P g^{-1} TSS	0.015 ± 0.003 (10)	0.029 ± 0.004 (11)	0.010 (1)	0.019 (1)
Ca	g Ca g^{-1} TSS	0.026 ± 0.004 (4)	0.051 ± 0.012 (4)	NA	NA
Mg	g Mg g^{-1} TSS	0.0027 ± 0.0006 (4)	0.0048 ± 0.002 (4)	NA	NA
K	g K g^{-1} TSS	0.0054 ± 0.0018 (4)	0.011 ± 0.003 (4)	NA	NA
N-NH_4	mg L^{-1}	248 ± 48 (12)	1427 ± 48 (12)	817 (1)	1209 (1)
P-PO_4	mg L^{-1}	105 ± 48 (11)	62 ± 12 (11)	36.7 (1)	6 (1)
Ca^{2+}	mg L^{-1}	271 ± 59 (12)	67 ± 4.7 (12)	420 (1)	205 (1)
Mg^{2+}	mg L^{-1}	43 ± 5.9 (12)	18 ± 7 (12)	109 (1)	67 (1)
K^+	mg L^{-1}	154 ± 26 (12)	216 ± 18 (12)	76 (1)	102 (1)
Na^+	mg L^{-1}	144 ± 20 (12)	143 ± 35 (12)	145 (1)	157 (1)
Ca^{2+} : Mg^{2+}	mol Ca mol^{-1} Mg	3.84 ± 0.69 (12)	2.86 ± 0.9 (12)	2.34 (1)	1.86 (1)
Ca^{2+} : SIP	mol Ca mol^{-1} P	2.42 ± 1.40 (11)	0.86 ± 0.14 (11)	8.85 (1)	27.1 (1)

Table 3.4 - Characteristics of mixed and digested sludge and operating conditions of WRRF 1 and 2 from historical data (mean value ± standard deviation (number of data))

		WRRF 1		WRRF 2	
Parameter	**Unit**	**Mixed sludge**	**Digested sludge**	**Mixed sludge**	**Digested sludge**
Flowrate	$m^3\ d^{-1}$	77.2 ± 6.2 (487/487)		0.12 ± 0.07 (365/365)	
TS	$g\ L^{-1}$	49.4 ± 6.2 (136/149)	27.4 ± 3.2 (97/97)	42.4 ± 16 (143/153)	25.3 ± 11.4 (156/176)
VS	$g\ VS\ g^{-1}\ TS$	0.814 ± 0.038 (136/139)	0.688 ± 0.040 (95/95)	0.638 ± 0.097 (139/141)	0.543 ± 0.08 (154/174)
pH		6.04 ± 0.3 (475/487)	7.32 ± 0.08 (67/67)	7.16 ± 0.28 (228/228)	8.16 ± 0.28 (195/195)
Alkalinity	$mg\ CaCO_3\ L^{-1}$		4682 ± 459 (38/38)	5001 ± 1502 (175/175)	8216 ± 2095 (198/198)
Biogas	$Nm^3\ d^{-1}$		1730 ± 291 (486/487)		1.358 ± 0.51 (159/159)

3.5.2 Results of the calibration procedure

All simulation results of calibration steps are summarised in Table 3.5 and 3.6 for WRRF 1 and 2, respectively. Each step of the calibration procedure are discussed below.

Table 3.5 - Summary of simulation results for WRRF 1

		Experimental results	Step 1 *All parameters by default*	Step 2 *Calibrated $f_{XI,COD}$*	Step 3 *Step 2 + model correction to consider organic Ca, Mg and K*	Step 4 *Step 3 + joint calibration of Kr (same parameter set for both WRRFs)*	Step 5 *Step 3 + separated calibration of Kr (unique parameter set for each WRRF)*
Model parameters	*Unit*						
$f_{XI,COD}$	-	-	0.3	0.36	0.36	0.36	0.36
Kr,CaCO3	day^{-1}	-	0.5	0.5	0.5	0.3	21
Kr,MgCO3	day^{-1}	-	50	50	50	50	274
Kr,ACP	day^{-1}	-	350	350	350	350	270
Kr,Stru	day^{-1}	-	3000	3000	3000	3000	3000
Kr,KStru	day^{-1}	-	100	100	100	100	100
Kr,New	day^{-1}	-	0.05	0.05	0.05	0.05	0.05
Model variables							
TS	$g\ L^{-1}$	26.3 ± 1.8	25	27	27.3	27.3	27.4
VS	$g\ L^{-1}$	18.6 ± 1.5	15.8	17.9	17.9	17.9	17.9
pH	-	7.38 ± 0.08	7.43	7.41	7.38	7.38	7.38
Alkalinity	$mg\ CaCO_3\ L^{-1}$	5124 ± 254	5487	5178	4881	4879	4813
N-NH_4	$mg\ L^{-1}$	1427 ± 47	1530	1423	1424	1424	1424
Biogas	$Nm^3\ d^{-1}$	1836 ± 170	1980	1825	1827	1831	1831
P-PO_4	$mg\ L^{-1}$	62 ± 12	59	57	45	45	63
Ca^{2+}	$mg\ L^{-1}$	67 ± 5	54	59	79	79	67
Mg^{2+}	$mg\ L^{-1}$	18 ± 7	14	16	23	23	18
K^{+}	$mg\ L^{-1}$	215 ± 18	156	156	222	222	222
X_{ACP}	$mg\ L^{-1}$	-	728	715	775	776	687
X_{CACO3}	$mg\ L^{-1}$	-	2.9	3.5	8	5	121
X_{Stru}	$mg\ L^{-1}$	-	0	0	0	0	0
X_{MgCO3}	$mg\ L^{-1}$	-	97	91	298	298	316
X_{NEW}	$mg\ L^{-1}$	-	6.5	5.35	4	4	3
X_{KStru}	$mg\ L^{-1}$	-	0	0	0	0	0

Table 3.6 – Summary of simulation results for WRRF 2

		Experimental results	Step 1 *All parameter by default*	Step 2 *Calibrated $f_{XI,COD}$*	Step 3 *Step 2 + model correction to consider organic Ca, Mg and K*	Step 4 *Step 3 + joint calibration of Kr (same parameter set for both WRRFs)*	Step 5 *Step 3 + separated calibration of Kr (unique parameter set for each WRRF)*
Model parameters	*Unit*						
$f_{XI,COD}$	-	-	0.43	0.53	0.53	0.53	0.53
Kr,CaCO3	day^{-1}	-	0.5	0.5	0.5	0.3	0.12
Kr,MgCO3	day^{-1}	-	50	50	50	50	0.4
Kr,ACP	day^{-1}	-	350	350	350	350	58
Kr,Stru	day^{-1}	-	3000	3000	3000	3000	3000
Kr,KStru	day^{-1}	-	100	100	100	100	100
Kr,New	day^{-1}	-	0.05	0.05	0.05	0.05	0.05
Model variables							
TS	$g\ L^{-1}$	41 ± 2.4	38.4	41.3	41.3	41.3	41
VS	$g\ L^{-1}$	21.5 ± 1.1	17.7	20.5	20.4	20.5	20.5
pH	-	7.85 ± 0.02	7.87	7.87	7.85	7.85	7.86
Alkalinity	$mg\ CaCO_3\ L^{-1}$	10090 ± 439	10027	9801	9519	9677	9830
$N\text{-}NH_4$	$mg\ L^{-1}$	1208 ± 87	1319	1220	1213	1220	1220
Biogas	$Nm^3\ d^{-1}$	2.07 ± 0.23	2.71	2.35	2.32	2.30	2.30
$P\text{-}PO_4$	$mg\ L^{-1}$	6 ± 2	3	3	3	2	6
Ca^{2+}	$mg\ L^{-1}$	207 ± 42	119	118	130	168	239
Mg^{2+}	$mg\ L^{-1}$	67 ± 3	6	6	7	7	63
K^{+}	$mg\ L^{-1}$	102	75	75	115	115	115
X_{ACP}	$mg\ L^{-1}$	-	1242	1247	1249	1253	1256
X_{CACO3}	$mg\ L^{-1}$	-	596	599	631	534	351
X_{Stru}	$mg\ L^{-1}$	-	0	0	0	0	0
X_{MgCO3}	$mg\ L^{-1}$	-	341	341	514	513	333
X_{NEW}	$mg\ L^{-1}$	-	39	39	39	43	14
X_{KStru}	$mg\ L^{-1}$	-	0	0	0	0	0

3.5.2.1 Simulation with parameters by default and calibration of $f_{XI,COD}$ (Steps 1 and 2)

For Steps 1 and 2, two periods were considered: the calibration, which corresponds to the measurement campaigns, and a validation period. The model was run first at steady state over the calibration period with the parameters set by default and using the fractionation of the model input components as described in section 2.5. Simulation outputs using these predetermined COD fractionation with $f_{XI,COD}$ = 0.3 for WRRF 1 and $f_{XI,COD}$ = 0.43 for WRRF 2 and resulted in an underestimation of TS and VS concentration in digested sludge as well as an overestimation of biogas production for both digesters. These results are in agreement with other studies that also used BMP results to define $f_{XI,COD.}$ and needed to increase this parameter at full-scale (Baquerizo et al., 2021; Mendes et al., 2015; Souza et al., 2013). In the present study, $f_{XI,COD}$ was increased from 0.30 to 0.36 (+20%) for WRRF 1 and from 0.43 to 0.53 (+23%) for WRRF 2 using the fitness function described in 2.6 and presented in Figure 3.2.

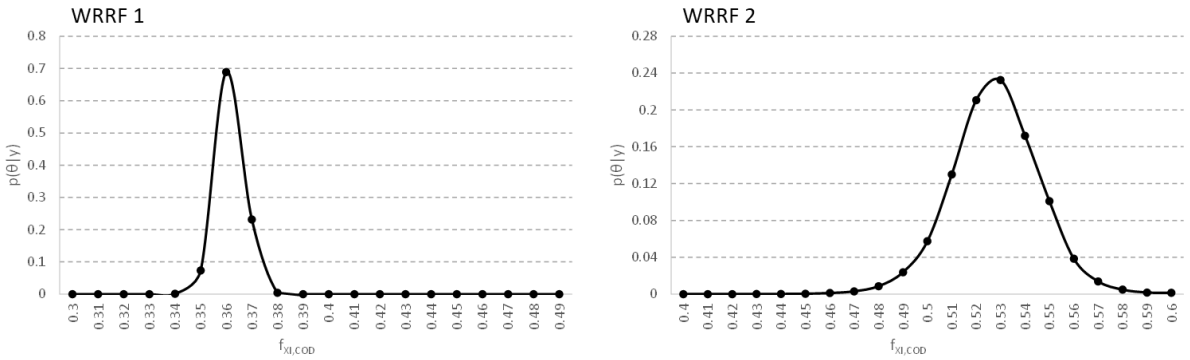

Figure 3.2 - Posterior probability density function according to the value of $f_{XI,COD}$ for both WRRFs

The model calibrated at steady state showed also good results under dynamic conditions for TS, VS in digested sludge as well as for biogas production for the overall validation period (Figure 3.3 and Figure 3.4). The model described the global trend of all measured variables for both digesters. For WRRF 1, the model underestimates TS and VS concentrations from day 200. For WRRF 2, the model slightly overestimated TS and VS concentrations at the beginning of the period (day 1 – 200). Similar results were reported by Otuzalti et al. (2018) and could be attributed to a variation of the stoichiometric parameter $f_{XI,COD}$ over a long-term period.

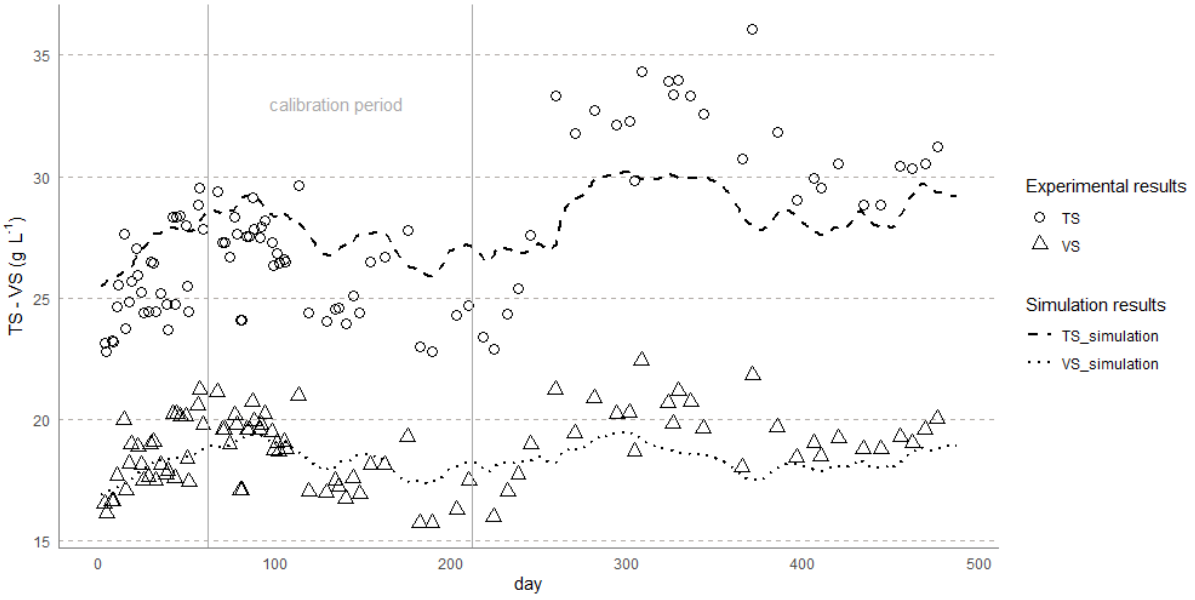

Figure 3.3 - Comparison of full-scale AD data and simulation results for the entire period for WRRF

Figure 3.4 - Comparison of full-scale AD data and simulation results for the entire period for WRRF2

3.5.2.2 Model modification to consider organic Ca, K, Mg in sludge (Step 3)

Among the 6 minerals included in the model, only ACP, $CaCO_3$, Newberyite and $MgCO_3$ were produced during AD according to model results. The release of K^+ in the digester, as well as Ca^{2+} and Mg^{2+}, is well-known and expected when having a sludge from enhanced biological phosphorus removal because of the decay of polyphosphates (X_{PP}) in anaerobic conditions (Martí et al., 2008). Despite the fact that WRRFs 1 and 2 do not have biological phosphorus removal treatment, a release of K^+ was noted. Indeed, the model does not take into account the Ca, Mg and K incorporated in the biomass (X_N, X_H, X_{SU}, X_{AA}, X_{FA}, X_{C4}, X_{PRO}, X_{AC}, X_{H2}, X_{PAO}, X_{PHA}, X_P) unlike other models (Barat et al., 2013; Wild et al., 1997). Consequently, calibrating the precipitation parameters could compensate the release of Ca^{2+}

and Mg^{2+} but not K^{+} as there is no K-Struvite present in the experimental conditions simulated. Therefore, a modification of the model was applied to take into account organic Ca, Mg and K in sludge according to the ratios proposed by Barat et al. (2009): 0.003 mg (K) mg VSS^{-1}; 0.004 mg (Mg) mg VSS^{-1}; 0.002 mg (Ca) mgVSS^{-1}. Table 3.7 presents the resulting ionic balance.

Table 3.7 – Mass balance of the cations in both anaerobic digesters

	WRRF 1	**WRRF 2**
Ca_{org} released during AD	44 mg L^{-1}	25 mg L^{-1}
Ca precipitated during AD (according to experimental results)	248 mg L^{-1}	238 mg L^{-1}
Mg_{org} released during AD	88 mg L^{-1}	51 mg L^{-1}
Mg precipitated during AD (according to experimental results)	115 mg L^{-1}	93 mg L^{-1}
K_{org} release during AD	66 mg L^{-1}	38 mg L^{-1}
K precipitated during AD (according to experimental results)	0 mg L^{-1}	0 mg L^{-1}

For WRRF 1, the simulations provided good results for all ions, but kinetic constants for precipitation could be calibrated to gain accuracy in predicting the model output variables: Ca^{2+}, Mg^{2+} and P-PO_4. For WRRF 2, simulations gave satisfactory results for P-PO_4 (± 5 mg/L) and K^{+} but the model significantly underestimated both Ca^{2+} and Mg^{2+} concentrations, calling for an adjustment of the parameters that impact those concentrations.

3.5.2.3 Joint calibration of $K_{r,CaCO3}$, $K_{r,ACP}$, $K_{r,Stru}$, $K_{r,KStru}$, $K_{r,MgCO3}$, $K_{r,New}$ for the two anaerobic digesters (Step 4)

To calibrate the kinetic precipitation constants $K_{r,CaCO3}$, $K_{r,MgCO3}$, $K_{r,ACP}$, $K_{r,Struvite}$, $K_{r,Kstruvite}$ and $K_{r,Newberyite}$ the Bayesian Monte Carlo techniques were applied. For Monte Carlo simulations, the range of values for each parameter (Table 3.8) was set according to the literature and to obtain a realistic range of Ca^{2+}, Mg^{2+} and P-PO_4 concentrations according to Devos et al. (2023).

Table 3.8 – Range of values applied for Monte Carlo simulations

Precipitation kinetic constants	Range of values (day^{-1})
$K_{r,CaCO3}$	0 – 50
$K_{r,MgCO3}$	0 – 500
$K_{r,ACP}$	0 – 700
$K_{r,Struvite}$	0 – 6000
$K_{r,Kstruvite}$	0 – 200
$K_{r,Newberyite}$	0 – 0.1

From the results of Monte Carlo simulations of this joint calibration procedure, the posterior probability density function showed a relation only with $K_{r,CaCO3}$ but not with $K_{r,MgCO3}$, $K_{r,ACP}$, $K_{r,Struvite}$, $K_{r,Kstruvite}$ nor $K_{r,Newberyite}$. Therefore, Figure 3.5 present $K_{r,CaCO3}$ result with the competing minerals ($K_{r,MgCO3}$ and $K_{r,ACP}$).

Figure 3.5 shows the best parameter sets to fit Ca^{2+}, Mg^{2+}, P-PO_4 and alkalinity concentrations for both anaerobic digesters at the same time using the fitness function presented in the section 2.5. The size of the spheres represents the value of the posterior probability density function; the higher the value, the best the parameter set. From these figures, $K_{r,CaCO3}$ can be identified with an optimum value of 0.16 when selecting the best parameter set.

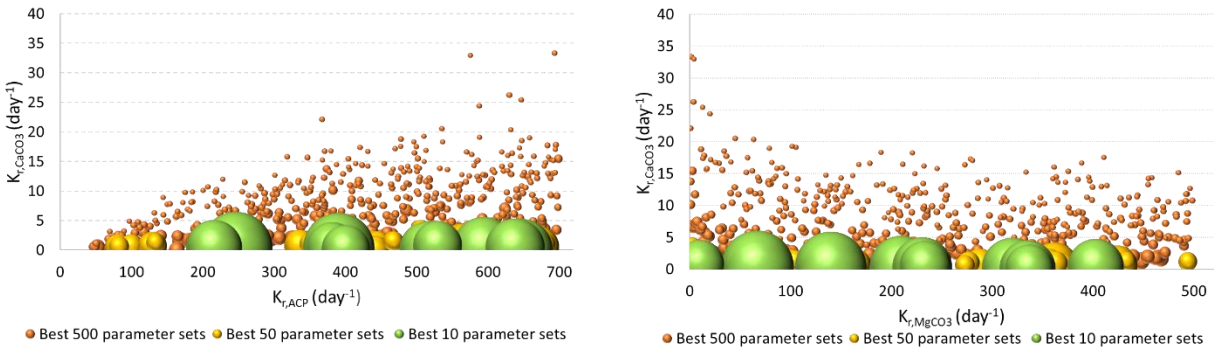

Figure 3.5 - Repartition of the posterior probability density function according to the value of the kinetic constants Kr for both WRRF 1 and WRRF 2

The simulation results obtained with the best set of parameters slightly improve the prediction for Ca^{2+} concentration in WRRF 2 without deteriorating WRRF 1 results. However, the optimisation with the joint parameter set was marginal and there were no improvements for the prediction of P-PO_4 and Mg^{2+}. These findings showed the inability to find a single reliable parameter set for the two different anaerobic digesters. The precipitation model probably misses some relevant mechanisms. This hinders the possibility of obtaining a reliable parameter set that can work for different application cases. Therefore, site-specific calibration of the precipitation kinetic constants is needed for reliable predictions. Simulation with default parameter values for all K_r gave more reliable results for WRRF 1 compared to WRRF 2. This is more likely due to the large differences in initial water hardness

(concentration of Ca^{2+} and Mg^{2+} in the initial sludge) and therefore to the initial saturation extent but also to different mixing conditions in both digesters (different reactor sizes).

3.5.2.4 Separate Calibration of $K_{r,CaCO3}$, $K_{r,ACP}$, $K_{r,Stru}$, $K_{r,KStru}$, $K_{r,MgCO3}$, $K_{r,New}$ for each anaerobic digester (Step 5)

The Bayesian Monte Carlo technique was applied again to each anaerobic digester in order to find the best $K_{r,CaCO3}$, $K_{r,ACP}$, $K_{r,Stru}$, $K_{r,KStru}$, $K_{r,MgCO3}$, $K_{r,New}$ values specific for each digested sludge concentrations of Ca^{2+}, Mg^{2+} and P-PO_4. The same ranges of values as for the joint calibration procedure (step 4) were used (Table 3.8). For both WRRFs, only the values of $K_{r,CaCO3}$, $K_{r,ACP}$, $K_{r,MgCO3}$ have an impact on the posterior probability density function. Thus, the results on $K_{r,Stru}$, $K_{r,KStru}$, and $K_{r,New}$ were not shown. Figure 3.6 and 3.7 represent the values of the posterior probability density function according to $K_{r,CaCO3}$, $K_{r,MgCO3}$ and $K_{r,ACP}$ for WRRF 1 and WRRF 2, respectively.

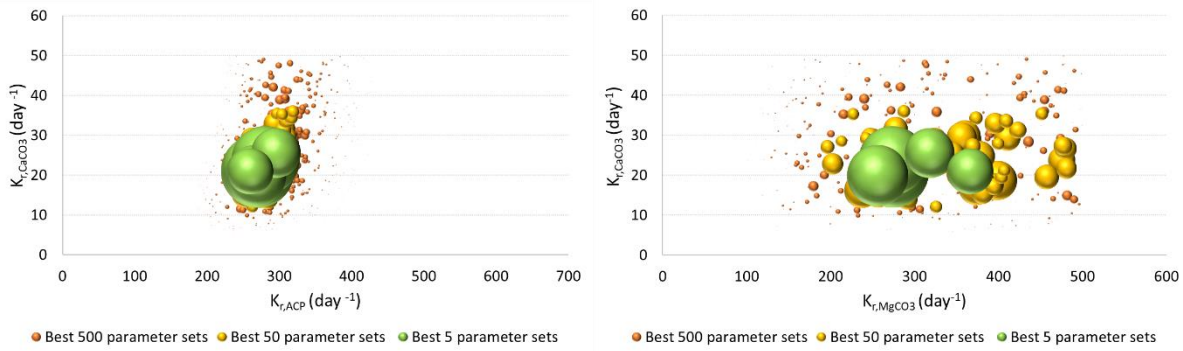

Figure 3.6 – Repartition of the posterior probability density function according to the values of the kinetic constants for precipitation in the case of WRRF 1

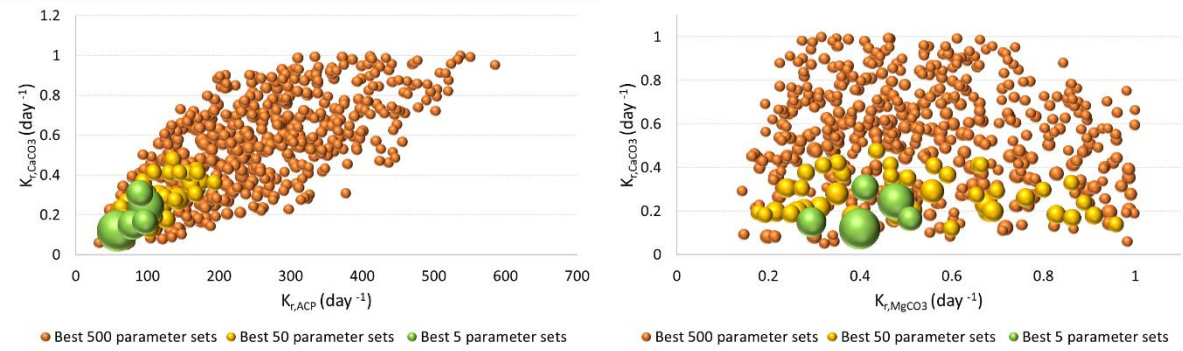

Figure 3.7 - Repartition of the posterior probability density function according to the values of the kinetic constants for precipitation in the case of WRRF 2

For WRRF 1, the best parameter set is clearly identifiable with the representation of the best 5 parameter sets in Figure 3.6. Simulation results with the best parameters set showed that the value of $K_{r,ACP}$ was slightly changed from 350 to 270, the value of $K_{r,CaCO3}$ was increased from 0.5 to 21 and $K_{r,MgCO3}$ from 50 to 274. For WRRF 2, all precipitation constants $K_{r,CaCO3}$, $K_{r,MgCO3}$ and $K_{r,ACP}$ needed to be reduced in a high extent: $K_{r,ACP}$ from 350 to 58, $K_{r,MgCO3}$ from 50 to 0.4 and $K_{r,CaCO3}$ from 0.5 to 0.12. For

both WRRFs, ACP was the mineral formed in the highest quantity followed by $CaCO_3$ and $MgCO_3$ (Tables 3.5 and 3.6).

In both WRRFs, the values of $K_{r,CaCO3}$ and $K_{r,MgCO3}$ needed to be calibrated; they are directly linked to the water hardness. Future research is required to understand why the values of $K_{r,CaCO3}$ and $K_{r,MgCO3}$ seem to be correlated to initial water hardness and to what extend other variables such as reactor geometry or mixing conditions may affect their value. Nevertheless, the model with default value gave more reasonable results for WRRF 1 which has concentration of Ca^{2+}, Mg^{2+} and alkalinity in digested sludge in the conventional range: 1 – 90 mg L^{-1} for S_{Mg} and 10 – 140 mg L^{-1} for S_{Ca} and 1000 – 6300 mg $CaCO_3$ L^{-1} for alkalinity (Devos et al., 2023). Particular attention must be devoted when the concentrations in digested sludge are outside this range, in order to reduce the uncertainty induced by $K_{r,crys}$ values.

3.6 Conclusion

An anaerobic digestion model with multiple mineral precipitation was calibrated for two case studies by adjusting a limited number of parameters. The main conclusions are as follows:

1) The value of the stoichiometric parameter $f_{XI,COD}$ obtained experimentally with BMP needs to be increased by approximatively 25% to fit TS, VS, biogas production, N-NH_4 and alkalinity concentrations in the ADs.

2) A modification of the original model to include a fraction of organic K, Ca and Mg in the biomass allowed to obtain reliable K^+ concentration in digested sludge. The release of ions from biomass was hidden for Ca^{2+} and Mg^{2+} due to the precipitation of these ions. This correction should be systematically included in the future if a good prediction of K^+, Ca^{2+} and Mg^{2+} is sought.

3) A Bayesian Monte Carlo technique was applied to identify which precipitation constants K_r must be adjusted to fit P-PO_4, Ca^{2+} and Mg^{2+} concentrations in digested sludge and estimate their values. $K_{r,CaCO3}$, $K_{r,MgCO3}$ & $K_{r,ACP}$ needed to be adjusted separately for each digester.

4) The WRRF with lower Ca^{2+}, Mg^{2+} and inorganic carbon concentrations in mixed sludge showed more reliable simulation results with precipitation kinetic constants by default. Nevertheless, estimated P-PO_4 concentrations were in the good order of magnitude for both anaerobic digesters without any calibration of the precipitation kinetic constants.

The calibration was necessary to reduce the uncertainty linked to the precipitation kinetics K_r in order to use this model in future scenario analysis to optimise P recovery in the next chapter. Results show the importance of calibrating the model especially when having high water hardness. This study highlights a link between the need for calibration and the initial Ca, Mg and inorganic carbon related to the water hardness but more experimental data and validation of AD model with multiple mineral precipitation would be required to confirm this observation. In addition, other operational conditions can also impact K_r as mixing and shear rates, pH, temperature and the presence of impurities. The variability of these kinetic constants leads to high uncertainty in simulation of precipitation reactions. More experimental data, especially on ion concentrations in the digesters, will be needed in the future in order to assign ranges of values for precipitation parameters $K_{r,crys}$ in relation to operating conditions.

CHAPTER 4 - EVALUATION OF SIDESTREAM MANAGEMENT FOR DIFFERENT SLUDGE CHARACTERISTICS AND WATER HARDNESS LEVEL

4.1 Abstract

The increasing number of anaerobic digesters installed in water resource recovery facilities as well as the interest for centralised anaerobic digesters integrating sludge from surrounding facilities has raised questions about sidestream management. The recovery of phosphorus in the form of struvite in anaerobic digestion sidestreams has been studied in the literature for WRRFs with enhanced biological phosphorus removal without paying particular attention to the effect of the water hardness level (concentration of Ca^{2+} and Mg^{2+}). The scenario analysis presented in this chapter aims to study the impact of different sludge characteristics (with varying PO_4 content and P fractionation mainly) and different levels of water hardness on the quantity of phosphorus in sidestreams by using a validated anaerobic digester model. The scenario analysis included an assessment of the operational costs and carbon footprint of the anaerobic digestion process, the struvite recovery process, and the biological treatment of nitrogen by nitrification/denitrification and partial nitritation/anammox in one-stage and two-stage configurations. Results show that the amount of phosphate in digested sludge is impacted by both the type of phosphorus treatment applied and the water hardness level. Indeed, even if the sludge from enhanced biological phosphorus removal induces the highest phosphate concentration in sidestreams, the quantity is divided by 2.4 between sludge with low (concentration in the sludge of Ca^{2+} = 50 mg/L and Mg^{2+} = 20 mg/L) and high (Ca^{2+} = 410 mg/L and Mg^{2+} = 166 mg/L) water hardness levels. For low and medium water hardness levels, the installation of a struvite recovery process can be viable for sludge from WRRF without specific phosphorus treatment because the phosphate concentration can be above 50 mg/L. These findings are explained by the precipitation during the aerobic digestion process encouraged by high concentrations of calcium, magnesium and inorganic carbon. For nitrogen treatment, the partial nitritation/anammox process can reduce the quantity of energy needed for the aeration but may also generate high N_2O emissions especially in the two-stage configuration. With median emission factors from scientific literature, the N_2O emissions of the 2-stage partial nitritation/anammox process is 3 and 3.5 times higher than respectively, nitrification/denitrification and 1-stage partial nitritation/anammox, which can jeopardise its benefits.

4.2 Highlights

- The quantity of phosphate in sidestreams from anaerobic digestion depends on the type of phosphorus treatment applied and on water hardness
- The anaerobic digestion of sludge with biological phosphorus removal results in higher phosphate concentration in sidestreams compared to chemical phosphorus removal and no specific phosphorus treatment
- For one type of phosphorus treatment the quantity of phosphate can be divided by 2 between low and high water hardness
- The carbon footprint of partial nitritation/anammox in the 2-stage configuration results in high N_2O emissions

4.3 INTRODUCTION

Anaerobic digestion (AD) has been proved to be an efficient process to reduce the volume of sludge as well as to valorise carbon from sewage sludge (Appels et al., 2008). The obtained digested sludge is dewatered and results in the production of sidestreams with high nitrogen and phosphorus content (Wild et al., 1997). Since the beginning of AD implementation in water resource recovery facilities (WRRFs), sidestreams have been pointed out because additional operational costs and a decrease in the effluent quality can be observed (Fujimoto et al., 1991; Grulois et al., 1993; Teichgräber and Stein, 1994). The impacts of anaerobic digestion sidestreams can be limited if the WRRF has been designed considering nitrogen and phosphorus flows from these streams. However, when an existing WRRF wants to implement an anaerobic digestion process, sidestream management can become a real challenge, especially if the WRRF operates close to its nominal capacity. In addition, the implementation of a centralised AD can be considered in some regions in order to process the sludge of nearby WRRFs on a single location. Such an installation emphasises the question of sidestream management as higher nitrogen and phosphorus mass flow should be treated in a same WRRF.

To upgrade the treatment capacity without expanding WRRF reactors, several sidestream processes have been developed for nitrogen or phosphorus treatment (Van Loosdrecht and Salem, 2006). The main biological processes for the treatment of nitrogen in sidestreams includes: nitrification-denitrification, nitritation-denitritation, partial nitritation/anammox, bioaugmentation and algae production (Eskicioglu et al., 2018). To initiate the recovery of nitrogen and phosphorus, physico-chemical processes are also considered: struvite precipitation, ammonia stripping, membrane filtration, electrodialysis, bio-electrochemical system, ammonia and phosphate sorption are the most investigated processes (Guilayn et al., 2020; Vaneeckhaute et al., 2017; Ye et al., 2018). Nevertheless, only partial nitritation/anammox (PN/anammox), nitrification/denitrification, nitritation/denitritation and phosphorus recovery as struvite have been implemented at full scale.

To assess the relevance of implementing struvite recovery or PN/anammox, different scenario analyses have been presented in the literature and are listed in Table 4.1. These scenario analyses have been carried out using plant wide models that couple biokinetics with a physicochemical framework.

Table 4.1 – Literature review on scenario analyses including sidestream management

Reference	WRRF	Scenarios	Performance criteria
Flores-Alsina et al. (2021)	Full scale study with biological COD, N and P removal + AD (Plant at 50% of its capacity)	Sludge line optimisation after the implementation of centralised AD on one full scale case study. Evaluation of scenarios with: thermal hydrolysis, struvite recovery, partial nitritation/anammox	Operating costs Effluent quality Quantity of struvite recovered
Roldán et al. (2020)	Full scale study with biological COD, N and P removal + AD	Evaluation of different scenarios with recovery of struvite upstream or downstream the AD	Operating costs Effluent quality Quantity of struvite recovered Life cycle analysis Life cycle cost analysis
Lizarralde et al. (2019)	Full scale study with biological COD and P removal + AD	Evaluation of the relevance of phosphorus recovery in the form of struvite	Operating costs Effluent quality Quantity of struvite recovered
Vaneeckhaute et al. (2019, 2018b, 2018a)	Virtual case study of AD to treat sludge and waste	Evaluation of struvite recovery and ammonia stripping and absorption processes	Operating costs Quantity of struvite recovered
Fernandez-Arevalo et al. (2017)	Virtual case study (benchmark simulation modelling – BSM): BSM1 with biological COD/N removal + AD	Evaluation of scenarios with: thermal hydrolysis and partial nitritation/anammox	Operating costs Effluent quality
Solon et al. (2017)	Virtual case study (benchmark simulation modelling – BSM): BSM2 with biological COD/N/P removal + AD	Evaluation of the relevance of phosphorus recovery in the form of struvite	Operating costs Effluent quality Quantity of struvite recovered
Martí et al. (2017)	Full scale study with biological COD, N and P removal + AD	Evaluation of different scenarios with recovery of struvite upstream or downstream the AD	Operating costs Effluent quality Quantity of struvite recovered

In Table 4.1, the literature review shows that the scenario analyses were carried out on similar case studies; all studies with struvite recovery process have enhanced biological phosphorus removal (Bio-P) and there is no analysis for other types of phosphorus treatment. For all case studies that investigated struvite recovery, the process was found relevant to decrease operating costs and to improve effluent quality as well as to provide P fertiliser. For example, total phosphorus concentration in the effluent decreased from 6.4 to 1.5 mg/L after the implementation of a struvite reactor on the BSM2 plant configuration (Solon et al., 2017). In a scenario analysis applied to a full case study, total phosphorus concentration in the effluent decreased from 12 mg/L to 2 mg/L with struvite recovery for a centralised AD with thermal hydrolysis pre-treatment step (Flores-Alsina et al., 2021). Similarly, in La Sur WRRF, the implementation of a struvite reactor could reduce the consumption of iron dosage by 50% (Lizarralde et al., 2019). However, in the different application cases, there is no information on the quantity of calcium throughout the WRRF while calcium can affect the quantity of phosphate in digested sludge. Indeed, Vaneeckhaute et al. (2018b) and Wild et al. (1997) found that the amount of calcium in sludge induced higher precipitation of ACP in the digester and therefore lowered potential P recovery in sidestreams. This was also observed in the previous chapter of the thesis where the AD model was validated to correctly predict phosphorus, calcium and magnesium content in sidestreams.

Few studies evaluated the implementation of biological nitrogen treatment and more specifically, the PN/anammox process and when assessed, the process was not found beneficial to the effluent quality because the main wastewater treatment line had the capacity to treat the

supplemental nitrogen load from sidestreams (Fernández-Arévalo et al., 2017a). The lack of inclusion of PN/anammox processes in scenario analysis may be due to the relative higher N_2O emissions that can have a negative impact on the carbon footprint of the facilities (Hauck et al., 2016) but also to the relative new development and applications of N_2O models to full-scale plants (Spérandio et al., 2022).

Assessing the impacts of implementing a centralised anaerobic digester have been studied in the work of Flores-Alsina et al. (2021) but the same type of sludge was considered for the surrounding facilities without including the variability of phosphorus treatment or different ion concentrations.

Finally, except for one case study who integrates life cycle assessment (LCA), there is no carbon footprint evaluation of the different sidestream processes while Solon et al. (2019) for example highlighted the need to include some performance criteria related to environmental impacts and the quality of the recovered product.

A model evaluation of a centralised anaerobic digester operated with sludge from different types of phosphorus treatment and for different Ca, Mg and SIC concentration was carried out. The management of the resulting streams by nitrogen treatment processes (nitrification/denitrification and PN/anammox) and a struvite recovery process was discussed considering both their operational costs and carbon footprint. Ultimately, the findings can serve as a basis for the choice of sidestream processes for a broader spectrum of sludge characteristics compared to literature.

4.4 Material and Methods

4.4.1 Case study description

The case study is based on the volume of sludge produced by an existing large WRRF having a primary settler and activated sludge lines for COD and N removal. Both sludge are thickened, then mixed and dewatered. This WRRF plans to implement a mesophilic AD to process both primary and biological sludge. This digester will operate at 50% of its capacity for a sludge retention time (SRT) of 44 days. In a second phase, the WRRF is considering to process the sludge of the nearby facilities to reach the anaerobic digester nominal capacity of 100% (corresponding to an SRT of 22 days). The surrounding facilities treat phosphorus differently: without specific P treatment, with a combination of biological and chemical phosphorus removal (Bio+Chem P) or by chemical phosphorus removal only (Chem P). Then, the digested sludge will be dewatered to reach a concentration of 250 g/L.

4.4.2 Definition of the scenarios

The first scenario S01 (50%_WH_High) explores the impacts of sidestream management when treating only internal sludge. The sludge in S01 is mixed primary and biological sludge without specific P treatment and the concentrations of Ca^{2+}, Mg^{2+} and soluble inorganic carbon (SIC) are high.

The different levels of Ca^{2+}, Mg^{2+} and soluble inorganic carbon (SIC) are presented in Table 4.2 and have been defined based on literature data (Astals et al., 2013; Fisgativa et al., 2020a, 2018; Metcalf & Eddy Inc. et al., 2003). The molar ratio Ca:Mg was set at 1.5 for the 3 levels.

Table 4.2 - Water hardness levels and associated concentration of Ca^{2+}, Mg^{2+} and soluble inorganic calcium (SIC)

Water hardness levels	Ca^{2+} (mg/L)	Mg^{2+} (mg/L)	SIC (mg/L)
Low	50	20	50
Medium	230	93	350
High	410	166	1000

Scenarios S02 (100%_WH_High), S03 (100%_Bio+ChemP_WH_High) and S04 (100%_ChemP_WH_High) look at the impacts of adding external sludge from nearby facilities and mix them with internal sludge in order to reach 100% capacity of the digester:

- The external sludge used in S02 (100%_WH_High) are considered to show the same characteristics as the ones of S01 (50%_WH_High) without phosphorus treatment and with high concentrations of Ca^{2+}, Mg^{2+} and SIC.
- The sludge in S03 (100%_Bio+ChemP_WH_High) is a mixture of primary and biological sludge with combined enhanced biological phosphorus (Bio-P) and chemical P (Chem-P) removal. The concentrations of Ca^{2+}, Mg^{2+} and SIC are high.
- The sludge in S04 (100%_ChemP_WH_High) is a mixture of primary and biological sludge with Chem-P removal. The concentrations of Ca^{2+}, Mg^{2+} and SIC are high.

Scenarios S05 (50%_WH_Medium), S06 (100%_WH_Medium), S07 (100%_Bio+ChemP_WH_Medium) and S08 (100%_ChemP_WH_Medium) repeat scenarios S01, S02, S03 and S04 but with medium Ca^{2+}, Mg^{2+} and SIC concentrations. Scenarios S09 (50%_WH_Low), S10 (100%_WH_Low), S11 (100%_Bio+ChemP_WH_Low) and S12 (100%_ChemP_WH_Low) repeat scenarios S01, S02, S03 and S04 but with low Ca, Mg and SIC concentrations. Table 4.2 summarises the different scenarios with their different sludge mixture and water hardness levels.

Table 4.3 – Summary of the different scenarios evaluated

Anaerobic Digester	External sludge	High Ca/Mg/SIC	Medium Ca/Mg/SIC	Low Ca/Mg/SIC
Conventional AD (50% capacity)				
Internal sludge (Mixed sludge - No specific P treatment)	None	S01 (50%_WH_High)	S05 (50%_WH_Medium)	S09 (50%_WH_Low)
Centralised AD (100% capacity)	Mixed sludge - No specific P treatment	S02 (100%_WH_High)	S06 (100%_WH_Medium)	S010 (100%_WH_Low)
Internal sludge (Mixed sludge - No specific P treatment) + External sludge	Mixed sludge – Combined Bio-P & Chem P removal	S03 (100%_Bio+ChemP_WH_High)	S07 (100%_Bio+ChemP_WH_Medium)	S11 (100%_Bio+ChemP_WH_Low)
	Mixed sludge – chemical P treatment	S04 (100%_ChemP_WH_High)	S08 (100%_ChemP_WH_Medium)	S12 (100%_ChemP_WH_Low)

4.4.3 Sludge characteristics

The 12 evaluated scenarios are based on the characteristics of 3 types of mixed sludge: without specific phosphorus treatment, with enhanced biological phosphorus removal (Bio-P) coupled with chemical phosphorus removal (Bio+Chem-P) and only with chemical removal (Chem-P).

The characteristics of the different sludge have been obtained from a steady-state simulation of a conventional WRRF with a primary settler and an activated sludge unit for carbon and nutrient removal. The simulations were run for 3 different types of phosphorus treatment while maintaining the same influent characteristics and the performance of nitrogen treatment, maintaining an identical sludge retention time for the aerobic and anoxic zone. The performance of the clarifier has also been kept constant and the effluent TSS concentration was fixed to 15 g/m^3. The pH of the mixed sludge have been defined with mean ratios from literature (Astals et al., 2013; de Gracia et al., 2009; Fisgativa et al., 2020b, 2018; Metcalf & Eddy Inc. et al., 2003). For simulation with biological and chemical or only with chemical phosphorus removal, the dosage of iron chloride was set to reach a total phosphorus concentration in the effluent of 1 g/m^3. Table 3 provides influent and effluent composition as well as reactor volume and sludge recycling flow. Table 4 shows the sludge characteristics obtained. The three different mixed sludge were thickened to a same total suspended solids concentration of 50 g/L.

Table 4.4 - Design of the WRRF used in the simulation to obtain sludge characteristics

	Simulation without P treatment	Simulation with Bio-P and Chem-P removal	Simulation with Chem-P removal
Influent		Flow = 24 000 m^3/day COD = 500 g/m^3 TKN = 50 g/m^3 TP = 7.1 g/m^3	
Primary settler		TSS removal = 60% TSS out = 5000 g/m3	
Activated sludge unit	vol. anoxic zone = 3000 m^3 vol. aerobic zone = 7000 m^3 sludge recirculation = 100%	vol. anoxic zone = 3000 m^3 vol. aerobic zone = 7000 m^3 vol. anaerobic zone = 2000 m^3 sludge recirculation = 100% molar ratio Fe:P = 0.7	vol. anoxic zone = 3000 m^3 vol. aerobic zone = 7000 m^3 vol. anaerobic zone = 2000 m^3 sludge recirculation = 100% molar ratio Fe:P = 1.6
Effluent	TSS = 15 g/m^3 COD = 35 g/m^3 TN = 10 g/m^3 TP = 5.9 g/m^3	TSS = 15 g/m^3 COD = 35 g/m^3 TN = 10 g/m^3 TP = 1 g/m^3	TSS = 15 g/m^3 COD = 35 g/m^3 TN = 10 g/m^3 TP = 1 g/m^3

Table 4.5 – Characteristics of feed sludge used in the different scenarios

	Unit	Mixed sludge – No P treatment	Mixed sludge – Bio-P and Chem-P removal	Mixed sludge – Chem-P removal
TSS	g/L	50	50	50
VSS:TSS	gVSS/gTSS	0.79	0.74	0.70
COD:VSS	gCOD/gVSS	1.52	1.51	1.46
TKN:VSS	gTKN/gVSS	0.0661	0.0657	0.0655
TP:VSS	gTP/gVSS	0.013	0.0384	0.0343
N-NH4:TKN	gN-NH4/gTKN	0.0655	0.0655	0.0653
P-PO4:TP	gP-PO4/gTP	0.25	0.0767	0.0766
pH	-	6.2	6.2	6.2
Fractionation total COD				
Protein - $f_{XPR,COD}$	g/gCOD	0.095	0.094	0.095
Lipids - $f_{XLI,COD}$	g/gCOD	0.132	0.131	0.132
Carbohydrates - $f_{XCH,COD}$	g/gCOD	0.108	0.107	0.108
Particulate inert - $f_{XI,COD}$	g/gCOD	0.41	0.40	0.41
Poly-hydroxy-alcanoates - $f_{XPHA,COD}$	g/gCOD	0.0003	0.0019	0.0003
Phosphorus accumulating bacteria - $f_{XPAO,COD}$	g/gCOD	0.0004	0.0625	0.0004
Heterotroph bacteria - $f_{XH,COD}$	g/gCOD	0.23	0.17	0.23
Nitrifying bacteria - $f_{XN,COD}$	g/gCOD	0.017	0.016	0.017
Volatile fatty acids - $f_{VFA,COD}$	g/gCOD	0.0016	0.0016	0.0016
Soluble biodegradable - $f_{SS,COD}$	g/gCOD	0.0047	0.0047	0.0047
Soluble inert - $f_{SSI,COD}$	g/gCOD	0.0029	0.0029	0.0029

Figure 4.1 represents the fractionation of phosphorus for the different types of sludge. Obviously, the mixed sludge without P treatment is characterised by the high fraction of P-PO_4 compared to the sludge with P treatment. The mixed sludge with Bio-P and Chem-P contains a high

polyphosphate fraction (XPP) due to the presence of polyphosphate accumulating organisms from the Bio-P sludge. The mixed sludge only with Chem-P removal shows the highest iron phosphate fraction (XFEPO4).

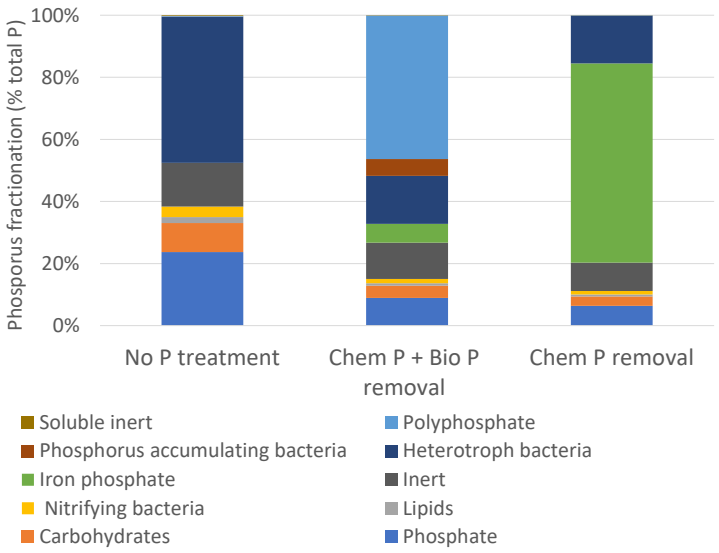

Figure 4.1 – Phosphorus fractionation for the different types of sludge

4.4.4 AD Model

The digesters for the different scenario analysis were simulated using the mathematical model detailed in Grau et al. (2007) and Lizarralde et al. (2015) and implemented in WEST. This model is the same as the one used in Chapter 3 and includes biochemical, multiphase and chemical transformations. The precipitation model includes the following minerals: calcium carbonate ($CaCO_3$), magnesium carbonate ($MgCO_3$), amorphous calcium phosphate (ACP) ($Ca_3(PO_4)_2$), struvite ($MgNH_4PO_4.6H_2O$), K-struvite ($MgKPO_4.6H_2O$) and newberyite ($MgHPO_4.3H_2O$). Iron phosphate is included in sludge characteristics but no further precipitation or dissolution were included in the anaerobic digester model. Default values taken from ADM 1 were used for all kinetic parameters since they were originally determined for the digestion of municipal wastewater sludge (Batstone et al., 2002) except for the precipitation kinetic parameters $K_{r,CaCO3}$, $K_{r,MgCO3}$, $K_{r,ACP}$, $K_{r,Struvite}$, $K_{r,Kstruvite}$ and $K_{r,Newberyite}$. For the latter, the parameter sets found in the Chapter 3 were used for the scenarios using sewage sludge with medium and high concentrations of Ca^{2+}, Mg^{2+} and soluble inorganic carbon (SIC) concentrations. For the scenario analysis using sludge with low concentration of Ca^{2+}, Mg^{2+} and K^{+}, K_r values obtained by Musvoto et al. (2000) were used, as they were obtained for a low water hardness level.

4.4.5 Evaluation Criteria

Performance indicators were calculated for three different processes: anaerobic digestion, struvite recovery and nitrogen treatment through nitrification-denitrification and PN/anammox in a one stage or two stages configuration. These indicators include operational costs (chemical or energy), carbon footprint (greenhouse gas emissions – GHGs) as well as an estimation of the recovered struvite quantity (Figure 4.2). No criteria were linked to the dewatering unit because the impacts of the different types of sludge on the polymer dosage were neglected. In addition, the anaerobic digestion funit was the only one to be modelled; struvite recovery, nitrification/denitrification, partial

nitritation/denitritation have been considered theoretically through stroichiometric coefficients. Therefore, the following assumptions and/or simplifications have been made:

- The scope of this study is focussed on the sludge line of a WRRF and the interactions between the water and sludge lines have not been considered nor the final dewatered sludge treatment/disposal. Consequently, the quantity of sludge produced by nitrification/denitrification and partial nitritation/anammox was also neglected.
- The dewatering unit produces dewatered sludge at a fixed concentration of 250 g/L.
- The struvite recovery unit has a phosphorus removal performance of 90% (Ueno and Fujii, 2001)
- Nitrification has a performance of 90% (Metcalf & Eddy Inc. et al., 2003)
- Denitrification has a performance of 80% (Metcalf & Eddy Inc. et al., 2003)
- Partial nitritration has a performance of 100%
- The anammox process has a performance of 80% (Lackner et al., 2014)

In Figure 4.2, nitrogen treatment and phosphorus recovery processes are evaluated independently. However, P recovery and N treatment processes can been set up in series (Driessen et al., 2020). There is no consensus on whether to implement the struvite reactor before or after the biological nitrogen removal reactor. The configuration with the struvite reactor implemented upstream of the PN/anammox reactor has been favoured in full scale installations because the struvite reactor can mitigate variable BOD_5 and TSS concentrations in sidestreams through settling and aeration incorporated into some technologies and therefore protect downstream PN/anammox system (Abma et al., 2010; Driessen et al., 2020). However, the configuration with PN/anammox upstream the struvite reactor was tested at pilot scale and ensured a good pH and temperature for the biological N treatment (Tuszynska and Czerwionka, 2021). For the scenario analysis, two configurations on the PN/anammox process were included: the one-stage process in which the 2 steps are conducted simultaneously in the same reactor and the two-stage process in which partial nitritation and anammox are performed in separate reactors.

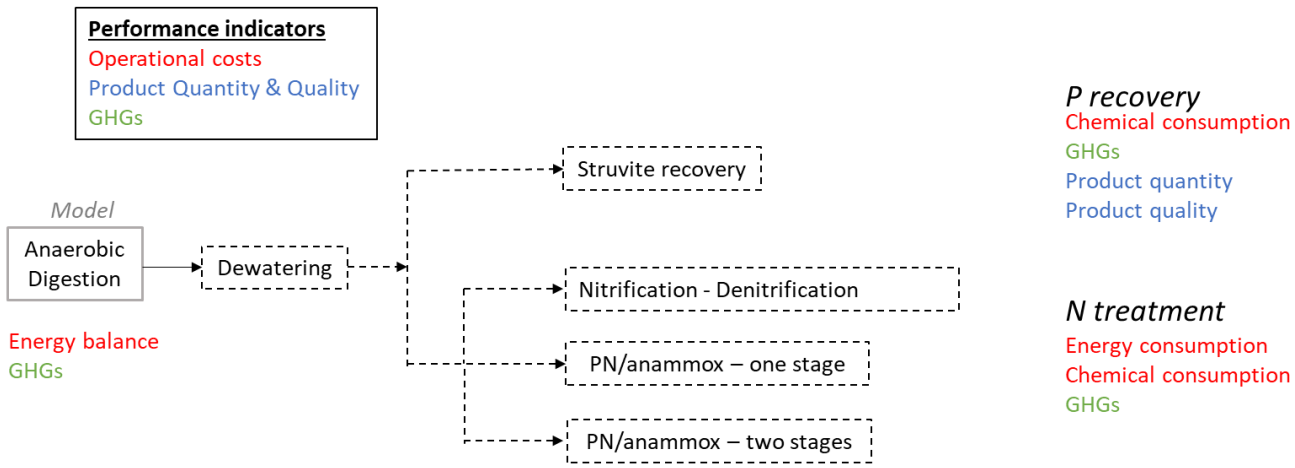

Figure 4.2 – Sludge line diagram and associated performance criteria for each unit

The equations used to calculate the performance indicators once the simulations of the different anaerobic digestion scenarios performed are presented below.

4.4.5.1 Anaerobic Digestion

The energy balance of the anaerobic digestion is performed using the production of biogas obtained from simulation and by calculating the heat energy required for sludge heating and electricity for sludge mixing. The different sources of greenhouse gas emissions considered are the consumption of electricity and the fugitive methane emissions. As the biogas produced by the digester is used to heat the sludge, greenhouse gas emissions for sludge heating are avoided.

The calculations for energy balance are presented below:

$$Energy\ produced\ from\ biogas\ \left(\frac{kWh}{day}\right) = Q_{CH_4 produced}\ \left(\frac{Nm^3}{day}\right) *\ 11\ \left(\frac{kWh}{Nm^3_{CH_4}}\right) \quad (1)$$

The value of 11 (kWh/Nm^3CH_4) corresponds to the heat value of methane (Taboada-Santos et al., 2019).

$$Heat\ required\ for\ AD\ \left(\frac{kWh}{day}\right) = \left(T°C_{AD} - T°C_{feedsludge}\right) * Q_{feed\ sludge}\left(\frac{m^3}{day}\right) * 1000\ \left(\frac{kg}{m^3}\right) * \frac{4.1\left(\frac{kJ}{kg\ .°C}\right)}{3600\left(\frac{kJ}{kWh}\right)} \quad (2)$$

$T°C_{AD}$ is the temperature of the mesophilic AD (38°C). $T°C_{feedsludge}$ is the temperature of the sludge (15°C). The value of $4.1\left(\frac{kJ}{kg\ .°C}\right)$ is the sludge heat capacity.

$$Energy\ required\ for\ mixing\ \left(\frac{kWh}{day}\right) = 3\ \left(\frac{kW}{m^3}\right) * \frac{24}{1000}\ \left(\frac{h}{day}\right) * vol_{AD}(m^3) \quad (3)$$

The value of $3\ \left(\frac{kW}{m^3}\right)$ is the energy required for sludge mixing according to Moletta (2008) and vol_{AD} is the volume of the AD (32120 m^3).

For the carbon footprint (CF), the following assumptions are made:

$$CF_{fugitive\ methane}\left(\frac{kg_{CO2}}{day}\right) = 0.03\ \left(\frac{m^3_{CH_4}}{m^3_{CH_4 produced}}\right) * 0.67\left(\frac{kg_{CH_4}}{m^3}\right) *\ \frac{24}{1000}\ \left(\frac{h}{day}\right) * Q_{CH_4}\ \left(\frac{Nm^3}{day}\right) * 30\ \left(\frac{kg_{CO_2}}{kg_{CH_4}}\right) \quad (4)$$

The value of $0.03\ \left(\frac{m^3_{CH_4}}{m^3_{CH_4 produced}}\right)$ is the value of fugitive methane according to Solis et al. (2022). $0.67\left(\frac{kg_{CH_4}}{m^3}\right)$ is the density of methane at 15°C (Metcalf & Eddy Inc. et al., 2003) and $30\ \left(\frac{kg_{CO_2}}{kg_{CH_4}}\right)$ is the global warming potential to 100 years of methane (ADEME, 2023).

$$CF_{electricity\ consumption}\ \left(\frac{kg_{CO2}}{day}\right) = 0.06\ \left(\frac{kg_{CO_2}}{kWh}\right) * Energy\ required\ for\ mixing\ \left(\frac{kWh}{day}\right) \quad (5)$$

$0.06\ \left(\frac{kg_{CO_2}}{kWh}\right)$ is the CO_2 emission relative to the French energy mix (ADEME, 2023).

4.4.5.2 Nitrogen removal

Oxygen requirements for nitrogen removal and the associated energy consumption are calculated based on stoichiometric ratios.

$$Aeration\ energy_{NitDenit}\ \left(\frac{kWh}{day}\right) = 4.33\ \left(\frac{gO_2}{gN-NH_4}\right) * Q_{N-NH_4}\left(\frac{kgN-NH_4}{day}\right) * 0.9\ \left(\frac{kgN_{nitrifyed}}{kgN-NH_{4_{applied}}}\right) * 1.5\ \left(\frac{kWh}{kgO_2}\right) * \frac{(10.5-2)}{10.5} \quad (6)$$

$4.33\ \left(\frac{gO_2}{gN-NH_4}\right)$ is the requirements of O_2 for a full nitrification. $0.9\ \left(\frac{kgN_{removed}}{kgN-NH_{4_{applied}}}\right)$ is the ammonia removal efficiency (Metcalf & Eddy Inc. et al., 2003). The value of $1.5\left(\frac{kWh}{kgO_2}\right)$ is the quantity of energy for the supply of 1 kg of O_2 linked to aeration (Gillot et al., 2005). The value of 10.5 mg O_2/L is the saturation concentration for a temperature of 20°C with a water height of 5 meters. The value of 2 mgO_2/L is the dissolved oxygen concentration in the reactor.

$$Aeration\ energy_{PN-A}\left(\frac{kWh}{day}\right) = 1.85\ \left(\frac{gO_2}{gN-NH_4}\right) * Q_{N-NH_4}\left(\frac{kgN-NH_4}{day}\right) * 1.5\ \left(\frac{kWh}{kgO_2}\right) * \frac{10.5}{(10.5-0.5)} \quad (7)$$

$1.85\ \left(\frac{gO_2}{gN-NH_4}\right)$ is the consumption of O_2 for the nitritation with 57% of N-NH_4 load converted into N-NO_2 (Baumgartner et al., 2022). The efficiency of the partial nitritation stage was considered to be 100%. The value of 10.5 mg O_2/L is the saturation concentration for a temperature of 20°C with a water height of 5 meters. The value of 0.5 and 1 mgO_2/L are respectively the dissolved oxygen concentration in the reactor for the one-stage and two-stage PN/anammox configurations (Lackner et al., 2014; Liu et al., 2020).

The consumption of methanol as a carbon source for the denitrification as well as the consumption of alkalinity for both complete nitrification and denitrification and PN/anammox are calculated as follows:

$$Q_{methanol_{NitDenit}}\left(\frac{kg}{day}\right) = \frac{\left(5.81\left(\frac{gCOD}{gN-NO_3}\right) * Q_{N-No_3 produced}\left(\frac{kgN-No_3}{day}\right) * 0.8\ \left(\frac{kgN-NO_3\ removed}{kgN-NO_3\ applied}\right)\right)}{1.5\left(\frac{g_{COD}}{g_{methanol}}\right)} \quad (8)$$

with $5.81\ \left(\frac{gCOD}{gN-NO_3}\right)$ the quantity of biodegradable COD needed for denitrification and based on stoichiometric reactions (Metcalf & Eddy Inc. et al., 2003). There is no need for biodegradable COD for the PN/anammox process.

$$Q_{NaHCO_3\ NitDenit}\left(\frac{kg}{day}\right) = \frac{\left(\left(7.09\left(\frac{gCaCO_3 consumed}{gN-NH_4 consummed}\right)\right) * Q_{N-NH_4 applied}\left(\frac{kgN-NH_4}{day}\right) * 0.9\left(\frac{kgN_{nitrifyed}}{kgN-NH_4 applied}\right) - 3.57\left(\frac{gCaCO_3 produced}{gN-NO_3 produced}\right) * Q_{N-NO_3}\left(\frac{kgN-NO_3}{day}\right) * 0.8\ \left(\frac{kgN-NO_3\ removed}{kgN-NO_3\ applied}\right)\right)}{1.22\left(\frac{g_{NaHCO_3}}{g_{CaCO_3}}\right)} \quad (9)$$

with $7.09\ \left(\frac{gCaCO_3 consumed}{gN-NH_4}\right)$ the quantity of alkalinity needed for nitrification and $3.57\ \left(\frac{gCaCO_3 produced}{gN-NO_3}\right)$ the quantity of alkalinity recovered from denitrification based stoichiometric reactions (Metcalf & Eddy Inc. et al., 2003)

$$Q_{NaHCO_3\ PN-A}\left(\frac{kg}{day}\right) = \frac{\left(\left(7.09\left(\frac{gCaCO_3 consumed}{gN-NH_4 cobsummed}\right) * 0.57\ \left(\frac{gN-NO_2}{gN-NH_4}\right) * Q_{N-NH_4}\left(\frac{kgN-NH_4}{day}\right) - 24.23 * \frac{14}{100}\left(\frac{g\ CaCO_3 produced}{g\ N\ processed}\right) * Q_{N processed}\left(\frac{kgN processed}{day}\right) * 0.8\ \left(\frac{kgN_{removed}}{kgN_{applied}}\right)\right)\right)}{1.22\left(\frac{g_{NaHCO_3}}{g_{CaCO_3}}\right)} \quad (10)$$

with $7.09\ \left(\frac{gCaCO_3 consumed}{gN-NH_4}\right)$ the quantity of alkalinity needed and $24.23\ \left(\frac{mol\ CaCO_3 produced}{mol\ N\ processed}\right)$ the quantity of alkalinity recovered from the anammox process based on stoichiometric reactions (Metcalf & Eddy Inc. et al., 2003). Same calculations have been made for one-stage and two-stage system assuming that in the two-stage system a recirculation will provide the alkalinity produced in the second step of the process.

The carbon footprint for electricity and chemical consumption are calculated similarly for the three N treatment processes considered as follows:

$$CF_{electricity}\left(\frac{kg_{CO2}}{day}\right) = 0.06\ \left(\frac{kg_{CO_2}}{kWh}\right) * Aeration\ energy\ \left(\frac{kWh}{day}\right) \quad (11)$$

The value of $0.06\ \left(\frac{kg_{CO_2}}{kWh}\right)$ is the CO_2 emission relative to the French energy mix (ADEME, 2023).

$$CF_{methanol}\left(\frac{kg_{CO2}}{day}\right) = 0.52\ \left(\frac{kg_{CO_2}}{kg_{methanol}}\right) *\ Q_{Methanol} \quad (12)$$

The value of $0.52\ \left(\frac{kg_{CO_2}}{kg_{methanol}}\right)$ is the CO_2 emission relative to the production of pure methanol (ADEME, 2023)

$$CF_{bicarbonate}\ \left(\frac{kg_{CO2}}{day}\right) = 1.2\ \left(\frac{kg_{CO_2}}{kg_{NaHCO_3}}\right) * Q_{NaHCO_3} \quad (13)$$

The value of $1.2\ \left(\frac{kg_{CO_2}}{kg_{NaHCO_3}}\right)$ is the CO_2 emission relative to the production of pure $NaHCO_3$ (ADEME, 2023).

The N_2O emission factors (EF), which are the ratio of the N_2O emission rate to the nitrogen removal rate, were defined based on a literature review. The details of the selected data are available in "Supplementary Information". More data have been found for the one-stage PN/anammox compared to the two-stage system. Median EF is for the one-stage and two-stage system of $0.011 \pm 0.0068\ \left(\frac{kg\ N-N_2O}{kg\ N_{removed}}\right)$ and $0.041\ \pm 0.02\ \left(\frac{kg\ N-N_2O}{kgN-NO_{2_{produced}}}\right)$, respectively. The higher emissions from the two stage system is most likely related to the higher level of nitrite ($N\text{-}NO_2$) concentration compared to the one stage system (Kampschreur et al., 2008). For nitrification/denitrification, only one extreme EF value of $0.1\ \left(\frac{kg\ N-N_2O}{kg\ N_{removed}}\right)$ was found. It was therefore not considered and we applied the EF of the one-stage PN/anammox system to the nitrification/denitrification system assuming that they had equivalent levels of nitrite concentration. The calculations of N_2O emissions for each process is detailed below with $273\ \left(\frac{kgCO_2}{kg\ N_2O}\right)$ the global warming potential to 100 years of N_2O (IPCC, 2021).

$$N_2O_{Nit-Denit\ \&\ PN-A_{onestage}}\ \left(\frac{kg_{CO2}}{day}\right) = Q_{N-NH_4}\left(\frac{kg\ N-NH_4}{day}\right) * 0.8\ \left(\frac{kgN_{removed}}{kgN-NH_{4_{applied}}}\right) * 0.011\ \left(\frac{kg\ N-N_2O}{kg\ N_{removed}}\right) * 1.57\ \left(\frac{kgN_2O}{kgN-N_2O}\right) * 273\ \left(\frac{kgCO_2}{kg\ N_2O}\right) \quad (14)$$

$$N_2O_{PN-A_{twostages}}\left(\frac{kg_{CO2}}{day}\right) = Q_{N-NH_4}\left(\frac{kg\ N-NH_4}{day}\right) * 0.57\ \left(\frac{\frac{kgN-NO_2}{day}}{Q_{\ N-NH_4}}\right) *\ 0.041\ \left(\frac{kg\ N-N_2O}{kgN-NO_2}\right) * 1.57\ \left(\frac{kgN_2O}{kgN-N_2O}\right) * 273\ \left(\frac{kgCO_2}{kg\ N_2O}\right) \quad (15)$$

4.4.5.3 P treatment

The struvite recovery process is based on the precipitation of $P\text{-}PO_4$ with $N\text{-}NH_4$ and $MgCl_2$ in a molar ratio of 1:1:1 (NH_4:PO_4:Mg). To enhance the degree of supersaturation and therefore phosphate removal an addition of magnesium chloride is added in a molar ratio $Mg\text{:}P\text{-}PO_4$ of 1.6 (Metcalf & Eddy Inc. et al., 2003). To reach the optimum pH concentration of 8.5, the quantity of sodium hydroxide needed was calculated using the chemical speciation part of the model.

$$MgCl_2\ required\ \ \left(\frac{kg}{day}\right) = 1.6\ \left(\frac{mol_{Mg}}{mol_P}\right) * \frac{Q_{P-PO_4}\left(\frac{kgP-PO_4}{day}\right)}{31\ \left(\frac{mol}{g}\right)} * 0.9\ \left(\frac{\frac{kgP_{removed}}{day}}{Q_{P-PO_4}}\right) \quad (16)$$

$$CF_{MgCl_2\ production}\ \left(\frac{kg_{CO2}}{day}\right) = 0.105\ \left(\frac{kg_{CO_2}}{kg_{MgCl_2}}\right) *\ Q_{MgCl_2} \quad (17)$$

The value of $0.105\ \left(\frac{kg_{CO_2}}{kg_{MgCl_2}}\right)$ is the CO_2 emission relative to the production of pure $MgCl_2$ (ADEME, 2023).

$$CF_{NaOH(50\%)}\ \left(\frac{kg_{CO2}}{day}\right) = 0.587\ \left(\frac{kg_{CO_2}}{kg_{NaOH_{50\%}}}\right) *\ Q_{NaOH_{50\%}} \quad (18)$$

The value of $0.587\ \left(\frac{kg_{CO_2}}{kg_{NaOH_{50\%}}}\right)$ is the CO_2 emission relative to the production of sodium hydroxide concentrated at 50% (ADEME, 2023).

4.6 Results

The results of the 12 scenarios according to the selected performance criteria are presented below by unit process (anaerobic digestion, N treatment, P treatment).

4.6.1 Anaerobic Digestion

The 12 scenarios resulted in a similar biogas production around 72,500 kWh/day for the anaerobic digester at 50% capacity and around 125,000 kWh/day for the anaerobic digester at 100% capacity (Figure 4.3). The anaerobic digester at 100% capacity does not produce exactly the double of the anaerobic digester at 50% capacity because of the different sludge retention time. The low variability in biogas production can be explained by the fact that the same sludge concentration (50 g/L) with similar COD to VSS ratio and biodegradability was considered in all simulations. The small variations are attributed to the differences of COD fractionation. Water hardness has no significant impact on the production of methane. All scenarios are energy self-sufficient thanks to the energy coming from the biogas.

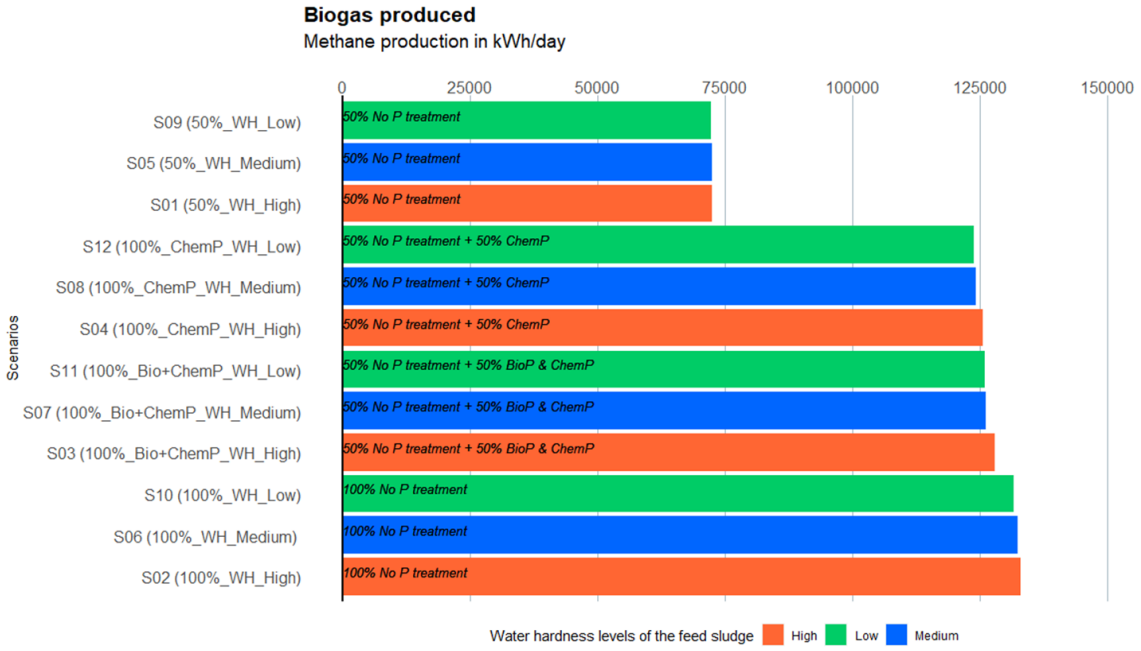

Figure 4.3 – Heat energy balance of the 12 scenarios evaluated

The 12 scenarios have similar operational costs and CO_2 balance with a carbon footprint of 795 $kgCO_2$/day for the anaerobic digester at 50% capacity and 1325 $kgCO_2$/day for the anaerobic digester at 100% capacity (Figure 4.4). CO_2 emissions for sludge heating are equals to 0 because part of the biogas produced is used to that purpose. CO_2 emissions for the anaerobic digestion process unit are broadly due to fugitive methane emissions and very slightly due to electricity consumption. These figures represent a carbon footprint in the range of 4.5 to 5.7 $kgCO_2/ML_{wastewater}$ which is in accordance with the range of 4 to 16 $kgCO_2/ML_{wastewater}$ found in Wu et al. (2022).

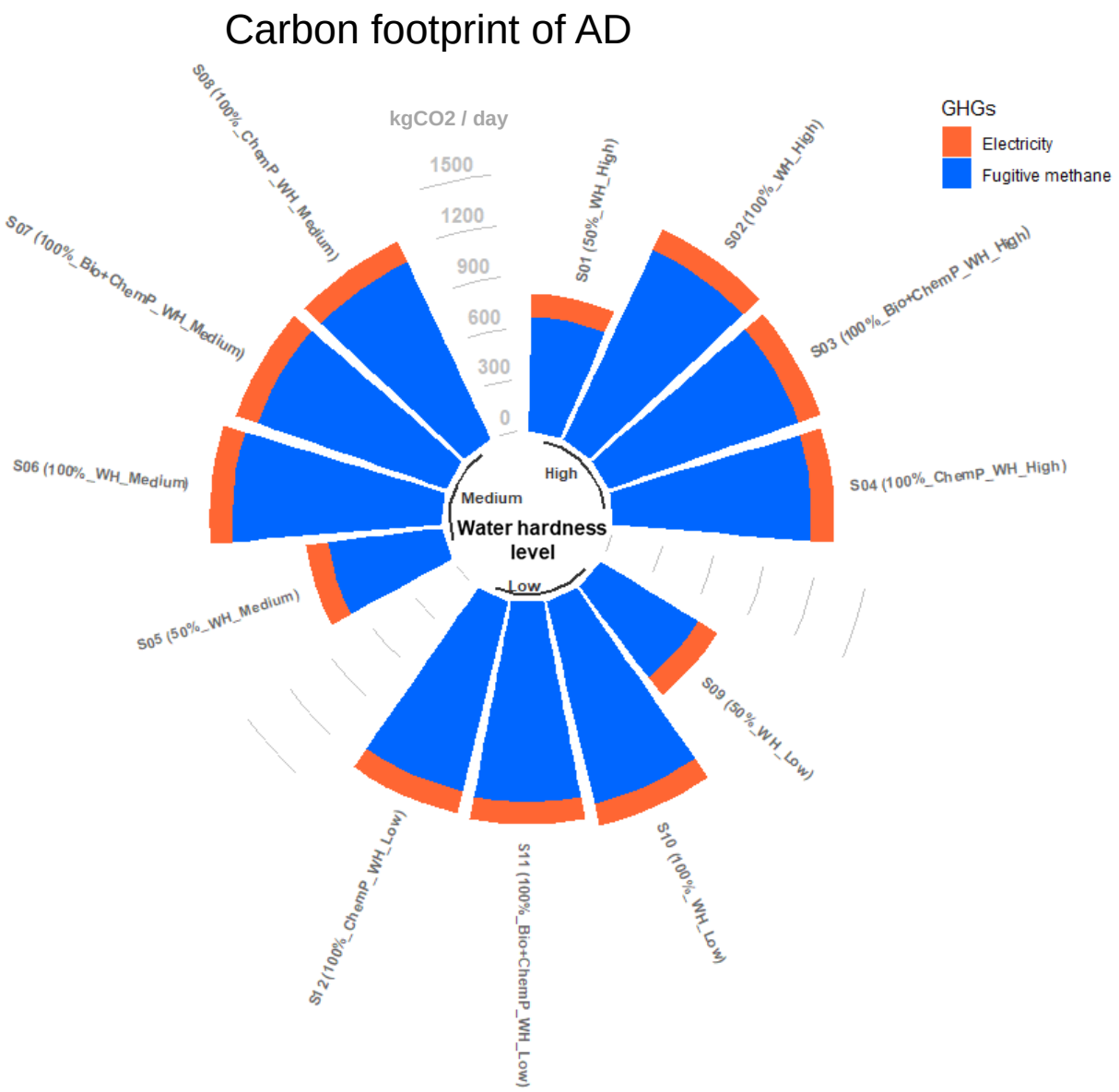

Figure 4.4 – CO_2 balance for the AD unit

4.6.2 Nitrogen treatment

The N-NH_4 mass flows from the 12 scenarios are equivalent and the small variations observed can be explained with the same explanations as for biogas production (Figure 4.5). The concentration of N-NH_4 resulting from the different AD simulations is between 1000 mg/L and 1100 mg/L which is in accordance with the data compilation by Devos et al. (2023). The quantity of nitrogen in sidestreams from the scenarios with the anaerobic digesters at 50% capacity is lower because the resulting flow of sidestreams is smaller than the anaerobic digesters at 100% capacity.

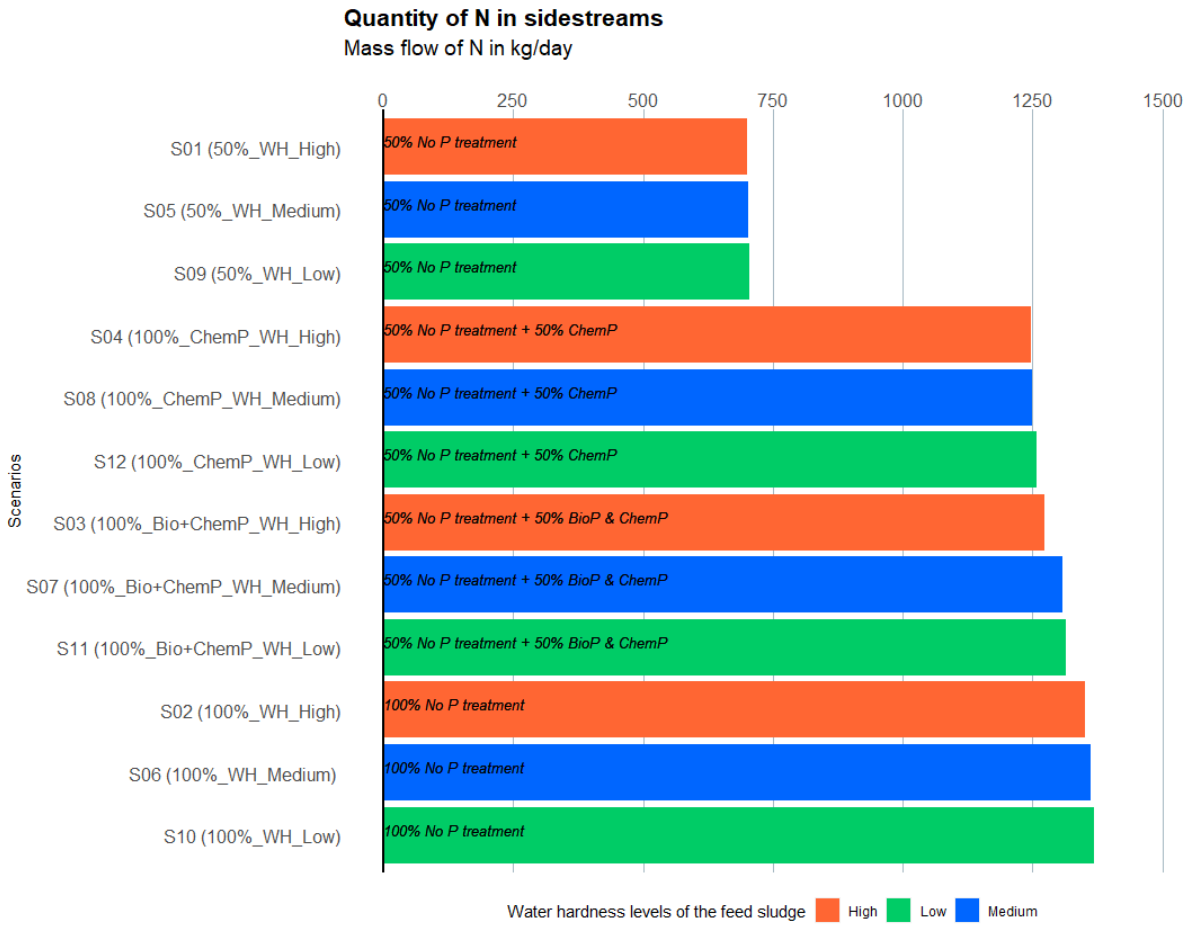

Figure 4.5 – Mass flows of N-NH_4 in sidestreams for the 12 evaluated scenarios

Figure 4.6, 4.7 and 4.8 represent the carbon footprint for the three possible N treatment processes: nitrification-denitrification, one stage and two stages partial nitritation-anammox (PN/A). As the nitrogen mass flows are similar, there are no differences on the carbon footprint between the 3 scenarios with AD at 50% capacity and between the 9 scenarios with AD at 100% capacity when considering one type of N treatment. Indeed, Figures 6 and 7 show that there is no chemical consumption and therefore no associated carbon footprint for PN/anammox processes compared to nitrification/denitrification. As expected, there is also is lower electricity consumption for PN/anammox. The calculations result in an energy consumption of between 3.5 and 3.7 kWh/$kgN_{applied}$ for the PN/anammox process which in accordance with the range of 1.05 - 4.2 kWh/$kgN_{applied}$ found in the review of Lackner et al. (2014). In comparison, the energy consumption for the nitrification/denitrification is of 7.2 kWh/$kgN_{applied}$. However, from an environmental point of view, the two-stage PN/anammox process is largely unfavourable compared to nitrification/denitrification and to the one stage PN/anammox due to the higher N_2O emissions. In second position is the nitrification/denitrification process due to the higher chemical and electricity consumption compared to the one stage PN/anammox process.

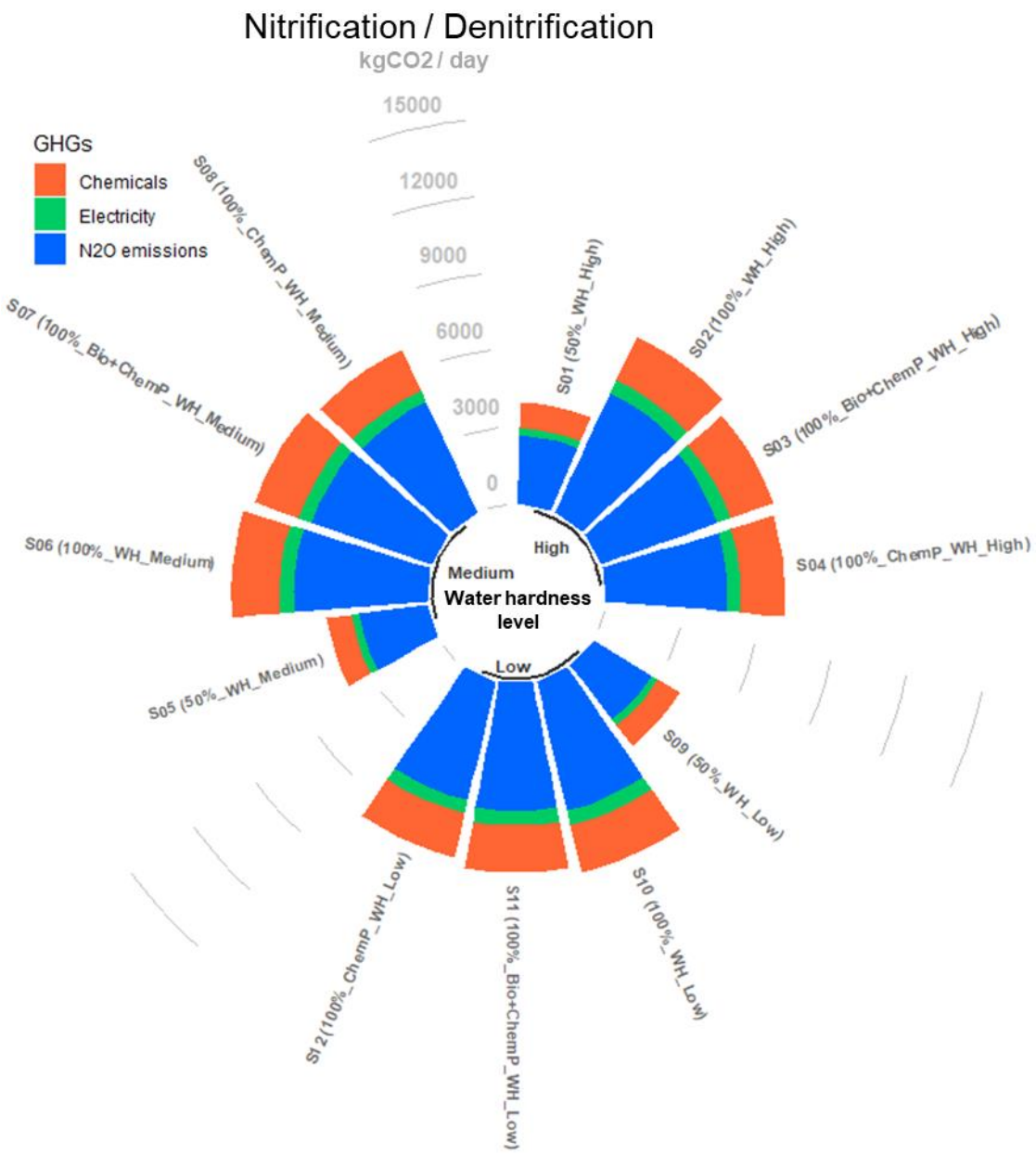

Figure 4.6 – Contribution of chemicals, electricity and N_2O emissions to the CO_2 balance of the nitrification/denitrification process

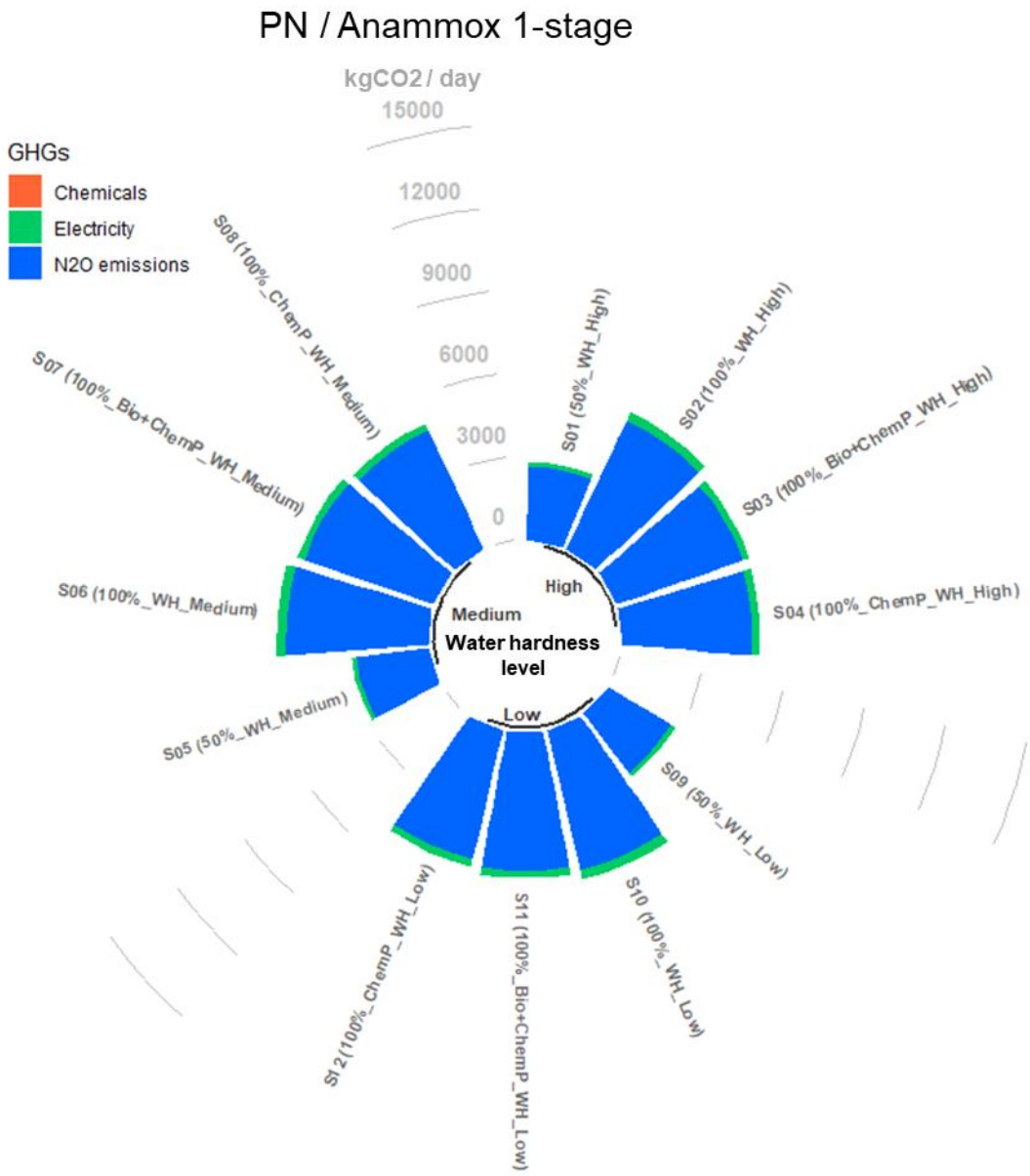

Figure 4.7 - Contribution of chemicals, electricity and N_2O emissions to the CO_2 balance of the 1-stage partial nitritation/anammox process

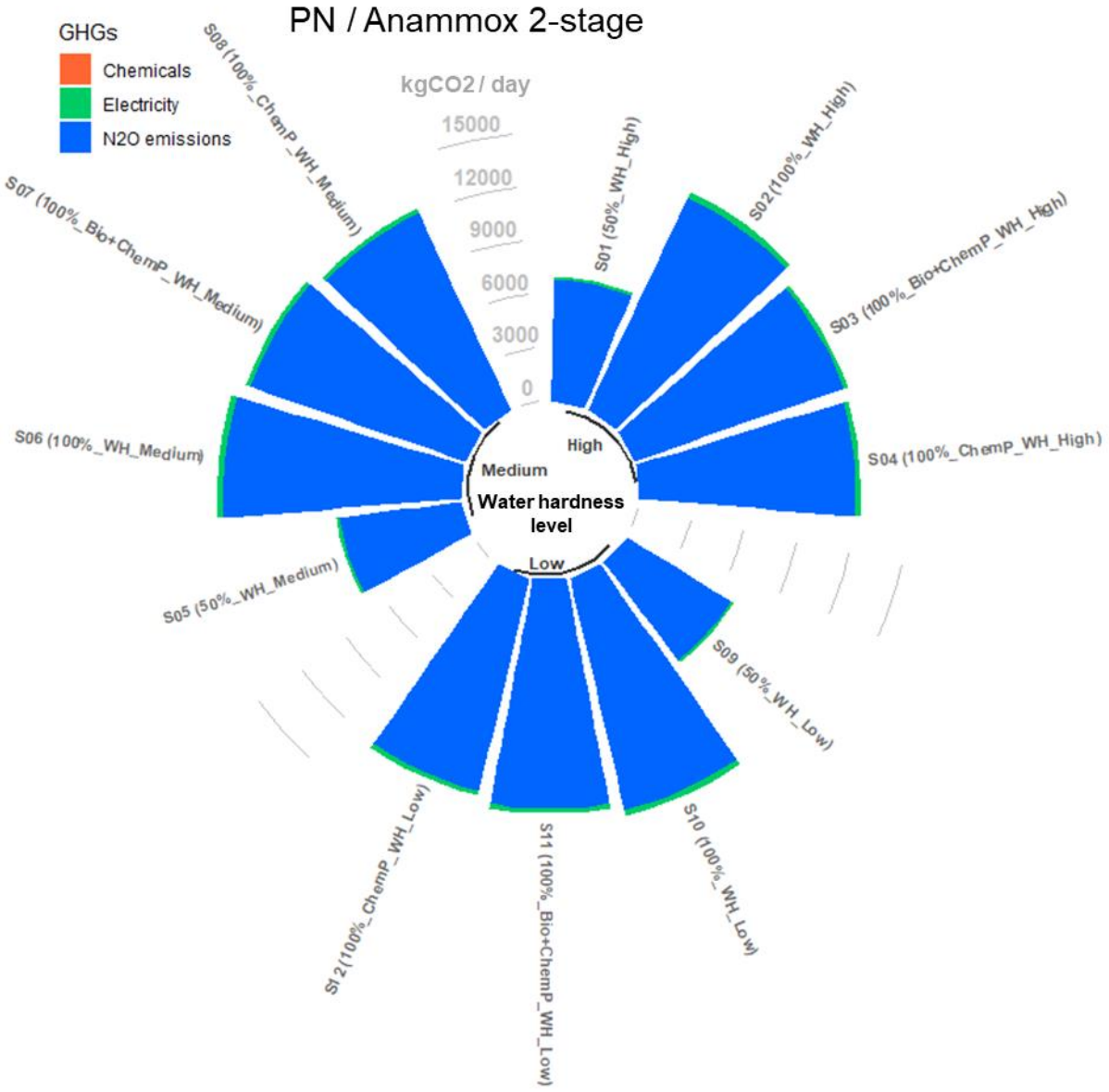

Figure 4.8 - Contribution of chemicals, electricity and N_2O emissions to the CO_2 balance of the 2-stage partial nitritation/anammox process

4.6.3 Phosphorus recovery as struvite

The mass flows of $P\text{-}PO_4$ generated for the 12 scenarios are different according to the types of sludge and to the different ion concentrations (Ca^{2+}, Mg^{2+}, SIC). Figure 4.9 shows that the 3 scenarios including Bio-P provide the highest potential for P recovery as struvite compared to the other types of sludge and regardless of the level of water hardness. However, between low and high level of water hardness, the potential for recovery is divided by more than 2 for a same type of sludge. This corresponds to a concentration of 127, 241 and 300 mg $(P\text{-}PO_4)/L$ for respectively high, medium and low water hardness level. Therefore, even if the scenarios with Bio-P removal sludge are the most

attractive, the scenarios with Chem-P removal sludge and without specific P treatment can also be economically viable if the water hardness of the sludge is low or medium. This is the case of scenarios S05, S06, S09, S10 and S12 that have a concentration of phosphorus in sidestreams higher than 50 mg/L which corresponds to the economic viability threshold of Wu et al (2022). However, higher struvite recovery is associated with higher consumption of sodium hydroxide and magnesium chloride and therefore higher carbon footprint. The carbon footprint of the struvite recovery unit can vary between 201.4 $kgCO_2$/day (S01) to 620 $kgCO_2$/day (S11).

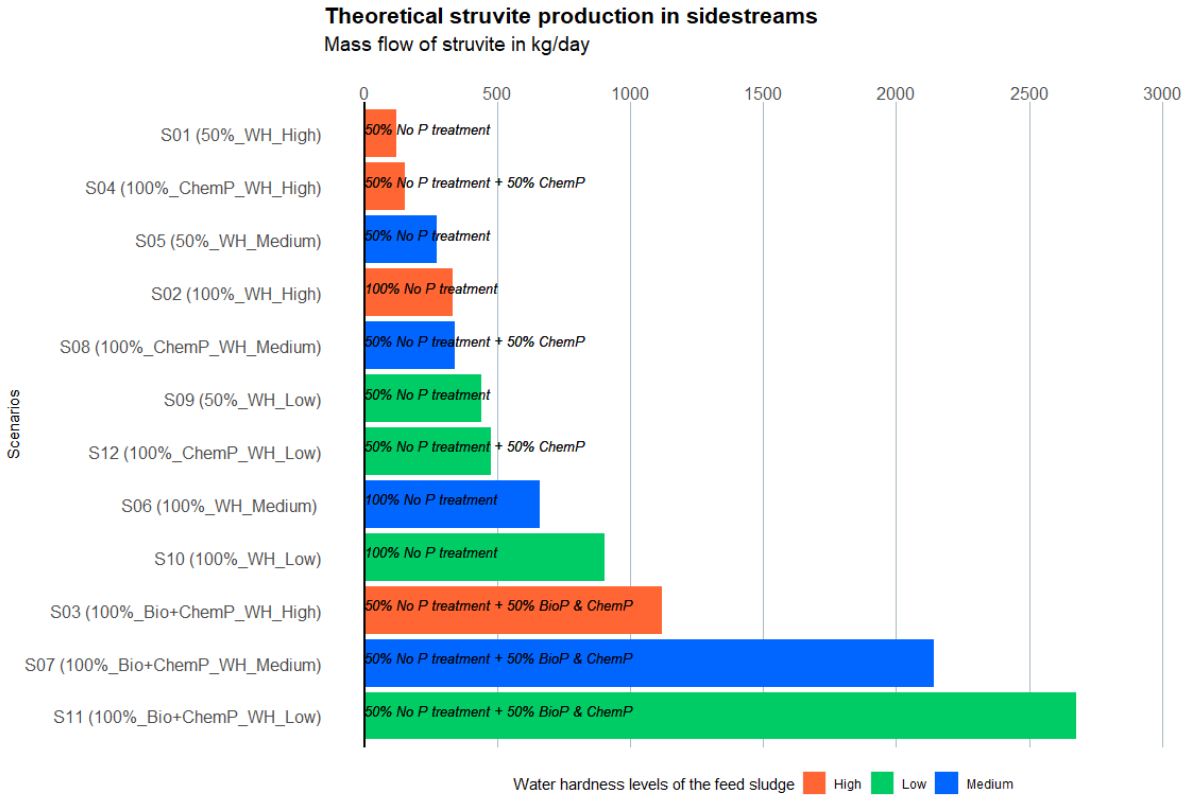

Figure 4.9 - Mass flows of theoretical struvite production in sidestreams for the different evaluated scenarios

The impact of the different water hardness levels on the potential for P recovery can be explained by precipitation mechanisms in the digester. Figure 4.10 shows that scenarios 01, 02, 03 and 04 with high water hardness level have the highest amount of precipitated minerals compared to low and medium water hardness levels. Indeed, the saturation extent is higher due to the highest concentrations of Ca, Mg and SIC which leads to a more important precipitation of Ca^{2+} and Mg^{2+} with phosphorus. This quantity is even accentuated for scenarios with Bio-P removal sludge (S03, S07 and S11) due to the release of Mg and P-PO_4 stored as polyphosphate. The minerals that precipitate mainly are Amorphous Calcium Phosphate (ACP) and $MgCO_3$. $CaCO_3$ is formed only with medium and high water hardness but its formation also depends on the concentration of P-PO_4 due to the competition with ACP. Struvite and newberyite (New) are formed only with Bio-P removal sludge because the release of Mg^{2+} and P-PO_4 modifies the ratio Ca:Mg and Mg:P-PO_4 which promotes struvite and newberyite formation.

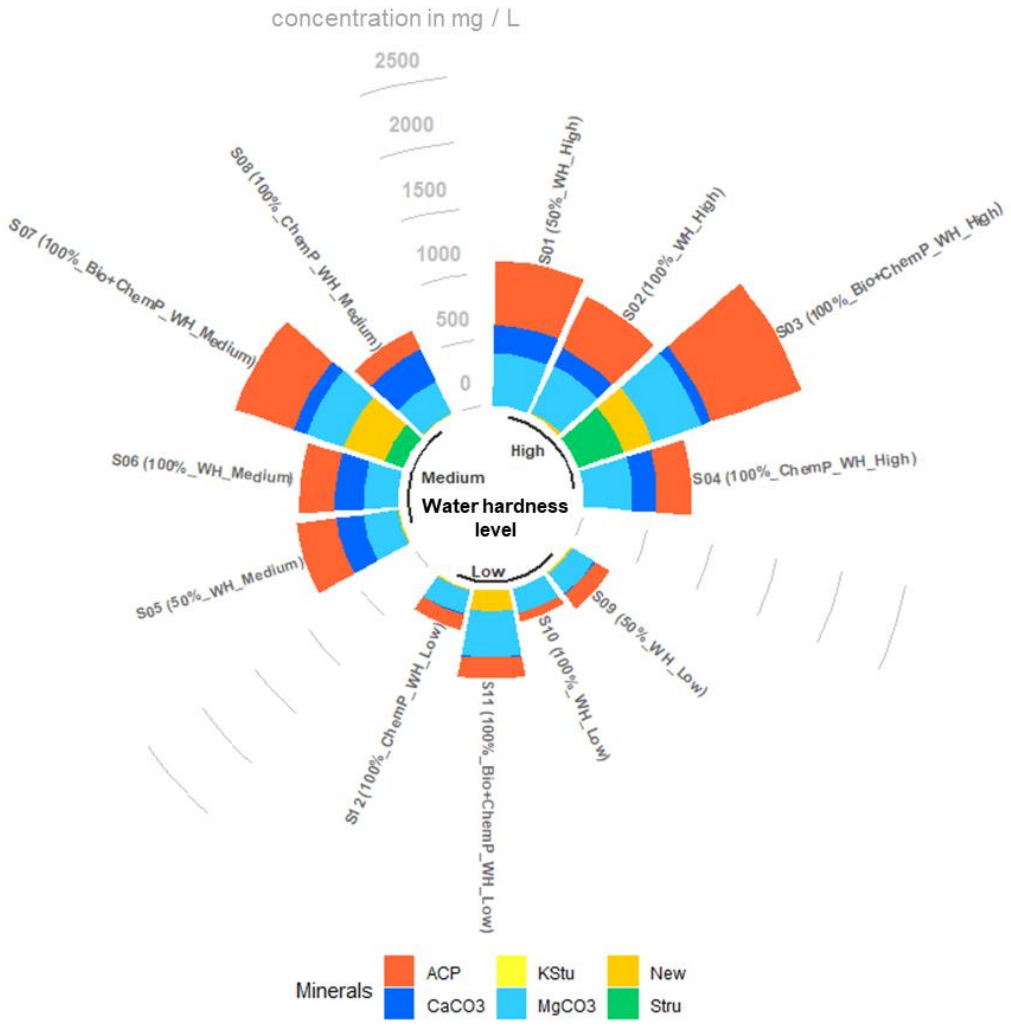

Figure 4.10 – Repartition of the minerals precipitated during AD for the different scenarios evaluated

The quality of the recovered product which can be defined by the percentage of pure struvite in the final product depends on the level of water hardness. High and medium water hardness levels will therefore tend to have a negative impact on the quality of the recovered product because the residual calcium concentration in sidestreams is high and can form ACP instead of struvite.

Additional graphs are available in appendix to illustrate the potential for P recovery in sidestreams using different units (kg struvite / kg P AD inlet, kg $P\text{-}PO_4$ / kg P AD inlet). A graph showing the fractionation of phosphorus in digested sludge is also presented in the appendix.

4.7 Discussion

4.7.1 Initial sludge characteristics

This scenario analysis was conducted using sludge characteristics obtained from a simulation of a WRRF treating conventional wastewater. This leads to a COD:VSS ratio of around 1.5 and an inert fraction of 0.4. The COD:VSS can be comprised in the range of 1.3 to 1.9 (Metcalf & Eddy Inc. et al., 2003) and the inert fraction between 0.30 to 0.55 (Astals et al., 2013; de Gracia et al., 2009; Fisgativa et al., 2020b, 2018; Metcalf & Eddy Inc. et al., 2003). These ratios can significantly impact the quantity of biogas, nitrogen and phosphorus in sidestreams. Nevertheless, the impact of the different types of sludge, without P treatment, with Bio-P and Chem-P removal sludge or only Chem-P removal sludge, as well as the level of water hardness, will not modify the main conclusions of this study. The order of the scenarios for which P recovery could be the most interesting or the comparison of the different nitrogen treatments will remain but the final value of the CO_2 emissions, the biogas production, the quantity of N or P in sidestreams may vary.

4.7.2 Uncertainty of kinetic precipitation constants

The values of kinetic precipitation constants obtained after the calibration done in Chapter 3 have been used in this scenario analysis. Nevertheless, no calibration could be performed for an anaerobic digester with low water hardness and default values from Ikumi et al. (2020) were used. In previous chapter, the simulation results obtained with precipitation kinetic constants by default gave reasonable results for the estimation of $P\text{-}PO_4$ but needed to be adjusted for Ca^{2+} and Mg^{2+} concentrations. In addition, the value of the kinetic precipitation constants does not depend only on the initial saturation extent, but also on the mixing conditions and reactor geometry. Consequently, there is an uncertainty for the values of kinetic precipitation constants that can induce a variation of $P\text{-}PO_4$ content in digested sludge as well as that of Ca^{2+} and Mg^{2+} according to the value of the precipitation kinetic constants used.

4.7.3 Sensitivity of CO_2 balance to the emission factors

The emission factors (EF) used to calculate fugitive emissions of methane and N_2O are extremely variable. For the fugitive methane emissions, it ranged from 0.5% (ADEME, 2023) to 3% (Solís et al., 2022) of the methane produced. In this scenario analysis, the highest value was chosen but this value can be reduced if the WRRF has an efficient air treatment of the digested sludge.

For nitrification/denitrification, the value of the EF for N_2O emissions was considered the same as for the one stage partial nitritation/anammox. This hypothesis has been done because limited information was found on N_2O emissions from activated sludge processes treating concentrated N streams, thus more measurements are required to further refine the value of the EF.

In order to evaluate the sensitivity of the sludge line carbon footprint to the EF, calculations were performed using the minimum, median and maximum values from the literature (see supplementary information). These calculations are presented in Table 4.6 for only one scenario, Scenario S1 (50%_WH_High) but similar conclusions can be drawn for the remaining 11 scenarios. For the one-stage PN/anammox, the EF is in the range of 0.2 –2.7 gN_2O/gTN removed; whereas, it is for the two-stage system of 3.3 – 7.12 $gN_2O/N\text{-}NH_4$ oxidised to $N\text{-}NO_2$. Even if the range is widespread, N_2O emissions from the two-stage PN/anammox remain higher than the one stage PN/anammox and nitrification/denitrification process when using the same level of EF (minimum, median or maximum).

However, between the minimum and maximum EF values, the carbon footprint can double for the two-stage PN/anammox and be multiplied by more than 10 for the two other processes (nitrification/denitrification and the one stage PN/anammox). Such differences should be considered in the assessment when selecting a sidestream process and be put in perspective to the overall WRRF carbon footprint. Such as concluded by Wu et al. (2022), N_2O mitigation will be an important challenge to achieve carbon neutrality.

Table 4.6 – Carbon footprint in $kgCO_2$/day of feed sludge of the different biological nitrogen treatment according to the different N_2O emission factor found in the literature.

	Minimum EF	Median EF	Maximum EF
Nitrification/Denitrification	433	2382	5847
PN/anammox one stage	385	2117	5197
PN/anammox two stage	5657	7028	12206

4.8 Conclusions

This scenario analysis performed is based on a model of AD including multiple mineral precipitation with different types of sludge and different water hardness levels to predict the quantity of biogas, N and P content in sidestreams. Then, calculation of operating costs (energy and chemicals) as well as the potential for struvite recovery and CO_2 balance have been performed to compare the different scenarios. The main conclusions are the followings:

1) The type of phosphorus treatment applied in the water line (no specific treatment, biological phosphorus removal and chemical phosphorus removal) does not have a major impact on the quantity of biogas produced for a feed sludge with a same total solid concentration and a same COD:VSS ratio. All scenarios are energy self-sufficient for the AD process unit and GHG emissions are mainly due to fugitive methane emissions.
2) The quantity of nitrogen in sidestreams, as for the biogas production does not depend on the type of phosphorus treatment applied in the WRRF nor on the level of water harness. The operating costs will be higher for the treatment of nitrogen by nitrification/denitrification process compared to partial nitritation/anammox due to more important oxygen and chemicals (methanol, alkalinity) requirements. However, from a carbon footprint point of view, the two stage partial/nitritation anammox system is responsible for higher emissions compared to nitrification/denitrification and one-stage anammox system.
3) The quantity of phosphorus available in sidestreams for recovery as struvite depends on both the type of phosphorus treatment applied and the level of water hardness. The lower the water hardness level, the higher the quantity of phosphorus in sidestreams. Feed sludge with Bio-P removal presents the largest amount of phosphorus but this quantity is divided by 2 between low and high water hardness level.

This scenario analyses have been conducted only for a sludge line and the impacts of sidestreams on the main wastewater treatment lines have not been considered. In the future, an assessment of the WRRF as a whole could help to evaluate the potential benefits of sidestream treatment on the performance of the water line.

CHAPTER 5 – CONCLUSION AND PERSPECTIVES

5.1 General conclusion

In the context of a paradigm shift from wastewater treatment to water resource recovery, urban facilities are increasingly considering sludge anaerobic digestion. This process provides different flows: a biogas, a digested sludge and a centrate, also called sidestreams, highly concentrated in nitrogen and phosphorus. To optimise the management of nitrogen and phosphorus throughout the entire water resource recovery facility (WRRF), the treatment or recovery of these nutrients may be relevant. Despite a growing interest in sidestream processes such as nitrification/denitrification, partial nitritation/anammox or struvite recovery, poor attention has been paid to sidestream characteristics and full-scale installations are still relatively rare compared to the number of anaerobic digesters implemented. Indeed, even if high concentrations of nitrogen and phosphorus are expected, an important variation can be observed from one facility to another, especially for phosphorus. This lack of knowledge is even more critical for anaerobic digesters that receive different types of sludge from surrounding facilities or for anaerobic digesters preceded by a pretreatment as thermal hydrolysis process. Models to simulate anaerobic digestion and sidestream processes could be a useful tool to help predict nitrogen and phosphorus levels as well as assess treatment or recovery options. However, a limited number of data restrains the validation of these models and their applications for different configurations of WRRFs. The recent implementation of full-scale sidestream processes associated with limited knowledge of sidestream characteristics could explain the absence of guidelines to support the choice for treatment or recovery of nitrogen and phosphorus in sidestreams.

The overall aim of this PhD study was to provide insights on sidestream characteristics and on the possible routes for nitrogen and phosphorus treatment or recovery. To start with, a comprehensive review of sidestream characteristics was performed (*Chapter 2*). It also includes the main treatment and recovery processes found in the literature, whatever their technology readiness levels. Concentration ranges of the different characteristics were obtained and allowed to understand in which extent sidestream characteristics can vary from one facility to another and how these characteristics can impact sidestream process performance. Then, a modified version of ADM1 (anaerobic digestion model n°1) including precipitation mechanisms was studied in order to validate the prediction of phosphate concentration in sidestreams (*Chapter 3*). This chapter was essential to calibrate model parameters and to reduce the uncertainty on the precipitation kinetic constants using data from two different full-scale digesters. The results of *Chapter 3* were then used in *Chapter 4* for the scenario analysis including anaerobic digestion of sludge with different characteristics, depending on the phosphorus treatment used in the water line and on the wastewater hardness. The objective was to assess how sludge characteristics were impacting the choice of implementation of a struvite recovery process. In this chapter, two biological nitrogen treatments of sidestreams were also compared based on operational performance indicators and on carbon footprint. The main conclusions related to these chapters are summarised in the following paragraphs. Potential future research directions are finally discussed.

5.2 State of the art of sidestream characteristics and existing processes

Anaerobic digestion sidestreams are known to contain high concentrations of nitrogen and phosphorus. However, explaining the variability encountered from one facility to another is not obvious because there is poor information on other characteristics such as COD, TSS or ions (Ca^{2+}, Mg^{2+}, Na^{+}, K^{+}, SO_4^{2-}, Cl^{-}). Chapter 2 provides concentration ranges for sidestream characteristics issued from conventional anaerobic digestion or anaerobic digestion preceded by a thermal hydrolysis process (Figure 1). This literature data compilation showed that nitrogen in sidestreams is mainly is the form of ammonia ($N\text{-}NH_4^{+}$) except for anaerobic digesters with THP where a fraction of refractory dissolved organic nitrogen, yet not quantified, has been observed. Thermal hydrolysis processes also result in higher nitrogen concentration compared to conventional anaerobic digester. The variability of ammonia concentration between the different facilities can be explained by a different TSS concentration of AD feed sludge, AD performance and the type of dewatering unit that can be operated with different washing system resulting in different sidestream dilution. For phosphorus, the concentration ranges differ according to the type of phosphorus treatment applied in the water line (no specific P treatment, biological or chemical phosphorus removal). However, compared to ammonia, there is no significant increase of phosphate concentration when adding a THP. This can be explained by precipitation of $P\text{-}PO_4$ in the digester with the ions that can also be released during the THP: Mg^{2+}, $Fe^{2+/3+}$, Ca^{2+} and Al^{3+}. The different concentration of ions, and especially Mg^{2+} and Ca^{2+}, can explain the variability between the different WRRFs for phosphate concentration with or without THP because they induce different levels of precipitation in the digester. For total COD and TSS, both characteristics are correlated and the variability is linked to the performance of the dewatering unit. However, for anaerobic digestion with THP the concentration of soluble COD is higher due to the important solubilisation with the THP but also to the higher sludge feed TSS concentration and the production of refractory COD compounds.

All sidestream processes found in the literature for nitrogen or phosphorus treatment or recovery can be impacted by the different characteristics of anaerobic digestion sidestreams. A list of characteristics to be checked for each process in order to avoid counter- performances is given on Figure 5.1. The threshold values could not be obtained because they are case dependent and there is not enough published experience to generalise the values found in literature. However, knowing the value before the implementation can give an indication on concentration level of the characteristics that may impact the process and take preventive measures. This chapter has also shown that the most common implemented processes are struvite recovery, the nitrification/denitrification and the partial nitritation/anammox process. Other processes either consume a lot of energy (ammonia stripping, membrane) or they are still at a development stage and their implementation at full scale is still complicated (electrodialysis, bioelectrochemical system, ion exchange resin and algae production).

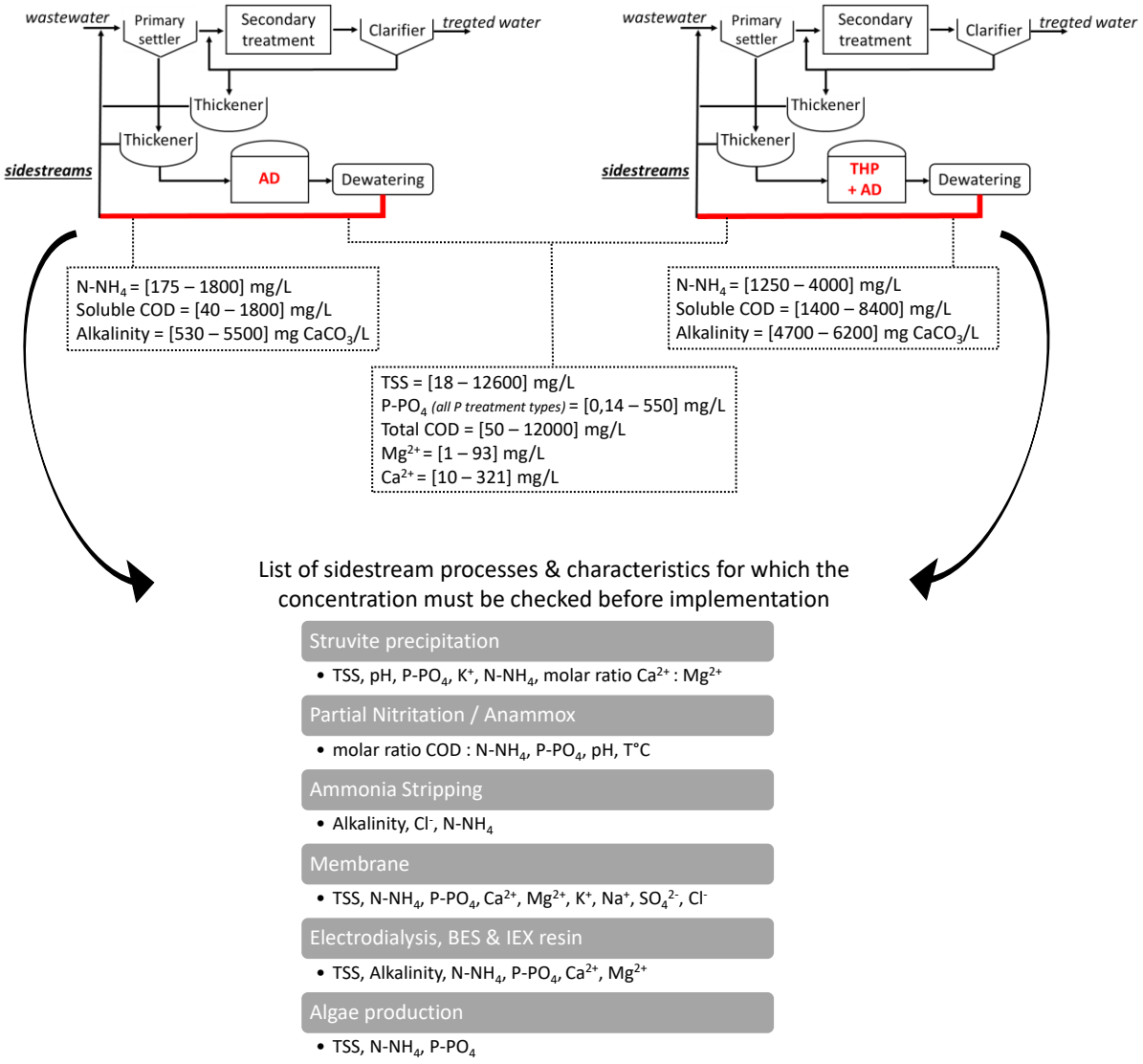

Figure 5.1 - Summary of the literature review on sidestream characteristics and processes

5.3 Calibration of an AD model with multiple mineral precipitation

The analysis of sidestream characteristics in *Chapter 2* has shown that phosphate concentration in anaerobic digestion sidestreams depends on the type of phosphorus treatment applied in the WRRF. However, precipitation of phosphate in the digester can also occur and impact phosphate concentration in sidestreams. This precipitation rate is affected by the concentration of other ions in solution, in particular calcium and magnesium, because they can interact with phosphate or inorganic carbon ions. The literature review has also highlighted the importance of calcium and magnesium on the performance of sidestream treatment or recovery processes such as struvite recovery, membranes, ion exchange resins, electrodialysis or bio electrochemical system.

In order to better predict the concentration of phosphorus in anaerobic digestion sidestreams, as well as the concentrations of magnesium and calcium, *Chapter 4* focused on calibrating an ADM1-based anaerobic digestion model coupled with multiple mineral precipitation mechanisms. This

calibration was carried out using data from two full-scale anaerobic digesters with different feed sludge characteristics and different levels of water hardness (concentration of calcium, magnesium and inorganic carbon). The precipitation model includes 6 minerals (struvite, K-struvite, amorphous calcium phosphate, calcium carbonate, magnesium carbonate, newberyite) whose precipitations are represented by six differential equations. These equations lie on the saturation of ions in solution and a kinetic constant K_r. The Bayesian Monte Carlo method was used to identify which K_r constant needed to be adjusted in order to determine the phosphate, calcium and magnesium concentration in digested sludge.

The results show that the constants linked to the precipitation of calcium carbonate, magnesium carbonate and amorphous calcium phosphate ($K_{r,CaCO3}$, $K_{r,MgCO3}$ and $K_{r,ACP}$, respectively) must be adjusted separately for each digester in order to fit the calcium and magnesium concentrations. In contrast, the simulated phosphate concentrations were already close to the observed values without adjustment of the Kr constants, for both digesters. The anaerobic digester with lower calcium and magnesium concentrations showed more consistent results without adjusting the precipitation kinetic constant K_r, suggesting that the calibration of the precipitation constants is particularly important when the water hardness is high. The inclusion of precipitation mechanisms when simulating an anaerobic digestion process is essential in order to obtain a consistent concentration of phosphate ions in the digested sludge. However, in order to reduce the degree of uncertainty of the precipitation kinetic constants, obtaining data on the concentrations of magnesium, calcium and phosphate is essential to consider while calibrating the anaerobic digestion model.

5.4 Influence of sludge typology and water hardness on the potential for phosphorus recovery

The recovery of phosphorus in the form of struvite from anaerobic digestion sidestreams is generally recommended for water resource recovery facilities with enhanced biological phosphorus removal since more release is expected in the anaerobic digester. However, there is no analysis in the literature of anaerobic digestion or centralised anaerobic digesters of sludge with different types of phosphorus treatment. In addition, water hardness (calcium and magnesium concentrations) are not presented as decision criteria in scenario analyses while these ions can impact the quantity of phosphate in digested sludge and therefore in anaerobic digestion sidestreams. *Chapter 4* provides a scenario analysis for a sludge line consisting of an anaerobic digester designed to treat internal sludge but also to treat sludge from surrounding facilities. This scenario analysis was carried out for different levels of water hardness (calcium, magnesium and inorganic carbon concentration) and used the anaerobic digestion models validated in *Chapter 3*.

Simulation results of the different anaerobic digester scenarios and simplified calculations of theoretical struvite production show that the centralised anaerobic digester including a part of sludge with biological phosphorus removal has the highest potential for P recovery in the form of struvite. On the other hand, for a same type of sludge, the amount of phosphate in the digested sludge can double if you move from a region with high water hardness to one with low water hardness. In addition, anaerobic digestion of sludge without specific phosphorus treatment can lead to phosphate concentrations that are compatible with an implementation of a struvite recovery unit for low or medium water hardness level. In conclusion, the decision criteria for implementing phosphorus recovery in the form of struvite should be based on the type of phosphorus treatment applied (without

specific phosphorus treatment, chemical and biological phosphorus removal) and on the level of water hardness.

5.5 Choice of a process for biological nitrogen treatment

The scenario analysis presented in *Chapter 4* also includes the assessment of different biological nitrogen treatments: nitrification/denitrification adding an external carbon source, one-stage and two-stage partial nitrification/anammox. A simplified carbon footprint assessment is presented because the literature highlights the important N_2O emissions of the partial nitritation/anammox process. In addition, most of the scenario analysis with partial nitritation/anammox process found in the literature only evaluate operational costs (chemical and energy consumption) and do not include a CO_2 balance.

The carbon footprint of biological nitrogen treatment in *Chapter 4* is based on the median value of N_2O emission factors found in the literature. The results of this CO_2 balance point out the elevated N_2O emissions when applying a two-stage partial nitritation/anammox process compared to nitrification/denitrification and to one-stage partial nitrification/anammox processes. The resulting carbon footprint of the two-stage partial nitritation/anammox process is twice the one obtained with the other processes. However, partial nitritation/anammox processes also requires less energy and chemicals so the operational costs and indirect CO_2 emissions are lower than the nitrification/denitrification scenario. In conclusion, the choice for a biological sidestream treatment cannot be based only on operational performance indicators but should also include the carbon footprint. This is paramount in order to come up with meaningful decisions for the evolution towards durable water resource recovery facilities.

5.6. Perspectives

5.6.1 Application of the precipitation model

This doctoral research uses the precipitation model developed in the work of Lizarralde et al. (2015) and Musvoto et al. (2000a, 2000b) and takes into account the precipitation kinetic constants K_r from Ikumi et al. (2020). However, different versions and writing of the precipitation models exist in the literature which makes difficult the comparison of the kinetic constant values. In addition, the relatively scarce application of precipitation models leads to limited knowledge about the range of values that can be attributed to the precipitation kinetic constants. In future research, more experimental data, especially on ion concentrations in the digesters, will be needed in order to assign ranges of values for precipitation parameters $K_{r,crys}$ in relation to operating conditions. To do so, experiments in controlled environment could be used to identify which operating conditions (water hardness, reactor form, mixing intensity or TSS concentration) has the greatest impact on the precipitation parameters $K_{r,crys}$ These constants $K_{r,crys}$ currently encompass many of these operating conditions and it is difficult to separate each effect when having full-scale data. To start with, a study of laboratory-scale AD pilots, varying only the types of sludge (with different water hardness Ca, Mg, P) could confirm that water hardness has an impact on the value of the $K_{r,crys}$ as it has been highlighted in this doctoral work. For this kind of experiment, the measurements of total phosphorus, phosphate, magnesium (total and soluble), Ca (total and soluble), pH, TSS ,VSS, biogas production as well as the

identification of the different minerals precipitated in the anaerobic digester will be required. In addition, a standardisation of the precipitation model with a same writing and units could also be helpful to compare different simulation results. The version suggested in the general physicochemical model (Batstone and Flores-alsina, 2022) could be systematically used in the future.

No struvite recovery reactor was simulated in this thesis because there was no monitoring data available for this technology and the validation of the model was not possible. A simulation would have provided the different minerals formed in the precipitation reactor. As with the precipitation in the anaerobic digester, access to data on phosphate, magnesium, calcium, alkalinity, pH as well as the identification of the minerals formed in the struvite recovery unit are essential to evaluate the potential and the quality of struvite recovery in future scenario analyses.

In this work, the interactions only between phosphorus, magnesium, calcium and inorganic carbon were considered in the precipitation mechanisms. Iron phosphate and iron oxides minerals were also used in the characterisation of the sludge in a simplified way. However, more accurate descriptions of the interactions between phosphorus, iron and sulfur are now available and integrated into model libraries (Hauduc et al., 2019; Solon et al., 2017). Nevertheless, the validation of these model is not straightforward because there is poor information on sulfur, iron and phosphate throughout the entire WRRF. Lab pilot of anaerobic digester could also help to obtain more data and validate this recent model.

In conclusion, precipitation mechanisms and interactions between phosphorus, magnesium, calcium, sulfur and iron have been integrated in recent model libraries but the validation and the application of the model is still scarce because of the lack of data and validation. Specific measurement campaigns and experiments under controlled environment to validate such models should be conducted in the future for different WRRF configurations and struvite recovery technologies. This is primordial to conduct reliable scenario analyses to optimise phosphorus recovery.

5.6.2 Plant wide evaluation of sidestreams

This work did not provide an assessment of the sidestream impacts on the entire WRRF functioning. However, a comparison of different sidestream treatment processes and their potential benefit for the WRRF cannot be made without considering the overall facility. Indeed, the conclusion on the performance of individual sidestream processes (energy and chemical consumption) can be different when the overall picture is viewed. Also, the impact of the nitrogen load from anaerobic digestion sidestreams on the nitrification and denitrification capacity of the WRRF is highly important. In addition, future plant wide simulations should consider the dynamics of streams. As an example, without sidestream treatment, the low concentrations of biodegradable COD during the night period associated with the high load of nitrogen from sidestreams could also impact the denitrification capacity.

In existing plant-wide models, the inclusion of precipitation kinetics has been applied mainly for the anaerobic digestion process. However, precipitation can also happen in other locations in the WRRF and particularly, in primary clarifiers, digested sludge storage tank, tubes and centrifuge. A discrepancy of phosphate quantity between digested sludge and sidestreams can therefore be observed at full scale but this is not represented in the model. In addition, thickening units or sludge storage tanks with high sludge retention time can lead to the formation of anaerobic zone and ion release. This could have an impact on the quantity of phosphate not only in anaerobic digestion

sidestreams but also on primary sludge or biological sludge sidestreams. Considering these mechanisms in the models could improve the prediction for phosphorus recovery.

5.6.3 Towards more integrated approaches

The evolution towards water resource recovery facility implies the existence of a market for the recovered products. Grid injection or combined heat and power with the production of biogas has already been well developed and implemented at full-scale. However, there are still few application cases showing a complete circularity of nutrients (nitrogen and phosphorus) from recovery in wastewater to application as a fertiliser. Nonetheless, struvite has been proved to be a slow-release fertiliser and can even reduce the risk of eutrophication compared to conventional fertiliser (Mancho et al., 2023). The low application of struvite as fertiliser can be due to different aspects (technical, social, and economic) and disciplines (engineers, physical, biologists, political scientists and policy makers) that have to be considered throughout the value chain of the resource. The most important aspects are having appropriate regulations and local demand for the recovered resource. For phosphorus recovery, annexes II and IV of the Regulation (EU) 2019/1009 of the European Parliament and of the Council have been recently modified to add precipitated phosphate salts and derivates as a component material category in EU fertilising products with application from July 2022. For the market, the phosphorus world demand could not be entirely sustain phosphorus recovery from wastewater but the recovery as struvite from wastewater can contribute partially and locally to the demand (Kok et al., 2018).

The integrated approaches that are able to include the potential for resource recovery in the WRRF, the need for this resource in surrounding areas, the existing market for this resource and all the costs relative to transport and resource transformation after the recovery in WRRF are the keys to achieve sustainable implementation of a WRRF. Without this complete integration, the water resource recovery facility could not be meaningful from a circular economy point of view. The challenge in the coming years is not only to make available data to enhance our model predictions but it is also to provide an efficient and sustainable end route of resource recovered from wastewater.

In this work, an attempt has been made to include carbon footprint and to consider the ions that can interfere with the quality of the recovered product. In the future, model platforms that can indicate the compatibility of the recovered product with market needs as well as a more accurate calculation of the carbon footprint could enable a better assessment of nutrient recovery in WRRFs. However, the inclusion of new performance criteria in addition of effluent quality and operational costs index also create more complex multi-criteria optimisation problems to solve.

References

Abdulhussein Alsaedi, A., Sohrab Hossain, M., Balakrishnan, V., Abdul Hakim Shaah, M., Mohd Zaini Makhtar, M., Ismail, N., Naushad, M., Bathula, C., 2022. Extraction and separation of lipids from municipal sewage sludge for biodiesel production: Kinetics and thermodynamics modeling. Fuel 325, 124946. https://doi.org/10.1016/j.fuel.2022.124946

Abma, W.R., Driessen, W., Haarhuis, R., Van Loosdrecht, M.C.M., 2010. Upgrading of sewage treatment plant by sustainable and cost-effective separate treatment of industrial wastewater. Water Sci. Technol. 61, 1715–1722. https://doi.org/10.2166/wst.2010.977

ADEME, 2023. base carbone® v19.0 [WWW Document]. URL https://data.ademe.fr/datasets/base-carbone(r) (accessed 3.20.23).

Ahn, Y.H., 2006. Sustainable nitrogen elimination biotechnologies: A review. Process Biochem. 41, 1709–1721. https://doi.org/10.1016/j.procbio.2006.03.033

Ahuja, N., 2015. Impact of Operating Conditions on Thermal Hydrolysis Pre-Treated Digestion Return Liquor.

Akhiar, A., Battimelli, A., Torrijos, M., Carrere, H., 2017. Comprehensive characterization of the liquid fraction of digestates from full-scale anaerobic co-digestion. Waste Manag. 59, 118–128. https://doi.org/10.1016/j.wasman.2016.11.005

Aktan, C.K., Yapsakli, K., Mertoglu, B., 2012. Inhibitory effects of free ammonia on Anammox bacteria. Biodegradation 23, 751–762. https://doi.org/10.1007/s10532-012-9550-0

Al-Sahari, M., Al-Gheethi, A., Radin Mohamed, R.M.S., Noman, E., Naushad, M., Rizuan, M.B., Vo, D.V.N., Ismail, N., 2021. Green approach and strategies for wastewater treatment using bioelectrochemical systems: A critical review of fundamental concepts, applications, mechanism, and future trends. Chemosphere 285, 131373. https://doi.org/10.1016/j.chemosphere.2021.131373

Al Momani, F., Örmeci, B., 2020. Assessment of algae-based wastewater treatment in hot climate region: Treatment performance and kinetics. Process Saf. Environ. Prot. 141, 140–149. https://doi.org/10.1016/j.psep.2020.03.031

Andreoli, C.V., Sperling, M. von, Fernandes, F., 2007. Sludge treatment and disposal. IWA Publishing.

APHA, 2005. Standard Methods for the Examination of Water and Wastewater. 21st Edition, American Public Health Association/American Water Works Association/Water Environment Federation, Washington DC.

Appels, L., Baeyens, J., Degrève, J., Dewil, R., 2008. Principles and potential of the anaerobic digestion of waste-activated sludge. Prog. Energy Combust. Sci. 34, 755–781. https://doi.org/10.1016/j.pecs.2008.06.002

Appels, L., Degrève, J., Van der Bruggen, B., Van Impe, J., Dewil, R., 2010. Influence of low temperature thermal pre-treatment on sludge solubilisation, heavy metal release and anaerobic digestion. Bioresour. Technol. 101, 5743–5748. https://doi.org/10.1016/j.biortech.2010.02.068

Appels, L., Lauwers, J., Degrve, J., Helsen, L., Lievens, B., Willems, K., Van Impe, J., Dewil, R., 2011. Anaerobic digestion in global bio-energy production: Potential and research challenges. Renew. Sustain. Energy Rev. https://doi.org/10.1016/j.rser.2011.07.121

Arabi, S., Nakhla, G., 2008. Impact of calcium on the membrane fouling in membrane bioreactors. J.

Memb. Sci. 314, 134–142. https://doi.org/10.1016/j.memsci.2008.01.037

Arienzo, M., Christen, E.W., Quayle, W., Kumar, A., 2009. A review of the fate of potassium in the soil-plant system after land application of wastewaters. J. Hazard. Mater. 164, 415–422. https://doi.org/10.1016/j.jhazmat.2008.08.095

Arora, A.S., Nawaz, A., Abdul, M., Ismail, S., Aslam, M., Tawfik, A., Mun, C., Lee, M., 2021. Energy saving anammox technology-based nitrogen removal and bioenergy recovery from wastewater : Inhibition mechanisms , state-of-the-art control strategies , and prospects. Renew. Sustain. Energy Rev. 135, 110126. https://doi.org/10.1016/j.rser.2020.110126

Astals, S., Esteban-Gutiérrez, M., Fernández-Arévalo, T., Aymerich, E., García-Heras, J.L., Mata-Alvarez, J., 2013. Anaerobic digestion of seven different sewage sludges: A biodegradability and modelling study. Water Res. 47, 6033–6043. https://doi.org/10.1016/j.watres.2013.07.019

Astals, S., Martínez-Martorell, M., Huete-Hernández, S., Aguilar-Pozo, V.B., Dosta, J., Chimenos, J.M., 2021. Nitrogen recovery from pig slurry by struvite precipitation using a low-cost magnesium oxide. Sci. Total Environ. 768. https://doi.org/10.1016/j.scitotenv.2020.144284

Baeten, J.E., Batstone, D.J., Schraa, O.J., van Loosdrecht, M.C.M., Volcke, E.I.P., 2019. Modelling anaerobic, aerobic and partial nitritation-anammox granular sludge reactors - A review. Water Res. https://doi.org/10.1016/j.watres.2018.11.026

Bakan, B., Bernet, N., Bouchez, T., Boutrou, R., Choubert, J.M., Dabert, P., Duquennoi, C., Ferraro, V., García-Bernet, D., Gillot, S., Mery, J., Rémond, C., Steyer, J.P., Trably, E., Tremier, A., 2022. Circular Economy Applied to Organic Residues and Wastewater: Research Challenges. Waste and Biomass Valorization. https://doi.org/10.1007/s12649-021-01549-0

Banks, D., Birke, M., Flem, B., Reimann, C., 2015. Inorganic chemical quality of European tap-water: 1. Distribution of parameters and regulatory compliance. Appl. Geochemistry 59, 200–210. https://doi.org/10.1016/j.apgeochem.2014.10.016

Baquerizo, G., Fiat, J., Buffiere, P., Girault, R., Gillot, S., 2021. Modelling the dynamic long-term performance of a full-scale digester treating sludge from an urban WRRF using an extended version of ADM1. Chem. Eng. J. 423, 128870. https://doi.org/10.1016/j.cej.2021.128870

Barat, R., Bouzas, A., Martí, N., Ferrer, J., Seco, A., 2009. Precipitation assessment in wastewater treatment plants operated for biological nutrient removal: A case study in Murcia, Spain. J. Environ. Manage. 90, 850–857. https://doi.org/10.1016/j.jenvman.2008.02.001

Barat, R., Serralta, J., Ruano, M. V., Jiménez, E., Ribes, J., Seco, A., Ferrer, J., 2013. Biological Nutrient Removal Model No. 2 (BNRM2): a general model for wastewater treatment plants. Water Sci. Technol. 67, 1481–1489. https://doi.org/10.2166/wst.2013.004

Barber, W.P.F., 2016. Thermal hydrolysis for sewage treatment: A critical review. Water Res. 104, 53–71. https://doi.org/http://dx.doi.org/10.1016/j.watres.2016.07.069

Barnes, D., Li, X., Chen, J., 2007. Determination of suitable pretreatment method for old-intermediate landfill leachate. Environ. Technol. 28, 195–203. https://doi.org/10.1080/09593332808618782

Barua, S., Zakaria, B.S., Chung, T., Hai, F.I., Haile, T., 2019. Microbial electrolysis followed by chemical precipitation for effective nutrients recovery from digested sludge centrate in WWTPs. Chem. Eng. J. 361, 256–265. https://doi.org/10.1016/j.cej.2018.12.067

Batstone, D.J., Amerlinck, Y., Ekama, G., Goel, R., Grau, P., Johnson, B., Kaya, I., Steyer, J.P., Tait, S., Takaćs, I., Vanrolleghem, P.A., Brouckaert, C.J., Volcke, E., 2012. Towards a generalized physicochemical framework. Water Sci. Technol. 66, 1147–1161.

https://doi.org/10.2166/wst.2012.300

Batstone, D.J., Flores-alsina, X., 2022. Generalised Physicochemical Model (PCM) for Wastewater Processes, Generalised Physicochemical Model (PCM) for Wastewater Processes. https://doi.org/10.2166/9781780409832

Batstone, D. J., Hülsen, T., Mehta, C.M., Keller, J., 2015. Platforms for energy and nutrient recovery from domestic wastewater: A review. Chemosphere 140, 2–11. https://doi.org/10.1016/j.chemosphere.2014.10.021

Batstone, D.J., Keller, J., Angelidaki, I., Kalyuzhnyi, S.V., Rozzi, A., Sanders, W.T.M., Siegrist, H., Vavilin, V.A., 2002. Anaerobic Digestion Model No.1.

Batstone, Damien J., Puyol, D., Flores-Alsina, X., Rodríguez, J., 2015. Mathematical modelling of anaerobic digestion processes: applications and future needs. Rev. Environ. Sci. Biotechnol. 14, 595–613. https://doi.org/10.1007/s11157-015-9376-4

Baumgartner, T., Jahn, L., Parravicini, V., Svardal, K., Krampe, J., 2022. Efficiency of Sidestream Nitritation for Modern Two-Stage Activated Sludge Plants. Int. J. Environ. Res. Public Health 19, 12871. https://doi.org/10.3390/ijerph191912871

Beckinghausen, A., Odlare, M., Thorin, E., Schwede, S., 2020. From removal to recovery: An evaluation of nitrogen recovery techniques from wastewater. Appl. Energy. https://doi.org/10.1016/j.apenergy.2020.114616

Benedetti, L., Claeys, F., Nopens, I., Vanrolleghem, P.A., 2011. Assessing the convergence of LHS Monte Carlo simulations of wastewater treatment models. Water Sci. Technol. 63, 2219–2224. https://doi.org/10.2166/wst.2011.453

Berends, D.H.J.G., Salem, S., Roest, H.F. Van Der, Loosdrecht, M.C.M. Van, 2000. Boosting nitrification with the BABE technology. Water Sci. Technol. 63–70.

Bhuiyan, M.I.H., Mavinic, D.S., Beckie, R.D., 2009. Determination of Temperature Dependence of Electrical Conductivity and Its Relationship with Ionic Strength of Anaerobic Digester Supernatant, for Struvite Formation. J. Environ. Eng. 135, 1221–1226. https://doi.org/10.1061/(ASCE)0733-9372(2009)135:11(1221)

Bi, Z., Wanyan, D., Li, X., Huang, Y., 2020. Biological conversion pathways of sulfate reduction ammonium oxidation in anammox consortia. Front. Environ. Sci. Eng. 14, 1–11. https://doi.org/10.1007/s11783-019-1217-1

Boehler, M.A., Heisele, A., Seyfried, A., Grömping, M., Siegrist, H., 2015. (NH4)2SO4 recovery from liquid side streams. Environ. Sci. Pollut. Res. 22, 7295–7305. https://doi.org/10.1007/s11356-014-3392-8

Bohutskyi, P., Liu, K., Nasr, L.K., Byers, N., Rosenberg, J.N., Oyler, G.A., Betenbaugh, M.J., Bouwer, E.J., 2015. Bioprospecting of microalgae for integrated biomass production and phytoremediation of unsterilized wastewater and anaerobic digestion centrate. Appl. Microbiol. Biotechnol. 99, 6139–6154. https://doi.org/10.1007/s00253-015-6603-4

Bougrier, C., Delgenès, J.P., Carrère, H., 2008. Effects of thermal treatments on five different waste activated sludge samples solubilisation, physical properties and anaerobic digestion. Chem. Eng. J. 139, 236–244. https://doi.org/10.1016/j.cej.2007.07.099

Bouzas, A., Martí, N., Grau, S., Barat, R., Mangin, D., Pastor, L., 2019. Implementation of a global P-recovery system in urban wastewater treatment plants. J. Clean. Prod. 227, 130–140. https://doi.org/10.1016/j.jclepro.2019.04.126

Bowden, G., Tsuchihashi, R., Stensel, H.D., 2015. Technologies for Sidestream Nitrogen Removal. Water Envirnment Res. Found.

Bretz, F., Hothorn, T., Westfall, P., 2010. Multiple Comparisons Using R, Multiple Comparisons Using R. https://doi.org/10.1201/9781420010909-f

Burgess, J.E., Quarmby, J., Stephenson, T., 1999. Micronutrient supplements for optimisation of the treatment of industrial wastewater using activated sludge. Water Res. 33, 3707–3714. https://doi.org/10.1016/S0043-1354(99)00094-9

Capdevila-Cortada, M., 2019. Electrifying the Haber–Bosch. Nat. Catal. 2, 1055. https://doi.org/10.1038/s41929-019-0414-4

Capson-Tojo, G., Moscoviz, R., Astals, S., Robles, Steyer, J.P., 2020. Unraveling the literature chaos around free ammonia inhibition in anaerobic digestion. Renew. Sustain. Energy Rev. 117, 109487. https://doi.org/10.1016/j.rser.2019.109487

Carrère, H., Dumas, C., Battimelli, A., Batstone, D.J., Delgenès, J.P., Steyer, J.P., Ferrer, I., 2010. Pretreatment methods to improve sludge anaerobic degradability: A review. J. Hazard. Mater. 183, 1–15. https://doi.org/http://dx.doi.org/10.1016/j.jhazmat.2010.06.129

Castro-Barros, C.M., Daelman, M.R.J., Mampaey, K.E., van Loosdrecht, M.C.M., Volcke, E.I.P., 2015. Effect of aeration regime on N2O emission from partial nitritation-anammox in a full-scale granular sludge reactor. Water Res. 68, 793–803. https://doi.org/10.1016/j.watres.2014.10.056

Chamchoi, N., Nitisoravut, S., Schmidt, J.E., 2008. Inactivation of ANAMMOX communities under concurrent operation of anaerobic ammonium oxidation (ANAMMOX) and denitrification. Bioresour. Technol. 99, 3331–3336. https://doi.org/10.1016/j.biortech.2007.08.029

Choubert, J.., Martin-Ruel, S., Budzinski, H., Miège, C., Esperanza, M., Soulier, C., Ugarrigue, C., Coquery, M., 2011. Évaluer les rendements des stations d'épuration Apports méthodologiques et résultats pour les micropolluants en filières conventionnelles et avancées. Tech. - Sci. - Methodes 44–62.

Christensson, M., Ekström, S., Chan, A.A., Le Vaillant, E., Lemaire, R., 2013. Experience from start-ups of the first ANITA Mox Plants. Water Sci. Technol. 67, 2677–2684. https://doi.org/10.2166/wst.2013.156

Constantine, T.A., 2006. North American Experience with Centrate Treatment Technologies for Ammonia and Nitrogen Removal, in: WEFTEC 2006. Water Environment Federation.

Cordell, D., Drangert, J.O., White, S., 2009. The story of phosphorus: Global food security and food for thought. Glob. Environ. Chang. 19, 292–305. https://doi.org/10.1016/j.gloenvcha.2008.10.009

Costamagna, P., Giordano, A., Lazzarini, Y., Delucchi, M., Busca, G., 2020. Process of ammonia removal from anaerobic digestion and associated ammonium sulphate production: Pilot plant demonstration. J. Environ. Manage. 259, 109841. https://doi.org/10.1016/j.jenvman.2019.109841

Couturier, C., Berger, S., Meiffren, I., 2001. La digestion anaérobie des boues urbaines. Etat des lieux, Etat de l'art. Solagro, l'Agence de l'eau Adour-Garonne 34p.

Cullen, N., Baur, R., Schauer, P., 2013. Three years of operation of North America's first nutrient recovery facility. Water Sci. Technol. 68, 763–768. https://doi.org/10.2166/wst.2013.260

Daneshgar, S., Vanrolleghem, P.A., Vaneeckhaute, C., Buttafava, A., Capodaglio, A.G., 2019. Optimization of P compounds recovery from aerobic sludge by chemical modeling and response

surface methodology combination. Sci. Total Environ. 668, 668–677. https://doi.org/10.1016/j.scitotenv.2019.03.055

Darestani, M., Haigh, V., Couperthwaite, S.J., Millar, G.J., Nghiem, L.D., 2017. Hollow fibre membrane contactors for ammonia recovery: Current status and future developments. J. Environ. Chem. Eng. 5, 1349–1359. https://doi.org/10.1016/j.jece.2017.02.016

de Fouchécour, F., Larzillière, V., Bouchez, T., Moscoviz, R., 2022. Systematic and quantitative analysis of two decades of anodic wastewater treatment in bioelectrochemical reactors. Water Res. 214. https://doi.org/10.1016/j.watres.2022.118142

de Gracia, M., Grau, P., Huete, E., Gómez, J., García-Heras, J.L., Ayesa, E., 2009. New generic mathematical model for WWTP sludge digesters operating under aerobic and anaerobic conditions: Model building and experimental verification. Water Res. 43, 4626–4642. https://doi.org/10.1016/j.watres.2009.07.014

De Ketele, J., Davister, D., Ikumi, D.S., 2018. Applying performance indices in plantwide modelling for a comparative study of wastewater treatment plant operational strategies. Water SA 44, 539–550. https://doi.org/10.4314/wsa.v44i4.03

Desmidt, E., Ghyselbrecht, K., Monballiu, A., Rabaey, K., Verstraete, W., Meesschaert, B.D., 2013. Factors influencing urease driven struvite precipitation. Sep. Purif. Technol. https://doi.org/10.1016/j.seppur.2013.03.010

Desmidt, E., Ghyselbrecht, K., Zhang, Y., Pinoy, L., Van Der Bruggen, B., Verstraete, W., Rabaey, K., Meesschaert, B., 2015. Global phosphorus scarcity and full-scale P-recovery techniques: A review. Crit. Rev. Environ. Sci. Technol. 45, 336–384. https://doi.org/10.1080/10643389.2013.866531

Devos, P., Filali, A., Grau, P., Gillot, S., 2023. Sidestream characteristics in water resource recovery facilities: A critical review. Water Res. 232, 119620. https://doi.org/10.1016/j.watres.2023.119620

Devos, P., Haddad, M., Carrère, H., 2020. Thermal Hydrolysis of Municipal sludge: Finding the Temperature Sweet Spot: A Review. Waste and Biomass Valorization 12, 2187–2205. https://doi.org/10.1007/s12649-020-01130-1

Donoso-Bravo, A., Olivares, D., Lesty, Y., Vanden, H., 2020. Exploitation of the ADM1 in a XXI century wastewater resource recovery facility (WRRF): The case of codigestion and thermal hydrolysis. Water Res. 175, 115654. https://doi.org/10.1016/j.watres.2020.115654

Driessen, W., Van Veldhoven, J.T.A., Janssen, M.P.M., Van Loosdrecht, M.C.M., 2020. Treatment of sidestream dewatering liquors from thermally hydrolised and anaerobically digested biosolids. Water Pract. Technol. 15, 142–150. https://doi.org/10.2166/wpt.2020.007

Dwyer, J., Kavanagh, L., Lant, P., 2008a. The degradation of dissolved organic nitrogen associated with melanoidin using a UV/H2O2 AOP. Chemosphere 71, 1745–1753. https://doi.org/10.1016/j.chemosphere.2007.11.027

Dwyer, J., Starrenburg, D., Tait, S., Barr, K., Batstone, D.J., Lant, P., 2008b. Decreasing activated sludge thermal hydrolysis temperature reduces product colour, without decreasing degradability. Water Res. 42, 4699–4709. https://doi.org/10.1016/j.watres.2008.08.019

Ebbers, B., Ottosen, L.M., Jensen, P.E., 2015. Electrodialytic treatment of municipal wastewater and sludge for the removal of heavy metals and recovery of phosphorus. Electrochim. Acta 181, 90–99. https://doi.org/10.1016/j.electacta.2015.04.097

Eggers, E., Dirkzwager, A.H., Van der Honing, H., 1991. Full-scale experiences with phosphate

crystallisation in a crystalactor. Water Sci. Technol. 24, 333–334. https://doi.org/10.2166/wst.1991.0533

Egle, L., Rechberger, H., Krampe, J., Zessner, M., 2016. Phosphorus recovery from municipal wastewater: An integrated comparative technological, environmental and economic assessment of P recovery technologies. Sci. Total Environ. 571, 522–542. https://doi.org/10.1016/j.scitotenv.2016.07.019

Elduayen-Echave, B., Lizarralde, I., Larraona, G.S., Ayesa, E., Grau, P., 2019. A New Mass-Based Discretized Population Balance Model for Precipitation Processes : Application to Struvite Precipitation. Water Res. 155, 26–41. https://doi.org/10.1016/j.watres.2019.01.047

Elduayen-Echave, B., Lizarralde, I., Schneider, P.A., Ayesa, E., Larraona, G.S., Grau, P., 2021. Inclusion of shear rate effects in the kinetics of a discretized population balance model: Application to struvite precipitation. Water Res. 200, 117242. https://doi.org/10.1016/j.watres.2021.117242

Eskicioglu, C., Galvagno, G., Cimon, C., 2018. Approaches and processes for ammonia removal from side-streams of municipal effluent treatment plants. Bioresour. Technol. 268, 797–810. https://doi.org/10.1016/j.biortech.2018.07.020

European Commission, 2019. Regulation (EU) 2019/1009 laying down rules on the making available on the market of EU fertilising products and amending Regulations (EC) No 1069/2009 and (EC) No 1107/2009 and repealing Regulation (EC) No 2003/2003. Off. J. Eur. Union.

Feng, Y., Lu, X., Al-Hazmi, H., Mąkinia, J., 2017. An overview of the strategies for the deammonification process start-up and recovery after accidental operational failures. Rev. Environ. Sci. Biotechnol. 16, 541–568. https://doi.org/10.1007/s11157-017-9441-2

Fenu, A., Smolders, S., De Gussem, K., Weemaes, M., 2019. Conflicting carbon footprint and energy saving in a side-stream Anammox Process. Biochem. Eng. J. 151, 107336. https://doi.org/10.1016/j.bej.2019.107336

Fernández-Arévalo, T., Lizarralde, I., Fdz-Polanco, F., Pérez-Elvira, S.I., Garrido, J.M., Puig, S., Poch, M., Grau, P., Ayesa, E., 2017a. Quantitative assessment of energy and resource recovery in wastewater treatment plants based on plant-wide simulations. Water Res. 118, 272–288. https://doi.org/10.1016/j.watres.2017.04.001

Fernández-Arévalo, T., Lizarralde, I., Maiza, M., Beltrán, S., Grau, P., Ayesa, E., 2017b. Diagnosis and optimization of WWTPs using the PWM library: Full-scale experiences. Water Sci. Technol. 75, 518–529. https://doi.org/10.2166/wst.2016.482

Fernández, I., Dosta, J., Fajardo, C., Campos, J.L., Mosquera-Corral, A., Méndez, R., 2012. Short- and long-term effects of ammonium and nitrite on the Anammox process. J. Environ. Manage. 95, S170–S174. https://doi.org/10.1016/j.jenvman.2010.10.044

Figdore, B., Wett, B., Hell, M., Murthy, S., 2011. Deammonification of Dewatering Sidestream from Thermal Hydrolysis-Mesophilic Anaerobic Digestion Process. Proc. Water Environ. Fed. 2011, 1037–1052. https://doi.org/10.2175/193864711802867289

Fisgativa, H., Marcilhac, C., Girault, R., Daumer, M., Trémier, A., Dabert, P., Béline, F., 2018. Data in Brief Physico-Chemical , biochemical and nutritional characterisation of 42 organic wastes and residues from France. Data Br. 19, 1953–1962. https://doi.org/10.1016/j.dib.2018.06.050

Fisgativa, H., Marcilhac, C., Jaudoin, C., Bareha, Y., Girault, R., Tremier, A., Béline, F., 2020a. Biological Nitrogen Potential (BNP): A New Methodology to Estimate Nitrogen Transformations During Anaerobic Digestion of Organic Substrates. Waste and Biomass Valorization 11, 525–537.

https://doi.org/10.1007/s12649-019-00683-0

Fisgativa, H., Zennaro, B., Charnier, C., Richard, C., Accarion, G., Fabrice, B., 2020b. Data in brief Comprehensive determination of input state variables dataset required for anaerobic digestion modelling (ADM1) based on characterisation of organic substrates. Data Br. 29. https://doi.org/10.1016/j.dib.2020.105212

Flores-Alsina, X., Arnell, M., Amerlinck, Y., Corominas, L., Gernaey, K. V., Guo, L., Lindblom, E., Nopens, I., Porro, J., Shaw, A., Snip, L., Vanrolleghem, P.A., Jeppsson, U., 2014. Balancing effluent quality, economic cost and greenhouse gas emissions during the evaluation of (plant-wide) control/operational strategies in WWTPs. Sci. Total Environ. 466–467, 616–624. https://doi.org/10.1016/j.scitotenv.2013.07.046

Flores-Alsina, X., Corominas, L., Snip, L., Vanrolleghem, P.A., 2011. Including greenhouse gas emissions during benchmarking of wastewater treatment plant control strategies. Water Res. 45, 4700–4710. https://doi.org/10.1016/j.watres.2011.04.040

Flores-Alsina, X., Kazadi Mbamba, C., Solon, K., Vrecko, D., Tait, S., Batstone, D.J., Jeppsson, U., Gernaey, K. V., 2015. A plant-wide aqueous phase chemistry module describing pH variations and ion speciation/pairing in wastewater treatment process models. Water Res. 85, 255–265. https://doi.org/10.1016/j.watres.2015.07.014

Flores-Alsina, X., Ramin, E., Ikumi, D., Harding, T., Batstone, D., Brouckaert, C., Sotemann, S., Gernaey, K. V., 2021. Assessment of sludge management strategies in wastewater treatment systems using a plant-wide approach. Water Res. 190, 116714. https://doi.org/10.1016/j.watres.2020.116714

Forouzanmehr, F., Le, Q.H., Solon, K., Maisonnave, V., Daniel, O., Buffiere, P., Gillot, S., Volcke, E.I.P., 2021. Plant-wide investigation of sulfur flows in a water resource recovery facility (WRRF). Sci. Total Environ. 801. https://doi.org/10.1016/j.scitotenv.2021.149530

Forouzanmehr, F., Solon, K., Maisonnave, V., Daniel, O., Volcke, E.I.P., Gillot, S., Buffiere, P., 2022. Sulfur transformations during two-stage anaerobic digestion and intermediate thermal hydrolysis. Sci. Total Environ. 810. https://doi.org/10.1016/j.scitotenv.2021.151247

Fujimoto, N., Mizuochi, T., Togami, Y., 1991. Phosphorus Fixation in the Sludge Treatment System of a Biological Phosphorus Removal Process. Water Sci. Technol. 23, 635–640. https://doi.org/10.2166/wst.1991.0513

Galvagno, G., Eskicioglu, C., Abel-Denee, M., 2016. Biodegradation and chemical precipitation of dissolved nutrients in anaerobically digested sludge dewatering centrate. Water Res. 96, 84–93. https://doi.org/10.1016/j.watres.2016.03.036

Gernaey, K. V., Jeppsson, U., Vanrolleghem, P.A., Copp, J.B., 2014. Benchmarking of Control Strategies for Wastewater Treatment Plants, IWA publishing. IWA Publishing. https://doi.org/10.2166/9781780401171

Ghosh, S., Lobanov, S., Lo, V.K., 2019. An overview of technologies to recover phosphorus as struvite from wastewater: advantages and shortcomings. Environ. Sci. Pollut. Res. 26, 19063–19077. https://doi.org/10.1007/s11356-019-05378-6

Gillot, S., Capela-Marsal, S., Roustan, M., Héduit, A., 2005. Predicting oxygen transfer of fine bubble diffused aeration systems—model issued from dimensional analysis. Water Res. 39, 1379–1387. https://doi.org/10.1016/j.watres.2005.01.008

Gillot, S., Choubert, J.-M., 2010. Biodegradable organic matter in domestic wastewaters: comparison of selected fractionation techniques. Water Sci. Technol. 62, 630–639.

https://doi.org/10.2166/wst.2010.341

Girault, R., Bridoux, G., Nauleau, F., Poullain, C., Buffet, J., Steyer, J., 2012. A waste characterisation procedure for ADM1 implementation based on degradation kinetics. Water Res. 6. https://doi.org/10.1016/j.watres.2012.04.028

Gopalakrishnan, K., Anderson, J., Carrio, L., Abraham, K., Stinson, B., 2000. Design and Operational Considerations for Ammonia Removal From Centrate By Steam Stripping. Proc. Water Environ. Fed. 2000, 89–109. https://doi.org/10.2175/193864700784607361

Gourdet, C., Girault, R., Berthault, S., Richard, M., Tosoni, J., Pradel, M., 2017. In quest of environmental hotspots of sewage sludge treatment combining anaerobic digestion and mechanical dewatering: A life cycle assessment approach. J. Clean. Prod. 143, 1123–1136. https://doi.org/10.1016/j.jclepro.2016.12.007

Grau, P., Beltrán, S., de Gracia, M., Ayesa, E., 2007a. New mathematical procedure for the automatic estimation of influent characteristics in WWTPs. Water Sci. Technol. 56, 95–106. https://doi.org/10.2166/wst.2007.603

Grau, P., de Gracia, M., Vanrolleghem, P.A., Ayesa, E., 2007b. A new plant-wide modelling methodology for WWTPs. Water Res. 41, 4357–4372. https://doi.org/10.1016/j.watres.2007.06.019

Grulois, P., Bousseau, A., Blin, E., Fayoux, C., 1993. Evaluation of the impact of return flows on the operation of a wastewater treatment plant. Water Sci. Technol. 28, 273–281. https://doi.org/10.2166/wst.1993.0059

Guérin, S., Mottelet, S., Azimi, S., Bernier, J., Andre, L., Ribeiro, T., Pauss, A., Rocher, V., 2017. Le pouvoir méthanogène des boues urbaines: Cartographie des boues de STEP et réduction du temps de mesure par un couplage « expérimentation en réacteur/modélisation ». Récents Progrès en Génie des Procédés 54–61.

Guilayn, F., Rouez, M., Crest, M., Patureau, D., Jimenez, J., 2020. Valorization of digestates from urban or centralized biogas plants: a critical review. Rev. Environ. Sci. Bio/Technology 19, 419–462. https://doi.org/10.1007/s11157-020-09531-3

Gupta, A., Novak, J.T., Zhao, R., 2015. Characterization of organic matter in the thermal hydrolysis pretreated anaerobic digestion return liquor. J. Environ. Chem. Eng. 3, 2631–2636. https://doi.org/10.1016/j.jece.2015.07.029

Gustavsson, D.J.I., la Cour Jansen, J., 2011. Dynamics of nitrogen oxides emission from a full-scale sludge liquor treatment plant with nitritation. Water Sci. Technol. 63, 2838–2845. https://doi.org/10.2166/wst.2011.487

Han, X., Zhang, S., Yang, S., Zhang, L., Peng, Y., 2020. Full-scale partial nitritation/anammox (PN/A) process for treating sludge dewatering liquor from anaerobic digestion after thermal hydrolysis. Bioresour. Technol. 297, 122380. https://doi.org/10.1016/j.biortech.2019.122380

Hanhoun, M., Montastruc, L., Azzaro-Pantel, C., Biscans, B., Frèche, M., Pibouleau, L., 2013. Simultaneous determination of nucleation and crystal growth kinetics of struvite using a thermodynamic modeling approach. Chem. Eng. J. 215–216, 903–912. https://doi.org/10.1016/j.cej.2012.10.038

Hauck, M., Maalcke-Luesken, F.A., Jetten, M.S.M., Huijbregts, M.A.J., 2016. Removing nitrogen from wastewater with side stream anammox: What are the trade-offs between environmental impacts? Resour. Conserv. Recycl. 107, 212–219. https://doi.org/10.1016/j.resconrec.2015.11.019

Hauduc, H., Wadhawan, T., Takács, I., Johnson, B., Bott, C., Ward, M., 2019. Incorporating sulfur reactions and interactions with iron and phosphorus into a general plant-wide model. Water Sci. Technol. 79, 26–34. https://doi.org/10.2166/wst.2018.482

Hellinga, C., Schellen, A.A.J.C., Mulder, J.W., van Loosdrecht, M.C.M., Heijnen, J.J., 1998. The sharon process: an innovative method for nitrogen removal from ammonium-rich waste water. Water Sci. Technol. 37, 135–142. https://doi.org/10.2166/wst.1998.0350

Henze, M., Comeau, Y., 2008. Wastewater Characterization, in: Publishing, I. (Ed.), Biological Wastewater Treatment : Principles, Modelling and Design.

Hodgson, B., Sharvelle, S., 2019. Development of generalized empirical models for comparing effectiveness of wastewater nutrient removal technologies. Environ. Sci. Pollut. Res. 26, 27915–27929. https://doi.org/10.1007/s11356-019-05761-3

Holliger, C., Alves, M., Andrade, D., Angelidaki, I., Astals, S., Baier, U., Bougrier, C., Buffière, P., Carballa, M., De Wilde, V., Ebertseder, F., Fernández, B., Ficara, E., Fotidis, I., Frigon, J.C., De Laclos, H.F., Ghasimi, D.S.M., Hack, G., Hartel, M., Heerenklage, J., Horvath, I.S., Jenicek, P., Koch, K., Krautwald, J., Lizasoain, J., Liu, J., Mosberger, L., Nistor, M., Oechsner, H., Oliveira, J.V., Paterson, M., Pauss, A., Pommier, S., Porqueddu, I., Raposo, F., Ribeiro, T., Pfund, F.R., Strömberg, S., Torrijos, M., Van Eekert, M., Van Lier, J., Wedwitschka, H., Wierinck, I., 2016. Towards a standardization of biomethane potential tests. Water Sci. Technol. 74, 2515–2522. https://doi.org/10.2166/wst.2016.336

Hori, M., Shozugawa, K., Sugimori, K., Watanabe, Y., 2021. A survey of monitoring tap water hardness in Japan and its distribution patterns. Sci. Rep. https://doi.org/10.1038/s41598-021-92949-8

Hosseinipour Dizgah, S., Taghavi, K., Jaafari, J., Roohbakhsh, E., Ashrafi, S.D., 2018. Data on pollutants content in the influent and effluent from wastewater treatment plant of Rasht in Guilan Province, Iran. Data Br. 16, 271–275. https://doi.org/10.1016/j.dib.2017.11.042

Howe, K.J., Hand, D.W., Crittenden, J.C., Trussell, R.R., Tchobanoglous, G., 2012. Principles of water treatment.

Huang, X., Guida, S., Jefferson, B., Soares, A., 2020. Economic evaluation of ion-exchange processes for nutrient removal and recovery from municipal wastewater. npj Clean Water 3. https://doi.org/10.1038/s41545-020-0054-x

Huete, E., Gracia, M. De, Ayesa, E., 2006. ADM1-based methodology for the characterisation of the influent sludge in anaerobic reactors. Water Sci. Technol. https://doi.org/10.2166/wst.2006.537

Husband, J.A., Phillips, J., Coughenour, J.R., Walz, T., Blatchford, G., 2010. Innovative approach to centrate nitrification accomplishes multiple goals: nitrogen removal and odour control. Water Sci. Technol. 61, 1097–1103. https://doi.org/10.2166/wst.2010.858

Ikumi, D., 2020. Sensitivity analysis on a three-phase plant-wide water and resource recovery facility model for identification of significant parameters. Water SA 46, 476–492. https://doi.org/10.17159/wsa/2020.v46.i3.8658

Ikumi, D.S., Harding, T.H., 2020. Kinetics of biological and chemical processes in anoxic-aerobic digestion of phosphorus rich waste activated sludge. Water Res. 170, 115333. https://doi.org/10.1016/j.watres.2019.115333

Im, J., Gil, K., 2019. Study on the application of nitritation, treating different wastewater streams with high nitrogen content. Environ. Earth Sci. 78, 1–9. https://doi.org/10.1007/s12665-019-8175-6

IPCC, 2021. Climate Change 2021: The Physical Science Basis: Working Group I Contribution to the Sixth

Assessment Report of the Intergovernmental Panel on Climate Change. Cambridge Univ. Press Cambridge, UK; New York, NY, USA.

Jaffer, Y., Clark, T.., Pearce, P., Parsons, S.., 2002. Potential phosphorus recovery by struvite formation. Water Res. 36, 1834–1842. https://doi.org/10.1016/S0043-1354(01)00391-8

Janus, H.M., van der Roest, H.F., 1997. Don't reject the idea of treating reject water. Water Sci. Technol. 35, 27–34.

Jin, R.C., Yang, G.F., Yu, J.J., Zheng, P., 2012. The inhibition of the Anammox process: A review. Chem. Eng. J. 197, 67–79. https://doi.org/10.1016/j.cej.2012.05.014

Jin, R.C., Yang, G.F., Zhang, Q.Q., Ma, C., Yu, J.J., Xing, B.S., 2013. The effect of sulfide inhibition on the ANAMMOX process. Water Res. 47, 1459–1469. https://doi.org/10.1016/j.watres.2012.12.018

Jin, Y., Li, Y., Li, J., 2016. Influence of thermal pretreatment on physical and chemical properties of kitchen waste and the efficiency of anaerobic digestion. J. Environ. Manage. 180, 291–300. https://doi.org/10.1016/j.jenvman.2016.05.047

Johansson, S., Ruscalleda, M., Colprim, J., 2017. Phosphorus recovery through biologically induced precipitation by partial nitritation-anammox granular biomass. Chem. Eng. J. 327, 881–888. https://doi.org/10.1016/j.cej.2017.06.129

Joss, A., Salzgeber, D., Eugster, J., König, R., Rottermann, K., Burger, S., Fabijan, P., Leumann, S., Mohn, J., Siegrist, H., 2009. Full-Scale Nitrogen Removal from Digester Liquid with Partial Nitritation and Anammox in One SBR. Environ. Sci. Technol. 43, 5301–5306. https://doi.org/10.1021/es900107w

Jung, J.Y., Kang, S.H., Chung, Y.C., Ahn, D.H., 2007. Factors affecting the activity of anammox bacteria during start up in the continuous culture reactor. Water Sci. Technol. 55, 459–468. https://doi.org/10.2166/wst.2007.023

Kacprzak, M., Neczaj, E., Fijałkowski, K., Grobelak, A., Grosser, A., Worwag, M., Rorat, A., Brattebo, H., Almås, Å., Singh, B.R., 2017. Sewage sludge disposal strategies for sustainable development. Environ. Res. 156, 39–46. https://doi.org/10.1016/j.envres.2017.03.010

Kampschreur, M.J., Poldermans, R., Kleerebezem, R., van der Star, W.R.L., Haarhuis, R., Abma, W.R., Jetten, M.S.M., van Loosdrecht, M.C.M., 2009. Emission of nitrous oxide and nitric oxide from a full-scale single-stage nitritation-anammox reactor. Water Sci. Technol. 60, 3211–3217. https://doi.org/10.2166/wst.2009.608

Kampschreur, M.J., van der Star, W.R.L., Wielders, H.A., Mulder, J.W., Jetten, M.S.M., van Loosdrecht, M.C.M., 2008. Dynamics of nitric oxide and nitrous oxide emission during full-scale reject water treatment. Water Res. 42, 812–826. https://doi.org/10.1016/j.watres.2007.08.022

Kanders, L., Yang, J.-J., Baresel, C., Zambrano, J., 2019. Full-scale comparison of N2O emissions from SBR N/DN operation versus one-stage deammonification MBBR treating reject water – and optimization with pH set-point. Water Sci. Technol. 79, 1616–1625. https://doi.org/10.2166/wst.2019.163

Kartal, B., Kuenen, J.G., Van Loosdrecht, M.C.M., 2010. Sewage treatment with anammox. Science (80-.). 328, 702–703. https://doi.org/10.1126/science.1185941

Karwowska, B., Sperczyńska, E., Wiśniowska, E., 2016. Characteristics of reject waters and condensates generated during drying of sewage sludge from selected wastewater treatment plants. Desalin. Water Treat. 57, 1176–1183. https://doi.org/10.1080/19443994.2014.989633

Kassouf, H., García Parra, A., Mulford, L., Iranipour, G., Ergas, S.J., Cunningham, J.A., 2020. Mass fluxes

of nitrogen and phosphorus through water reclamation facilities: Case study of biological nutrient removal, aerobic sludge digestion, and sidestream recycle. Water Environ. Res. 92, 478–489. https://doi.org/10.1002/wer.1239

Kazadi Mbamba, C., Batstone, D.J., Flores-alsina, X., Tait, S., 2015a. A generalised chemical precipitation modelling approach in wastewater treatment applied to calcite. Water Res. 68, 342–353. https://doi.org/10.1016/j.watres.2014.10.011

Kazadi Mbamba, C., Flores-Alsina, X., John Batstone, D., Tait, S., 2016. Validation of a plant-wide phosphorus modelling approach with minerals precipitation in a full-scale WWTP. Water Res. 100, 169–183. https://doi.org/10.1016/j.watres.2016.05.003

Kazadi Mbamba, C., Lindblom, E., Flores-alsina, X., Tait, S., Anderson, S., Saagi, R., Batstone, D.J., Gernaey, K. V, Jeppsson, U., 2019. Plant-wide model-based analysis of iron dosage strategies for chemical phosphorus removal in wastewater treatment systems. Water Res. 155, 12–25. https://doi.org/10.1016/j.watres.2019.01.048

Kazadi Mbamba, C., Tait, S., Flores-alsina, X., Batstone, D.J., 2015b. A systematic study of multiple minerals precipitation modelling in wastewater treatment. Water Res. 85, 359–370. https://doi.org/10.1016/j.watres.2015.08.041

Kehrein, P., van Loosdrecht, M., Osseweijer, P., Garfí, M., Dewulf, J., Posada, J., 2020. A critical review of resource recovery from municipal wastewater treatment plants – market supply potentials, technologies and bottlenecks. Environ. Sci. Water Res. Technol. 6, 877–910. https://doi.org/10.1039/C9EW00905A

Khiewwijit, R., Temmink, H., Rijnaarts, H., Keesman, K.J., 2015. Energy and nutrient recovery for municipal wastewater treatment: How to design a feasible plant layout? Environ. Model. Softw. 68, 156–165. https://doi.org/10.1016/j.envsoft.2015.02.011

Khunjar, W.O., Horne, M. Van, Pace, G., Bilyk, K., Sveum, K., 2019. Strategies for treating biodegradable and recalcitrant nutrient fractions generated from THP processes. WEF/IWA Residuals Biosolids Conf. 2019 343–344.

Kleemann, R., Chenoweth, J., Clift, R., Morse, S., Pearce, P., Saroj, D., 2015. Evaluation of local and national effects of recovering phosphorus at wastewater treatment plants: Lessons learned from the UK. Resour. Conserv. Recycl. 105, 347–359. https://doi.org/10.1016/j.resconrec.2015.09.007

Kok, D.-J.D., Pande, S., van Lier, J.B., Ortigara, A.R.C., Savenije, H., Uhlenbrook, S., 2018. Global phosphorus recovery from wastewater for agricultural reuse. Hydrol. Earth Syst. Sci. 22, 5781–5799. https://doi.org/10.5194/hess-22-5781-2018

Kor-Bicakci, G., Eskicioglu, C., 2019. Recent developments on thermal municipal sludge pretreatment technologies for enhanced anaerobic digestion. Renew. Sustain. Energy Rev. 110, 423–443. https://doi.org/10.1016/j.rser.2019.05.002

Korchef, A., Saidou, H., Amor, M. Ben, 2011. Phosphate recovery through struvite precipitation by CO2 removal: Effect of magnesium, phosphate and ammonium concentrations. J. Hazard. Mater. https://doi.org/10.1016/j.jhazmat.2010.11.045

Krhutkova, O., Novak, L., Pachmanova, L., Benakova, A., Wanner, J., Kos, M., 2006. In situ bioaugmentation of nitrification in the regeneration zone : practical application and experiences at full-scale plants. Water Sci. Technol. 39–46. https://doi.org/10.2166/wst.2006.404

Lackner, S., Gilbert, E.M., Vlaeminck, S.E., Joss, A., Horn, H., van Loosdrecht, M.C.M., 2014. Full-scale partial nitritation/anammox experiences - An application survey. Water Res. 55, 292–303.

https://doi.org/10.1016/j.watres.2014.02.032

Lahav, O., Telzhensky, M., Zewuhn, A., Gendel, Y., Gerth, J., Calmano, W., 2013. Struvite recovery from municipal-wastewater sludge centrifuge supernatant using seawater NF concentrate as a cheap Mg (II) source. Sep. Purif. Technol. 108, 103–110. https://doi.org/10.1016/j.seppur.2013.02.002

Laperche, D., 2022. Révision de la directive Eaux résiduaires urbaines : les pistes de la Commission européenne [WWW Document]. ACTU Environ. URL https://www.actu-environnement.com/ae/news/revision-deru-pistes-commission-europeennce-congres-fnccr-40371.php4 (accessed 4.4.23).

Larsen, T.A., Gujer, W., 1997. The concept of sustainable urban water management. Water Sci. Technol. 35, 3–10. https://doi.org/10.2166/wst.1997.0326

Latimer, R., Rohrbacher, J., Nguyen, V., Khunjar, W.O., Jeyanayagam, S., 2016. Towards a Renewable Future: Assessing Resource Recovery as a Viable Treatment Alternative. WERF. https://doi.org/10.2166/9781780407920

Le Corre, K.S., Valsami-Jones, E., Hobbs, P., Parsons, S.A., 2009. Phosphorus recovery from wastewater by struvite crystallization: A review, Critical Reviews in Environmental Science and Technology. https://doi.org/10.1080/10643380701640573

Le Corre, K.S., Valsami-Jones, E., Hobbs, P., Parsons, S.A., 2005. Impact of calcium on struvite crystal size, shape and purity. J. Cryst. Growth 283, 514–522. https://doi.org/10.1016/j.jcrysgro.2005.06.012

Ledda, C., Romero Villegas, G.I., Adani, F., Acién Fernández, F.G., Molina Grima, E., 2015. Utilization of centrate from wastewater treatment for the outdoor production of Nannochloropsis gaditana biomass at pilot-scale. Algal Res. 12, 17–25. https://doi.org/10.1016/j.algal.2015.08.002

Liu, M., Smal, N., Barry, J., Morton, R., Tang, C.-C., Friess, P.L., Bell, J., Zhao, H., 2014. Pilot-Scale Evaluation of ANITA TM Mox for Centrate Nitrogen Removal at the Joint Water Pollution Control Plant, in: Proceedings of the Water Environment Federation. WEFTEC 2014. New Orleans, LA USA, pp. 4460–4482. https://doi.org/10.2175/193864714815941199

Liu, X., Kim, M., Nakhla, G., Andalib, M., Fang, Y., 2020. Partial nitrification-reactor configurations, and operational conditions: Performance analysis. J. Environ. Chem. Eng. 8, 103984. https://doi.org/10.1016/j.jece.2020.103984

Liu, Y., Qu, H., 2017. Interplay of digester supernatant composition and operating pH on impacting the struvite particulate properties. J. Environ. Chem. Eng. 5, 3949–3955. https://doi.org/10.1016/j.jece.2017.07.065

Lizarralde, I., Fernández-Arévalo, T., Brouckaert, C., Vanrolleghem, P., Ikumi, D.S., Ekama, G.A., Ayesa, E., Grau, P., 2015. A new general methodology for incorporating physico-chemical transformations into multi-phase wastewater treatment process models. Water Res. 74, 239–256. https://doi.org/10.1016/j.watres.2015.01.031

Lizarralde, I., Fernández-Arévalo, T., Manas, A., Ayesa, E., Grau, P., 2019. Model-based optimization of phosphorus management strategies in Sur WWTP, Madrid. Water Res. 153, 39–52. https://doi.org/10.1016/j.watres.2018.12.056

Lizarralde, I., Guida, S., Canellas, J., Jefferson, B., Grau, P., Soares, A., 2021. Development and calibration of a new mathematical model for the description of an ion-exchange process for ammonia removal in the presence of competing ions. Water Res. 206, 117779. https://doi.org/10.1016/j.watres.2021.117779

Mampaey, K.E., De Kreuk, M.K., van Dongen, U.G.J.M., van Loosdrecht, M.C.M., Volcke, E.I.P., 2016. Identifying N 2 O formation and emissions from a full-scale partial nitritation reactor. Water Res. 88, 575–585. https://doi.org/10.1016/j.watres.2015.10.047

Mancho, C., Diez-Pascual, S., Alonso, J., Gil-Díaz, M., Lobo, M.C., 2023. Assessment of Recovered Struvite as a Safe and Sustainable Phosphorous Fertilizer. Environments 10, 22. https://doi.org/10.3390/environments10020022

Mannina, G., Rebouças, T.F., Cosenza, A., Chandran, K., 2019. A plant-wide wastewater treatment plant model for carbon and energy footprint: Model application and scenario analysis. J. Clean. Prod. 217, 244–256. https://doi.org/10.1016/j.jclepro.2019.01.255

Marazzi, F., Bellucci, M., Rossi, S., Fornaroli, R., Ficara, E., Mezzanotte, V., 2019. Outdoor pilot trial integrating a sidestream microalgae process for the treatment of centrate under non optimal climate conditions. Algal Res. 39. https://doi.org/10.1016/j.algal.2019.101430

Martí, N., Barat, R., Seco, A., Pastor, L., Bouzas, A., 2017. Sludge management modeling to enhance P-recovery as struvite in wastewater treatment plants. J. Environ. Manage. 196, 340–346. https://doi.org/10.1016/j.jenvman.2016.12.074

Martí, N., Bouzas, A., Seco, A., Ferrer, J., 2008. Struvite precipitation assessment in anaerobic digestion processes. Chem. Eng. J. 141, 67–74. https://doi.org/10.1016/j.cej.2007.10.023

Massara, T.M., Solís, B., Guisasola, A., Katsou, E., Baeza, J.A., 2018. Development of an ASM2d-N2O model to describe nitrous oxide emissions in municipal WWTPs under dynamic conditions. Chem. Eng. J. 335, 185–196. https://doi.org/10.1016/j.cej.2017.10.119

Melia, P.M., Cundy, A.B., Sohi, S.P., Hooda, P.S., Busquets, R., 2017. Trends in the recovery of phosphorus in bioavailable forms from wastewater. Chemosphere 186, 381–395. https://doi.org/10.1016/j.chemosphere.2017.07.089

Mendes, C., Esquerre, K., Matos Queiroz, L., 2015. Application of Anaerobic Digestion Model No. 1 for simulating anaerobic mesophilic sludge digestion. Waste Manag. 35, 89–95. https://doi.org/10.1016/j.wasman.2014.10.013

Metcalf & Eddy Inc., Tchobanoglous, G., Burton, F.L., Stencel, H.D., 2003. Wastewater Engineering: Treatment and Reuse, McGraw-Hill International Edition.

Moletta, R., 2008. Méthanisation de la biomasse. Tech. l'Ingénieur 33.

Molinuevo, B., García, M.C., Karakashev, D., Angelidaki, I., 2009. Anammox for ammonia removal from pig manure effluents: Effect of organic matter content on process performance. Bioresour. Technol. 100, 2171–2175. https://doi.org/10.1016/j.biortech.2008.10.038

Mondor, M., Ippersiel, D., Lamarche, F., Masse, L., 2009. Fouling characterization of electrodialysis membranes used for the recovery and concentration of ammonia from swine manure. Bioresour. Technol. 100, 566–571. https://doi.org/10.1016/j.biortech.2008.06.072

Morel, F.M.M., Hering, J.G., 2013. Principles and applications of aquatic chemistry; 1st edition. Wiley-Interscience.

Münch, E. V, Barr, K., 2001. Controlled struvite crystallisation for removing phosphorus from anaerobic digester sidestreams. Water Res. 35, 151–159. https://doi.org/10.1016/S0043-1354(00)00236-0

Musvoto, E.V., Wentzel, M.C., Ekama, G.A., 2000a. Integrated chemical–physical processes modelling—II. simulating aeration treatment of anaerobic digester supernatants. Water Res. 34, 1868–1880. https://doi.org/10.1016/S0043-1354(99)00335-8

Musvoto, E.V., Wentzel, M.C., Loewenthal, R.E., Ekama, G.A., 2000b. Integrated chemical–physical processes modelling—I. Development of a kinetic-based model for mixed weak acid/base systems. Water Res. 34, 1857–1867. https://doi.org/10.1016/S0043-1354(99)00334-6

Muys, M., Phukan, R., Brader, G., Samad, A., Moretti, M., Haiden, B., Pluchon, S., Roest, K., Vlaeminck, S.E., Spiller, M., 2020. A systematic comparison of commercially produced struvite: Quantities, qualities and soil-maize phosphorus availability. Sci. Total Environ. 756, 143726. https://doi.org/10.1016/j.scitotenv.2020.143726

Nancharaiah, Y. V., Venkata Mohan, S., Lens, P.N.L., 2016. Recent advances in nutrient removal and recovery in biological and bioelectrochemical systems. Bioresour. Technol. https://doi.org/10.1016/j.biortech.2016.03.129

Nanda, S., Sarangi, P.K., 2022. Biomethane. Apple Academic Press, Boca Raton. https://doi.org/10.1201/9781003277163

Nopens, I., Batstone, D.J., Copp, J.B., Jeppsson, U., Volcke, E., Alex, J., Vanrolleghem, P.A., 2009. An ASM/ADM model interface for dynamic plant-wide simulation. Water Res. 43, 1913–1923. https://doi.org/10.1016/j.watres.2009.01.012

Noutsopoulos, C., Mamais, D., Statiris, E., Lerias, E., Malamis, S., Andreadakis, A., 2018. Reject water characterization and treatment through short-cut nitrification/denitrification: assessing the effect of temperature and type of substrate. J. Chem. Technol. Biotechnol. 93, 3638–3647. https://doi.org/10.1002/jctb.5745

Ochs, P., Martin, B.D., Germain, E., Stephenson, T., van Loosdrecht, M., Soares, A., 2021. Ammonia removal from thermal hydrolysis dewatering liquors via three different deammonification technologies. Sci. Total Environ. 755, 142684. https://doi.org/10.1016/j.scitotenv.2020.142684

Parsons, S.A., Wall, F., Doyle, J., Oldring, K., Churchley, J., 2001. Assesing the Potential for Struvite Recovery at Sewage Treatment Works. Environ. Technol. 22, 1279–1286. https://doi.org/10.1080/09593332208618188

Paul, E., Liu, Y., 2012. Biological Sludge Minimization and Biomaterials/bioenergy Recovery Technologies. John Wiley & Sons, Inc., Publication.

Peralta, E., Jerez, C.G., Figueroa, F.L., 2019. Centrate grown Chlorella fusca (Chlorophyta): Potential for biomass production and centrate bioremediation. Algal Res. 39. https://doi.org/10.1016/j.algal.2019.101458

Perret, J.M., Garcia, O., Amsaleg, C.R., Laverman, A., Pichon, S., Azimi, S., Rocher, V., Canler, J.P., Perret, J.M., Garcia, O., Amsaleg, C.R., Laverman, A., Pichon, S., 2018. Le traitement des jus de digestion par le procédé de nitritation sharon ® cas de la station Seine Grésillons du SIAAP, in: Journées Information Eaux 2018. Potiers, France. https://hal.archives-ouvertes.fr/hal-01951172.

Ping, Q., Li, Y., Wu, X., Yang, L., Wang, L., 2016. Characterization of morphology and component of struvite pellets crystallized from sludge dewatering liquor: Effects of total suspended solid and phosphate concentrations. J. Hazard. Mater. 310, 261–269. https://doi.org/10.1016/j.jhazmat.2016.02.047

Pörtner, H.-O., Roberts, D.C., Tignor, M., Poloczanska, E.S., Mintenbeck, K., Alegría, A., Craig, M., Langsdorf, S., Löschke, S., Möller, V., Okem, A., Rama, B., 2022. IPCC, 2022: Climate Change 2022: Impacts, Adaptation, and Vulnerability. Contribution of Working Group II to the Sixth Assessment Report of the Intergovernmental Panel on Climate Change. Cambridge Univ. Press 3056. https://doi.org/110.1017/9781009325844

Pradel, M., Aissani, L., 2019. Environmental impacts of phosphorus recovery from a “product” Life Cycle Assessment perspective: Allocating burdens of wastewater treatment in the production of sludge-based phosphate fertilizers. Sci. Total Environ. 656, 55–69. https://doi.org/10.1016/j.scitotenv.2018.11.356

Pradel, M., Aissani, L., Villot, J., Baudez, J.-C., Laforest, V., 2016. From waste to added value product: towards a paradigm shift in life cycle assessment applied to wastewater sludge – a review. J. Clean. Prod. 131, 60–75. https://doi.org/10.1016/j.jclepro.2016.05.076

Preisner, M., Neverova-Dziopak, E., Kowalewski, Z., 2020. An Analytical Review of Different Approaches to Wastewater Discharge Standards with Particular Emphasis on Nutrients. Environ. Manage. 66, 694–708. https://doi.org/10.1007/s00267-020-01344-y

Puchongkawarin, C., Gomez-Mont, C., Stuckey, D.C., Chachuat, B., 2015. Optimization-based methodology for the development of wastewater facilities for energy and nutrient recovery. Chemosphere 140, 150–158. https://doi.org/10.1016/j.chemosphere.2014.08.061

Qadir, M., Drechsel, P., Jiménez Cisneros, B., Kim, Y., Pramanik, A., Mehta, P., Olaniyan, O., 2020. Global and regional potential of wastewater as a water, nutrient and energy source. Nat. Resour. Forum 1–12. https://doi.org/10.1111/1477-8947.12187

Ramalingam, K., Fillos, J., Mehrdad, M., Halim, D., Deur, A., Orpianesi, M., 2017. Side stream treatment nitrogen removal: alternatives for New York City. Water Pract. Technol. 12, 179–185. https://doi.org/10.2166/wpt.2017.024

Razaviarani, V., Buchanan, I.D., 2015. Calibration of the Anaerobic Digestion Model No. 1 (ADM1) for steady-state anaerobic co-digestion of municipal wastewater sludge with restaurant grease trap waste. Chem. Eng. J. https://doi.org/10.1016/j.cej.2014.12.080

Rey-Martínez, N., Guisasola, A., Baeza, J.A., 2022. Assessment of the significance of heavy metals, pesticides and other contaminants in recovered products from water resource recovery facilities. Resour. Conserv. Recycl. 182, 106313. https://doi.org/10.1016/j.resconrec.2022.106313

Richter, L., Wichern, M., Grömping, M., Robecke, U., Haberkamp, J., 2020. Ammonium recovery from process water of digested sludge dewatering by membrane contactors. Water Pract. Technol. 15, 84–91. https://doi.org/10.2166/wpt.2020.002

Rieger, L., Gillot, S., Langergraber, G., Ohtsuki, T., Shaw, A., Takacs, I., Winkler, S., 2012. Guidelines for Using Activated Sludge Models.

Rivera, F., Muñoz, R., Prádanos, P., Hernández, A., Palacio, L., 2022. A Systematic Study of Ammonia Recovery from Anaerobic Digestate Using Membrane-Based Separation. Membranes (Basel). 12. https://doi.org/10.3390/membranes12010019

Robles, Á., Aguado, D., Barat, R., Borrás, L., Bouzas, A., Giménez, J.B., Martí, N., Ribes, J., Ruano, M.V., Serralta, J., Ferrer, J., Seco, A., 2020. New frontiers from removal to recycling of nitrogen and phosphorus from wastewater in the Circular Economy. Bioresour. Technol. 300. https://doi.org/10.1016/j.biortech.2019.122673

Rodier, J., Legube, B., Merlet, N., 2016. L’analyse de l’eau, 10ème. ed. fFrance.

Roldán, M., Bouzas, A., Seco, A., Mena, E., Mayor, Á., Barat, R., 2020. An integral approach to sludge handling in a WWTP operated for EBPR aiming phosphorus recovery: Simulation of alternatives, LCA and LCC analyses. Water Res. 175, 115647. https://doi.org/10.1016/j.watres.2020.115647

Romero Villegas, G.I., Fiamengo, M., Acién Fernández, F.G., Molina Grima, E., 2017. Outdoor production of microalgae biomass at pilot-scale in seawater using centrate as the nutrient source.

Algal Res. 25, 538–548. https://doi.org/10.1016/j.algal.2017.06.016

Sagberg, P., Ryrfors, P., Berg, K.G., 2006. 10 years of operation of an integrated nutrient removal treatment plant: Ups and down. Background and water treatment. Water Sci. Technol. 53, 83–90. https://doi.org/10.2166/wst.2006.409

Salem, S., Roest, H.F. Van Der, Kuij, R.J. Van Der, 2004. Full-scale application of the BABE ® technology. Water Sci. Technol. 87–96.

Saoudi, M.A., Dabert, P., Ponthieux, A., Vedrenne, F., Daumer, M.L., 2022. Correlation between phosphorus removal technologies and phosphorus speciation in sewage sludge: focus on iron-based P removal technologies. Environ. Technol. (United Kingdom). https://doi.org/10.1080/09593330.2021.2023222

Schaubroeck, T., De Clippeleir, H., Weissenbacher, N., Dewulf, J., Boeckx, P., Vlaeminck, S.E., Wett, B., 2015. Environmental sustainability of an energy self-sufficient sewage treatment plant: Improvements through DEMON and co-digestion. Water Res. 74, 166–179. https://doi.org/10.1016/j.watres.2015.02.013

Seco, A., Aparicio, S., González-Camejo, J., Jiménez-Benítez, A., Mateo, O., Mora, J.F., Noriega-Hevia, G., Sanchis-Perucho, P., Serna-García, R., Zamorano-López, N., Giménez, J.B., Ruiz-Martínez, A., Aguado, D., Barat, R., Borrás, L., Bouzas, A., Martí, N., Pachés, M., Ribes, J., Robles, A., Ruano, M. V., Serralta, J., Ferrer, J., 2018. Resource recovery from sulphate-rich sewage through an innovative anaerobic-based water resource recovery facility (WRRF). Water Sci. Technol. 78, 1925–1936. https://doi.org/10.2166/wst.2018.492

Sengupta, S., Nawaz, T., Beaudry, J., 2015. Nitrogen and Phosphorus Recovery from Wastewater. Curr. Pollut. Reports 1, 155–166. https://doi.org/10.1007/s40726-015-0013-1

Shaddel, S., Bakhtiary-Davijany, H., Kabbe, C., Dadgar, F., Østerhus, S.W., 2019. Sustainable Sewage Sludge Management: From Current Practices to Emerging Nutrient Recovery Technologies. https://doi.org/10.3390/su11123435

Shaddel, S., Grini, T., Andreassen, J.P., Østerhus, S.W., Ucar, S., 2020. Crystallization kinetics and growth of struvite crystals by seawater versus magnesium chloride as magnesium source: towards enhancing sustainability and economics of struvite crystallization. Chemosphere 256, 126968. https://doi.org/10.1016/j.chemosphere.2020.126968

Shao, Y., Florentino, A.P., Buchanan, I., Mohammed, A., Liu, Y., 2019. Microbial population dynamics in a partial nitrification reactor treating high ammonia strength supernatant from anaerobically digested sludge: Role of the feed water characteristics. Int. Biodeterior. Biodegradation 137, 109–117. https://doi.org/10.1016/j.ibiod.2018.12.006

Sheng, H., Ni, S., Wang, Y., Yuan, R., Su, K., Hao, T., 2022. Uncertainty and sensitivity analysis of algal-bacterial model under different ranges of parameter variation. Biochem. Eng. J. 179, 108334. https://doi.org/10.1016/j.bej.2022.108334

Solís, B., Guisasola, A., Flores-Alsina, X., Jeppsson, U., Baeza, J.A., 2022. A plant-wide model describing GHG emissions and nutrient recovery options for water resource recovery facilities. Water Res. 215, 118223. https://doi.org/10.1016/j.watres.2022.118223

Solon, K., Flores-Alsina, X., Kazadi Mbamba, C., Ikumi, D., Volcke, E.I.P., Vaneeckhaute, C., Ekama, G., Vanrolleghem, P.A., Batstone, D.J., Gernaey, K. V., Jeppsson, U., 2017. Plant-wide modelling of phosphorus transformations in wastewater treatment systems: Impacts of control and operational strategies. Water Res. 113, 97–110. https://doi.org/10.1016/j.watres.2017.02.007

Solon, K., Flores-Alsina, X., Mbamba, C.K., Volcke, E.I.P., Tait, S., Batstone, D., Gernaey, K. V., Jeppsson, U., 2015. Effects of ionic strength and ion pairing on (plant-wide) modelling of anaerobic digestion. Water Res. 70, 235–245. https://doi.org/10.1016/j.watres.2014.11.035

Solon, K., Jia, M., Volcke, E.I.P., 2019a. Evaluation criteria for water resource recovery facilities, in: Watermatex 2019.

Solon, K., Volcke, E.I.P., Spérandio, M., Van Loosdrecht, M.C.M., 2019b. Resource recovery and wastewater treatment modelling. Environ. Sci. Water Res. Technol. 5, 631–642. https://doi.org/10.1039/c8ew00765a

Song, M., Li, M., 2019. Adsorption and regeneration characteristics of phosphorus from sludge dewatering filtrate by magnetic anion exchange resin. Environ. Sci. Pollut. Res. 26, 34233–34247. https://doi.org/10.1007/s11356-018-4049-9

Souza, T.S.O., Carvajal, A., Donoso-Bravo, A., Peña, M., Fdz-Polanco, F., 2013. ADM1 calibration using BMP tests for modeling the effect ofautohydrolysis pretreatment on the performance ofcontinuous sludge digesters. Water Res. 47, 3244–3254. https://doi.org/10.1016/j.watres.2013.03.041

Spérandio, M., Lang, L., Sabba, F., Nerenberg, R., Vanrolleghem, P., Domingo-Félez, C., Smets, B.F., Duan, H., Ni, B.-J., Yuan, Z., 2022. Modelling N2O production and emissions, in: Quantification and Modelling of Fugitive Greenhouse Gas Emissions from Urban Water Systems. IWA Publishing, pp. 167–196. https://doi.org/10.2166/9781789060461_0167

Steele, J.C., Meng, X.Z., Venkatesan, A.K., Halden, R.U., 2022. Comparative meta-analysis of organic contaminants in sewage sludge from the United States and China. Sci. Total Environ. https://doi.org/10.1016/j.scitotenv.2022.153423

Svennevik, O.K., Nilsen, P.J., Solheim, O.E., Westereng, B., Horn, S.J., 2020. Quantification of soluble recalcitrant compounds in commercial thermal hydrolysis digestates. Water Environ. Res. wer.1351. https://doi.org/10.1002/wer.1351

Taboada-Santos, A., Lema, J.M., Carballa, M., 2019. Energetic and economic assessment of sludge thermal hydrolysis in novel wastewater treatment plant configurations. Waste Manag. 92, 30–38. https://doi.org/10.1016/j.wasman.2019.05.003

Talan, A., Tyagi, R.D., Drogui, P., 2021. Critical review on insight into the impacts of different inhibitors and performance inhibition of anammox process with control strategies. Environ. Technol. Innov. 23, 101553. https://doi.org/10.1016/j.eti.2021.101553

Tao, W., Fattah, K.P., Huchzermeier, M.P., 2016. Struvite recovery from anaerobically digested dairy manure: A review of application potential and hindrances. J. Environ. Manage. 169, 46–57. https://doi.org/10.1016/j.jenvman.2015.12.006

Teichgräber, B., Stein, A., 1994. Nitrogen elimination from sludge treatment reject water – comparison of the steam-stripping and denitrification processes. Water Sci. Technol. 30, 41–51. https://doi.org/10.2166/wst.1994.0251

Tong, J., Chen, Y., 2007. Enhanced biological phosphorus removal driven by short-chain fatty acids produced from waste activated sludge alkaline fermentation. Environ. Sci. Technol. 41, 7126–7130. https://doi.org/10.1021/es071002n

Toutian, V., Barjenbruch, M., Unger, T., Loderer, C., Remy, C., 2020. Effect of temperature on biogas yield increase and formation of refractory COD during thermal hydrolysis of waste activated sludge. Water Res. 171, 115383. https://doi.org/10.1016/j.watres.2019.115383

Turk, O., Mavinic, D.S., 1986. Preliminary assessment of a shortcut in nitrogen removal from wastewater. Can. J. Civ. Eng. 13, 600–605. https://doi.org/10.1139/l86-094

Tuszynska, A., Czerwionka, K., 2021. Nutrient recovery from deammonification effluent in a pilot study using two-step reject water treatment technology. Water Resour. Ind. 25, 100148. https://doi.org/10.1016/j.wri.2021.100148

Ueno, Y., Fujii, M., 2001. Three Years Experience of Operating and Selling Recovered Struvite from Full-Scale Plant. Environ. Technol. 22, 1373–1381. https://doi.org/10.1080/09593332208618196

Urrea, J.L., Collado, S., Laca, A., Díaz, M., 2015. Rheological behaviour of activated sludge treated by thermal hydrolysis. J. Water Process Eng. 5, 153–159. https://doi.org/10.1016/j.jwpe.2014.06.009

Uysal, A., Yilmazel, Y.D., Demirer, G.N., 2010. The determination of fertilizer quality of the formed struvite from effluent of a sewage sludge anaerobic digester. J. Hazard. Mater. 181, 248–254. https://doi.org/10.1016/j.jhazmat.2010.05.004

Van Hulle, S.W.H., Vandeweyer, H.J.P., Meesschaert, B.D., Vanrolleghem, P.A., Dejans, P., Dumoulin, A., 2010. Engineering aspects and practical application of autotrophic nitrogen removal from nitrogen rich streams. Chem. Eng. J. 162, 1–20. https://doi.org/10.1016/j.cej.2010.05.037

van Loosdrecht, M.C.M., Nielsen, P.H., Lopez-Vazquez, C.M., Brdjanovic, D., 2016. Experimental Methods in Wastewater Treatment, Water Intelligence Online. https://doi.org/10.2166/9781780404752

van Loosdrecht, M.C.M., Salem, S., 2006. Biological treatment of sludge digester liquids. Water Sci. Technol. 53, 11–20. https://doi.org/10.2166/wst.2006.401

Van Loosdrecht, M.C.M., Salem, S., 2006. Biological treatment of sludge digester liquids. Water Sci. Technol. 53, 11–20. https://doi.org/10.2166/wst.2006.401

van Rensburg, P., Musvoto, E.., Wentzel, M.., Ekama, G.., 2003. Modelling multiple mineral precipitation in anaerobic digester liquor. Water Res. 37, 3087–3097. https://doi.org/10.1016/S0043-1354(03)00173-8

Van Vuuren, D.P., Bouwman, A.F., Beusen, A.H.W., 2010. Phosphorus demand for the 1970-2100 period: A scenario analysis of resource depletion. Glob. Environ. Chang. 20, 428–439. https://doi.org/10.1016/j.gloenvcha.2010.04.004

Vaneeckhaute, C., Belia, E., Meers, E., Tack, F.M.G., Vanrolleghem, P.A., 2018a. Nutrient recovery from digested waste: Towards a generic roadmap for setting up an optimal treatment train. Waste Manag. 78, 385–392. https://doi.org/10.1016/j.wasman.2018.05.047

Vaneeckhaute, C., Claeys, F.H.A., Tack, F.M.G., Meers, E., Belia, E., Vanrolleghem, P.A., 2018b. Development, implementation, and validation of a generic nutrient recovery model (NRM) library. Environ. Model. Softw. 99, 170–209. https://doi.org/10.1016/j.envsoft.2017.09.002

Vaneeckhaute, C., Ghekiere, G., Michels, E., Vanrolleghem, P.A., Tack, F.M.G., Meers, E., 2014. Assessing nutrient use efficiency and environmental pressure of macronutrients in biobased mineral fertilizers: A review of recent advances and best practices at field scale, in: Advances in Agronomy. Academic Press Inc., pp. 137–180. https://doi.org/10.1016/B978-0-12-802139-2.00004-4

Vaneeckhaute, C., Lebuf, V., Michels, E., Belia, E., Vanrolleghem, P.A., Tack, F.M.G., Meers, E., 2017. Nutrient Recovery from Digestate: Systematic Technology Review and Product Classification. Waste and Biomass Valorization 8, 21–40. https://doi.org/10.1007/s12649-016-9642-x

Vaneeckhaute, C., Remigi, E., Tack, F.M.G., Meers, E., Belia, E., Vanrolleghem, P.A., 2018c. Optimizing the configuration of integrated nutrient and energy recovery treatment trains: A new application of global sensitivity analysis to the generic nutrient recovery model (NRM) library. Bioresour. Technol. 269, 375–383. https://doi.org/10.1016/j.biortech.2018.08.108

Vaneeckhaute, C., Remigi, E.U., Tack, F.M.G., Meers, E., Belia, E., Vanrolleghem, P.A., 2019. Model-based optimisation and economic analysis to quantify the viability and profitability of an integrated nutrient and energy recovery treatment train. J. Environ. Eng. Sci. 14, 2–12. https://doi.org/10.1680/jenes.18.00005

Varennes, E., Blanc, D., Azaïs, A., Choubert, J.M., 2023. Upgrading wastewater treatment plants to urban mines: Are metals worth it? Resour. Conserv. Recycl. 189, 106738. https://doi.org/10.1016/j.resconrec.2022.106738

Vriens, B., Voegelin, A., Hug, S.J., Kaegi, R., Winkel, L.H.E., Buser, A.M., Berg, M., 2017. Quantification of Element Fluxes in Wastewaters: A Nationwide Survey in Switzerland. Environ. Sci. Technol. 10943–10953. https://doi.org/10.1021/acs.est.7b01731

Vu, M.T., Price, W.E., He, T., Zhang, X., Nghiem, L.D., 2019. Seawater-driven forward osmosis for pre-concentrating nutrients in digested sludge centrate. J. Environ. Manage. 247, 135–139. https://doi.org/10.1016/j.jenvman.2019.06.082

Wäeger-Baumann, F., Fuchs, W., 2012. The Application of Membrane Contactors for the Removal of Ammonium from Anaerobic Digester Effluent. Sep. Sci. Technol. 47, 1436–1442. https://doi.org/10.1080/01496395.2011.653468

Ward, A.J., Arola, K., Thompson Brewster, E., Mehta, C.M., Batstone, D.J., 2018. Nutrient recovery from wastewater through pilot scale electrodialysis. Water Res. 135, 57–65. https://doi.org/10.1016/j.watres.2018.02.021

Weissenbacher, N., Takacs, I., Murthy, S., Fuerhacker, M., Wett, B., 2010. Gaseous Nitrogen and Carbon Emissions from a Full-Scale Deammonification Plant. Water Environ. Res. 82, 169–175. https://doi.org/10.2175/106143009X447867

Wett, B., Alex, J., 2003. Impacts of separate rejection water treatment on the overall plant performance. Water Sci. Technol. 48, 139–146. https://doi.org/10.2166/wst.2003.0240

Wild, D., Kisliakova, A., Siegrist, H., 1997. Prediction of recycle phosphorus loads from anaerobic digesion. Water Res. 31, 2300–2308.

Wilfert, P., Kumar, P.S., Korving, L., Witkamp, G.J., Van Loosdrecht, M.C.M., 2015. The relevance of phosphorus and iron chemistry to the recovery of phosphorus from wastewater: a review. Environ. Sci. Technol. 49, 9400–9414. https://doi.org/10.1021/acs.est.5b00150

Wilfert, P., Mandalidis, A., Dugulan, A.I., Goubitz, K., Korving, L., Temmink, H., Witkamp, G.J., Van Loosdrecht, M.C.M., 2016. Vivianite as an important iron phosphate precipitate in sewage treatment plants. Water Res. 104, 449–460. https://doi.org/10.1016/j.watres.2016.08.032

Wilson, C.A., Novak, J.T., 2009. Hydrolysis of macromolecular components of primary and secondary wastewater sludge by thermal hydrolytic pretreatment. Water Res. 43, 4489–4498. https://doi.org/10.1016/j.watres.2009.07.022

Wilson, C.A., Tanneru, C.T., Banjade, S., Murthy, S.N., Novak, J.T., 2011. Anaerobic Digestion of Raw and Thermally Hydrolyzed Wastewater Solids Under Various Operational Conditions. Water Environ. Res. 83, 815–825. https://doi.org/10.2175/106143011X12928814444934

Wu, H., Vaneeckhaute, C., 2022. Nutrient recovery from wastewater: A review on the integrated

Physicochemical technologies of ammonia stripping, adsorption and struvite precipitation. Chem. Eng. J. 433. https://doi.org/10.1016/j.cej.2021.133664

Wu, Z., Duan, H., Li, K., Ye, L., 2022. A comprehensive carbon footprint analysis of different wastewater treatment plant configurations. Environ. Res. 214, 113818. https://doi.org/10.1016/j.envres.2022.113818

Xavier, L.D., Cammarota, M.C., Yokoyama, L., Volschan, I., 2014. Study of the recovery of phosphorus from struvite precipitation in supernatant line from anaerobic digesters of sludge. Water Sci. Technol. 14, 751–757. https://doi.org/10.2166/ws.2014.033

Yadav, A., Rene, E.R., Sharma, M., Jatain, I., Mandal, M.K., Dubey, K.K., 2022. Valorization of wastewater to recover value-added products: A comprehensive insight and perspective on different technologies. Environ. Res. 214, 113957. https://doi.org/10.1016/j.envres.2022.113957

Yan, H., Shih, K., 2016. Effects of calcium and ferric ions on struvite precipitation: A new assessment based on quantitative X-ray diffraction analysis. Water Res. 95, 310–318. https://doi.org/10.1016/j.watres.2016.03.032

Yang, J., Trela, J., Plaza, E., 2016. Nitrous oxide emissions from one-step partial nitritation/anammox processes. Water Sci. Technol. 74, 2870–2878. https://doi.org/10.2166/wst.2016.454

Yang, J., Trela, J., Plaza, E., Tjus, K., 2013. N2O emissions from a one stage partial nitrification/anammox process in moving bed biofilm reactors. Water Sci. Technol. 68, 144–152. https://doi.org/10.2166/wst.2013.232

Yang, S., Xu, S., Florentino, A.P., Mohammed, A., Ashbolt, N.J., Liu, Y., 2019. Importance of controlling phosphate concentration in nitritation-anammox reactor operation. Environ. Sci. Water Res. Technol. 5, 1234–1243. https://doi.org/10.1039/c9ew00203k

Ye, Y., Ngo, H.H., Guo, W., Liu, Y., Chang, S.W., Nguyen, D.D., Liang, H., Wang, J., 2018. A critical review on ammonium recovery from wastewater for sustainable wastewater management. Bioresour. Technol. 268, 749–758. https://doi.org/10.1016/j.biortech.2018.07.111

Ye, Y., Ngo, H.H., Guo, W., Liu, Yiwen, Li, J., Liu, Yi, Zhang, X., Jia, H., 2017. Insight into chemical phosphate recovery from municipal wastewater. Sci. Total Environ. https://doi.org/10.1016/j.scitotenv.2016.10.078

Yoshida, H., Christensen, T.H., Guildal, T., Scheutz, C., 2015. A comprehensive substance flow analysis of a municipal wastewater and sludge treatment plant. Chemosphere 138, 874–882. https://doi.org/10.1016/j.chemosphere.2013.09.045

Yoshino, M., Yao, M., Tsuno, H., Somiya, I., 2003. Removal and recovery of phosphate and ammonium as struvite from supernatant in anaerobic digestion. Water Sci. Technol. 48, 171–178. https://doi.org/10.2166/wst.2003.0045

Zhang, Q., Cheng, Y.F., Huang, B.C., Jin, R.C., 2022. A review of heavy metals inhibitory effects in the process of anaerobic ammonium oxidation. J. Hazard. Mater. 429, 128362. https://doi.org/10.1016/j.jhazmat.2022.128362

Zhang, Q., De Clippeleir, H., Su, C., Al-Omari, A., Wett, B., Vlaeminck, S.E., Murthy, S., 2016. Deammonification for digester supernatant pretreated with thermal hydrolysis: overcoming inhibition through process optimization. Appl. Microbiol. Biotechnol. 100, 5595–5606. https://doi.org/10.1007/s00253-016-7368-0

Zhang, Q., Vlaeminck, S.E., DeBarbadillo, C., Su, C., Al-Omari, A., Wett, B., Pümpel, T., Shaw, A., Chandran, K., Murthy, S., De Clippeleir, H., 2018. Supernatant organics from anaerobic digestion

after thermal hydrolysis cause direct and/or diffusional activity loss for nitritation and anammox. Water Res. 143, 270–281. https://doi.org/10.1016/j.watres.2018.06.037

Zhang, Z.Z., Hu, H.Y., Xu, J.J., Shi, Z.J., Deng, R., Ji, Z.Q., Shi, M.L., Jin, R.C., 2017. Effects of inorganic phosphate on a high-rate anammox system: Performance and microbial community. Ecol. Eng. 101, 201–210. https://doi.org/10.1016/j.ecoleng.2017.02.002

Zhao, X., Kumar, K., Gross, M.A., Kunetz, T.E., Wen, Z., 2018. Evaluation of revolving algae biofilm reactors for nutrients and metals removal from sludge thickening supernatant in a municipal wastewater treatment facility. Water Res. 143, 467–478. https://doi.org/10.1016/j.watres.2018.07.001

Zhen, G., Lu, X., Kato, H., Zhao, Y., Li, Y.Y., 2017. Overview of pretreatment strategies for enhancing sewage sludge disintegration and subsequent anaerobic digestion: Current advances, full-scale application and future perspectives. Renew. Sustain. Energy Rev. 69, 559–577. https://doi.org/10.1016/j.rser.2016.11.187

APPENDIX OF CHAPTER 1

The table below summarizes the literature on sidestream processes used to establish figure S1.1.

Table S1.1 - Summary of scientific literature on sidestream processes

Processes	Technology maturity	Operational costs
Nitrification/Denitrification	Full scale[1]	g O_2/g N-NH_4 : 4.57 [8] g COD / g N-NO_3 : 2.86 [8] 4 – 12,5 kWh/ g N [6]
Nitritation/Denitritation	Demonstration at full scale [2]	g O_2/g N-NH_4 : 3.43 [3] g COD / g N-NO_3 : 1.72 [8]
PN-Deammonification	Demonstration at full scale [3]	g O_2/g N-NH_4 : 1.9 [3] 0,8 – 4,2 kWh/kgN [3]
N stripping	Demonstration at full scale [4]	26 - 28 kWh/kgN [5,9]
Bioelectrochemical system	Pilot at lab scale [5]	3 – 5,8 kWh/kg N [5,9]
Algae production	Pilot at full scale [6]	-11%[10] to –45%[11] compared to energy consumption of nitrification/denitrification
Ion exchange resin	Pilot at full scale [6]	Zeolite dosing 71,4 g/g N-NH_3 [6]
Membrane	Pilot at full scale [6]	-20% compared to N stripping energy consumption [12]
Struvite recovery	Demonstration at full scale [7]	Magnesium consumption: molar ratio Mg:P > 1.3 [13]

[1] Husband et al., 2010; Krhutkova et al., 2006; Salem et al., 2004
[2] Perret et al., 2018; Ramalingam et al., 2017
[3] Lackner et al., 2014
[4] Sagberg et al., 2006
[5] Ye et al., 2018
[6] Eskicioglu et al., 2018
[7] Le Corre et al., 2009
[8] Rieger et al., 2012
[9] Barua et al., 2019
[10] Marazzi et al., 2019
[11] Sheng et al., 2022
[12] Darestani et al., 2017
[13] Hanhoun et al., 2013

APPENDIX OF CHAPTER 2

Chapter 2 is based on the collection of data from literature. This document describes the dataset organisation, the method for data collection and the value of the data. The dataset is not exhaustive and could be completed with new references.

Data description

As part of sewage sludge handling in WRRFs, sludge thickening and dewatering units result in the production of different types of sidestreams, also called reject water, which are usually recycled to the inlet of the wastewater treatment line. Even if the volumes of sidestreams are generally small, their concentrations in organic and inorganic matters may be different from the composition of the influent and may negatively impact the performance of the facilities. Relatively recent concerns arise with the overall tightening of WWRFs at created opportunities for nutrient recovery. This dataset thus compiles literature data of sidestream characteristics from different locations in WRRFs.

This dataset is available in Data Gouv repository (https://doi.org/10.57745/FOHRHY) into 3 files:

1) « sidestreams_data »: main data table with all sidestream characteristics (conventional parameters: TSS, COD, BOD_5, Ammonium, Total Phosphorus, Phosphate), ions, pH, flow and metals
2) List of references: complete list of references used in « sidestreams_data »
3) Data column description: column description of the table « sidestreams_data »

All figures presented in this document have been created with the RStudio software. The code is available in supplementary material.

The dataset contains data from 87 documents:

- 75 peer reviewed papers
- 5 technical reports
- 5 conference proceedings
- 1 PhD thesis
- 1 master thesis.

Each line of the sidestreams_data file corresponds to the concentration of one component or to the proportion of the total inlet flux of one component. It is considered in the following as one data.

Figure S2.1 shows the breakdown of data according to sidestream sources. The distribution corresponds to the percentage of data (percentage of lines in the file “sidestream_data”) according to each sidestream source:

- anaerobic_digestion for sidestreams resulting from the dewatering of digested sludge
- biological_sludge for sidestreams resulting from the thickening of biological sludge
- primary_sludge for sidestreams resulting from the thickening of primary sludge
- THP_anaerobic_digestion for sidestreams resulting from the dewatering of digested sludge preceded by a thermal hydrolysis process (THP)

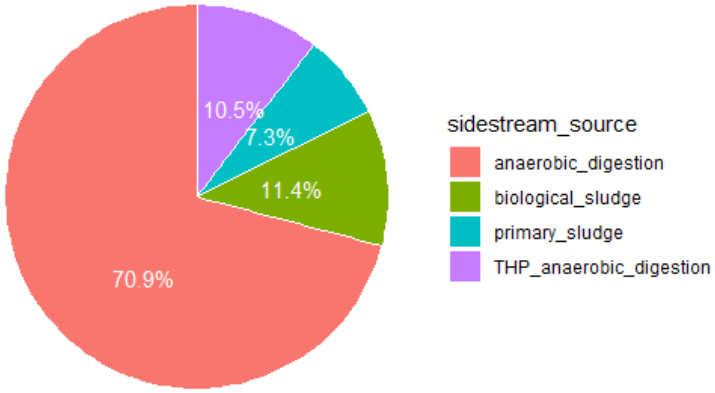

Figure S2.1 – Sidestream data by source

Figure S2.2 and S2.3 present the number of occurrences of the different secondary treatment types and of the different phosphorus treatment types, respectively.

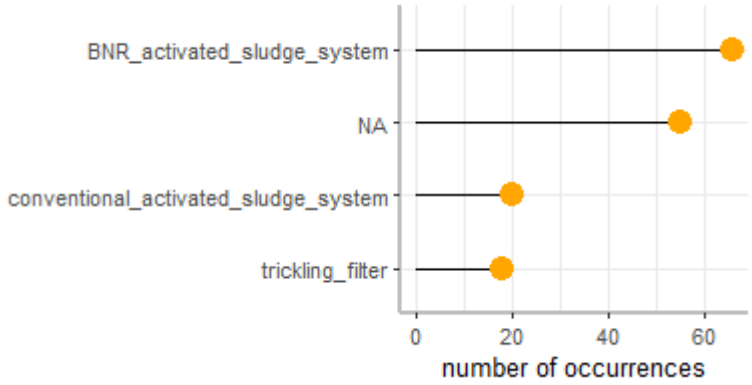

Figure S2.25 – Secondary treatment types included in the dataset. NA means "information not available for the sample"

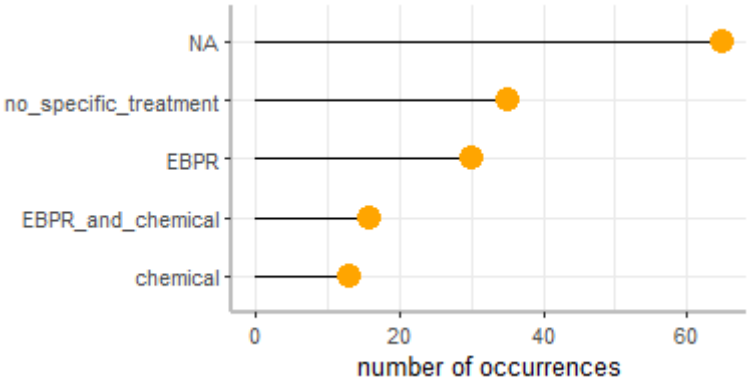

Figure S2.3 – Phosphorus treatment types included in the dataset. NA means "information not available for the sample"

The different dewatering and thickening equipment types found in the dataset are presented in Fifure S2.4, S2.5, S2.6.

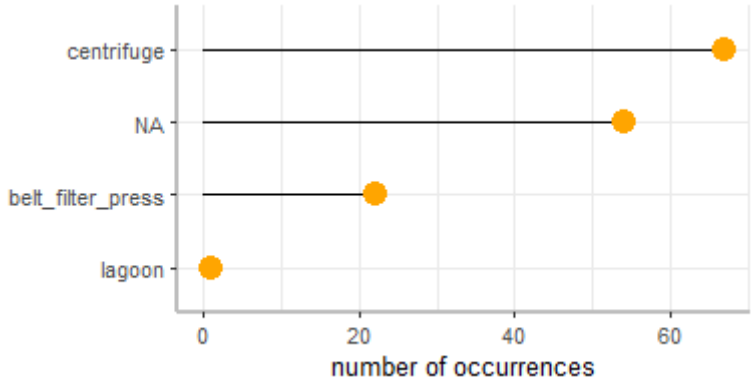

Figure S2.4 – Distribution of the different dewatering equipment types for anaerobic digestion sidestreams (conventional anaerobic digestion and THP anaerobic digestion). NA means "information not available for the sample"

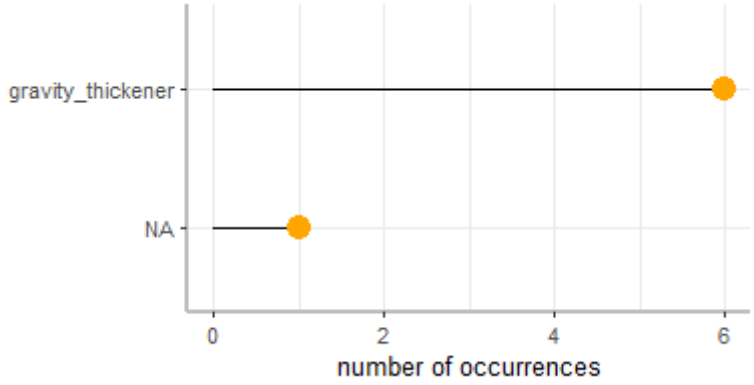

Figure S2.5 - Distribution of the different dewatering equipment types for primary sludge sidestreams. NA means "information not available for the sample"

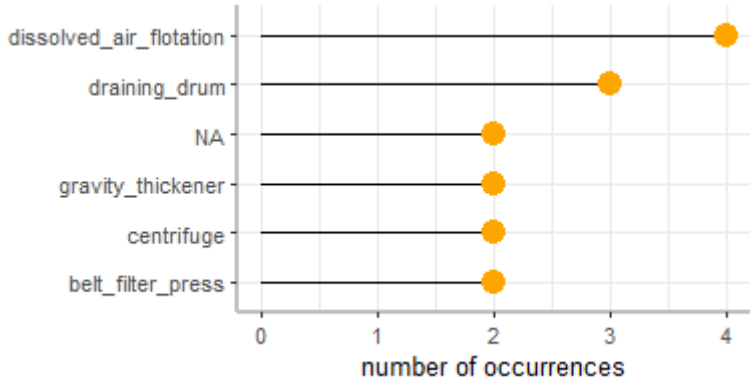

Figure S2.6 – Distribution of the different thickening equipment types for secondary sludge sidestreams. NA means "information not available for the sample"

Figure 2.7 shows the number of occurrences of the 66 characteristics included in the dataset.

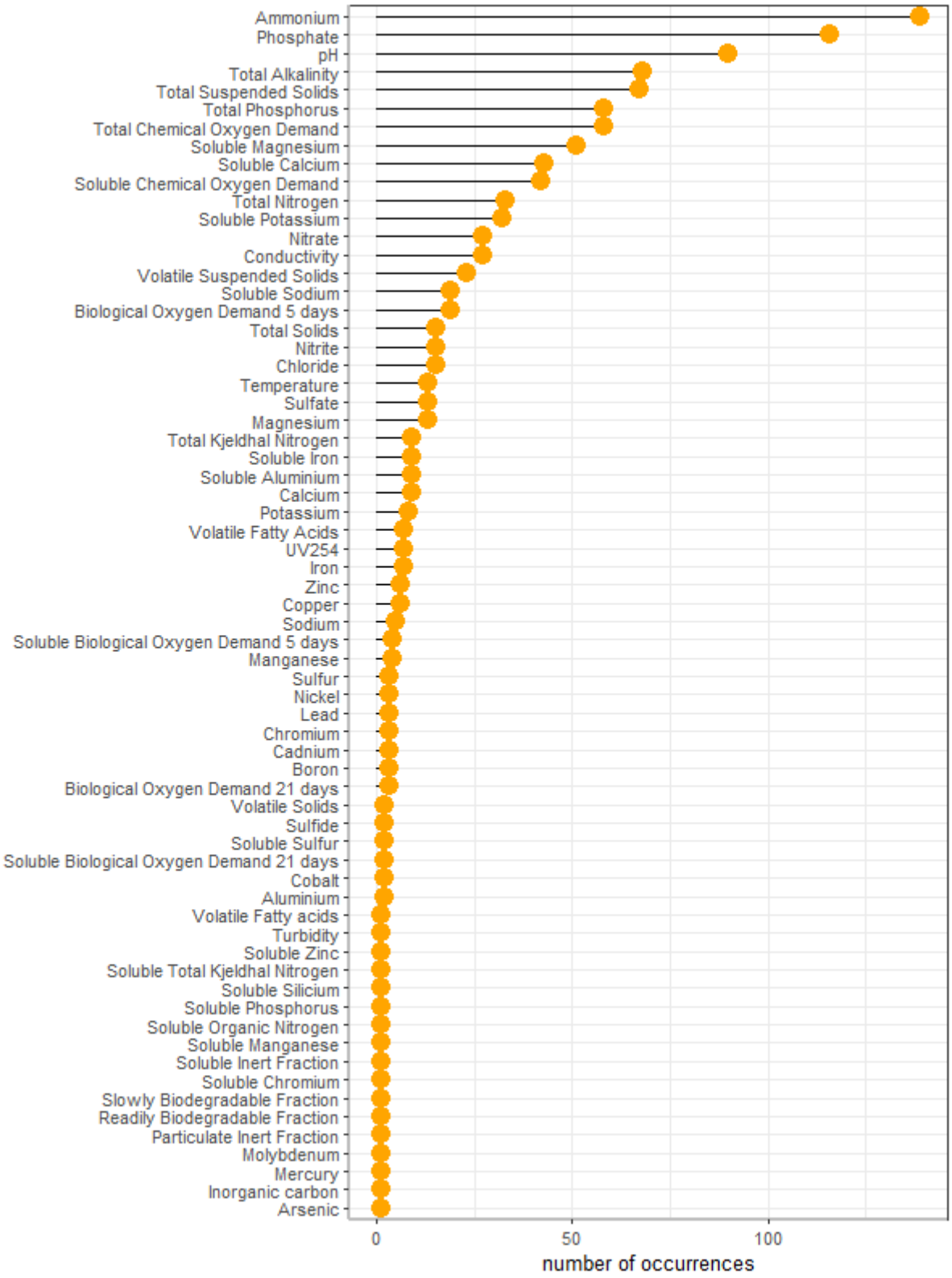

Figure S2.7 – List of sidestream characteristics compiled in the dataset

Figure S2.8 shows the number of occurrences of the different mass flows calculated when information on flows was available both at the inlet of the WRRF and for sidestreams.

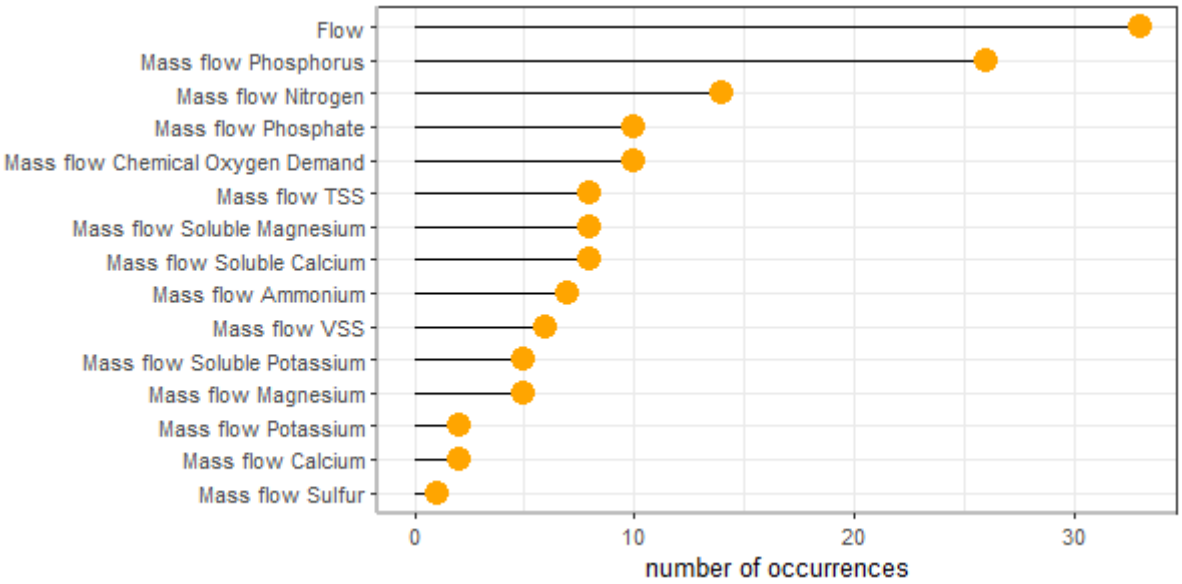

Figure S2.8 – List of calculated mass flows

Method for data collection

To set up the dataset of sidestream characteristics, SCOPUS database was used. The reference section of the selected research articles were also screened. Few internal documents were also used to complete the dataset.

The research query in SCOPUS was defined with a combination of expressions organised as follow:

- Publications containing the expressions related to sidetreams: sidestream, side-stream, supernatant, centrate, filtrate, reject water, sludge liquor, liquid phase or fraction, (return, recycle, dewatering, thickening, concentrated, or enriched) followed by (liquor or flow or load or flux or stream).

- Associated to the sidestreams location and context: "wastewater treatment plant" OR wwtp or "water resource recovery facility" OR sewage OR ((domestic or municipal or urban or sewage OR primary or biological or "waste activated" or digest*) PRE/1 (wastewater or effluent or sludge)

Only papers with clear information on sidestream sources were selected. Sidestreams from full-scale measurements only were included in the dataset. All characteristics of sidestreams coming from primary sludge thickening, waste activated sludge thickening, digested sludge dewatering were included. The digested sludge can be from conventional mesophilic anaerobic digestion or advanced anaerobic digestion with THP upstream of the digester.

When available, information about the WRRF configuration have been identified. These information include:

- the type of digester feed (primary sludge, biological sludge or mixed sludge)

- the type of phosphorus treatment (enhanced biological phosphorus removal, chemical, combination of biological and chemical or no treatment)
- the type of secondary treatment: activated sludge or trickling filter
- information on the thickening or dewatering equipment: centrifuge, belt filter press, draining drum, gravity thickener, dissolved air flotation
- Pore size of the filters used to characterise the soluble forms: 0.45 µm or 0.2 µm.
- Standard deviation: when available, standard deviation associated to sample size and measurement campaigns duration were provided.

The results of the analysis from the literature were not modified. Only a standardisation to express the results with the same units was carried out. If not reported, the soluble elements were assumed to be the predominant ions species for the following elements: sNa as Na^+, sCa as Ca^{2+}, sK as K^+, Mg as Mg^{2+}, Fe as Fe^{2+}, Cl as Cl^-, Al as Al^{3+}**.** When possible, the contribution of sidestreams to the total load was calculated as follows:

$$Mass\ flow_{[i]} = \frac{Flow_{sidestream} * [i]_{sidestream}}{Flow_{inlet_{WRRF}} * [i]_{inlet_{WRRF}} + Flow_{sidestream} * [i]_{sidestream}} * 100$$

Where:

- Mass flow $_{[i]}$ represents the mass flow brought by sidestreams compared to the inlet mass flows of the WRRF in %
- Flow $_{sidestream}$: flow of sidestream expressed as m3/day
- [i] $_{sidestream}$: concentration of the characteristic [i] in sidestream expressed as g/L or mg/L
- Flow $_{inlet\ WWRF}$: total flow at the inlet of the WRRF expressed as m3/day
- [i] $_{inlet\ WWRF}$: concentration of the characteristic [i] at the inlet of the WRRF expressed as g/L or mg/L

Value of the data

• This dataset presents a large data collection of sidestream characteristics in WRRFs. Data have been standardised (same units) and classified according to the WRRF configuration (type of secondary treatment, type of specific phosphorus treatment, dewatering or thickening equipment).

• For the first time, this dataset provides information on conventional characteristics of wastewater (e.g., Total Suspended Solids, Chemical Oxygen Demand) but also on the ionic strength, metal concentrations and organic matter biodegradability at full scale. This may be valuable for modellers or designers of sidestream treatment or recovery technologies that usually need information especially on the physico-chemical equilibria.

- This dataset allows the generation of average values and concentration ranges of the different characteristics according to the source of sidestreams and the configuration of the WRRF. This can be interesting for the development and the assessment of sidestream treatment or recovery technologies (e.g., phosphorus recovery as struvite, partial nitritation/anammox).

APPENDIX OF CHAPTER 3

List of model components

	Variable name	Formula	Description	Unit
1	S_{H2O}	H_20	Water	$gH2O/m^3$
2	S_{O2}	O_2	Dissolved oxygen	$gO2/m^3$
3	S_{ALK}	H^+	Total hydrogen	gH/m^3
4	S_{IP}	H2PO4-	Total inorganic phosphorus	gP/m^3
5	SIN	$(NH_4)^+$	Total inorganic nitrogen	gN/m^3
6	SIC	CO_2	Total inorganic carbon	gC/m^3
7	S_{TVA}	$C_5H_{10}O_2$	Total valerate	$gCOD/m^3$
8	S_{TBU}	$C_4H_8O_2$	Total butyrate	$gCOD/m^3$
9	S_{TPRO}	$C_3H_6O_2$	Total propionate	$gCOD/m^3$
10	S_{TAC}	$C_2H_4O_2$	Total acetate	$gCOD/m^3$
11	S_{Ca}	Ca^{2+}	Total dissolved calcium	gCa/m^3
12	S_{Mg}	Mg^{2+}	Total dissolved magnesium	gMg/m^3
13	S_{Na}	Na^+	Total dissolved sodium	gNa/m3
14	S_K	K^+	Total dissolved potassium	gK/m3
15	S_{Cl}	Cl^-	Chloride	gCl/m3
16	S_{Fe}	Fe^{3+}/Fe^{2+}	Soluble iron	gFe/m3
17	S_{SU}	$C_6H_{12}O_6$	Monosacarides	$gCOD/m^3$
18	S_{AA}	$C_4H_{6.1}0_{1.2}N$	Aminoacids	$gCOD/m^3$
19	S_{FA}	$C_{16}O_2H_{32}$	Long chain fatty acids (LCFA)	$gCOD/m^3$
20	S_{H2}	H_2	Dissolved hydrogen	$gCOD/m^3$
21	S_{CH4}	CH_4	Dissolved methane	$gCOD/m^3$
22	S_{N2}	N_2	Dissolved nitrogen	gN/m^3
23	S_{NO3}	$(NO_3)^-$	Nitrates	gN/m^3
24	S_I	$C_7H_{9.1}O_{2.65}NP_{0.05}$	Soluble inerts	$gCOD/m^3$
25	S_P	$C_5H_{6.9}O_2NP_{0.1}$	Lysis soluble product	$gCOD/m^3$
26	X_{C1}	$C_XH_XO_XNP_X$	Composites	$gCOD/m^3$
27	X_{C2}	$C_5H_{6.9}O_2NP_{0.1}$	Decay products	$gCOD/m^3$
28	X_{CH}	$C_6H_{9.95}O_5P_{0.05}$	Carbohydrates	$gCOD/m^3$
29	X_{PR}	$C_4H_{6.1}O_{1.2}N$	Proteins	$gCOD/m^3$
30	X_{LI}	$C_{51}H_{97.9}O_6P_{0.1}$	Lipids	$gCOD/m^3$
31	X_H	$C_5H_{6.9}O_2NP_{0.1}$	Heterotrophic bacteria	$gCOD/m^3$
32	X_N	$C_5H_{6.9}O_2NP_{0.1}$	Nitrifying bacteria	$gCOD/m^3$
33	X_{SU}	$C_5H_{6.9}O_2NP_{0.1}$	Sugar degrading bacteria	$gCOD/m^3$
34	X_{AA}	$C_5H_{6.9}O_2NP_{0.1}$	Aminoacid degrading bacteria	$gCOD/m^3$
35	X_{FA}	$C_5H_{6.9}O_2NP_{0.1}$	LCFA degrading bacteria	$gCOD/m^3$
36	X_{C4}	$C_5H_{6.9}O_2NP_{0.1}$	VAL/BUT degrading bacteria	$gCOD/m^3$
37	X_{PRO}	$C_5H_{6.9}O_2NP_{0.1}$	Propionate degrading bacteria	$gCOD/m^3$
38	X_{AC}	$C_5H_{6.9}O_2NP_{0.1}$	Acetate degrading bacteria	$gCOD/m^3$
39	X_{H2}	$C_5H_{6.9}O_2NP_{0.1}$	Hydrogen degrading bacteria	$gCOD/m^3$
40	X_I	$C_7H_{9.1}O_{2.65}NP_{0.05}$	Particulate inert	$gCOD/m^3$
41	X_P	$C_5H_{6.9}O_2NP_{0.1}$	Lysis particulate inert	$gCOD/m^3$
42	X_{II}	X	Inorganic	gSS/m^3
43	X_{CACO3}	CaCO3	Calcite	gSS/m^3
44	X_{MGCO3}	MgCO3	Magnesite	gSS/m^3
45	X_{ACP}	Ca3(PO4)2	Amorphous calcium phosphate	gSS/m^3
46	X_{STRU}	MgNH4PO4	Struvite	gSS/m^3
47	X_{KSTRU}	MgKPO4	Potassium struvite	gSS/m^3
48	X_{NEW}	MgHPO4	Newberyite	gSS/m^3
49	X_{PAO}	$C_5H_{6.9}O_2NP_{0.1}$	Phosphorus accumulating bacteria	gCOD
50	X_{PHA}	$C_4H_6O_2$	Poli-hydroxy-alcanoates	gCOD
51	X_{PP}	$K_{0.33}Mg_{0.33}PO_3$	Polyphosphates	gP
52	X_{FePO4}	$FePO_4$	Ferric phosphate	gSS/m^3
53	X_{FeCl3}	$FeCl_3$	Ferric Chloride	gSS/m^3
54	X_{FeOH3}	$Fe(OH)_3$	Ferric hydroxide	gSS/m^3
55	G_{CO2}	CO_2	Carbon dioxide	g C
56	G_{H2}	H_2	Hydrogen	g COD
57	G_{CH4}	CH_4	Methane	g COD
58	G_{NH3}	NH_3	Ammonium	g N
59	G_{N2}	N_2	Nitrogen	g N
60	G_{O2}	O_2	Oxygen	g 0_2
61	G_{H20}	H_20	Water Steam	g H_2O

List of transformations

1.Biochemical transformation

1.1 Intracellular	1	S_{SU} acidogenesis
	2	S_{AA} acidogenesis
	3	S_{FA} acetogenesis
	4	S_{HVA} acetogenegis
	5	S_{HBU} acetogenesis
	6	S_{HPRO} acetogenesis
	7	S_{TAC} methanogenesis
	8	S_{H2} methanogenesis
1.2 Extracellular / Enzymatic hydrolysis	9	X_{C2} anaerobic desintegration
	10	X_{CH} anerobic hydrolysis
	11	X_{PR} anerobic hydrolysis
	12	X_{LI} anerobic hydrolysis
	13	Thermal solubilization of X_{C2}
1.3 Biomass decay	17	X_{SU} decay
	15	X_{AA} decay
	16	X_{FA} decay
	17	X_{C4} decay
	18	X_{PRO} decay
	19	X_{AC} decay
	20	X_{H2} decay

2. Multiphase transformation

2.1 Liquid - solid transfer	21	Calcite precipitation-redissolution
	22	Magnesite precipitation-redissolution
	23	Magnesite precipitation-redissolution
	24	Struvite precipitation-redissolution
	25	K-Struvite precipitation-redissolution
	26	Newberyite precipitation-redissolution
	27	$FeCl_3$ precipitation-redissolution
	28	$FePO_4$ precipitation-redissolution
	29	$Fe(OH)_3$ precipitation-redissolution
2.2 Liquid - gas transfer	30	CO_2 dissolution
	31	O_2 dissolution
	32	H_2O evaporation
	33	NH_3 dissolution
	34	CH_4 dissolution
	35	N_2 dissolution
	36	H_2 dissolution

3. Chemical transformation

3.1 Acid base	37	$H_2O \leftrightarrow H^+ + OH^-$
	38	$H_2O + CO_2 \leftrightarrow 2H^+ + CO_3^{2-}$
	39	$HCO_3^- \leftrightarrow H^+ + CO_3^{2-}$
	40	$H_2PO_4^- \leftrightarrow 2H^+ + PO_4^{3-}$
	41	$HPO_4^= \leftrightarrow H^+ + PO_4^{3-}$
	42	$NH_4 \leftrightarrow H^+ + NH_3$
	43	$HAc \leftrightarrow H^+ + Ac^-$
	44	$HVa \leftrightarrow H^+ + Va^-$
	45	$HBu \leftrightarrow H^+ + Bu^-$
	46	$HPro \leftrightarrow H^+ + Pro^-$
	47	$CaCO_3 \leftrightarrow Ca^{2+} + CO_3^{2-}$
3.2 Ion pairing	48	$MgCO_3 \leftrightarrow Mg^{2+} + CO_3^{2-}$
	49	$CaHCO_3^+ \leftrightarrow Ca^{2+} + H^+ + CO_3^{2-}$
	50	$MgHCO_3^+ \leftrightarrow Mg^{2+} + H^+ + CO_3^{2-}$
	51	$MgPO_4^- \leftrightarrow Mg^{2+} + PO_4^{3-}$
	52	$CaPO_4^- \leftrightarrow Ca^{2+} + PO_4^{3-}$
	53	$MgHPO_4 \leftrightarrow Mg^{2+} + H^+ + PO_4^{3-}$
	54	$CaHPO_4 \leftrightarrow Ca^{2+} + H^+ + PO_4^{3-}$
	55	$CaOH^+ \leftrightarrow Ca^{2+} + H_2O - H^+$
	56	$MgOH^+ \leftrightarrow Mg^{2+} + H_2O - H^+$
	57	$NaHPO_4 \leftrightarrow Na^+ + H^+ + PO_4^{3-}$
	58	$NaCO_3^- \leftrightarrow Na^+ + CO_3^{2-}$
	59	$NaHCO_3 \leftrightarrow Na^+ + H^+ + CO_3^-$
	60	$MgH_2PO_4^+ \leftrightarrow Mg^{2+} + 2H^+ + PO_4^{-3}$
	61	$CaAc^+ \leftrightarrow Ca^{2+} + Ac^-$
	62	$NaAc \leftrightarrow Na^+ + Ac^-$
	63	$MgAc^+ \leftrightarrow Mg^{2+} + Ac^-$
	64	$CaPr^+ \leftrightarrow Ca^{2+} + Pr^-$
	65	$MgPr^+ \leftrightarrow Mg^{2+} + Pr^-$
	66	$MgBu^+ \leftrightarrow Mg^{2+} + Bu^-$
	67	$CaBu^+ \leftrightarrow Ca^{2+} + Bu^-$
	68	$CaH_2PO_4^+ \leftrightarrow Ca^{2+} + 2H^+ + PO_4^{3-}$

Biochemical transformations

Stoichiometric matrix

	S_{SU}	S_{AA}	S_{FA}	S_{TVA}	S_{TBU}	S_{TPRO}	S_{TAC}	S_{H2}	S_{CH4}	Sp	X_{SU}	X_{AA}	X_{FA}	X_{C4}	X_{PRO}	X_{AC}	X_{H2}	X_{C2}	X_{CH}	X_{PR}	X_{LI}	X_P
1	S_{SU} acidogen.	-1			$(1-Y_{SU})\cdot f_{BU,SU}$	$(1-Y_{SU})\cdot f_{PRO,SU}$	$(1-Y_{SU})\cdot f_{AC,SU}$	$(1-Y_{SU})\cdot f_{H2,SU}$			Y_{SU}											
2	S_{aa} acidogen.	-1		$(1-Y_{AA})\cdot f_{VA,AA}$	$(1-Y_{AA})\cdot f_{BU,AA}$	$(1-Y_{AA})\cdot f_{PRO,AA}$	$(1-Y_{AA})\cdot f_{AC,AA}$	$(1-Y_{AA})\cdot f_{H2,AA}$				Y_{AA}										
3	S_{FA} acetog.		-1										Y_{FA}									
4	S_{TVA} acetog.			-1		$(1-Y_{C4})\cdot f_{PRO,VA}$	$(1-Y_{C4})\cdot f_{AC,VA}$	$(1-Y_{C4})\cdot f_{H2,VA}$						Y_{C4}								
5	S_{TBU} acetog.				-1		$(1-Y_{C4})\cdot f_{AC,BU}$	$(1-Y_{C4})\cdot f_{H2,BU}$						Y_{C4}								
6	S_{TPRO} acetog.					-1	$(1-Y_{PRO})\cdot f_{AC,PRO}$	$(1-Y_{PRO})\cdot f_{H2,PRO}$							Y_{PRO}							
7	S_{TAC} Methanog.						-1		$1-Y_{AC}$							Y_{AC}						
8	S_{H2} Methanog.							-1	$1-Y_{H2}$								Y_{H2}					
9	X_{C2} anaerobic disintegration									$f_{SP,XC2}$								-1	$f_{CH,XC2}$	$f_{PR,XC2}$	$f_{LI,XC2}$	$f_{XP,XC2}$
10	X_{CH} anaerobic hydrolysis	1																	-1			
11	X_{PR} anaerobic hydrolysis		1																	-1		
12	X_{LI} anaerobic hydrolysis	$1-f_{FA,LI}$		$f_{FA,LI}$																	-1	
13	X_{C2} thermal solubilisation	$f_{TS}\cdot f_{CH,XC2}$	$f_{TS}\cdot f_{PR,XC2}$	$f_{TS}\cdot f_{LI,XC2}$						$f_{SP,XC2}$								-1	$(1-f_{TS})\,f_{CH,XC2}$	$(1-f_{TS})\,f_{PR,XC2}$	$(1-f_{TS})\,f_{LI,XC2}$	$f_{XP,XC2}$
14	X_{SU} decay										-1							1				
15	X_{AA} decay											-1						1				
16	X_{FA} decay												-1					1				
17	X_{C4} decay													-1				1				
18	X_{PRO} decay														-1			1				
19	X_{AC} decay															-1		1				
20	X_{H2} decay																-1	1				

rate
$r_1 = k_{m,XSU} * S_{SU} / (K_{SU,XSU} + S_{SU}) * [I_{O2} * I_{NOX} * A_{IN} * A_{IC} * A_{IP} * I_{pH,AA}] * X_{SU}$
$r_2 = k_{m,XAA} * S_{AA} / (K_{AA,XAA} + S_{AA}) * [I_{O2} * I_{NOX} * A_{IN} * A_{IC} * A_{IP} * I_{pH,AA}] * X_{AA}$
$r_3 = k_{m,XFA} * S_{FA} / (K_{FA,XFA} + S_{FA}) * [I_{O2} * I_{NOX} * A_{IN} * A_{IC} * A_{IP} * I_{H2,FA} * I_{pH,AA}] * X_{FA}$
$r_4 = k_{m,XC4} * S_{TVA} / (K_{C4,XC4} + S_{TVA}) * S_{TVA} / (S_{TVA} + S_{TBU}) * [I_{O2} * I_{NOX} * A_{IN} * A_{IC} * A_{IP} * I_{H2,C4} * I_{pH,AA}] * X_{C4}$
$r_5 = k_{m,XC4} * S_{TBU} / (K_{C4,XC4} + S_{TBU}) * S_{TBU} / (S_{TVA} + S_{TBU}) * [I_{O2} * I_{NOX} * A_{IN} * A_{IC} * A_{IP} * I_{H2,C4} * I_{pH,AA}] * X_{C4}$
$r_6 = k_{m,XPRO} * S_{PRO} / (K_{PRO,XPRO} + S_{PRO}) * [I_{O2} * I_{NOX} * A_{IN} * A_{IC} * A_{IP} * I_{H2,PRO} * I_{pH,PRO}] * X_{PRO}$
$r_7 = k_{m,XAC} * S_{TAC} / (K_{AC,XAC} + S_{TAC}) * [I_{O2} * I_{NOX} * A_{IN} * A_{IC} * A_{IP} * I_{NH3} * I_{pH,AC}] * X_{AC}$
$r_8 = k_{m,XH2} * S_{H2} / (K_{H2,XH2} + S_{H2}) * [I_{O2} * I_{NOX} * A_{IN} * A_{IC} * A_{IP} * I_{pH,H2}] * X_{H2}$
$r_9 = k_{dis,ANAER,XC2} * [I_{O2} * I_{NOX} * A_{IN} * A_{IC} * A_{IP} * I_{pH,H2}] * X_{C2}$
$r_{10} = k_{hid,ANAER,XCH} * [I_{O2} * I_{NOX} * A_{IN} * A_{IC} * A_{IP}] * X_{CH}$
$r_{11} = k_{his,ANAER,XPR} * [I_{O2} * I_{NOX} * A_{IN} * A_{IC} * A_{IP}] * X_{PR}$
$r_{12} = k_{his,ANAER,XLI} * [I_{O2} * I_{NOX} * A_{IN} * A_{IC} * A_{IP}] * X_{LI}$
$r_{13} = k_{FS} * [A_{IN} * A_{IC} * A_{IP}] * X_{C2}$
$r_{14} = k_{dec,XH,ANAER} * [I_{O2} * I_{NOX}] * X_{SU}$
$r_{15} = k_{dec,XH,ANAER} * [I_{O2} * I_{NOX}] * X_{AA}$
$r_{16} = k_{dec,XH,ANAER} * [I_{O2} * I_{NOX}] * X_{FA}$
$r_{17} = k_{dec,XH,ANAER} * [I_{O2} * I_{NOX}] * X_{C4}$
$r_{18} = k_{dec,XH,ANAER} * [I_{O2} * I_{NOX}] * X_{PRO}$
$r_{19} = k_{dec,XH,ANAER} * [I_{O2} * I_{NOX}] * X_{AC}$
$r_{20} = k_{dec,XH,ANAER} * [I_{O2} * I_{NOX}] * X_{H2}$

List of parameters

Acidogenesis

Parameter	Description	Unit	Default Value	Reference
Y_{SU}	Biomass Yield	$gCOD_X/gCOD_S$	0.1	Batstone et al., 2002
Y_{AA}	Biomass Yield	$gCOD_X/gCOD_S$	0.08	Batstone et al., 2002
$f_{BU,SU}$	Butyrate from sugars	----	0.13	Batstone et al., 2002
$f_{PRO,SU}$	Propionate from sugars	----	0.27	Batstone et al., 2002
$f_{AC,SU}$	Acetate from sugars	----	0.41	Batstone et al., 2002
$f_{H2,SU}$	Hydrogen from sugars	----	0.19	Batstone et al., 2002
$f_{VA,AA}$	Valerate from aminoacids	----	0.23	Batstone et al., 2002
$f_{BU,AA}$	Butyrate from aminoacids	----	0.26	Batstone et al., 2002
$f_{PRO,AA}$	Propionate from aminoacids	----	0.05	Batstone et al., 2002
$f_{AC,AA}$	Acetate from aminoacids	----	0.4	Batstone et al., 2002
$f_{H2,AA}$	Hydrogen from aminoacids	----	0.06	Batstone et al., 2002
$k_{m,XSU(T=35ºC)}$	Maximum specific uptake rate for sugars at 35ºC	$g\ COD_S/g\ COD_x \cdot d$	30	Batstone et al., 2002
$k_{m,XSU(T=55ºC)}$	Maximum specific uptake rate for sugars at 55ºC	$g\ COD_S/g\ COD_x \cdot d$	70	Batstone et al., 2002
$K_{SU,XSU(T=35ºC)}$	Sugar saturation constant	$g\ COD/m^3$	500	Batstone et al., 2002
$q_{SU,XSU}$	Temperature correction factor	----	0.035	Batstone et al., 2000
$k_{m,XAA(T=35ºC)}$	Maximum specific uptake rate for amino acids at 35ºC	$g\ COD_S/g\ COD_x \cdot d$	50	Batstone et al., 2002
$k_{m,XAA(T=55ºC)}$	Maximum specific uptake rate for amino acids at 55ºC	$g\ COD_S/g\ COD_x \cdot d$	70	Batstone et al., 2002
$K_{AA,XAA(T=35ºC)}$	Amino acid saturation constant for heterotrophic biomass	$g\ COD/m^3$	300	Batstone et al., 2002
$q_{AA,XAA}$	Temperature correction factor	----	0	Batstone et al., 2000
$K_{A,NOX}$	Activation/ Inhibition constant for NO_2^- and NO_3^-	$g\ N/m^3$	0.1	Batstone et al., 2002
$K_{I,H,XAA}$	Inhibition constant for pH in the acidogenesis and acetogenesis	$g\ H/m^3$	0.0155	Batstone et al., 2002

Acetogenesis

Parameter	Description	Unit	Default Value	Reference
Y_{FA}	Biomass Yield	$gCOD_X/gCOD_S$	0.06	Batstone et al., 2002
Y_{C4}	Biomass Yield	$gCOD_X/gCOD_S$	0.06	Batstone et al., 2002
Y_{PRO}	Yield coefficient of biomass on propionate	$gCOD_X/gCOD_S$	0.04	Batstone et al., 2002
$f_{AC,FA}$	Acetate from fatty acids	----	0.7	BSM2
$f_{H2,FA}$	Hydrogen from fatty acids	----	0.3	BSM2
$f_{AC,VA}$	Acetate from valerate	----	0.31	BSM2
$f_{H2,VA}$	Hydrogen from valerate	----	0.15	BSM2
$f_{PRO,VA}$	Propionate from valerate	----	0.54	BSM2
$f_{AC,BU}$	Acetate from butyrate	----	0.8	BSM2
$f_{H2,BU}$	Hydrogen from butyrate	----	0.2	BSM2
$f_{AC,PRO}$	Acetate from propionate	----	0.57	BSM2
$f_{H2,PRO}$	Hydrogen from propionate	----	0.43	BSM2
$k_{m,XFA(T=35ºC)}$	Maximum specific uptake rate for Fatty acids at 35ºC	$g\ COD_S/g\ COD_X \cdot d$	6	Batstone et al., 2002
$k_{m,XFA(T=55ºC)}$	Maximum specific uptake rate for Fatty acids at 55ºC	$g\ COD_S/g\ COD_X \cdot d$	10	Batstone et al., 2002
$K_{FA,XFA\ (T=35ºC)}$	Fatty acid saturation constant	g COD/m3	400	Batstone et al., 2002
$q_{FA,XFA}$	Temperature correction factor	----	0	Batstone et al., 2002
$K_{I,H2,FA\ (T=35ºC)}$	Inhibition of acidogenesis on fatty acids due to hydrogen	g COD/m3	0.005	Batstone et al., 2002
$q_{I,H2,FA}$	Temperature correction factor	----	0	Batstone et al., 2000
$k_{m,XC4(T=35ºC)}$	Maximum specific uptake rate for valerate-butyrate at 35ºC	$g\ COD_S/g\ COD_X \cdot d$	20	Batstone et al., 2002
$k_{m,XC4(T=55ºC)}$	Maximum specific uptake rate for valerate-butyrate at 55ºC	$g\ COD_S/g\ COD_X \cdot d$	30	Batstone et al., 2002
$K_{C4,XC4\ (T=35ºC)}$	Butyrate/ valerate saturation constat	$g\ COD/m^3$	200	Batstone et al., 2002
$q_{C4,XC4}$	Temperature correction factor	----	0.035	Batstone et al., 2002
$K_{I,H2,C4\ (T=35ºC)}$	Inhibition of acidogenesis on butyrate/ valerate due to hydrogen	$g\ COD/m^3$	0.01	Batstone et al., 2002
$q_{I,H2,C4}$	Temperature correction factor	----	0.055	Batstone et al., 2000
$k_{m,XPRO(T=35ºC)}$	Maximum specific uptake rate for Propionate at 35ºC	$g\ COD_S/g\ COD_X \cdot d$	13	Batstone et al., 2002
$k_{m,XPRO(T=55ºC)}$	Maximum specific uptake rate for Propionate at 55ºC	$g\ COD_S/g\ COD_X \cdot d$	20	Batstone et al., 2002
$K_{PRO,XPRO\ (T=35ºC)}$	Propionate saturation constant	g COD/m3	100	Batstone et al., 2002
$q_{PRO,XPRO}$	Temperature correction factor	----	0.055	Batstone et al., 2002
$K_{I,H2,PRO\ (T=35ºC)}$	Inhibition of acidogenesis on propionic acid due to hydrogen	g COD/m3	0.0035	Batstone et al., 2002
$q_{I,H2,PRO}$	Temperature correction factor	----	0.055	Batstone et al., 2000

Methanogenesis

Parameter	Description	Unit	Default Value	Reference
Y_{AC}	Biomass Yield	$gCOD_X/gCOD_S$	0.05	Batstone et al., 2002
Y_{H2}	Biomass Yield	$gCOD_X/gCOD_S$	0.06	Batstone et al., 2002
$K_{m,XAC(T=35ºC)}$	Maximum specific uptake rate for Acetate at 35ºC	$g\ COD_S/g\ COD_X \cdot d$	8	Batstone et al., 2002
$K_{m,XAC(T=55ºC)}$	Maximum specific uptake rate for Acetate at 55ºC	$g\ COD_S/g\ COD_X \cdot d$	16	Batstone et al., 2002
$K_{AC,XAC\ (T=35ºC)}$	Acetate saturation constant for methanogenic biomass	$g\ COD/m^3$	150	Batstone et al., 2002
$q_{AC,XAC}$	Temperature correction factor	----	0.035	Batstone et al., 2002
$K_{I,H,XAC}$	Inhibition of acetoclastic methanogenesis due to pH	$g\ H/m^3$	0.000316	Batstone et al., 2002
$K_{I,NH3\ (T=35ºC)}$	Inhibition coefficient due to NH_3	$g\ N/m^3$	25.2	Batstone et al., 2002
$q_{I,NH3}$	Temperature correction factor	----	0.091	Batstone et al., 2000
$K_{m,XH2(T=35ºC)}$	Maximum specific uptake rate for Hydrogen at 35ºC	$g\ COD_S/g\ COD_X \cdot d$	35	Batstone et al., 2002
$K_{m,XH2(T=55ºC)}$	Maximum specific uptake rate for Hydrogen at 55ºC	$g\ COD_S/g\ COD_X \cdot d$	35	Batstone et al., 2002
$K_{H2,XH2\ (T=35ºC)}$	Hydrogen saturation constant for methanogenic biomass	$g\ COD/m^3$	0.007	Estimated
$q_{H2,XH2}$	Temperature correction factor	----	0.018	Batstone et al., 2002
$K_{I,H,XH2}$	Inhibition of hydrogenophilic methanogenesis due to pH	$g\ H/m^3$	0.00316	Batstone et al., 2002

Extracellular enzymatic biomass disintegration

Parameter	Description	Unit	Default Value	Reference
$f_{SP.XC2}$	Lysis sol. Product from decay complex	---	0.015	Estimated
$f_{CH.XC2}$	Carbohydrates from decay complex	---	0.103	Estimated
$f_{PR.XC2}$	Proteins from decay complex	---	0.413	Estimated
$f_{LI.XC2}$	Lipids from decay complex	---	0.285	Estimated
$f_{XP.XC2}$	Lysis particulate product from decay complex	---	0.184	Estimated
$k_{dis,ANAER,XC2\ (T=35ºC)}$	Disintegration rate of X_{C2} in anaerobic conditions	1/d	0.5	Batstone et al., 2002
$q_{dis,ANAER,\ XC2\ (T=35ºC)}$	Temperature correction factor	----	0.035	Batstone et al., 2002

Extracellular enzymatic hydrolysis

Parameter	Description	Unit	Default Value	Reference
$f_{FA,LI}$	Fatty acids from lipids	----	0.95	Batstone et al., 2002
$k_{hid,ANAER,XCH\ (T=35ºC)}$	Hydrolysis rate of carbohydrates in anaerobic conditions	1/d	10	Batstone et al., 2002
$k_{hid,ANAER,XLI\ (T=35ºC)}$	Hydrolysis rate of lipids in anaerobic conditions	1/d	10	Batstone et al., 2002
$k_{hid,ANAER,XPR\ (T=35ºC)}$	Hydrolysis rate of proteins in anaerobic conditions	1/d	10	Batstone et al., 2002
$q_{hid,ANAER,XCH\ (T=35ºC)}$	Temperature correction factor	----	0.024	Estimated
$q_{hid,ANAER,XLI\ (T=35ºC)}$	Temperature correction factor	----	0	Estimated
$q_{hid,ANAER,XPR\ (T=35ºC)}$	Temperature correction factor	----	0.024	Estimated
$K_{x\ (T=20ºC)}$	Half saturation coefficient for hydrolysis of slowly biodegradable substrate	gCOD/ gCOD	0.03	Henze et al., 2000
$q_{hid,x}$	Temperature correction factor	---	1.116	Henze et al., 2000

Extracellular enzymatic thermal solubilisation of XC2

Parameter	Description	Unit	Default Value	Reference
f_{TS}	Solubilised fraction	----	0.1	Estimated
$k_{TS\ (T=35ºC)}$	Thermal solubilisation rate of X_{C2}	1/d	20	Estimated
q_{TS}	Temperature correction factor	----	0.82	Estimated

Biomass decay

Parameter	Description	Unit	Default Value	Reference
$k_{dec,XSU,ANAER\ (T=35ºC)}$	Sugars degraders decay rate in anaerobic conditions	1/d	0.02	Batstone et al., 2002
$q_{dec,XSU,ANAER\ (T=35ºC)}$	Temperature correction factor	----	0.035	Siegrist et al., 2002
$k_{dec,XAA,ANAER\ (T=35ºC)}$	Amino acid degraders decay rate in anaerobic conditions	1/d	0.02	Batstone et al., 2002
$q_{dec,XAA,ANAER\ (T=35ºC)}$	Temperature correction factor	----	0.035	Siegrist et al., 2002
$k_{dec,XFA,ANAER\ (T=35ºC)}$	Fatty acids degraders decay rate in anaerobic conditions	1/d	0.02	Batstone et al., 2002
$q_{dec,XFA,ANAER\ (T=35ºC)}$	Temperature correction factor	----	0.035	Siegrist et al., 2002
$k_{dec,XC4,ANAER\ (T=35ºC)}$	Butyrate- valerate degraders decay rate in anaerobic conditions	1/d	0.02	Batstone et al., 2002
$q_{dec,XC4,ANAER\ (T=35ºC)}$	Temperature correction factor	----	0.035	Siegrist et al., 2002
$k_{dec,XPRO,ANAER\ (T=35ºC)}$	Propionate degraders decay rate in anaerobic conditions	1/d	0.02	Batstone et al., 2002
$q_{dec,XPRO,ANAER\ (T=35ºC)}$	Temperature correction factor	----	0.035	Siegrist et al., 2002
$k_{dec,XAC,ANAER\ (T=35ºC)}$	Acetoclastic methanogenic bacteria decay rate in anaerobic conditions	1/d	0.02	Batstone et al., 2002
$q_{dec,XAC,ANAER\ (T=35ºC)}$	Temperature correction factor	----	0.035	Siegrist et al., 2002
$k_{dec,XH2,ANAER\ (T=35ºC)}$	Hydrogenophilic methanogenic bacteria decay rate in anaerobic conditions	1/d	0.02	Batstone et al., 2002
$q_{dec,XH2,ANAER\ (T=35ºC)}$	Temperature correction factor	----	0.035	Siegrist et al., 2002

Calculated variables

Variables	Description
$k_{m,XSU}$	$A_{(T=35°C)} * k_{m,XSU(T=35°C)} * e^{[-0,01*(Tw-35)^2]} + A_{(T=55°C)} * k_{m,XSU(T=55°C)} * e^{[-0,01*(Tw-55)^2]}$
$k_{m,XAA}$	$A_{(T=35°C)} * k_{m,XSU(T=35°C)} * e^{[-0,01*(Tw-35)^2]} + A_{(T=55°C)} * k_{m,XAA(T=55°C)} * e^{[-0,01*(Tw-55)^2]}$
$k_{m,XFA}$	$A_{(T=35°C)} * k_{m,XFA(T=35°C)} * e^{[-0,01*(Tw-35)^2]} + A_{(T=55°C)} * k_{m,XFA(T=55°C)} * e^{[-0,01*(Tw-55)^2]}$
$k_{m,XC4}$	$A_{(T=35°C)} * k_{m,XC4(T=35°C)} * e^{[-0,01*(Tw-35)^2]} + A_{(T=55°C)} * k_{m,XC4(T=55°C)} * e^{[-0,01*(Tw-55)^2]}$
$k_{m,XPRO}$	$A_{(T=35°C)} * k_{m,XPRO(T=35°C)} * e^{[-0,01*(Tw-35)^2]} + A_{(T=55°C)} * k_{m,XPRO(T=55°C)} * e^{[-0,01*(Tw-55)^2]}$
$k_{m,XAC}$	$A_{(T=35°C)} * k_{m,XAC(T=35°C)} * e^{[-0,01*(Tw-35)^2]} + A_{(T=55°C)} * k_{m,XAC(T=55°C)} * e^{[-0,01*(Tw-55)^2]}$
$k_{m,XH2}$	$A_{(T=35°C)} * k_{m,XH2(T=35°C)} * e^{[-0,01*(Tw-35)^2]} + A_{(T=55°C)} * k_{m,XH2(T=55°C)} * e^{[-0,01*(Tw-55)^2]}$
$k_{m,dis,ANAER,XC2}$	$A_{(T=35°C)} * k_{m,dis,ANAER,XC2(T=35°C)} * e^{[\theta dis,ANAER,XC2*(Tw-35)]}$
$k_{hid,ANAER,XCH}$	$A_{(T=35°C)} * k_{m,hid,ANAER,XCH(T=35°C)} * e^{[\theta hid,ANAER,XCH(T=35°C)*(Tw-35)]}$
$k_{hid,ANAER,XLI}$	$A_{(T=35°C)} * k_{m,hid,ANAER,XLI(T=35°C)} * e^{[\theta hid,ANAER,XLI(T=35°C)*(Tw-35)]}$
$k_{hid,ANAER,XPR}$	$A_{(T=35°C)} * k_{m,hid,ANAER,XPR(T=35°C)} * e^{[\theta hid,ANAER,XPR(T=35°C)*(Tw-35)]}$
k_{TS}	$A_{(T=35°C)} * k_{TS(T=35°C)} * e^{[\theta TS*(Tw-35)]}$
$k_{dec,XSU,ANAER}$	$A_{(T=35°C)} * k_{dec,XSU,ANAER(T=35°C)} * e^{[\theta decXSU,ANAER(T=35°C)*(Tw-35)]}$
$k_{dec,XAA,ANAER}$	$A_{(T=35°C)} * k_{dec,XAA,ANAER(T=35°C)} * e^{[\theta decXAA,ANAER(T=35°C)*(Tw-35)]}$
$k_{dec,XFA,ANAER}$	$A_{(T=35°C)} * k_{dec,XFA,ANAER(T=35°C)} * e^{[\theta decXFA,ANAER(T=35°C)*(Tw-35)]}$
$k_{dec,XC4,ANAER}$	$A_{(T=35°C)} * k_{dec,XC4,ANAER(T=35°C)} * e^{[\theta decXC4,ANAER(T=35°C)*(Tw-35)]}$
$k_{dec,PRO,ANAER}$	$A_{(T=35°C)} * k_{dec,PRO,ANAER(T=35°C)} * e^{[\theta decXCPRO,ANAER(T=35°C)*(Tw-35)]}$
$k_{dec,XAC,ANAER}$	$A_{(T=35°C)} * k_{dec,XAC,ANAER(T=35°C)} * e^{[\theta decXAC,ANAER(T=35°C)*(Tw-35)]}$
$k_{dec,XH2,ANAER}$	$A_{(T=35°C)} * k_{dec,XH2,ANAER(T=35°C)} * e^{[\theta decXH2,ANAER(T=35°C)*(Tw-35)]}$

Variables	Description
$k_{SU,XSU}$	$k_{SU,XSU(T=35°C)} * e^{[\theta SU,XSU*(Tw-35)]}$
$k_{AA,XAA}$	$k_{AA,XAA(T=35°C)} * e^{[\theta AA,XAA*(Tw-35)]}$
$k_{FA,XFA}$	$k_{FA,XFA(T=35°C)} * e^{[\theta FA,XFA*(Tw-35)]}$
$k_{C4,XC4}$	$k_{C4,XC4(T=35°C)} * e^{[\theta C4,XC4*(Tw-35)]}$
$k_{PRO,XPRO}$	$k_{PRO,XPRO(T=35°C)} * e^{[\theta PRO,XPRO*(Tw-35)]}$
$k_{AC,XAC}$	$k_{AC,XAC(T=35°C)} * e^{[\theta AC,XAC*(Tw-35)]}$
$k_{H2,XH2}$	$k_{H2,XH2(T=35°C)} * e^{[\theta H2,XH2*(Tw-35)]}$

Variables	Description
I_{NOX}	$K_{A,NOX} / (K_{A,NOX} + S_{NO3-})$
$I_{pH,AA}$	$K_{I,H,XAA}^2 / (K_{I,H,XAA}^2 + S_{H+}^2)$
$k_{I,H2,FA}$	$k_{I,H2,FA(T=35°C)} * e^{[\theta I,H2,FA*(Tw-35)]}$
$k_{I,H2,C4}$	$k_{I,H2,C4(T=35°C)} * e^{[\theta I,H2,C4*(Tw-35)]}$
$k_{I,H2,PRO}$	$k_{I,H2,PRO(T=35°C)} * e^{[\theta I,H2PRO*(Tw-35)]}$
$I_{H2,FA}$	$K_{I,H2,FA} / (K_{I,H2,FA} + S_{H2})$
$I_{H2,C4}$	$K_{I,H2,C4} / (K_{I,H2,C4} + S_{H2})$
$I_{H2,PRO}$	$K_{I,H2,PRO} / (K_{I,H2,PRO} + S_{H2})$
$k_{I,NH3}$	$k_{I,NH3(T=35°C)} * e^{[\theta I,NH3*(Tw-35)]}$
I_{NH3}	$K_{I,NH3} / (K_{I,NH3} + S_{NH3})$
$I_{pH,Ac}$	$K_{I,H,XAC}^3 / (K_{I,H,XAC}^3 + S_H^3)$
$I_{pH,H2}$	$K_{I,H,XH2}^3 / (K_{I,H,XH2}^3 + S_H^3)$

Multiphase transformations

Liquid-solid transfer

Stoichiometric matrix

		S_{IP}	S_{H2O}	S_{IN}	S_{IC}	S_{Mg}	S_K	S_{Ca}	X_{CaCO3}	X_{MgCO3}	X_{ACP}	X_{stru}	X_{kstru}	X_{new}
21	Calcite				-1			-40/12	100/12					
22	Magnesite				-1	-24.3/12				84.31/12				
23	ACP	-1						-120/61			246/61			
24	Struvite	-1	-108/31	-14/31		-24.3/31						245.31/31		
25	k-Struvite	-1				-24.3/31	-39/31						153.3/31	
26	Newberyite	-1					-24.3/31							120.3/31

rate
$r_{21} = k_{r,CaCO3} * ((S_{Ca}/40000)^{1/2} * (S_{CO3}/12000)^{1/2} - K_{sp,CaCO3}^{1/2})^2$
$r_{22} = k_{r,MgCO3} * ((S_{Mg}/24300)^{1/2} * (S_{CO3}/12000)^{1/2} - K_{sp,MgCO3}^{1/2})^2$
$r_{23} = k_{r,ACP} * ((S_{Ca}/40000)^{3/5} * (S_{PO4}/31000)^{2/5} - K_{sp,ACP}^{1/5})^2$
$r_{24} = k_{r,stru} * ((S_{Mg}/24300)^{1/3} * (S_{PO4}/31000)^{1/3} * S_{NH4}/14000)^{1/3} * - K_{sp,stru}^{1/3})^3$
$r_{25} = k_{r,kstru} * ((S_{Mg}/24300)^{1/3} * (S_{PO4}/31000)^{1/3} * S_K/39000)^{1/3} * - K_{sp,kstru}^{1/3})^3$
$r_{26} = k_{r,new} * ((S_{Mg}/24300)^{1/2} * (S_{HPO4}/31000)^{1/2} - K_{sp,MgCO3}^{1/2})^2$

List of parameters

Parameter	Description	Unit	Default Value (298 K)	Reference
$K_{r,caco3}$	Precipitation rate constant	1/d	0.5	Musvoto et al 2000
$K_{r,mgco3}$	Precipitation rate constant	1/d	50	Musvoto et al 2000
$K_{r,ACP}$	Precipitation rate constant	1/d	350	Musvoto et al 2000
$K_{r,stru}$	Precipitation rate constant	1/d	3000	Musvoto et al 2000
$K_{r,kstru}$	Precipitation rate constant	1/d	100	Ikumi et al. 2020
K_{rnew}	Precipitation rate constant	1/d	0.05	Musvoto et al 2000
$K_{sp,caco3\ (T=.25ºC)}$	Solubility product of $CaCO_3$	mol/L	$10^{-6.45}$	Musvoto et al 2000
$K_{sp,mgco3\ (T=.25ºC)}$	Solubility product of $MgCO_3$	mol/L	$10^{-7.0}$	Musvoto et al 2000
$K_{sp,ACP\ (T=.25ºC)}$	Solubility product of ACP	mol/L	$10^{-25.46}$	Musvoto et al 2000
$K_{sp,stru\ (T=.25ºC)}$	Solubility product of struvite	mol/L	$10^{-13.16}$	Musvoto et al 2000
$K_{sp,kstru\ (T=.25ºC)}$	Solubility product of K-struvite	mol/L	$10^{-13.16}$	Musvoto et al 2000
$K_{sp,new\ (T=.25ºC)}$	Solubility product of newberyite	mol/L	$10^{-5.8}$	Musvoto et al 2000

Calculated variables

Variables	Description
$k_{sp,CaCO3}$	$K_{sp,CaCO3\ (T°C=25°C)} * e^{[12348/8,314\ *(1/298,15\ -\ 1/(Tw+273,15))]}$
$k_{sp,MgCO3}$	$K_{sp,MgCO3\ (T°C=25°C)} * e^{[487906/8,314\ *(1/298,15\ -\ 1/(Tw+273,15))]}$
$k_{sp,ACP}$	$K_{sp,ACP\ (T°C=25°C)} * e^{[2308000/8,314\ *(1/298,15\ -\ 1/(Tw+273,15))]}$
$k_{sp,Stru}$	$K_{sp,Stru\ (T°C=25°C)} * e^{[0/8,314\ *(1/298,15\ -\ 1/(Tw+273,15))]}$
$k_{sp,KStru}$	$K_{sp,KStru\ (T°C=25°C)} * e^{[0/8,314\ *(1/298,15\ -\ 1/(Tw+273,15))]}$
$k_{sp,New}$	$K_{sp,new\ (T°C=25°C)} * e^{[0/8,314\ *(1/298,15\ -\ 1/(Tw+273,15))]}$

Liquid-gas transfer

Stroichiometric matrix

		S_{H2O}	S_{O2}	S_{IN}	S_{IC}	S_{H2}	S_{CH4}	S_{N2}	G_{CO2}	G_{H2}	G_{CH4}	G_{NH3}	G_{N2}	G_{O2}	G_{H2O}
27	CO_2 dissolution-evaporation				1				-1						
28	O_2 dissolution-evaporation		1											-1	
29	H_2O dissolution-evaporation	-1													1
30	NH_3 dissolution-evaporation			1								-1			
31	CH_4 dissolution-evaporation						1				-1				
32	N_2 dissolution-evaporation							1					-1		
33	H_2 dissolution-evaporation					1				-1					

rate
$r_1 = k_{L\_a,CO2} * (K_{H,CO2} * 12000 * p_{g,CO2} - CS_{CO2})$
$r_2 = k_{L\_a,O2} * (K_{H,O2} * 32000 * p_{g,O2} - CS_{O2})$
$r_3 = k_{M\_a,H2O} * 18000 / (0{,}082 * (273{,}15 + T_g)) * (P_{g,H2O}^{SAT} - p_{g,H2O})$
$r_4 = k_{L\_a,NH3} * (K_{H,NH3} * 14000 * p_{g,NH3} - CS_{NH3})$
$r_5 = k_{L\_a,CH4} * (K_{H,CH4} * 64000 * p_{g,CH4} - CS_{CH4})$
$r_6 = k_{L\_a,N2} * (K_{H,N2} * 28000 * p_{g,N2} - CS_{N2})$
$r_7 = k_{L\_a,H2} * (K_{H,H2} * 16000 * p_{g,H2} - CS_{H2})$

List of parameters

Parameter	Description	Unit	Default Value (298.15 K)	Reference
$K_{H,CO2\ (T=.25ºC)}$	Henry´s constant for CO_2	mol/L·bar	0.035	Perry and Chilton, 1973
$K_{H,H2\ (T=.25ºC)}$	Henry´s constant for H_2	mol/L·bar	0.00078	Perry and Chilton, 1973
$K_{H,CH4\ (T=.25ºC)}$	Henry´s constant for CH_4	mol/L·bar	0.0014	Perry and Chilton, 1973
$K_{H,NH3\ (T=.25ºC)}$	Henry´s constant for NH_3	mol/ L·bar	59	Perry and Chilton, 1973
$K_{H,N2\ (T=.25ºC)}$	Henry´s constant for N_2	mol/ L·bar	0.00065	Perry and Chilton, 1973
$K_{H,O2\ (T=.25ºC)}$	Henry´s constant for O_2	mol/ L·bar	0.0013	Perry and Chilton, 1973
$k_{M,H2O}$	Evaporation constant	m/d	calibration	Estimated

Parameter	Description	Unit	Default Value	Reference
$k_{L\_a,O2}$	0_2 transfer coefficient	1/d	100	Estimated
$k_{L\_a,CO2}$	CO_2 transfer coefficient	1/d	100	Estimated
$k_{L\_a,H2}$	H_2 transfer coefficient	1/d	100	Estimated
$k_{L\_a,CH4}$	CH_4 transfer coefficient	1/d	100	Estimated
$k_{L\_a,NH3}$	NH_3 transfer coefficient	1/d	100	Estimated
$k_{L\_a,N2}$	N_2 transfer coefficient	1/d	100	Estimated
$k_{M\_a,H2O}$	H_20 transfer coefficient	1/d	100	Estimated
m	a water moleculate weight	g	$2.99 \cdot 10^{-23}$	Perry and Chilton, 1973
k_B	Boltzmann constant	J/K	$1.3806504 \cdot 10^{-23}$	Perry and Chilton, 1973

State	Description	Unit
$p_{g,CO2}$	$C0_2$ partial pressure	Bar
$p_{g,O2}$	O_2 partial pressure	Bar
$p_{g,H2O}$	H_2O partial pressure	Bar
$p_{g,NH3}$	NH_3 partial pressure	Bar
$p_{g,CH4}$	CH_4 partial pressure	Bar
$p_{g,N2}$	N_2 partial pressure	Bar
$p_{g,H2}$	H_2 partial pressure	Bar
$p^{SAT}_{g,H2O}$	H_20 partial pressure	Bar

Calculated variables

Variables	Description
$k_{H,CO2}$	$K_{H,CO2\ (T°C=25°C)} * e^{[-19410/8,314\ *(1/298,15\ -\ 1/(Tw+273,15))]}$
$k_{H,O2}$	$K_{H,O2\ (T°C=25°C)} * e^{[-12741/8,314\ *(1/298,15\ -\ 1/(Tw+273,15))]}$
$k_{H,NH3}$	$K_{H,NH3\ (T°C=25°C)} * e^{[-34100/8,314\ *(1/298,15\ -\ 1/(Tw+273,15))]}$
$k_{H,CH4}$	$K_{H,CH4\ (T°C=25°C)} * e^{[-14240/8,314\ *(1/298,15\ -\ 1/(Tw+273,15))]}$
$k_{H,N2}$	$K_{H,N2\ (T°C=25°C)} * e^{[-10808/8,314\ *(1/298,15\ -\ 1/(Tw+273,15))]}$
$k_{H,H2}$	$K_{H,H2\ (T°C=25°C)} * e^{[-4180/8,314\ *(1/298,15\ -\ 1/(Tw+273,15))]}$

Chemical transformations

Tableau method

	Model components																
Species	H_2O	H	$C\text{-}CO_3$	$P\text{-}PO_4$	$N\text{-}NO_3$	Ac	Bu	Prop	Va	Cl	$N\text{-}NH_4$	Ca	Mg	Na	K	Fe^{3+}	LogK
H_2O	1																0
H^+		1															0
OH^-	1	-1															-14
CaOH	1	-1										1					12.7
MgOH	1	-1											1				11.4
NaOH	1	-1												1			-1.3
$Fe(OH)_3$	3	-3														1	-13.2
H_2CO_3		2	1														-16.7
HCO_3		1	1														-10.3
CO_3			1														0
$CaCO_3$			1									1					-3.2
$CaHCO_3$		1	1									1					-11.6
$MgCO_3$			1										1				-2.9
$MgHCO_3$		1	1										1				-11.3
$NaCO_3$			1											1			-1.3
$NaHCO_3$		1	1											1			-10.1
H_2PO_4		2		1													-19.6
HPO_4		1		1													-12.7
PO_4				1													0
CaH_2PO_4		2		1								1					-20.9
$CaHPO_4$		1		1								1					-15
$CaPO_4$				1								1					-6.5
MgH_2PO_4		2		1									1				-21.2
$MgHPO_4$		1		1									1				-15.2
$MgPO_4$				1									1				-4.5
$NaHPO_4$		1		1										1			-13.4
$KHPO_4$		1		1											1		-15.3
NH_4^+											1						0
NH_3		-1									1						-9.2
Ac						1											0
Bu							1										0
Prop								1									0
Va									1								0
HVA		1							1								-4.6
HBu		1					1										-4.8
Hprop		1						1									-4.8
Hac		1				1											-4.7
CaAc						1						1					-1.2
CaBu							1					1					-0.9
CaProp								1				1					-0.9
MgAc						1							1				-1.3
MgBu							1						1				-1
MgProp								1					1				1
NaAc						1								1			0.2
NO_3^-					1												0
$FeCl_3$										3						1	0
Na														1			0
Cl										1							0
Ca												1					0
Mg													1				0
Fe^{3+}																1	0
K															1		0

Mass balances

The mass balances were carried out according to the Lavoisier matter conservation principle.

WRRF 1

Total COD mass balance

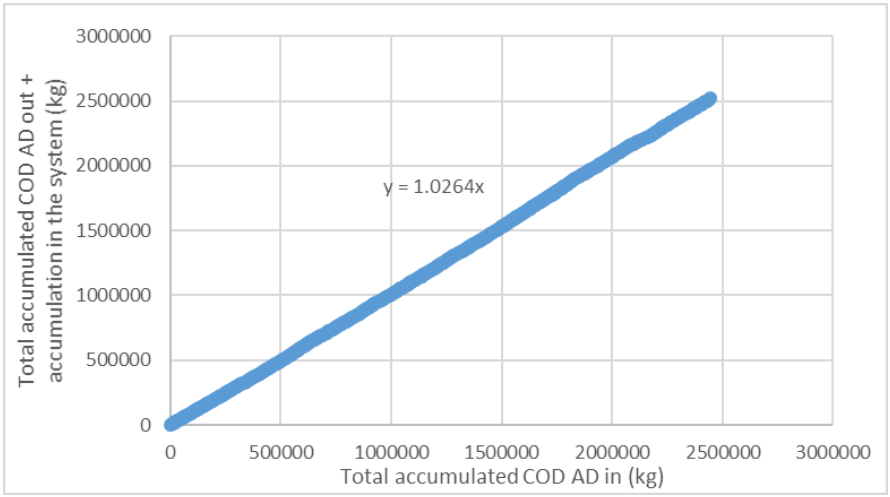

Mineral matter mass balance

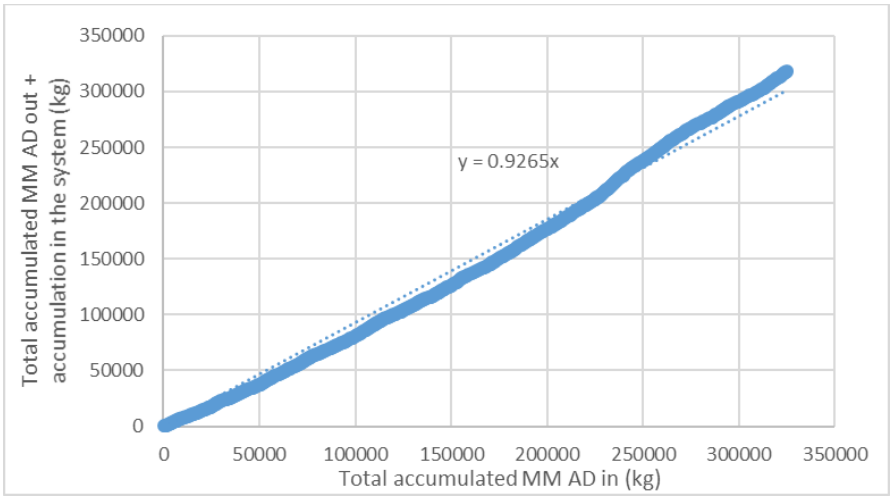

Total Kjeldhal Nitrogen balance

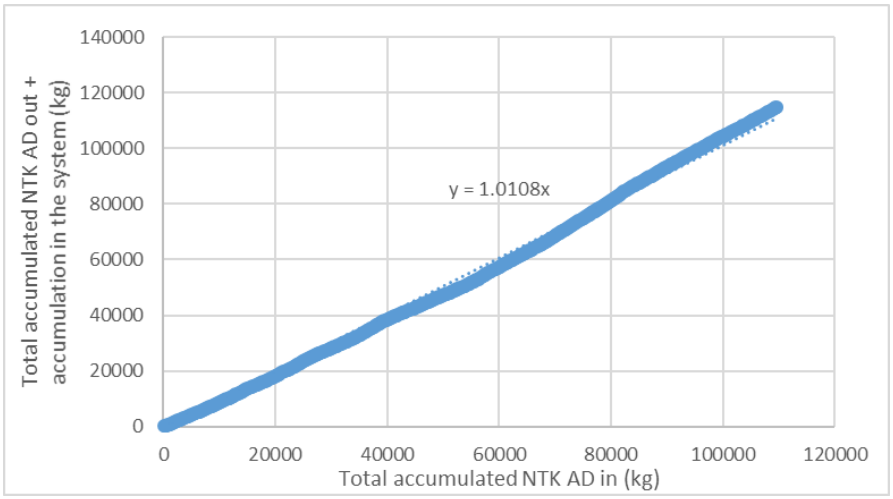

Total phosphorus mass balance

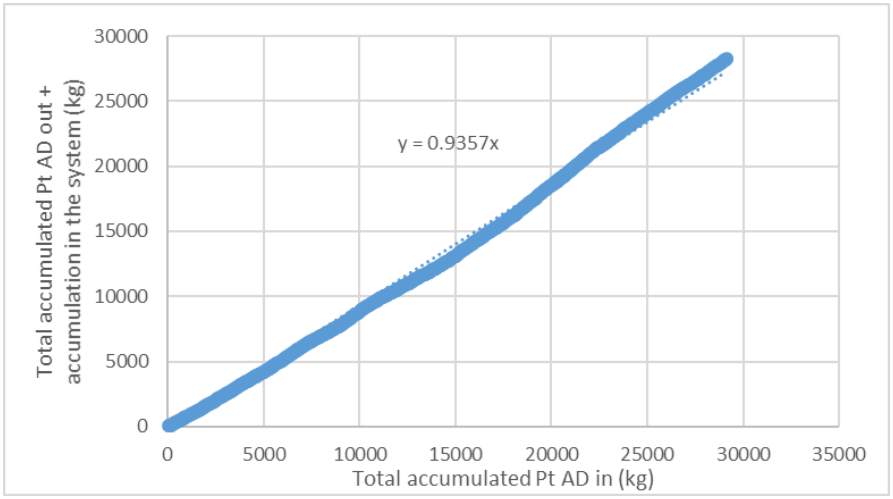

Total Calcium mass balance

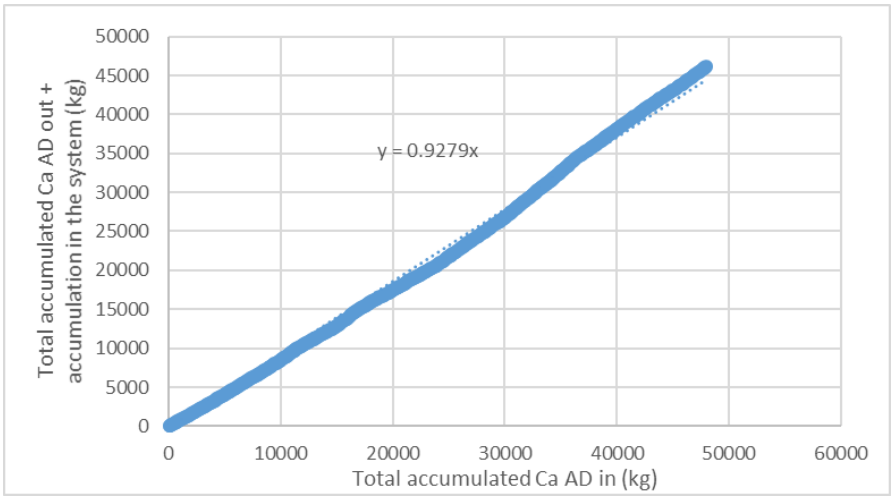

Total Potassium mass balance

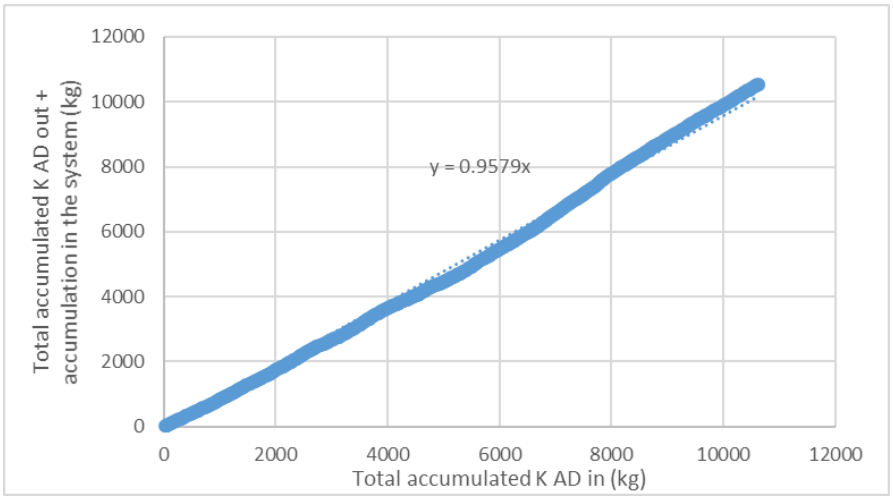

Total Magnesium mass balance

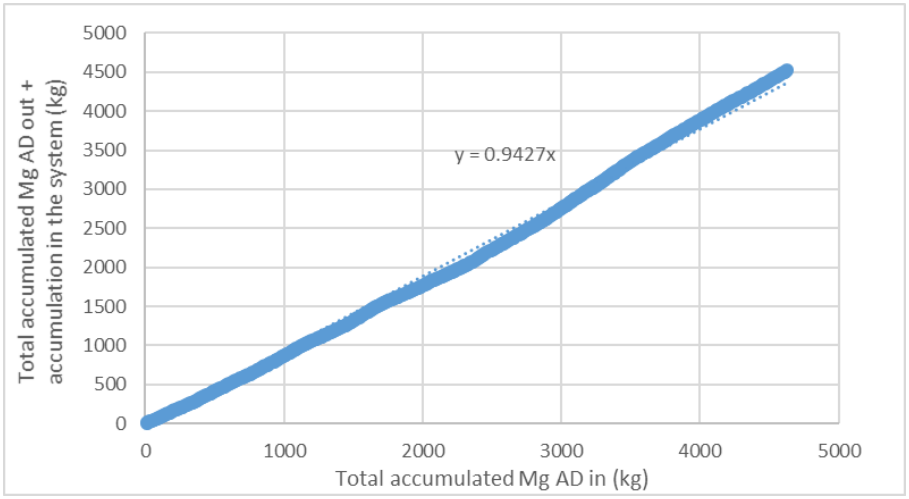

WRRF 2

Total COD mass balance

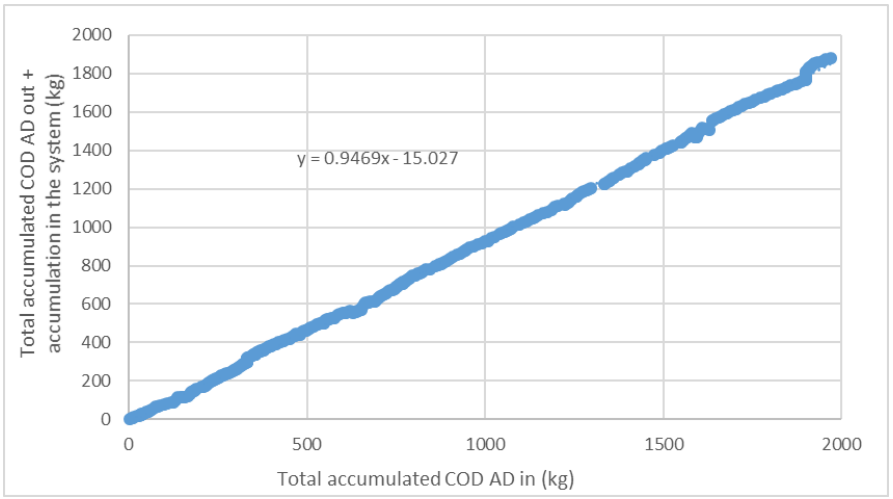

Mineral matter mass balance

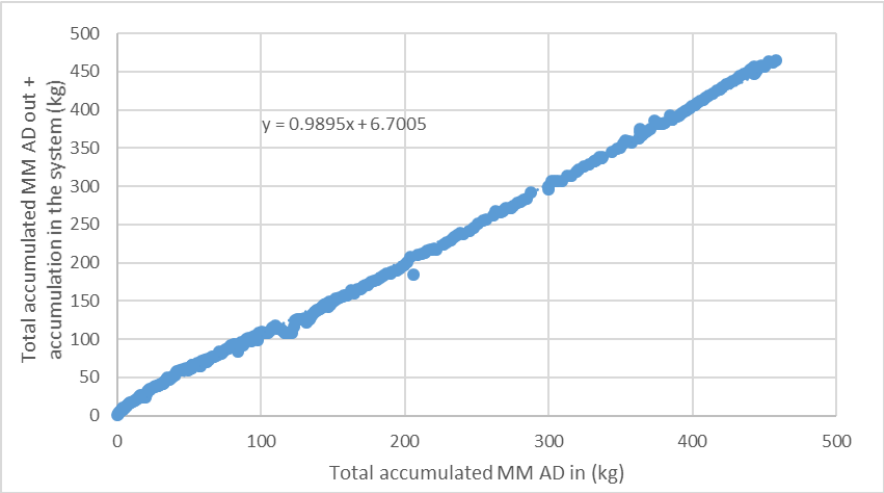

APPENDIX OF CHAPTER 4

The table below presents the review on N_2O emission factor found in the literature according to the type of biological N treatment.

Table S4.1 - N_2O emission factor found in the literature

Reference	Process	EF (% NLR)	EF (% NRR)
(Kanders et al., 2019)	Nitrification/Denitrification	10.4	
(Kampschreur et al., 2008)	2-stage PN/anammox	1.7	3.3
(Mampaey et al., 2016)	2-stage PN/anammox	3.7	7.12
(Gustavsson and la Cour Jansen, 2011)	2-stage PN/anammox	3.8	4.10
(Kanders et al., 2019)	1-stage PN/anammox	0.43	
(Kampschreur et al., 2009)	1-stage PN/anammox	1.23	1.67
(Joss et al., 2009)	1-stage PN/anammox		0.5
(Castro-Barros et al., 2015)	1-stage PN/anammox	2	2.70
(Schaubroeck et al., 2015)	1-stage PN/anammox	1.3	1.46
(Weissenbacher et al., 2010)	1-stage PN/anammox	1.3	1.45
(Yang et al., 2016)	1-stage PN/anammox	0.51	0.62
(Christensson et al., 2013)	1-stage PN/anammox		0.55
(Christensson et al., 2013)	1-stage PN/anammox		0.75
(Fenu et al., 2019)	1-stage PN/anammox		1.3
(Yang et al., 2016)	1-stage PN/anammox	0.97	1.21
(Yang et al., 2013)	1-stage PN/anammox	1.2	00.9

NLR = Nitrogen Loading Rate, NRR = Nitrogen Removal rate. For the 2-stage PN/anammox, NRR corresponds to the oxidation of NH_4^+ into NO_2^-.

The two graphs below represent the quantity of phosphorus in sidestreams per kg of phosphoris in the AD feed sludge.

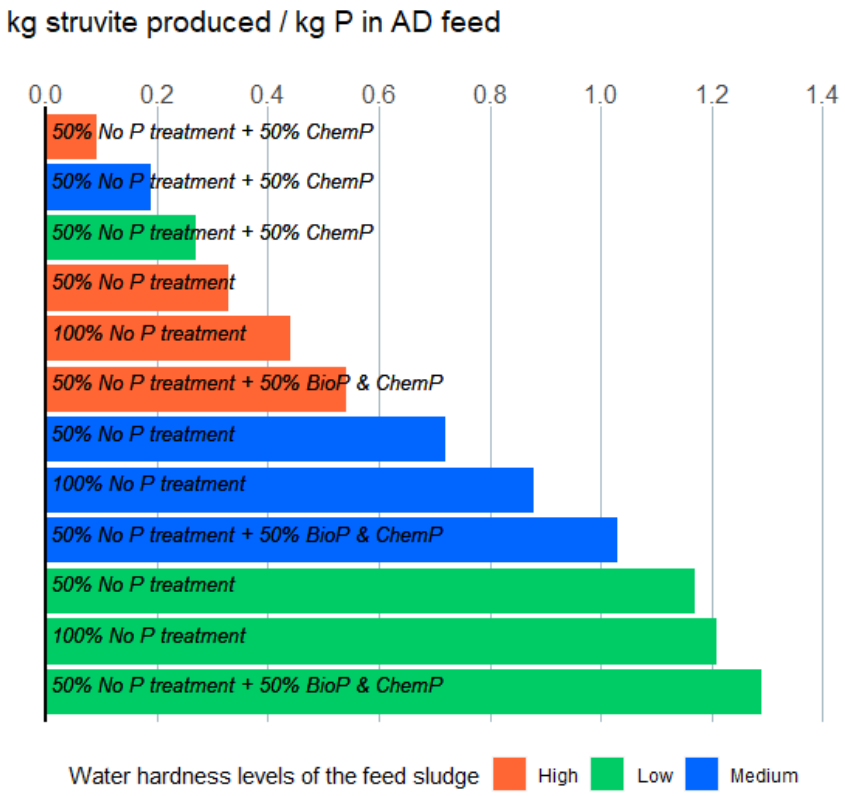

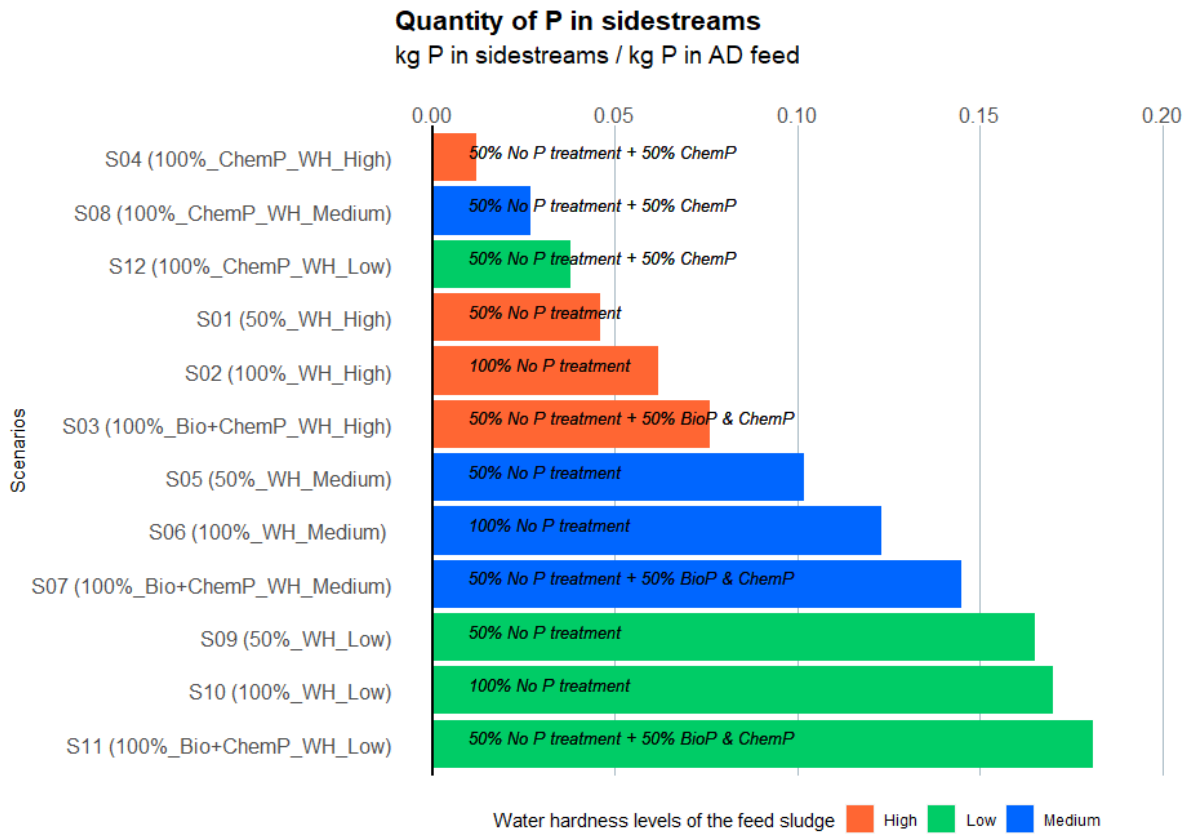

The graph below represents the quantity of minerals in digested sludge for scenarios S03, S07 and S11 (scenarios with 50% No P treatment + 50% BioP & Chem P and different water hardness levels).

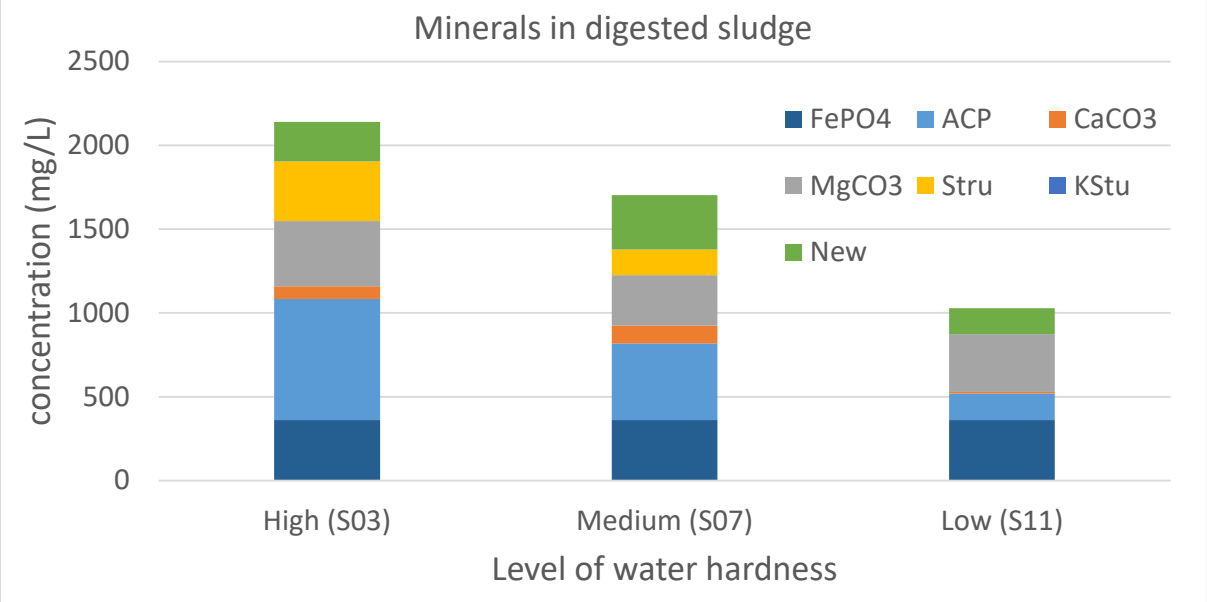

The graph below represents the fractionation of phosphorus in digested sludge for scenarios S10, S11 and S12 (scenarios for low water hardness level with different types of sludge: 50% No P treatment + 50% BioP & Chem P, 50% No P treatment + 50% Chem P, 100% No P treatment). The fraction “other” represents the biomass, lipids, carbohydrates and inerts.

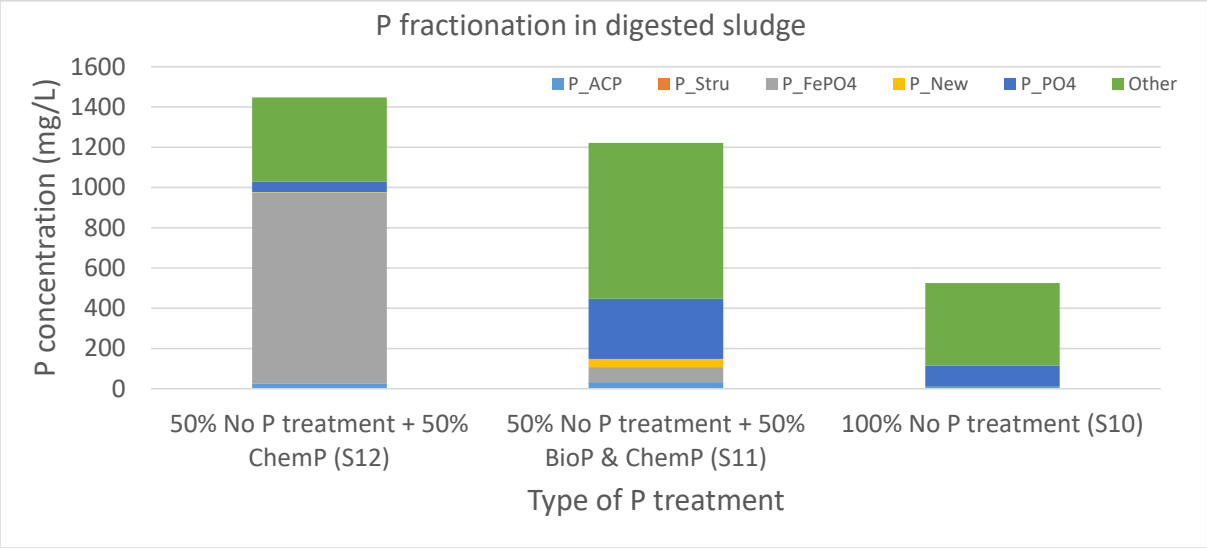

FOLIO ADMINISTRATIF

THESE DE L'INSA LYON, MEMBRE DE L'UNIVERSITE DE LYON

NOM : DEVOS DATE de SOUTENANCE : 12/09/2023

Prénoms : Perrine, Marie, Marie-Thérèse

TITRE : Traitement et valorisation des retours en tête: de la mesure à la modélisation

NATURE : Doctorat Numéro d'ordre : 2023ISAL0056

Ecole doctorale : Ecole doctorale de chimie de Lyon

Spécialité : Génie des Procédés

RESUME : La thèse porte sur le traitement et la valorisation des flux secondaires en stations d'épuration. Les flux secondaires (ou retours en tête) proviennent de l'étape d'épaississement ou de déshydratation des boues d'épuration et peuvent contenir des quantités importantes d'azote et de phosphore. Il convient de valoriser ou de traiter ces flux pour d'une part ne pas détériorer les performances des installations de traitement des eaux résiduaires, et d'autre part maximiser les ressources qu'elles contiennent. Dans un contexte d'évolution de la STEP (Station d'épuration) vers la StaRRE (Station de Récupération des Ressources de l'Eau), l'objectif de la thèse est d'accroitre les connaissances sur les caractéristiques des flux secondaires afin d'évaluer l'impact d'un traitement ou d'une valorisation de ces flux sur les performances globales de l'installation. Pour y répondre, la thèse s'appuie sur des campagnes expérimentales sur stations réelles et sur des outils de modélisation de la station d'épuration dans son intégralité (traitement des eaux résiduaires, des boues d'épuration et des flux secondaires). La thèse est organisée en trois grandes parties :
1) Caractérisation des retours et impact sur les performances des procédés de traitement ou de valorisation de l'azote et du phosphore
2) Validation d'un modèle de digestion anaérobie incluant la précipitation afin d'optimiser la récupération du phosphore
3) Analyse de scénarios pour évaluer les quantités de phosphore et d'azote dans les flux secondaires pour un digesteur centralisé mélangeant différents types de boues

MOTS-CLÉS : station d'épuration, digestion anaérobie, valorisation du phosphore, traitement de l'azote, modélisation

Laboratoire (s) de recherche : UR REVERSAAL

Directrice de thèse : Sylvie Gillot

Président de jury : Pierre Buffière, Professeur des Universités, INSA-LYON

Composition du jury :
GILLOT Sylvie, Directrice de recherche, INRAE
SPERANDIO Mathieu, Professeur des Universités, INSA Toulouse
FLORES ALSINA Xavier, Senior Researcher,Technical University of Denmark (DTU)
VANEECKHAUTE Céline, Associate Professor, Université Laval
BUFFIERE Pierre, Professeur des Universités, INSA-LYON
GRAU Paloma, Full Professor, TECNUN